



HUNGARIAN UNIVERSITY OF AGRICULTURE AND LIFE SCIENCES

# Tribological applicability of polymer composites in farm- machines

DOI: 10.54598/001030

PhD Dissertation

by

Hasan Muhandes

Gödöllő

2021

**Doctoral school**

**Denomination:** Doctoral School of Mechanical Engineering

**Science:** Mechanical Engineering

**Leader:** Prof. Dr. István Farkas  
Institute of Technology  
Hungarian University of Agriculture and Life Sciences, Gödöllő, Hungary

**Supervisor:** Prof. Dr. Gábor Kalácska  
Institute of Technology  
Hungarian University of Agriculture and Life Sciences, Gödöllő, Hungary

.....  
Affirmation of supervisor

.....  
Affirmation of head of school

## CONTENTS

NOMENCLATURE AND ABBREVIATIONS .....	5
1. INTRODUCTION, OBJECTIVES .....	7
<b>1.1. Introduction</b> .....	7
<b>1.2. Objectives</b> .....	7
2. LITERATURE REVIEW .....	9
<b>2.1. Friction</b> .....	9
<b>2.2. Wear</b> .....	11
<b>2.3. Abrasive wear</b> .....	16
2.3.1. <i>Effect of temperature on abrasive wear</i> .....	21
2.3.2. <i>Effect of hardness</i> .....	21
2.3.3. <i>Moisture effect on abrasive wear</i> .....	22
2.3.4. <i>Effect of abrasive grain size</i> .....	22
<b>2.4. Polymers and polymer abrasion</b> .....	23
<b>2.5. Bio-composite abrasion</b> .....	28
<b>2.6. Lubrication and effect on abrasion</b> .....	32
<b>2.7. Conclusion of the literature review</b> .....	36
3. MATERIALS AND METHODS .....	39
<b>3.1. Materials and preparations</b> .....	39
3.1.1. <i>Experimental materials</i> .....	39
<b>3.2. Test systems</b> .....	45
3.2.1. <i>Abrasive pin-on-plate test system</i> .....	45
3.2.2. <i>Slurry pot test system</i> .....	48
<b>3.4. Topography</b> .....	54
<b>3.5. Dimensionless numbers</b> .....	56
<b>3.6. Statistical analysis</b> .....	57
4. RESULTS .....	58
<b>4.1. Pin-on-plate system</b> .....	58
4.1.1. <i>The effect of the load</i> .....	58
4.1.2. <i>The effect of the speed</i> .....	60
4.1.3. <i>The effect of the wear interface</i> .....	61
4.1.4. <i>Comparing the materials for wear</i> .....	63
4.1.5. <i>Comparing the materials for friction temperature evolution</i> .....	68
4.1.6. <i>Comparing the materials for friction force</i> .....	70
4.1.7. <i>Abrasive wear against dimensionless parameters of mechanical properties</i> .....	71
4.1.8. <i>Multiple linear regression analysis</i> .....	79
4.1.9. <i>3D microscopy results and regression models</i> .....	81
4.1.10. <i>Abrasive sensitivity of the tested materials with the pin-on-plate system</i> .....	87

<b>4.2. Slurry-pot system</b> .....	89
4.2.1. <i>The effect of the speed</i> .....	89
4.2.2. <i>The effect of the collision</i> .....	91
4.2.3. <i>Evaluation of the relative wear</i> .....	92
4.2.4. <i>The daily relative wear</i> .....	96
4.2.5. <i>The statistical analysis of the wear results</i> .....	96
4.2.6. <i>3D surface microscopy results</i> .....	98
4.2.7. <i>Statistical evaluation of the 3D surface parameters</i> .....	107
<b>4.3. New scientific results</b> .....	110
5. CONCLUSIONS AND SUGGESTIONS .....	112
6. SUMMARY .....	113
7. ÖSSZEFOGLALÁS (SUMMARY IN HUNGARIAN) .....	114
8. APPENDICES.....	115
<b>A1: Bibliography</b> .....	115
<b>A2: Publications related to the dissertation</b> .....	123
<b>A3: Comparing the materials for wear</b> .....	124
<b>A4: The wear line equation and the slope value for the 12 test conditions</b> .....	125
<b>A5: Specific wear comparison</b> .....	127
<b>A6: Comparing the materials for friction temperature evolution</b> .....	128
<b>A7: Comparing the materials for friction force</b> .....	129
<b>A8: 3D surface microscopy results</b> .....	130
<b>A9: The relative wear different polymer samples (daily cumulative) of the weight loss in percentage (%), compared to the zero day weight</b> .....	133
<b>A10: The daily relative wear of the weight loss as a percentage (%) compared to the previous day's weight</b> .....	137
<b>A11: The other position results of the 3D surface microscopy results with the corundum medium</b> .....	139
<b>A12: The other position results of the 3D surface microscopy results with the gravel slurry</b> .....	142
<b>A13: The other position results of the 3D surface microscopy results with the loamy slurry</b> .....	145
<b>A14: The other position results of the 3D surface microscopy results with the sandy slurry</b> .....	148
9. ACKNOWLEDGEMENTS .....	151

## NOMENCLATURE AND ABBREVIATIONS

$A_p$	ploughed layer
$c$	Cohesion, kPa
$C_p$	Heat capacity at constant pressure, J/(kg $\times$ $^{\circ}$ C)
$C_p$	Plasticity criterion
$e$	elongation to break, %
$E$	Young's modulus, MPa
$e$	Pore index
$E$	Linear deformation modulus, kPa
$f_{ab}$	the ratio of the amount of material removed by the passage of grit, to the volume of the wear groove, N
$F_f$	friction force, N
$F_n$	normal force, N
$H$	Hardness
$HV$	Vickers hardness
$I_c$	Consistency index
$M$	Edometric deformation modulus, kPa
$n$	Porosity, %
$p_v$	contact pressure x sliding speed, MPa ms $^{-1}$
$S$	ultimate tensile strength, MPa
$s$	Sliding distance, m
$S_a$	3D surface roughness parameter indicates to Arithmetical mean height, $\mu$ m
$S_{ku}$	3D surface roughness parameter indicates to Kurtosis
$S_p$	3D surface roughness parameter indicates to Maximum peak height, $\mu$ m
$S_q$	3D surface roughness parameter indicates to Root mean square height, $\mu$ m
$S_{sk}$	3D surface roughness parameter indicates to Skewness
$S_v$	3D surface roughness parameter indicates to Maximum pit height, $\mu$ m
$S_z$	3D surface roughness parameter indicates to Maximum height, $\mu$ m
$T_m$	melting temperature, $^{\circ}$ C
$v$	Volumetric weight in the state of natural moisture content, kN/m $^3$
$v$	Sliding velocity, m/s
$V_f$	Fiber volume fraction, %
$V_m$	Matrix volume fraction, %
$V_p$	Porosity volume fraction, %
$v_d$	Volumetric weight in the dry state, kN/m $^3$
$v_s$	Specific gravity, kN/m $^3$
$W$	Natural moisture content, %
$WL$	The upper limit of plasticity, %
$Wp$	The lower limit of plasticity, %

### *Greek symbols*

$\Delta v$	relative velocity
$\varepsilon$	the corresponding elongation, %
$\varepsilon_B$	Elongation at break, %

$\rho$	Density, g/cm <sup>3</sup>
$\lambda$	Thermal conductivity, W/(m×°C)
$\alpha$	Coefficient of thermal expansion, 1/°C
$\rho_c$	Composite density, g/cm <sup>3</sup>
$\sigma$	the tensile stress, MPa
$\sigma_F$	Flexural strength, MPa
$\sigma_y$	Yield stress, MPa
$\sigma_F$	Flexural strength, MPa
$\sigma_M$	Tensile strength, MPa
$\sigma_C$	Compressive strength 1%, MPa
$\omega$	The angular velocity
$\Phi$	Internal friction angle, °

### *Abbreviations*

AFM	Atomic force microscope
CLTE	Coefficient of linear thermal expansion
CTI	Comparative tracking index
FEM	Finite element method
GFR	Glass Fiber Reinforced
HDPE	High Density Polyethylene
HPM	High-performance materials
LDPE	Low Density Polyethylene
PA	Polyamide
PA6	Polyamide 6
PA66	Polyamide 66
PA66GF30	Polyamide 66 glass fibre reinforced composite
PA6E	Extruded polyamide 6
PA6G	Cast polyamide 6
PE	Polyethylene
PEEK	Polyetheretherketone
PLA	Polylactic acid
PLA-HF	Biodegradable polymer composite - hemp fibre reinforced polylactic acid
PP	Polypropylene
PTFE	Polytetrafluoroethylene
PVC	Polyvinyl chloride
SECM	Scanning electrochemical microscopy
SiC	Silicon carbide
SLM	Self-lubricating materials
UHMW	Ultra high molecular weight
UHMW-PE	Ultra high molecular weight polyethylenes
UHMW-PE HD1000	Ultra High Molecular Weight Polyethylene High Density 1000

## 1. INTRODUCTION, OBJECTIVES

In this chapter, the importance of the research topic is presented along with the objectives of this research.

### 1.1. Introduction

A significant proportion of agricultural machinery is subject to abrasive wear, either in the field of crop production or in animal husbandry machinery. Every year, significant damage is caused by the need to provide spare parts instead of worn machine parts, there is downtime at the machines, and a technological process stops unexpectedly. Machine repairs and maintenance must be provided, and machines must often be equipped with lubrication technology.

The abrasive wear is a phenomenon in agricultural machinery that is present in the machine components or even in the complete equipment due to the operating conditions.

Components of field and horticultural machinery - from cultivators to harvesters - often have to operate in dusty, earthy, gravel environments. According to a large body of the relevant literature, hard mineral particles, in extremely wide fraction sizes, usually cause scratches, micro-cutting, cutting and fatigue processes on the working surfaces of machines and equipment, thus changing the surface, size or dimensional tolerances of machine parts. Some machines have to operate in a medium with a significant water content, they typically suffer from abrasive erosion (eg rice harvesting machines, washing and crop processing lines, manure handling equipment in animal husbandry, biogas systems etc.).

Also in the case of these critical abrasion machine parts, a design approach has emerged to replace the heavier, less corrosion-resistant, more expensive and / or more difficult-to-machine metal parts with engineering plastics. The use of polymers alone offers lighter machines (thus less soil compaction), corrosion-resistant and lubricant-free solutions at a competitive price with easier machinability. A key issue from the point of view of technical reliability is the wear life, especially the determining abrasion resistance.

In engineering practice, the polyamide (PA) plastic family as well as some variants of ultra high molecular weight polyethylenes (UHMW-PE) are generally characterized by good abrasion resistance. These conventional engineering plastics are all polymers produced from monomers provided by the petrochemical industry, i.e., oil and natural gas based products. Nowadays, along with the intensification of environmental protection, the question has arisen that e.g. where the polymer particles that wear out in the field go, what will happen to them. Do they increase the micro-plastic load in the environment? If so, is it currently possible to find a fully biodegradable polymer commercially or even in the development phase that could potentially partially or completely replace conventional engineering plastics?

In my research, I investigate this issue and use laboratory abrasion tribological modelling to find the relationship between abrasive resistance and material properties for conventional and bio-polymeric materials in systems modelling different abrasion mechanisms.

### 1.2. Objectives

The main aim of the research to describe (or/and find) useful data about the tribological behaviour of conventional and bio-polymeric materials. The objectives of this work are:

Development of laboratory models of two dominant abrasion effects (cutting, micro-cutting and abrasive erosion) typical of agricultural machinery according to DIN50322 wear test standard in accordance with the description of the category VI. Design of abrasive pin-on-plate and slurry-pot systems, conversion of the existing tribotesters to the planned abrasion tests.

In the developed two test systems abrasive tribotesting with the following materials. Among the polymers used for abrasion in general engineering practice are cast polyamide 6 (PA6G), extruded polyamide 6 (PA6E), polyamide 66 glass fibre reinforced composite (PA66GF30), antistatic cast polyamide 6 composite (PA 6G ESD) and an ultra high molecular weight polyethylene (UHMW-PE HD1000) with a density category of 1000 are selected. Furthermore, a fully biodegradable polymer composite - hemp fibre reinforced polylactic acid (PLA / HF) – is involved into the tests.

Comparison of wear test results, evaluation of a large number of measurement data by multiple linear regression. Processing of wear test results as a function of material properties ( $H, E, \sigma_y, \sigma_c, \varepsilon_B, \sigma_F, \sigma_M$ ), and the dimensionless numbers formed from them.

Based on the coefficients of multiple linear regression, to define the “abrasion sensitivity” for each tested material, to determine the material properties and the dimensionless parameters formed from them dominant in terms of abrasive resistance.

In the light of dimensionless parameters exploring the similarity between the two test systems (abrasive pin-on-plate and slurry-pot) based on the independent variables describing the abrasion sensitivity obtained.

To answer the hypothetical question: can a realistic abrasive operating condition be determined where the PLA / HF bio-composite is not inferior in terms of wear resistance than the engineering polymers currently used.



## 2. LITERATURE REVIEW

In this chapter, the scientific method and the critical literature which is related to the research will be reviewed, in addition to identifying the gap in the knowledge base. The progressive development of polymer tribology will be shown to give insight into the obstacles encountered by former researchers and the solutions they reached. This is considered to be the base, and this was the catalyst that inspired us to launch this research.

### 2.1. Friction

All artificial and natural mechanical systems contain relative motion between solid components. Sliding or rolling of two surfaces against each other would lead to frictional resistance, and this is where surfaces become worn. The response of the faces is called a tribological one. The nature of the materials and the contact conditions of the faces are what cause these conditions to arise (Hutchings et al., 2006).

The friction and frictional force can be defined as good or bad, it is impossible to use the car's tires on a road without this friction. The friction is also important and necessary to transmit the power and in the braking system. In other cases, friction is not the preferred thing, for example, in rotating and sliding components (Jeyaprakash and Yang, 2021).

The frictional characteristics are usually measured by a friction test along with abrasion resistance test. The coefficient of friction is used to calculate the results of these tests.

While the changes in conditions caused by friction are measured by a wear test. Deformation, scratches, and indentations on the interacting surfaces are the main factors in obtaining the test results (Keyence America, 2021).

Five categories has been given for the classification of the results of this friction and wear as follows (Ludema, 1996):

1. *Friction and wear usually cost money*, in several forms such as energy loss or material loss, and also in the social system which uses the mechanical devices. In general, wear costs between \$25 and \$250 for each person per year.
2. *Friction and wear can decrease national productivity*. Repairing the items due to wear or break down will occupy people with maintenance instead of contributing to national productivity.
3. *Friction and wear can affect national security*. For example, decreasing the efficiency of military hardware will lead to a decrease in the ability to perform a military mission.
4. *Friction and wear can affect the quality of life*, by improving the artificial part, which can be used inside our body when our natural parts wear out, for example, tooth fillings, artificial teeth and artificial skeletal joints.
5. *Wear causes accidents*. Worn brakes, for example, will lead to traffic accidents.

The motion resistance phenomena between two materials during sliding contact, with certain surface roughness, is defined as sliding friction (Encycloids, 2020a).

Fig. 2.1 shows a microscopic section of sliding contact surfaces (Li et al., 2020).

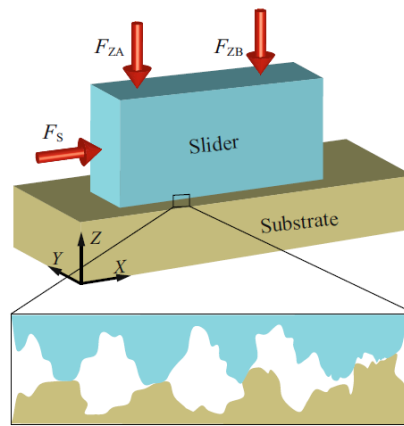


Fig. 2.1. Macroscopic section of sliding contact surfaces (Li et al., 2020)

The friction points of polymers sliding on smooth metal surfaces are generally characterized by two distinct dependencies on a normal load, sensitivity at low stress levels followed by a sharp decrease in friction, and increasing pressure at levels above the plastic flow limit of the polymer (Quaglini and Dubini, 2011).

During friction between a polymer pad and a metal surface, there are two processes which contribute to the friction force. The first one is the shearing of the junctions, and it is a result of adhesion between the asperities of the contacting surfaces. The second one is the dissipation of energy (Stachowiak and Batchelor, 2005) as a result of plastic deformation and abrasion (Bely et al., 1982).

Early studies used the adhesion process, which was originally developed for metals, to explain the friction of polymers. (Pascoe and Tabor, 1956) In his study he showed that there are two main ways the intricate behaviors differ from that of metals. The first one is that during sliding, it appears to have a little or no junction growth. The second one is that the deformation is neither purely elastic nor purely plastic but intermediate over a very wide range.

The friction of elastomers is usually considered as a joint effect of friction on a surface. This effect is caused by adhesion and the internal friction generated by the hysteresis of the deformation (Békési, 2012).

In the last 50 years, the polymers' sliding behavior has been studied excessively. Several models of friction have been well acknowledged (Myshkin and Petrokovets, 2004).

The friction and wear of materials are not simple characteristics that can be found in their properties. They are measured in the tribological system. (Axén et al., 2001). This is because the tribological characteristics of the system are affected by surface contact (mechanical, physical, chemical, and geometrical) and the surrounding atmospheric conditions.

The phenomenon of friction - its origin and course - has been thoroughly researched and known to engineers, and the role of adhesion and deformation of the contact surfaces is discussed in detail in the significant literature. This dissertation deals primarily with abrasive wear processes, which are the result of friction, so I go on the wear processes in the next, ignoring the friction details.

## 2.2. Wear

Stachowiak and Batchelor (2001) gave a definition of wear as film failure, which impairs the relative motion between solid bodies and causes severe damage to the contacting surfaces. The consequences of film failure were considered as severe wear. Wear is the major wastage and loss of material of mechanical performance. Reducing the wear can make considerable savings as a result. Wear and energy dissipation is an effect of friction.

Devine (1976), during a workshop on wear control, to achieve product durability, in the USA, in 1976, gave a report about the total cost of wear. It had been calculated as 243.87 US\$ per flight hour for a single US naval aircraft. The details of this 243.87 were as follows, the scheduled maintenance for wear \$67, unscheduled maintenance \$140, and overhaul \$36.87.

Devine (1976) also gave data on the wear cost of diesel engines. The data provided showed that the maintenance and repairing of diesel engines for 20 ships (120 engines) costs 38.92\$ as a wear cost per hour per ship, while fuel costs about 75\$ per hour per ship.

Due to this unexpected high cost as a result of wear, (Devine, 1976) mentioned several technical and professional societies which work to minimize the effects of wear in an effort to control them. Some examples are ASLE, ASTM, MFPG and ASME.

Fig. 2.2 shows the relation between the operation conditions and the type of wear.

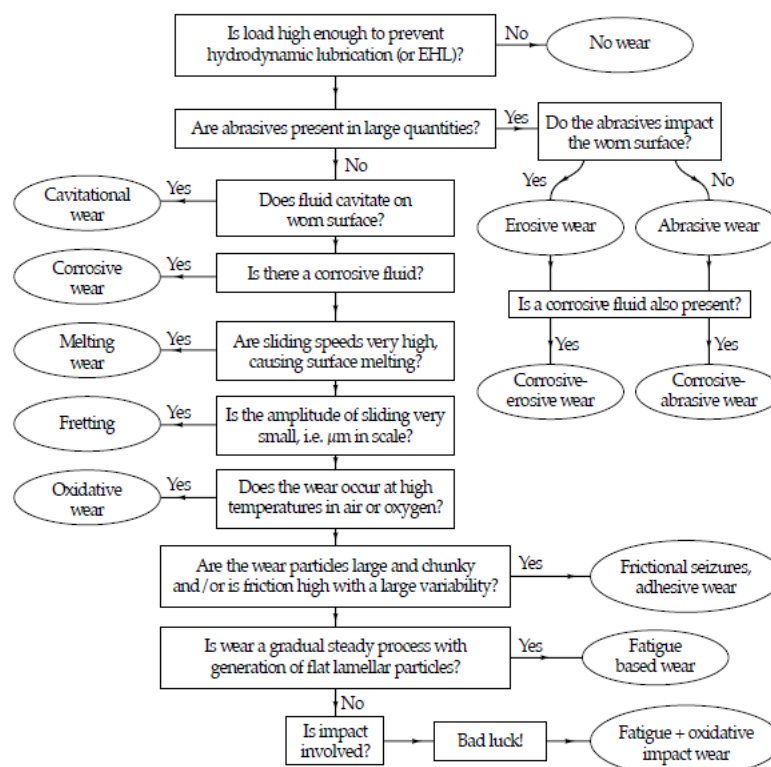


Fig. 2.2. The relationship between operating conditions and type of wear (Stachowiak and Batchelor, 2001)

While studying wear and wear mechanisms, (Li, 2009a) gave a definition of wear as “the relative motion between contacting surfaces leads to a progressive loss of materials, this loss can be defined as wear”.

Wear is one of three primary factors besides fatigue and corrosion. These affect the performance and limit the life of any engineering system.

Li (2009b) classified the damage of wear into two sections:

- The first, due to the loss of material. The dimension of a component will decrease and lead to high vibration, high noise, system malfunction and reduced efficiency. With the presence of dynamic load, fatigue fracture could happen, which leads to a catastrophic failure.
- Secondly, wear debris, this is detached material from the worn surfaces that can be harmful to machinery, it can increase wear rate, block valves, oil filters or it may cause contamination if the machinery is used for food production.

In order to classify wear, (Li, 2009a) mentioned that in the industry there are several forms of wear. To categorize wear, several methods can be used, one classification can be described as:

- lubricated wear and dry wear;
- severe wear and mild wear;
- Sliding wear, rolling contact wear and impact wear.

These forms can happen with the presence of one or a combination of wear mechanisms. Studying and understanding the wear mechanisms involved is the first step to solve wear problems.

Several types of wear are mentioned, including, ‘adhesive wear, fatigue wear, abrasive wear, cavitation wear, corrosive wear, oxidative wear, fretting wear, impact wear, melting wear, diffusive wear’.

Stachowiak and Batchelor (2001) mentioned, that choosing materials which have specific properties, can have an effect on wear control. Fig. 2.3 illustrates and guides, for wear control, by general material properties.

Critical materials property	Wear mechanism							
	Abrasive	Erosive	Cavitation	Corrosive	Fretting	Adhesive	Melting	Fatigue
Hardness	✓	✓	○	○	○	✓	○	○
Toughness	○	✓	✓	○	○	○	○	✓
Fatigue resistance	✓	✓	✓	○	✓	○	○	✓
Inertness	○	○	○	✓	✓ <sup>①</sup>	○	○	○
High melting point	○	○	○	○	○	✓	✓	○
Heterogeneous microstructure	✓	○	○	✗ <sup>②</sup>	○	✓	○	○
Non-metallic character	○	○	○	✓	○	✓	○	○

✓ Important

○ Marginal

✗ Unfavourable

① Fretting in air for metals

② Homogeneous microstructure inhibits electrochemical corrosion and, with it, most forms of corrosive wear

Fig. 2.3. General materials selection guide for wear control (Stachowiak and Batchelor, 2001)

Varenberg (2013) gave a definition of wear according to the "Standard terminology relating to wear and erosion. ASTM G40-01, 2001" as "that wear is defined, as the damage to a solid surface, generally involving progressive loss of material, due to relative motion between that surface and a contacting substance or substances".

After analysis of this definition, three criteria can be used to classify which issues are applicable to particular parts of the system. These three criteria are the answers to the following questions: 1) Why does it happen? 2) How does it happen? and 3) Where does it happen?

Then he gave a more in depth explanation about these three questions as follows:

- As usual, the question “why” can determine the reason. This is defined and explicitly specified in the definition of ASTM. So it is clarified that the first classification will be the type of relative motion.
- The question “how” is used to illuminate the mechanism. The interaction of the contacting surfaces with “a contacting substance or substances”, lead to external forces being exerted on them. With the presence of relative motion, forces will act through certain distances, and mechanical work will be performed on the surfaces. This mechanical work will accumulate energy which should be dissipated. The form of surface damage can be determined by the amount of energy involved in this process. This allows us to clarify the second classification, which is based on energy dissipation.
- The question “where” is used to define the significance, and it refers to the scale of the problem. This may be recognized on either macroscopic, or microscopic, or nano level as surface color, reflectivity, texture, integrity, homogeneity, etc.

Varenberg (2013) during his study of wear classification, he mentioned that a lot of studies, classifications, and schemes had been devised. However, though covering the whole field, and the fact they were still connected loosely to each other, they did not give a complete or clear picture. To achieve this goal, he combined several existing approaches to unify the field, to create a simple approach to wear types. This simple scheme is based on the three previous classifications which answers the questions, “why”, “how” and “where”. As a result, he created a 3D cubic or space to understand wear types.

Varenberg (2013) understood that answering the three questions (why, how, where), would lead to producing this 3D space, shown in Fig. 2.4. This is a combination of two surface states, four mechanisms of surface disturbance, and five types of relative motion, and then filling the space with the known wear types.

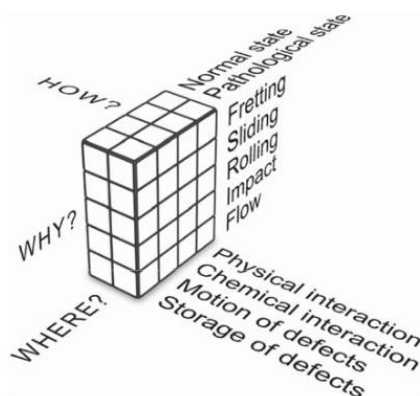


Fig. 2.4. 3D classification space (Varenberg, 2013)

Varenberg (2013) introduced a table for the pathological surface state, with the 5×4 slice, and by arranging the remaining wear types, filled the vacant places as shown in Fig. 2.5. Eleven types of wear can be categorized, and they can be further subdivided into smaller subgroups for specific ones.

## 2. Literature review








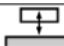

Surface disturbance Relative motion	Generation of defects		Generation of heat	
	 Storage of defects	 Motion of defects	 Chemical interaction	 Physical interaction
 Fretting	Fretting fatigue	Fretting wear		
 Sliding	Fatigue wear	Abrasive wear		Adhesive wear
 Rolling	Pitting	Solid-particle crushing		
 Impact	Impact wear	Solid-particle erosion		Ablation erosion
 Flow	Liquid-impact erosion	Solid-particle erosion		

Fig. 2.5. Pathological wear types determined by relative motion and surface disturbance

Kovaříková et al. (2009) gave a general idea about wear, as soon as the contact between the base body and counter body takes place, which happens when the lubricant film is unavailable or is not thick enough, wear occurs. Wear comes about by mechanical causes, by a progressive loss of material from the surface of a solid. Signs of wear can be in several forms, like small detached wear particles, or material removed and transferred from one friction body to the other. That leads to changes in the material and the new shape changes the tribologically loaded material zone of one or both friction partners.

According to the type of tribological load and the materials involved, the wear is classified into different types, like sliding wear, fretting wear, abrasive wear, and material cavitation.

Wear can be caused by a number of mechanisms, the following four being especially important:

- Surface fatigue
- Abrasion
- Adhesion
- Tribochemical reaction

Fig. 2.6 was introduced to illustrate the effective wear mechanisms. These four essential wear mechanisms can occur individually, successively or concomitantly.

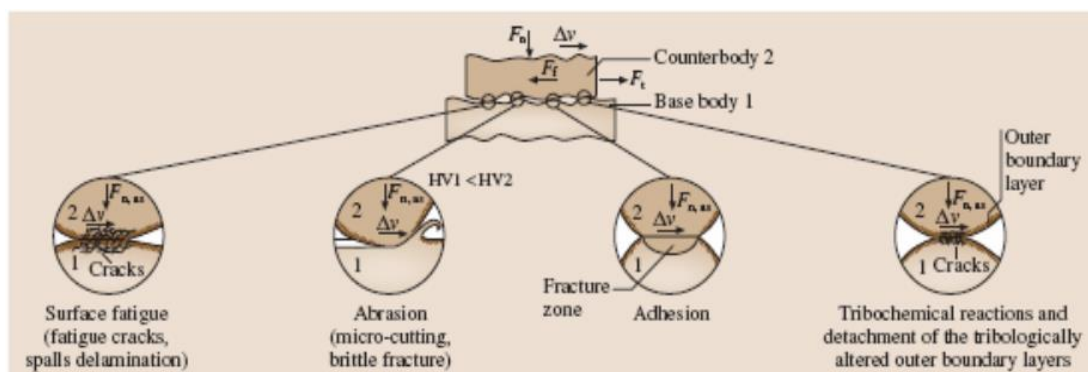


Fig. 2.6. Basic wear mechanisms viewed microscopically ( $F_n$  normal force on the apparent contact surface,  $F_f$  friction force between the base body and counter body,  $F_n$ , as a normal force on asperity contact,  $\Delta v$  relative velocity, HV Vickers hardness) (Kovaříková et al., 2009)

The first mechanism which is *surface fatigue* manifests itself through cracking, crack growth, and detachment of wear particles, and is caused by alternating loads in the near-surface zones of the two bodies (base body and counter body).

*Abrasion* can be caused by:

- Repeated ploughing which leads to fatigue and micro cuttings.
- Counterbody's hard asperities which lead to fracturing of the base body.
- Wear caused by the hard particles in the interfacial medium.

With *adhesion*, after braking the protective surface layers, the atomic bonds between the base body and counter body deform in a plastic way. Materials detach from the softer body and transfer to the harder one, this happens if the adhesive bonds of the softer body are less than the strength of the bonds between the two bodies.

The last mechanism "*tribochemical reactions*" happen for two reasons, the activation of friction due to the load near surface zones, or the chemical reaction of the counter body with lubricant or an ambient medium. These two reasons can happen together or in a separate way. But in both cases, the properties of the objects acted on will be changed. After a certain thickness, brittle chipping could occur or it could even produce properties that reduce friction and/or wear.

Knowing wear mechanisms and wear phenomena is important for interpreting wear results, these can happen in several forms, like changes in a surface layer or the accumulation of wear particles. Electron microscopes can be used to clarify this. (Kovaříková et al., 2009) introduced a table (Table 2.1) of typical wear phenomena caused by the main wear mechanisms.

Table 2.1. The main wear mechanisms (Kovaříková et al., 2009)

<b>Wear mechanism</b>	<b>Wear phenomenon</b>
Adhesion	Scuffing or galling areas, holes, plastic shearing, material transfer
Abrasion	Scratches, grooves, ripples
Surface fatigue	Cracks, pitting
Tribochemical reaction	Reaction products (layers, particles)

Li (2009b) dealt with wear measurement, and mentioned that after the test, the material removed from the specimen could be determined by weight loss, volume loss, changing of the linear dimension, the test specimens size and geometry. For mass loss, it can be determined by using precision balance. After cleaning the sample, the difference in weight between, the before and after states, represents a mass loss. The unit of this loss is in grams (g) or milligrams ( $\mu\text{g}$ ). For volume, by knowing the geometry of the wear track (depth, length, width) or by scar profile, the wear volume can be calculated. The unit of wear volume loss is  $\text{mm}^3$  or  $\mu\text{m}^3$ . With these wear volume calculations, the wear of several materials which have different densities can be compared.

In case of an irregular track, it's not easy to calculate the volume, so in this case, the mass loss and the wear volume can be determined by having the density calculated. In some cases, when a certain dimension is more important than the function of the system, calculating wear by linear dimension change becomes very useful in many engineering situations.

All of these wear measurements (mass loss, volume loss, or linear dimension changing) reflected by wear rates, can be expressed in different ways. Li gave a table (Table 2.2) with some examples:

Table 2.2. Wear measurement methods and typical units of wear quantification (Li, 2009b)

	Measurement Methods	Units of Wear	Units of wear rate
<b>Mass loss</b>	<ul style="list-style-type: none"> <li>Direct measurement by a precision balance.</li> <li>Calculated from volume loss for known density material.</li> </ul>	$\mu\text{g}$ $\text{g}$	$\mu\text{g}/\text{m}$ , $\text{g}/\text{m}$ , $\mu\text{g}/\text{N}$ , $\text{g}/\text{N}$ , $\mu\text{g}/(\text{N}\cdot\text{m})$ , $\text{g}/(\text{N}\cdot\text{m})$ .
<b>Volume loss</b>	<ul style="list-style-type: none"> <li>Calculated from depth, width, wear profile and/or other dimensions data of a wear track. Surface <u>profilometry</u> or microscopy techniques can be used for the measurement.</li> <li>Calculated from mass loss for known density material.</li> </ul>	$\text{mm}^3$	$\text{mm}^3/\text{m}$ $\text{mm}^3/\text{N}$ $\text{mm}^3/(\text{N}\cdot\text{m})$ ,
<b>Linear dimension</b>	<ul style="list-style-type: none"> <li>Direct measurement by surface <u>profilometry</u>, microscopy and other dimension measurement techniques.</li> </ul>	$\mu\text{m}$ $\text{mm}$	$\mu\text{m}/\text{year}$ $\text{mm}/\text{year}$

To have better control of wear and friction, several production methods have been developed including, composite structuring and soft or hard film coating. These aspects would lead to better properties for friction and wear since it makes the materials and their surfaces perform better (Kato, 2000).

Walczak et al. (2017) presented an analysis of the tribological properties of a ball on a disc as sliding elements in agricultural machinery. They conducted dry friction tests for polymer-metal pairs to obtaining the corrosion rate and friction coefficient of the samples used. Three pairs of Iglidur samples were used.

Sarankó et al. (2017) studied the effect of the mass load (static) and vibration loads (dynamic) which are the result of the vibration of the machine elements for several materials on fatigue-sliding models. The authors gave an idea of how the loads can affect the friction coefficient and the wear.

### 2.3. Abrasive wear

Nowadays, abrasive wear of engineering and agricultural machine components caused by the abrasive particles is a major industrial problem. Therefore, a full understanding of the effects of all system variables on the abrasive wear rates is necessary to undertake appropriate steps in the design of the machinery and the choice of materials to reduce/control wear (Mishra, 2014).

Agricultural machine components are affected by typical but markedly different operating conditions that shape abrasive wear. Hence, a wide range of materials from different families are used for these machine elements. Tillage or cultivator implements are characterized by micro-cutting and fatigue acting on their location specific surfaces (Kalácska et al., 2020), in this way alloyed martensitic steels are considered most commonly used. Often, hard alloy coatings are applied to further enhance the wear resistance of these elements (Sidorov et al., 2017).

Abrasive wear happens when a soft surface is passed over by hard particles or a hard surface and causes material loss (Bhushan, 1999).



However, with sliding friction of similar metals, abrasive grooves can be found (Kato, 1997).

If a solid object comes in contact with particles of a material which have equal or greater hardness "Abrasive wear" occurs. Wear of buckets on earth-moving machinery is a common example of this problem (Stachowiak and Batchelor, 2001).

Kovaříková et al. (2009) dealt with abrasive wear and showed that contact between the particles of solid materials could cause abrasion, which is a wear form.

In their study about wear, (Stachowiak and Batchelor, 2001; Kovaříková et al., 2009) showed that abrasion shares some common features with erosion and cavitation. There are also fundamental differences between these wear forms. These differences are due to the microscopic mechanisms of wear for these wear forms, which lead to the different practical considerations for materials selected, in regard to wear resistance.

Based on that, during the wear process, the abrasive particles can be formed due to phase transformations and work hardening (Rigney, 1997).

There are three different forms of abrasive wear: micro-cutting, wedge formation and ploughing (Hokkirigawa and Kato, 1988).

In 1985 (Lim and Brunton, 1985) built a scanning electron microscope with a pin-on-disc rig inside it, this allowed for ground breaking observation of a wear mechanism. Not only that, he recorded the process on a videotape, and by using a data-logging system, measured the variations on normal load and frictional force. These experiments formed a sheet or flake like debris when high purity copper pins slid on casehardened mild steel disks. The amount of debris produced was influenced by small variations in the surface roughness of the disks for the same sliding distance.

A schematic to was given illustrate the scanning electron microscope (Fig. 2.7), it consisted of a stationary pin, held in place by a load cell which slid on a rotating disk (Lim and Brunton, 1985).

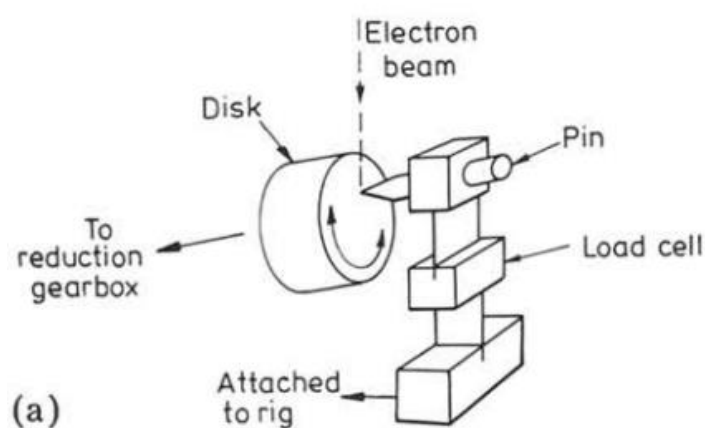


Fig. 2.7. A schematic representation of the low angle pin-on-disc wear rig (Lim and Brunton, 1985)

By using a scanning electrochemical microscopy, (SECM) high-resolution three-dimensional images were generated, by measuring the variation in the tip current due to perturbations in the diffusion layer (Ellis et al., 1995).

A study of surface roughness of thin silicon films deposited on SiO<sub>2</sub> was done by using an atomic force microscope. Several silicon films were used, like amorphous silicon and low-pressure, chemically-vapour-deposited silicon films, on silicon dioxide (Nasrullah et al., 2005).

The atomic force microscope and profilometer was used to calculate the surface roughness in ceramic specimens, where the surface had different finishing techniques. Three ceramic materials were used: Vitadur Alpha, IPS Empress 2 and AllCeram. Five surface finished systems were used. The stylus profilometer and an atomic force microscope (AFM) are the two roughness measuring instruments used (Tholt et al., 2006).

Bates et al. (1974) built a similar device to "Lim & Brunton" in order to study the mechanisms of penetrative wear (Fig. 2.8). By the applied load, three modes of penetration can be distinguished.

- Plate-like wear debris during the most severe penetration from the leading edge of the slider.
- A series of slip line fields are presented to approximate this debris formation process.
- A plastic constraint is seen to be an important factor in wear particle formation.

It was found that debris was formed like random plate debris by a stylus scratching cast iron.

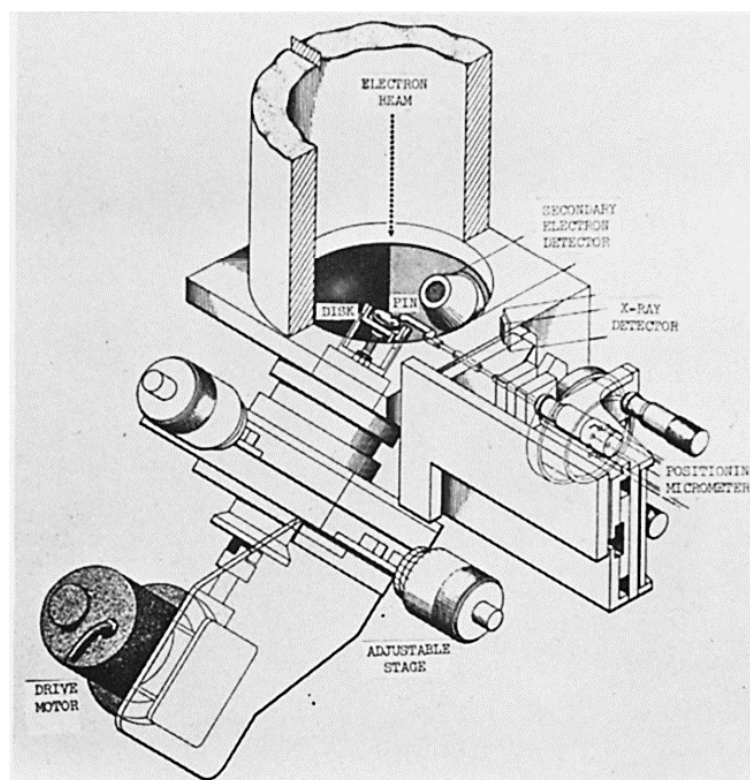


Fig. 2.8. Pin-on disk wear machine mounted in a scanning electron microscope (Bates et al., 1974)

During the study about wear and wear mechanisms, similar abrasive wear mechanisms were found during machining and grinding, in the manufacturing process (Li, 2009a). With normal pressure, the harder asperities penetrate the softer surface. With tangential motion and with the combined effects of 'micro-ploughing', 'micro-cutting' and 'micro-cracking', the materials of the softer surface will be removed, which leads to the creation of grooves and scratches, as shown in Fig. 2.9.

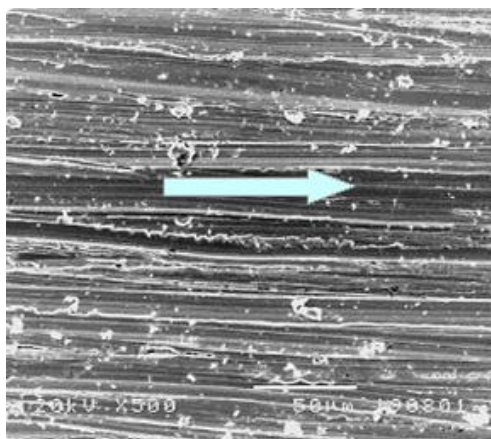


Fig. 2.9. The steel surface is worn by abrasion (Li, 2009a)

Stachowiak and Batchelor (2001) mentioned in their book about tribology, that the scientists previously thought that grits or hard asperities which cause abrasive wear, look like a cutting process by a machine tool or a file. The microscopic examination has now shown, that the sharpest of grits and more indirect mechanisms take place in the cutting process.

The particles or grits that are subjected to abrasive wear can be removed by micro-cutting, micro-fracture, accelerated fatigue by repeated deformations or by the “pull-out” of individual grains. Fig. 2.10 illustrates these mechanisms.

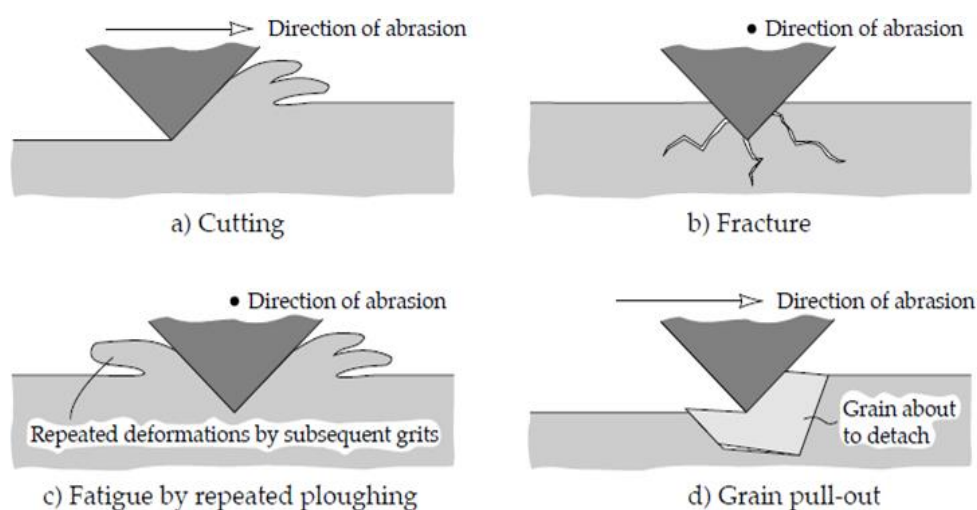


Fig. 2.10. Mechanisms of abrasive wear (Stachowiak and Batchelor, 2001)

The first mechanism "cutting" which is illustrated by Fig. 2.10. (a), sharp grit or hard asperity goes through and cuts the softer surface, the cut material is removed as debris. This mechanism presents the classic model.

The literature review indicates two basic modes of abrasive wear: two-body and three-body abrasive wear.

In the three-body abrasion, the particles which are formed during the operation or which come from outside the system cause the abrasive wear. While for two-body mode, the role of the abrasive is played by one of the materials (Moore, 1974).

Moving or switching from one mode to another can result during the system operation, as well as modes acting simultaneously (Kitsunai et al., 1990).

The simplest example of two-body abrasive wear is sandpaper, the action of sandpaper is like a cutting tool when the hard asperities pass over the surface.

While in three-body abrasive wear, the grits aren't held rigidly, they can rollover the surface freely. These two modes are illustrated schematically in Fig. 2.11.

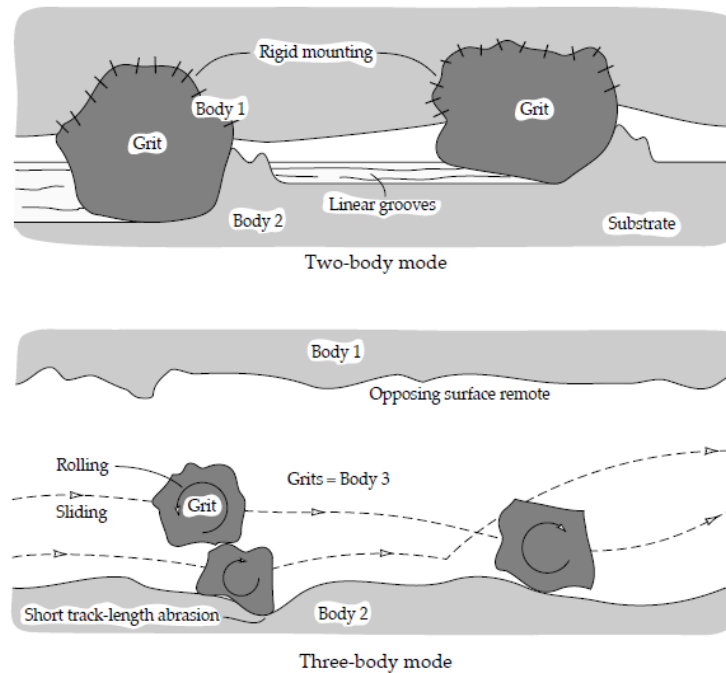


Fig. 2.11. Two and three-body modes of abrasive wear (Stachowiak and Batchelor, 2001)

The material removal model for two-body is close to 'cutting tool', while the material removal model for three-body involves slower mechanisms. For two-body abrasive wear, the worn material is not removed by a series of scratches but through gradual removal of surface layers by the successive contact of grit, due to the worn surface's random topography.

The same result has been produced by (Rabinowicz et al., 1961) by analyzing the abrasive wear data of several investigations and using them to develop a simple quantitative expression. As a result, he found that the abrasive wear for three-body abrasion rates are ten times less than those for two-body abrasion. The reason for this is because of the time it takes for the average loose abrasive grain to be divided in to two parts, the first one causing 90% when rolling and then 10% when abrading the sliding surfaces between which it is situated.

Depending on different interactions between wearing material and the abrasive particles, (Gahr, 1988) gave another model for abrasive wear as showed in Fig. 2.12.

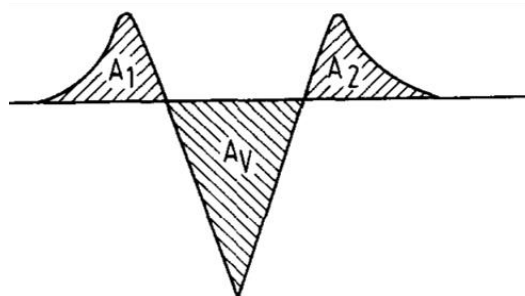


Fig. 2.12. Model of material removal and displacement in ductile abrasive wear

The idea for this model is to show that the removed materials don't disappear, but they transform in to wear debris. A large amount of these materials become displaced on the grit path sides, especially if the material is ductile.

Then (Gahr, 1988) introduced a value " $f_{ab}$ ", which is the ratio of micro-cutting to micro-ploughing or the amount of volume loss, to the volume of the wear groove. It can be calculated by Eq. 2.1:

$$f_{ab} = \frac{A_v - (A_1 + A_2)}{A_v} \quad (2.1)$$

Where  $f_{ab}$  is the ratio of the amount of material removed by the passage of grit, to the volume of the wear groove;  $f_{ab} = 1$  for ideal micro-cutting,  $f_{ab} = 0$  for ideal micro-ploughing and  $f_{ab} > 1$  for micro-cracking.

### 2.3.1. Effect of temperature on abrasive wear

During abrasive wear, temperature has an affect in two situations (Stachowiak and Batchelor, 2001):

- The influence of ambient temperature
- The deformation of the worn plastic material raising the temperature and effecting the contact with grits.

To study the effects of temperature, (Soemantri et al., 1985) did experiments on pure aluminum and copper with an ambient temperature reaching 400 °C, for two-body abrasive wear. The temperature had no effect on aluminum, while on copper there was an effect, and a significant one at 250 °C where an increase occurred.

For three-body abrasive wear, a disc-shaped specimen pressed against a rotating disc containing loose abrasive particles was used. The temperature caused weight loss in very small amounts on aluminum, while for copper it caused an increase in apparent wear rate. The reason for this changing is that the long tests lead to oxidation.

### 2.3.2. Effect of hardness

The effect of the hardness was studied by (Rabinowicz et al., 1961). They did several tests for several types of metals, the upper and bottom specimens were from the same metal, and the wear rate calculated was an average loss in volume in the two specimens.

By knowing the weight lost and by dividing the worn volume (cm<sup>3</sup>) in to the load (g) and sliding distance (cm), the wear rate can be calculated. In doing this, the main characteristic, that the wear rate doesn't have a relation with the load and the sliding distance, can be considered predominantly independent.

Fig. 2.13 represents the results, and it is clear that the wear resistance is approximately proportional to the hardness;

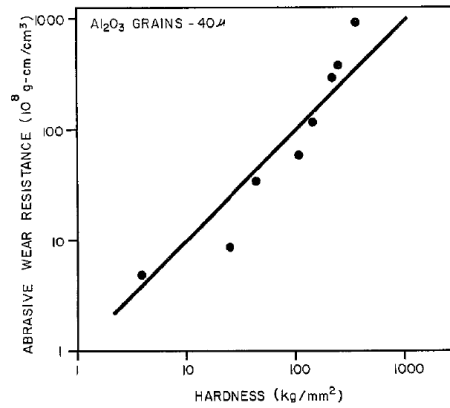


Fig. 2.13. The abrasive wear resistance of a number of metals plotted as a function of hardness (Rabinowicz et al., 1961)

### 2.3.3. Moisture effect on abrasive wear

Moisture has a strong influence on abrasive wear rates. In general, the abrasive wear rate will increase when the moisture content in the atmosphere is increased, but sometimes there is a reverse action. (Larsen-Basse and Sokoloski, 1975) while studying the influence of atmospheric humidity on abrasive wear, it was shown that it is difficult to know the exact effect of moisture for a particular case. Moisture can make the grit sufficiently weak, which produces new cutting edges, or alternately can cause the disintegration of the grits into nonabrasive and fine particles. Not only does moisture have an effect on the grits but also on the worn materials which can become weak like glass.

Modes of abrasive wear have a role in moisture effect, abrasive wear increases with humidity for two-body abrasive wear, while abrasive wear rate may increase or decrease for three-body abrasive wear.

### 2.3.4. Effect of abrasive grain size

To study the effect of the grain's size on abrasive wear, (Sasada et al., 1984) did several sliding metal experiments by using Sic abrasives with a grain size range of 3 - 150  $\mu m$ . These tests involved a tube end against a flat surface using the following metals; pure aluminum, copper, iron, nickel and zinc.

They show the results in Fig. 2.14.

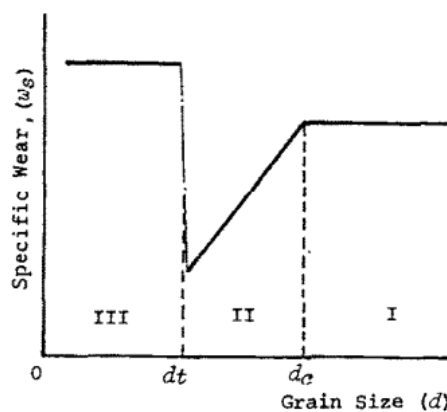


Fig. 2.14. Effect of abrasive grain size on three-body wear (Sasada et al., 1984)

Three different effects of grain size can be noticed.

The first one is when the grain's size is larger than the critical size  $d$  (about 50  $\mu\text{m}$ ) which is the first rank. It was noticed that the wear rate has no relation with the size of grains. A different result occurred during the second rank, where the wear decreases as abrasive grains become smaller. In this rank the grain's size is located between the critical size and transition size (about 10  $\mu\text{m}$ ). In the third rank where the grains are smaller than the transitional size, it was observed that the wear rate is high and independent of abrasive grain size.

By applying a sliding contact between two specimens made from the same metal, maintaining sliding conditions and changing the abrasive particle size, (Rabinowicz et al., 1961) gave a figure to illustrate what the role of the abrasive grain's size is on wear rate.

This shows that the wear produced was very small when the abrasive grain size was small, and started to increase when the grain size was increased, it then reached a value where there is no relation between the wear rate and the size of the grain, as illustrated by the plateauing line, in Fig. 2.15.

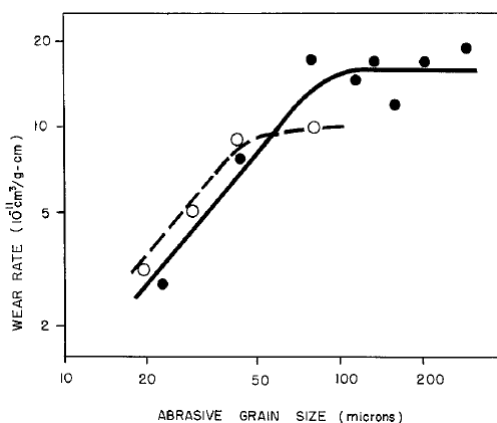


Fig. 2.15. Wear rate of metals as a function of abrasive grain size. ● Bronze on bronze; ○ steel on steel (Rabinowicz et al., 1961)

#### 2.4. Polymers and polymer abrasion

Abhi (2010) In this report explaining polymers, it shows that materials which are able to be molded by heating them to a higher temperature than their melting point, in order to make a specific shape, are known as thermoplastic polymers. To describe thermoplastic polymers in engineer's language, polymers are molecules which contain atoms with a strong bond between themselves, but have weak bonds to nearby molecules. Polymers are prepared by joining a large number of small molecules called monomers. In other words, monomers are like bricks in the big building "polymers".

Polymers have very good properties (chemical and physical) due to their large molecular size. When a chain of polymers has a sufficient length, these properties are created.

Chanda and Roy (2006) in their book about plastics technology, they show a figure which illustrates some polymer properties like impact strength, tensile strength and melt viscosity against molecular weight. From this figure (Fig. 2.16), they noticed that by increasing the chain length (or molecular weight), the strength properties would increase to a certain point then level off, while melt viscosity will keep increasing in a rapid way. One of the most important results that occurred, was that very high molecular weight polymers have high melt viscosities, which leads to face

fabricating and processing difficulties. From this discovery, a range called a “commercial range” was created, where polymers show a compromise between process-ability and maximum properties.

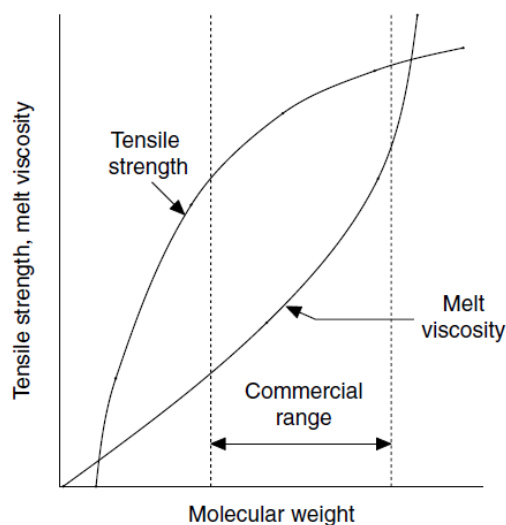


Fig. 2.16. Polymer properties (Tensile strength, and melt viscosity) versus polymer size (Chanda and Roy, 2006)

Many properties of polymeric materials depend on the microscopic arrangement of their molecules. Polymers can have an amorphous (disordered) or semi-crystalline (partially crystalline, partially ordered) structure (Fig. 2.17).



Fig. 2.17. (a) Amorphous polymer and (b) simplified model of a Semi-crystalline polymer (Koutsos, 2009)

Fig. 2.18. shows the polymeric pyramid, which consists of three main sections. The first one is mass product plastics, which is positioned at the base of the pyramid, the second is general engineering plastics, which is in the middle of the pyramid, and within that the polyamide (PA) family is considered a 'Strategic polymer'. The third section is HPM or high-performance materials, and these polymers are expensive and used in specific cases. Fig. 2.18 divides the polymers in to semi-crystalline (right side) and amorphous structures (left side) (Kalacska, 2017).



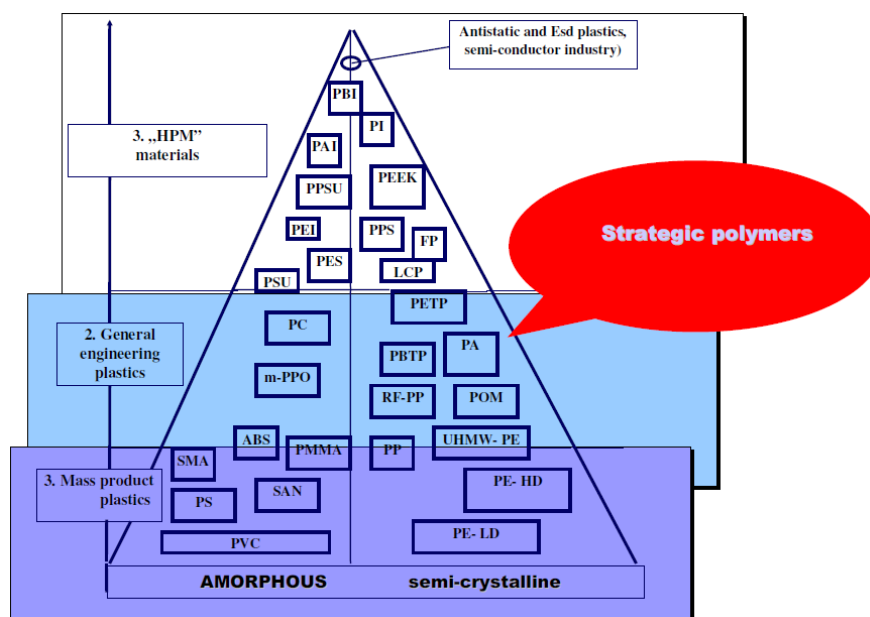


Fig. 2.18. Polymeric pyramid (Kalacska, 2017)

It is generally accepted that engineering polymers can be advantageously used as a moving machine element due to their favourable tribo-mechanical properties, corrosion resistance and high design flexibility (Myshkin and Kovalev, 2018).

The tribological literature on polymers and their composites is growing tremendously, in line with the proliferation of industrial applications and the emergence of newer materials. According to a review based on the ‘Web of Science’ database (Quintelier, 2007), the number of publications in the field of polymer tribology reached thousands in the second half of the 2000s, accounting for about 25% of the total literature on polymers and composites.

The main mechanisms of polymer wear are adhesion, abrasion and fatigue (Bahadur, 2000). Abrasion is caused by hard asperities on the mating surface and hard particles moving on the polymer surfaces. This phenomenon of the wear occurs when roughness is a dominant factor during the friction processes.

Earlier research on polymer abrasive processes (Myshkin et al., 2005) and describes that the abrasive wear often occurs on the surfaces as scratches, holes and pits and other deformed marks (Sinha and Briscoe, 2009). The debris generated by wear is often in the form of fine-cut chips, rather than that generated during machining, albeit in a much finer size (Myshkin et al., 2005). Most models related to abrasive wear have geometric asperity descriptions, so the degree of wear depends on the shape and apex angles of the grinding points moving on the surface. There are two different ways for deformation to occur when an abrasive particle acts on the plastic (Myshkin et al., 2005). The first mode is plastic grooving, often referred to as ploughing. It occurs when the moving particles or asperities are pushed onto the mating surface, and the material is continuously displaced laterally to form grooves and ridges. No material loss on the surface is detected. The second mode is called cutting because it is similar to micro-machining and all material displaced by the particle is removed as a chip. There is another approach to describing abrasive wear (Sinha and Briscoe, 2009).

Experiments have shown that the degree of abrasive wear is proportional to  $1/(\sigma \epsilon)$ , where  $\sigma$  is the tensile stress and  $\epsilon$  is the corresponding elongation. The connection was found by Lancaster and Ratner in the 60s and are often referred to them (Lancaster, 1969).

In engineering practice, the most common technical plastic family is the various polyamide 6 (PA6) and polyamide 66 (PA66) variants, as well as the ultra-high molecular weight polyethylene high density 1000 grade (UHMW-PE HD1000) polymer. There is a lot of information about these materials today (Bahadur, 2000), a huge amount of research has been done on their abrasion resistance. Relationships between some material properties and specific wear have been found, as introduced later, but a comprehensive evaluation between combinations of properties and a large number of variables is not in the literature yet.

Rajesh et al. (2002) examined two types of PAs. Abrasive wear studies were carried out with a single pass condition, by abrading a polymer pin against a waterproof silicon carbide (SiC) abrasive paper having different loads. They found that CH<sub>2</sub>/CONH ratio had a significant influence on some mechanical properties e.g. tensile strength, elongation to break, fracture toughness, fracture energy and the abrasive wear performance. It was observed that CH<sub>2</sub>/CONH ratio and various mechanical properties did not show linear relation in most of the cases, however the specific wear rate in the function of some mechanical properties (e.g. tensile strength, elongation) showed good correlation.

The same research team presented (Rajesh et al., 2001) results about the abrasive wear behaviour of numerous PA6 based composites. They applied short glass fibre, polytetrafluoroethylene (PTFE) and metal powders e.g. copper and bronze as reinforcing and filling materials. The samples were produced in lab scale and characterised for their properties such as tensile strength, tensile elongation, flexural strength, hardness and impact strength. In the test system, the wear in a function of product of hardness, elongation to break ( $\epsilon$ ) and ultimate tensile strength ( $S$ ) showed better correlation than the correlation Ratner-Lancaster had found.

Patnaik et al. (Patnaik et al., 2010) studied the erosion behaviour of solid particles on the fibre and particulate filled polymer composites. This review focused on the problems related to the processes of polymer matrix composites with several aspects and used the Taguchi method to optimize the process parameters and analyse that wear behaviour.

Harsha (2011) extended the specified PA6-based composite testing to the HPM (high performance materials). Three-body abrasion tests have been carried out on more unreinforced thermoplastic HPM polymers by means of rubber wheel, abrasion test equipment. The applied abrasive particle was dry silica sand, used as loose abrasive in the size range between 150 and 250  $\mu\text{m}$ . They applied constant sliding velocity ( $v = 2.4 \text{ m/s}$ ) of a rubber wheel at different loads (5–20 N). The abrasive wear rates were influenced by the load and type of polymeric materials. On the worn surfaces it was found that semi-crystalline polymers reflected ductile failure mode whereas amorphous polymers resulted in brittle failure. An attempt was also made to correlate the abrasive wear rates with mechanical properties.

Concerning UHMW-PE HD1000 grade polymer as a widely used, abrasion resistant polymer – unfortunately due to low mechanical loadbearing capacity, the engineering application is limited – the abrasive performance of many PE family members were already investigated. (Tervoort et al., 2002) examined the abrasive wear resistance of many PE grades, including UHMW-PE as

well. They found that an effective number of physical cross-links per macromolecular chain influences the abrasive wear resistance.

Lee et al. (2002) introduced a simple model of composite materials abrasive wear. This model is based on the mechanics and mechanisms associated with sliding wear in soft matrix composites, which contain solid reinforcement particles. The model supposes that any removed part of the reinforcement as wear debris, participate to the wear resistance of the matrix material.

Yapici et al. (2014) studied safety frames to provide protection for tractor drivers in the event of the tractor overturning. In the industry, safety criteria are considered, so the tractor frames need high strength, high fatigue strength, high rigidity, high wear resistance and low weight. To consider all of these specifications, new generation materials are needed, and polymer matrix composite materials are the most suitable choice. Thermoset epoxy was selected as matrix material due to its properties and glass fibers as a reinforcement material.

Andó et al. (2008) selected cast polyamide 6 material for semi-finished structural materials because it has excellent mechanical and chemical properties and is easy for composite production. They selected magnesium catalytic cast polyamide 6 natural polymer matrix as basic grade composites to accommodate the need of the agricultural sector. Indeed a new composite version was developed to improve tribology grade abrasion resistance, also an anti-static composite version and an improved fire-resistant version.

Kalácska (2007) studied improving the tribology properties by adding several materials like graphite, silicon dioxide, polytetrafluoroethylene, polyethylene, lead, oils, calcium silicate, waxes and silicone.

Kumar and Panneerselvam (2016) used PA6 and Glass Fiber Reinforced (GFR) PA6 composites specimens and studied the mechanical and abrasive wear behaviour. The specimens were prepared by injection moulding. Four proportions of glass fiber contents were used (0, 10, 20 and 30 wt. %). They performed the test on a pin-on-disc configuration with 320 grit size abrasive paper, at 23 °C and RH 67±10 %, 50m sliding distance at constant sliding velocity (0.5 m/s), with several loads (5, 10, 15 and 20 N). They found that the specific wear rate decreases with increasing sliding distance. That happened because the polymer formed a transfer layer which filled the space between the abrasive particles, causing a reduced depth of penetration.

To study the polymer composite materials properties (Kumar and Panneerselvam, 2016) used Nylon 6 and Glass Fiber Reinforced (GFR) Nylon 6 composites specimens. They studied mechanical and abrasive wear behavior. The reinforced specimens were prepared by injection molding. To study the effect of reinforcing materials they used four proportions of glass fiber contents as (0, 10, 20 and 30wt. %), by using a pin-on-disc configuration with 320 grit size abrasive paper, 23 C temperature under humid atmospheric conditions (67 ±10 %), 50m as the sliding distance at constant sliding velocity (0.5 m/s), by applying several loads (5, 10, 15 and 20 N).

Kalácska et al. (2008) studied what affects soils and sands can have on polymers by studying the abrasive wear of polymer/steel gear pairs in different soil types. According to these tests, it has been found that the wear resistance can be strongly influenced by physical types of soils, this is a very important point in designing and maintaining agricultural machines. As a result of these tests, the sand (H) and loam (A) caused very high wear values (10 – 12%) with a certain polymer, but

regarding the average behavior of loamy sand (HV) and small pebble sand resulted a lesser high wear.

The abrasive role of soil particles established a new maintenance strategy due to the specific wear-resistance ranking of structural materials in the function of dominant soil types.

Even though Polymers are soft compared to metals, a higher degree of resistance to abrasive wear on the same hardness of metals can be recognized. That's what was observed by (Bartenev and Lavrentev, 1981) by plotting wear resistance against hardness for polymers like L54, L68, nylon 6, low-pressure polyethylene, high-pressure polyethylene and polyfluoroethylene, and metals like silver, zinc, cadmium and lead, on the same graph. This is illustrated in Fig. 2.19.

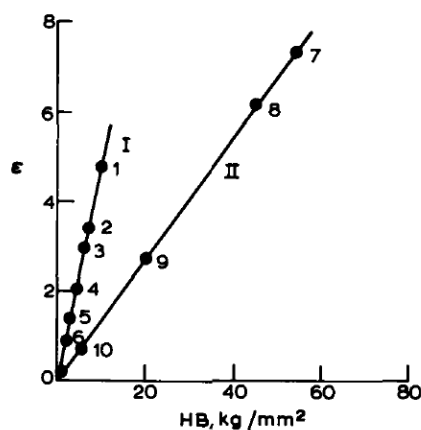


Fig. 2.19. Dependence on relative wear resistance upon hardness (HB) for (I) plastics and (II) metals: (1) L54; (2) L68; (3) nylon 6; (4) low-pressure polyethylene; (5) high-pressure polyethylene; (6) polyfluoroethylene; (7) Ag; (8) Zn; (9) Cd; (10) Pb. (Bartenev and Lavrentev, 1981)

it was noticed that the wear resistance of polymers could be improved by mixing different polymers, and gave an example of this situation; by adding natural rubber into cross-linked phenol-formaldehyde at the first step, will reduce wear and increase wear resistance (Bartenev and Lavrentev, 1981).

## 2.5. Bio-composite abrasion

Nowadays, in addition to the normal use of engineering plastics, more and more attention is being paid to bio-polymers. The research of the wear resistance of bio-polymers and their composites, and the exploration of the peculiarities of the wear processes appear independently in more and more research programs. From a practical point of view, however, it would be extremely important to compare bio-polymers with already known engineering plastics in a typical test systems.

Gupta et al. (2015) also justified the importance of the developments of bio-composites, focusing on jute fibre reinforced bio-composites.

La Mantia and Morreale (2011) showed that using biodegradable composites (where reinforcement and matrix are made up of biodegradable materials) can significantly reduce the environmental impact.

Fig. 2.20 shows the life cycle of bio-composites materials.

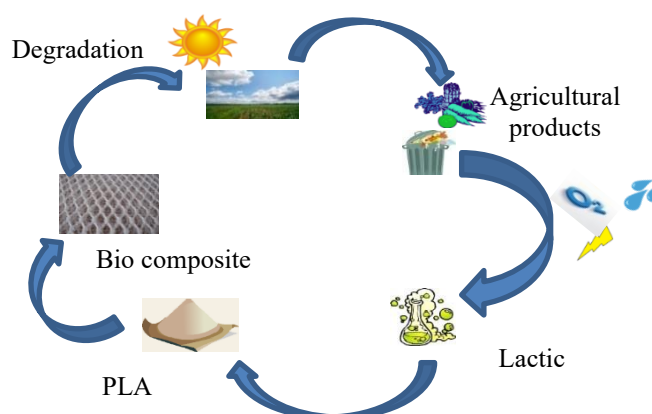


Fig. 2.20. The life cycle of bio-composites materials

Thermoplastic bio-composites are experiencing a continuing demand for various industrial applications (Sawpan et al., 2011). This is due to several specific advantageous characteristics that can be combined in these materials (Thakur et al., 2014).

Thermoplastics, reduced processing times, highly increased storage times, and have favorable recycling capabilities. (Kim and Park, 2017), by using thermoplastics, the components can be separated after use, making the process easier, cleaner and faster (Svensson et al., 1998).

Environmentally friendly, degradable biomaterials, used to create true bio-composites, possess the ability to significantly improve the environmental impact of commonly used composite materials (La Mantia and Morreale, 2011). This includes both natural fibers and matrix materials from renewable resources, being used for the reinforcement component of a composite.

The use of thermoplastic matrices is better than using thermo-sets because thermoplastics has facilitated recycling, by being able to be molten and then reshaped numerous times (Biron, 2013). (Khondker et al., 2006) demonstrate that thermoplastic materials like PP (polypropylene), PE (polyethylene) and PVC (polyvinyl chloride) dominate as matrices for natural fibers.

Singha and Thakur (2008) and others reported in their research that interest in using natural fibers had been increased because of the environmental questions and awareness, and that this interest led to the consideration of natural fibers as a good replacement for artificial fibers in various fields.

Wahit et al. (2012) reported that natural fibers had been extracted from natural substances, a long time before synthesizing the first polymers, and natural fibers were used then in textile applications. In previous decades, natural fibers have been used to enhance materials.

A figure was given to illustrate how compression molding process works as Fig. 2.21 (Park and Lee, 2012).

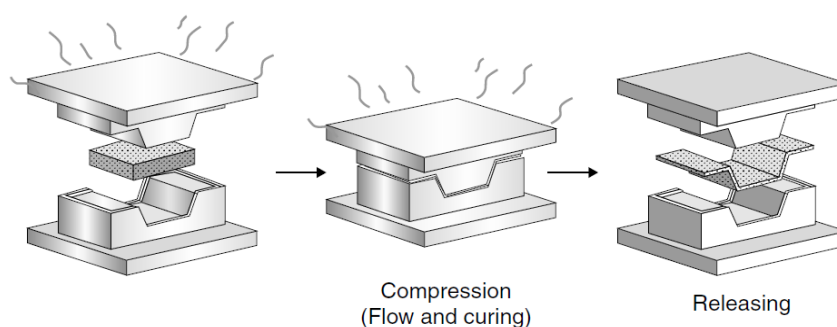


Fig. 2.21. Compression molding process

1. Preparing the materials and placing them in the heated mold.
2. Closing the mold, in this step one of the two mold's pieces will move to the other one and compresses the composite materials, during this step the pressure will be built up slowly, and air will be pressed out of the structure.
3. With maintained pressure and temperature application, consolidation takes place and the liquefied matrix spreads and impregnates the fibers. The required time for this step depends on the material used, the thickness of the lay-up and applied temperature and pressure.
4. The structure is removed and left to cool down outside of the mold.

Summerscales et al. (2010), in their study about bast fibers, showed that cellulose has a potential Young's modulus value which reaches 140 GPa and that this value is near to the Young's modulus of aramid fibers (synthetic fibers).

Mukherjee and Kao (2011) showed that inter-facial bonding between the fibers and matrix can be affected by the type of fibers used, and as a result affect mechanical performance.

Gupta et al. (2015), in their study gave a table that shows the mechanical properties of thermoplastic and thermosetting polymers subjected to the production of natural fibre reinforced polymers (Table 2.3).

Table 2.3. The mechanical properties of thermoplastic and thermosetting polymers subjected to the production of natural fibre reinforced polymers

Polymers	Density (g/cm <sup>3</sup> )	Tensile Strength (MPa)	Tensile Modulus (GPa)	Flexural Strength (MPa)	Flexural Modulus (GPa)	Impact Strength
Epoxies	-	55-130	2.7-4.1	110-150	3-4	-
Phenolic	-	50-60	4-7	80-135	2-4	-
Polyesters	-	34-105	2.1-3.5	70-110	2-4	-
Vinylesters	-	73-81	3-3.5	130-140	3	-
Poly lactide	1.24	56.3	3.6	-	-	-
Polyester	1.2	61	4	-	-	-
Polyvinyl chloride (PVC)	1.35	48	3.300	-	-	0.32 J/cm
Polystyrene	-	46	2.9	-	-	0.17 J/cm
Polypropylene (PP)	0.899 - 0.920	26 - 41.4	0.95 -1.776	55.2	0.83-1.73	21.4 -267 J/m
Low density polyethylene(LDPE)	0.910 - 0.925	4-78.6	0.055 -0.38	-	-	>854 J/m
High density polyethylene (HDPE)	0.941-1	14.5- 38	0.413- 1.490	-	0.41-1.07	26.7 J/m

Mahapatra and Mohanty (2007) realized the important effect of deformation, strain, on the mechanical applicability of jute fibre reinforced composites and examined the failure mechanism of the materials. They emphasized that matrix material must be ductile and not chemically reacting with natural fibers.

Sawpan et al. (2011) highlighted that the (PLA) represents the most common example of a polymer matrix from renewable resources. It has an acceptable mechanical behaviour for low load applications, but it will degrade to carbon dioxide, water and methane in the environment after several months to two years, unlike petroleum-based polymers, which need hundreds of years to

degrade. It is considered as one of the most important bio-polymers compared to the petroleum-based polymers as it was presented by (Thakur et al., 2014) too.

There are several different fiber materials that can be used as the reinforcement component in bio-composites (Summerscales et al., 2010) as it shows, using flax, hemp, jute and kenaf for the composites. The critical disadvantage in using natural fibers is their hydrophilic nature, which leads to a high moisture absorption (La Mantia and Morreale, 2011).

To examine the mechanical properties of the composites materials affected by the correlation between the matrix and the supporting material, (Girisha et al., 2014) used epoxy and polyester as a matrix of the composite material, while Jute and Hemp fibers where the reinforcing materials, these fibers were oriented into three different directions ( $30^\circ$ ,  $45^\circ$ ,  $90^\circ$ ) by using simple hand lay-up technique. Mechanical properties like impact strength, tensile strength and flexural strength were studied.

Alagirusamy et al. (2006) showed fast and improved impregnation of the reinforcing fibers. This occurs by uniformly distributing the matrix and reinforcement components in the hybrid yarns, which lead to a significant reduction in the flow path of the melting thermoplastic, after heat application.

Some mechanical (but not abrasive tribological) experiments were done using bio-composite materials like (Khondker et al., 2006) when they prepared three samples of bio-composite materials. They processed at  $170^\circ\text{C}$ , jute was used as reinforcement material and PLA as matrix material, then the tensile and 3 point bending properties were evaluated (Fig 2.23). The three samples had a variation in fiber contents (fiber volume fraction ( $V_f$ )) as  $V_{f1}$  (38%),  $V_{f2}$  (27.5%) and  $V_{f3}$  (22.5%) (Fig 2.22).

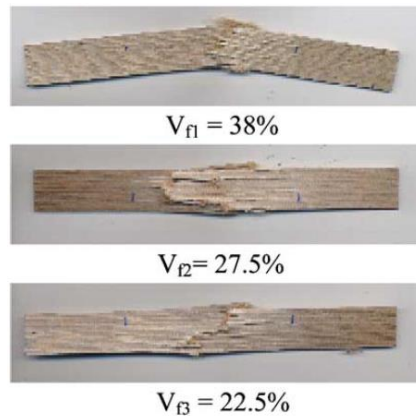


Fig. 2.22. Tensile tested jute/PLA composite specimens processed at  $170^\circ\text{C}$

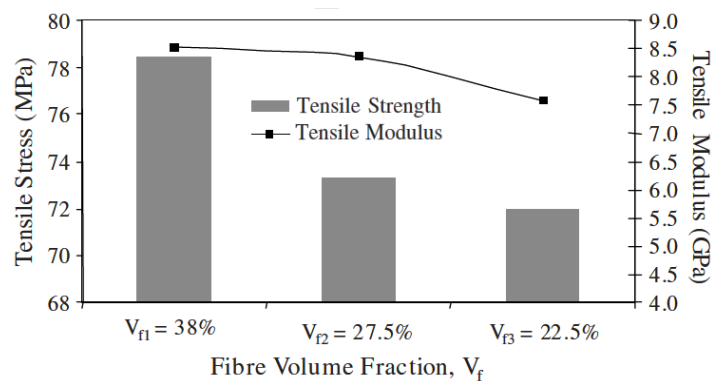


Fig. 2.23. Tensile properties of jute/PLA composites processed at  $170^\circ\text{C}$

Another experiment had also been done by (Khondker et al., 2006) in order to study the effect of molding temperatures and pressures. Examining the temperature's effect by comparing the bending properties of samples at 170, 175 °C and the matrix content  $V_m$  were 62% and 77.5%. For examining the effect of pressure, they used two values 2.3 and 2.7 MPa with a stable temperature, which equals to 175. The results are displayed in Fig. 2.24.

These results support what was described earlier, that in this optimized processing condition, matrix resins were adequately fused and the presence of voids between the fibers and the matrices was at a minimum.

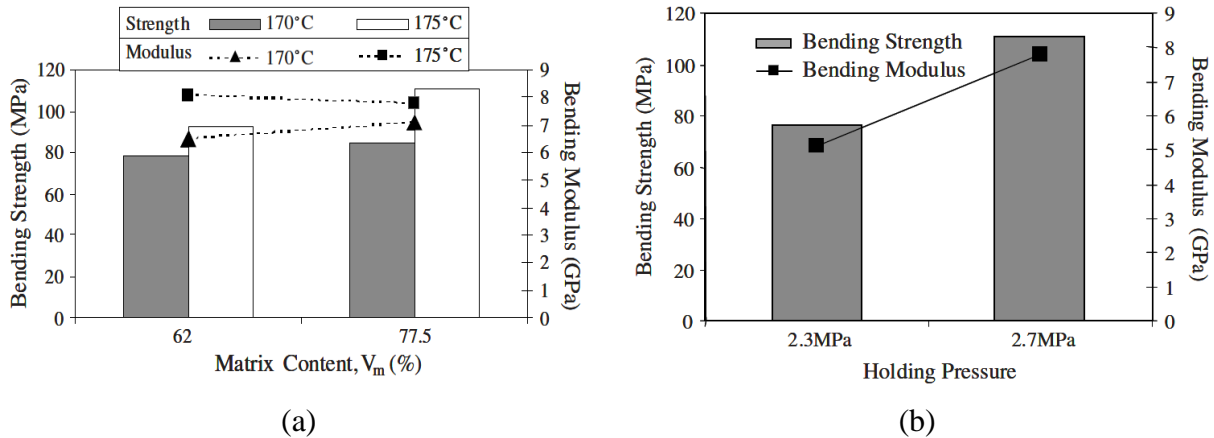


Fig. 2.24. (a) Effect of molding temperature on bending properties of jute/PLA composites - (b) Effect of molding pressure on bending properties of jute/PLA composites molded at 175 °C

## 2.6. Lubrication and effect on abrasion

Lubricants represent a solution to reduce the coefficients of friction and, hence, reduce the wear.

In the last ten years, an advanced approach took place in the materials science and technologies to create a better friction coefficient. The final goal of tribology and surface physics is to have almost frictionless surfaces (Ciraci et al., 2007).

In modern mechanics, it is essential to use lubricant in every mechanism with moving parts. The lubrication function differs based on the relative motion of the contact parts (Encyclios, 2020b). During sliding between dry bodies, both the mechanical action of surface roughness and the intermolecular electrical actions are the main cause of friction.

Lubricant can be used in several ways based on its nature. It can be used to supply the contact with additives, eliminate heat and wear debris, or even transmit power (Harris and Kotzalas, 2006).

Lubricants can be found in several forms. They can be liquid like water and oil, they can be solid like graphite and graphene, they can be gas like air, and they can be semisolid like grease. To improve the performance of the lubricants, they can contain up to 30% in additives (Tribonet, 2017).

Based on the perspective of lubrication theory, several main properties can determine the lubricants' performance. The viscosity and density of a lubricant are considered the most important properties. These two properties play the main role in determining the thickness of the lubricant film (Wen and Huang, 2017).



SKF has mentioned that, “bearings can have an infinite life when particles larger than the lubricant film are removed.” which means that bearing wear can be prevented by removing abrasive particles (Knight, 2016). The investigation in to bearing failure showed that 60% of the damage is related to lubrication. Fig. 2.25 shows a macroscopic section of contact surfaces with lubricant film against abrasion.

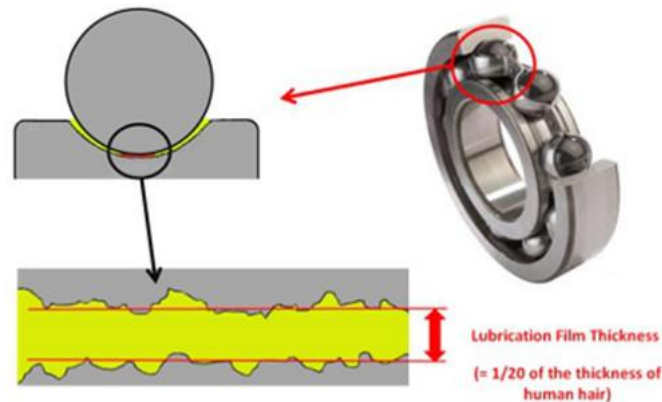


Fig. 2.25. Macroscopic section of contact surfaces with lubricant film against abrasion (Knight, 2016)

Normal lubricants disintegrate above temperatures of 300 °C and the health and environmental hazards they cause, have required scientists to look for alternatives. Self-lubrication materials are one answer and represent a new generation of lubricants. They utilize solid-lubricating compounds to minimize friction and wear over a wide range of temperatures (Kumar and Antonov, 2020).

During the machining process, cutting fluids are considered as an aid to the process as a cooling agent, via lubrication. During severe contact conditions, where the temperature is very high, the tribology of the tool-chip and tool-workpiece interfaces are considered as a key aspect in machining (Singh and Bajpai, 2014).

Busch et al. (2016) presented an investigation of four strategies to supply the cooling lubricants (Fig. 2.26); the first one (a) is when the lubricant is directed on to the rake face, while the second one (b) is when the coolant has been supplied between the machined surface and the clearance face. The third way (c) is a combination of the first and the second ways. The fourth way (d) is a high-pressure jet which passes liquid through a hole in the rake face.

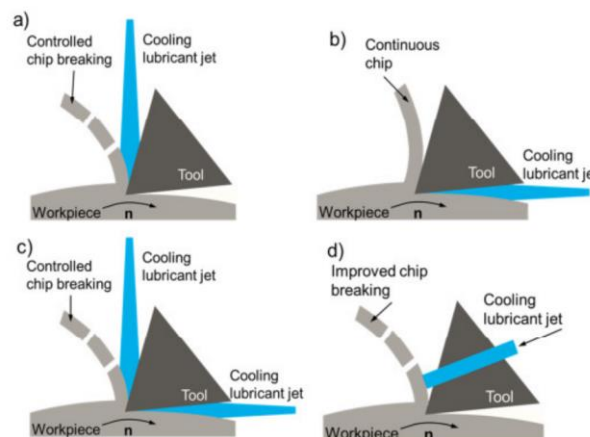


Fig. 2.26. Possible directions of cooling lubricant supply into the cutting zone (Busch et al., 2016)

Yan et al. (2016) suggested that the effect of cutting fluid on machined surface quality and performance will become a very important direction of research. Several factors have to be taken under consideration, like the physical and chemical properties of the cutting fluid, the long-term effects of the process, and an evaluation method for the effective use of cutting fluid.

Su (2016) developed a three-dimensional model of cryogenic minimum quantity lubrication machining, by using a finite element method, in order to check the role of the cooling/lubrication effect of cryogenic minimum quantity lubrication in the machining of AISI H13 steel. The cooling effect was provided by refrigerated compressed air at temperatures of  $-10^{\circ}\text{C}$ ,  $-30^{\circ}\text{C}$ ,  $-50^{\circ}\text{C}$ ,  $-100^{\circ}\text{C}$  and  $-140^{\circ}\text{C}$ . The results showed that both the cryogenic and lubrication cooling effects led to reduced cutting force and tool temperature. Although there was a reduction in cutting force and tool temperature, they didn't decrease continuously, as the refrigerated compressed air temperature decreased after some time (Fig. 2.27).

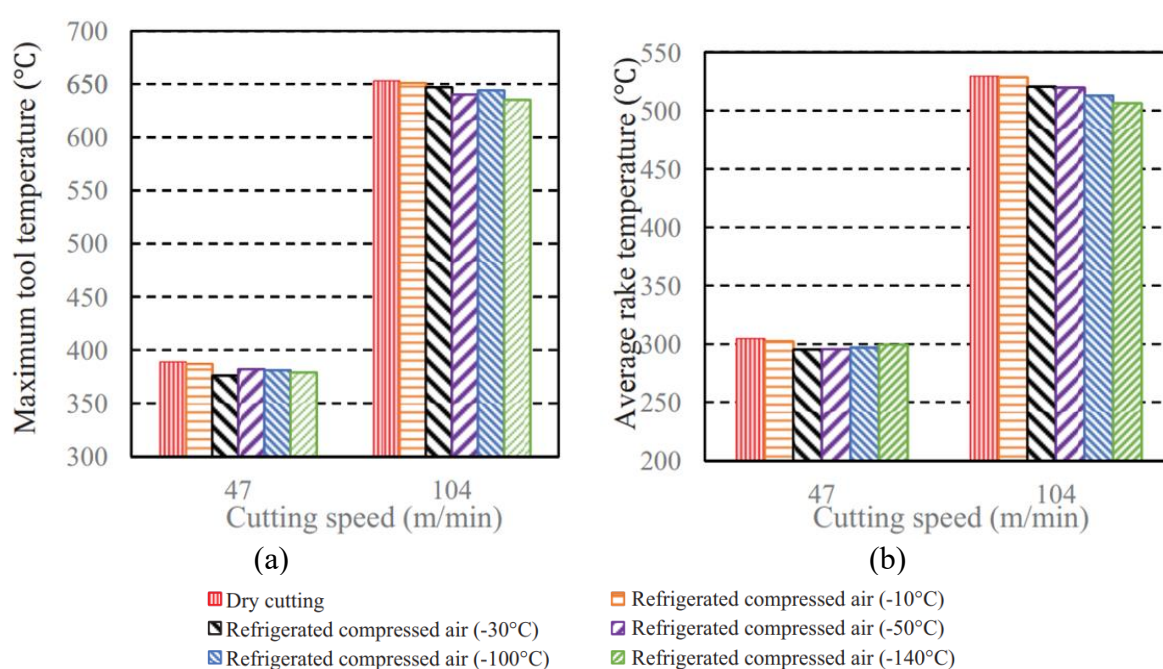


Fig. 2.27. Comparison of tool temperature for dry cutting and refrigerated compressed air, with different temperatures obtained from the simulation: (a) maximum tool temperature, (b) average rake temperature (Su, 2016)

Machines which are working in hostile environments are more likely to be contaminated with dust or moisture. In these conditions, any performed operation with the machine could lead to external particles contaminating the lubrication system. For example, changing the lubricant or checking its levels, can let abrasive particles or water to mix with the lubricant, which will negatively affect the potency of the lubricant and the machine operation conditions (Miro, 2018).

By using a high frequency reciprocating rig (HFRR), (Sari et al., 2010) has studied the effect of different contaminant concentrations on the friction and surface wear of machine elements under fully submerged oil conditions. As a result, the proper operation of the lubricant has been disturbed by the presence of the solid particles, and led to noticeable fluctuations in the film thickness, and a higher coefficient of friction.

A Tribometer has been used to study the wear and friction of lubricated sliding (continuous and reciprocate) for AISI 52100 and counter-faces of AISI 8640 steel. The presence of additives and

contamination in the lubricant was investigated. As a result, a wear increase was detected due to the contamination of the lubricant. As for the abrasive action at the contact area, particle "anchoring" at the asperity valleys was suggested (Maru and Tanaka, 2006).

To study the effect of contamination particles in lubricants during surface contact, (Sari et al., 2007) studied the degradation of lubricated spur gears in an extremely dusty environment (Fig. 2.28). As a result, using a lubricant contaminated by very fine sand particles, led to significant wear in the first few operating cycles. The friction was also increased with the presence of the contamination particles, and this led to an increase in temperature, and the roughness of the lubricant.

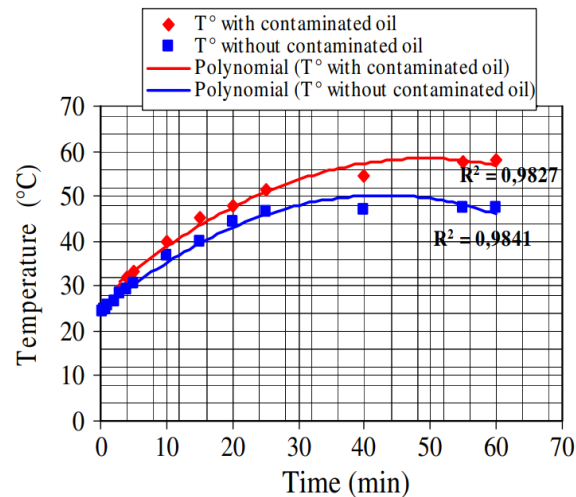


Fig. 2.28. Temperature evolution during the surface contact with and without contaminated oil (Sari et al., 2007)

In addition to the use of lubricants, coolants, another way to reduce friction and wear is when developing and using self-lubricants. These are usually composite materials where the lubricating particles incorporated in the base matrix are able to reduce the surface energy and adhesion of the composite. self-lubricants can be used advantageously primarily on clean contact surfaces, their effect in abrasion systems is not clear.

Prajapati et al. (2018) divided the plastics and fillers for self-lubricating composites for several groups:

- Thermoplastics: Polyethylene (high MW and UHMW), Polyacetal (homo- and co-polymer), Nylons (types 6, 6.6, 11), Poly (phenylene sulfide), Poly (tetrafluoroethylene) and Poly (p-oxybenzoate)
- Thermosetting: Phenolics, Cresylics, Epoxies, Silicones and Polyimides.
- Reinforcements: Glass fibers, Asbestos fibers, Textiles (polyester, "Nomex," cotton) and Mica.
- Friction and wear reducing additives: Graphite, Molybdenum disulfide, Polytetrafluoroethylene (PTFE), Metal oxides and Silicon fluids.
- Thermal conductivity adjunctives: Bronze, Graphite, and Silver.

In the absence of external lubrication, the self-lubricity of polymers and polymer-based materials properties, ensure the friction unit operation. These Polymer-based self-lubricating materials

(SLM) include polymers with high intrinsic lubricity, like polytetrafluoroethylene (PTFE) and linear polyethylenes (PE) (Aderikha and Krasnov, 2013).

Zhu et al. (2020) studied the dry friction and wear behavior of several polyetheretherketone (PEEK) composites (30 wt % carbon fiber reinforced PEEK, 30 wt % glass fiber reinforced PEEK, each 10 wt % of PTFE, graphite and carbon fiber modified PEEK and neat PEEK). When PEEK composite was reinforced with PTFE, both the graphite and carbon fiber showed superior properties (lower friction, lower temperature increase, self-lubrication, reduced energy consumption and enhanced bearing life) compared to the other composites.

### 2.7. Conclusion of the literature review

Due to the fact previously reviewed research showed that polymers and their composites had been tested with several methods, they have been selected as a replacement for several applications.

The developments in polymer and bio-composite materials and their use, according to the reviewed literature, are summarized in the following points:

All artificial and natural mechanical systems contain relative motion between solid components. The friction and friction force can be defined as good or bad. The frictional characteristics are usually measured by a friction test along with an abrasion resistance test. The coefficient of friction is used to calculate the results of these tests.

During friction between a polymer pad and a metal surface, there are two mechanisms which contribute to the friction force. Shearing of the junctions and the dissipation of energy.

The main cause of wastage and loss of material in mechanical performance is wear. Reducing the wear can make considerable savings as a result. Wear and energy dissipation occur because of friction. Due to loss of material, the dimensions of the component will decrease and lead to high vibration, high noise and system malfunction, which reduces efficiency.

Several mechanisms can cause wear, the following four being especially important (Surface fatigue, Abrasion, Adhesion and Tribochemical reaction)

Abrasive wear happens when a soft surface is passed over by hard particles or a hard surface, causing material loss. Abrasion shares some common features with erosion and cavitation but there are also some fundamental differences between these wear forms.

Several scanning electron microscopes were built which allowed for ground breaking observations of a wear mechanisms. The process was also recorded on videotape, and by using a data-logging system, the variations on normal load and frictional force were measured.

Polymers have very good properties (chemical and physical) due to their large molecular size. When a chain of polymers has a sufficient length, these properties will appear. Engineering polymers can be advantageously used as a moving machine element due to their favourable tribo-mechanical properties, corrosion resistance and high design flexibility.

The polymer abrasive process describes the way abrasive wear often occurs on surfaces as scratches, holes and pits and other deformed marks. The debris generated by wear is often in the form of fine-cut chips rather than those generated during machining

In engineering practice, the most common technical plastics are the various polyamide 6 (PA6) and polyamide 66 (PA66) variants, as well as the ultra-high molecular weight polyethylene high

density 1000 grade (UHMW-PE HD1000) polymer. There is a lot of information about these materials today, a huge number of research studies have been done on their abrasion resistance.

Several sciences studied the improvement of tribology properties by adding several materials like graphite, silicon dioxide, polytetrafluoroethylene, polyethylene, lead, oils, calcium silicate, waxes and silicone.

Even though polymers are soft compared with metals, a higher degree of resistance to abrasive wear on the same hardness of metals can be recognized

More and more attention is being paid to bio-polymers. The research of the wear resistance of bio-polymers and their composites, and the exploration of the peculiarities of the wear processes appear independently in more and more research programs.

The interest in using natural fibers has been increased because of the environmental questions and awareness. This interest led to the consideration of natural fibers as a good substitute for artificial fibers in various fields.

There are several different options of fiber materials that can be used as the reinforcement component in bio-composites, like flax, hemp, jute and kenaf.

The mechanical properties of a composite's materials are affected by the correlation between the matrix and the supporting material. The bonding interface between the fibers and matrix can be affected by the type of fibers used, and as a result it affects the mechanical performance.

Lubricants represent a solution to have lower coefficients of friction and to reduce the wear in machining. Several properties can determine a lubricants' performance, the viscosity and density of a lubricant are considered as the most important properties.

In the absence of external lubrication, self-lubricity of polymers and polymer-based materials' properties ensure the friction unit operation. PTFE and PE are examples of polymer-based self-lubricating materials.

Some machines have to operate in a medium with a significant water content, they typically suffer from abrasive erosion, like rice harvesting machines.

The erosion behaviour of solid particles on the fibre and particulate filled polymer composites has been studied, focused on the problems related to the processes of polymer matrix composites with several aspects and used the Taguchi method to optimize the process parameters and analysis that wear behaviour.

In the literature, there is no comprehensive or global assessment of the abrasion sensitivity in those material families, taking into account the most important mechanical features and the dimensionless numbers that can be formed from them. Furthermore, there are ultimately no published results comparing engineering plastics and a bio-polymer over a wide range of operating conditions. Even a connection between wear and combined properties, valid for polyamides and UHMW-PE together, have not been published yet.

Dependant on all the articles, books and experiments that have been reviewed up to now, and by comparing the knowledge and results that have been shown above chronologically, then the table below is a practical conclusion for the scientific development of the tribological testing of engineered polymers and bio-composites (which related to our PhD topic) over time.

Table 2.4. The practical conclusion for the scientific development of the tribological testing

<b>Date</b> <b>Topic</b>	<b>1960</b>	<b>1970</b>	<b>1980</b>	<b>1990</b>	<b>2000</b>	<b>2010</b>	<b>Current decade</b>
Examination of Friction and wear on natural fibers (natural polymers)	X	X	X	X	X	X	X
Tribological testing of composite polymers		X	X	X	X	X	X
Microscopic scanning of tested composite materials			X	X	X	X	X
Abrasive testing of composite materials			X	X	X	X	X
The effect of the reinforced material on polymers properties			X	X	X	X	X
Manufacturing and testing the mechanical properties of Bio-composites					X	X	X
Tribological testing of Bio-composites							X
Abrasive sensitivity of engineering polymers and bio-composites							

And as a summary, laboratory abrasion tribological modelling has to be used to find the relationship between abrasive resistance and material properties for conventional and bio-polymeric materials to understand their behavior with different abrasion mechanisms.

### 3. MATERIALS AND METHODS

This chapter is an introduction to the materials and their preparations which I used in my research. I also show the engineering and scientific methods involved in experimental measurements, characteristics, methodology and descriptions of the test systems used to achieve the research goals.

#### 3.1. Materials and preparations

##### 3.1.1. Experimental materials

###### 1. Engineering polymers

Concerning the engineering practice, based on the literature and commercial data of semi-finished polyamide product grades, it is clear that the agricultural machinery prefers the PA6 and PA66 polymer families, as well the UHMW-PE HD1000 grade that are subjected to abrasive effects during operation.

There is no comprehensive or global assessment of the abrasion sensitivity in those material families, taking into account the most important mechanical features and the dimensionless numbers that can be formed from them. and the same thing for comparing engineering plastics and a selected bio-polymer over a wide range of operating conditions.

Five types of engineering polymers and composites were recommended for investigation, and they are extruded polyamide 6 (PA6E), cast polyamide 6 (PA6G), electrostatic dissipative cast polyamide 6 composite (PA6G-ESD), extruded polyamide 66 composite reinforced with 30% glass fiber (PA66GF30), ultrahigh molecular weight polyethylene, high density grade “1000” (UHMW-PE HD1000) and one kind of bio-composite materials (PLA reinforced by hemp fibers, PLA-HF).

The engineering polymers and composites are commercial grade semi-finished plastics, distributed and partly produced by Quattroplast Ltd, Budapest, Hungary. The actual test specimens were machined out from the semi-finished rods or plates, Table 3.1 shows the properties of the engineering polymers used.

###### 2. Bio composite material

The bio-composite PLA-HF was produced by Boras University, a fully biodegradable product. The materials used part form the two distinctive components of composites – the reinforcement and matrix (Fig. 3.1). The materials used are from renewable resources and are biodegradable, this allows them to produce bio-composites.

For the reinforcement component, cottonized hemp, staple fibers were used. The fibers have an average length of 22 mm, an average diameter of 25-45  $\mu\text{m}$ , and a density of 1.48  $\text{g}/\text{cm}^3$ .

Polylactic acid (PLA) staple fibers were used as the matrix. The Polylactic acid fibers were provided by the company Trevira GmbH (Hattersheim, Germany), with a fiber length of 38 mm and a linear density of 1.7 dtex, this PLA has a density of 1.24  $\text{g}/\text{cm}^3$  and a melting temperature ( $T_m$ ) of 160-170  $^{\circ}\text{C}$ .

Table 3.1. The properties of the selected engineering materials (Quattroplast, 2019)

Properties	PA6G	PA6E	PA66GF30	UHMW-PE HD1000	PA6G ESD
Density (g/cm <sup>3</sup> )	1.15	1.14	1.34	0.94	1.19
Water absorption in air, 24 h / 96 h, (23°C) (%)	0.2 / 0.4	0.3 / 0.6	0.1 / 0.2	<0.01	2.5
Dielectric constant	3.7	3.9		2.3	-
Volume resistivity ( $\Omega$ *cm)	1014	10 <sup>14</sup>	10 <sup>14</sup>	>10 <sup>14</sup>	10 <sup>5</sup> -10 <sup>8</sup>
Surface resistivity ( $\Omega$ )	1014	10 <sup>14</sup>	10 <sup>14</sup>	>10 <sup>14</sup>	10 <sup>6</sup> -10 <sup>9</sup>
Dielectric strength (kV/mm)	20	20		45	
Dielectric dissipation factor (50 Hz)	0.02	0.02		0.0001	
Comparative tracking index (CTI)	600	600		600	
Thermal conductivity (W/ (K.m))	0.38	0.37	0.39	0.41	
Melting temperature (°C)	216	220	260	135	
Glass transition temperature (°C)	40	45	48		
Specific heat (J/(g.K))	1.7	1.7	1.2	1,9	
Coefficient of linear thermal expansion (CLTE): 23 - 60°C (m/(m.K)x10 <sup>-5</sup> )	12	12	5	150	
Coefficient of linear thermal expansion (CLTE): 23 - 100°C (m/(m.K)x10 <sup>-5</sup> )	12	13	5	230	
Max. allowable service temperature in air, short term (°C)	170	160	170	130	
Max. allowable service temperature in air, long term (°C)	100	100	110	80	
Min. allowable service temperature in air, long term (°C)	- 40	- 40	- 20	- 250	
Heat deflection temperature (°C)	95	75	150	80	
Yield stress (MPa)	80	78	91	19	75
Modulus of elasticity (tensile test) (MPa)	3500	3300	5500	750	4000
Elongation at break (%)	130	130	13	>50	5
Flexural strength (MPa)	109	100	135	21	102
Impact strength, Charpy (kJ/m <sup>2</sup> )	Doesn't break	Doesn't break	87		
Tensile strength (MPa)	83	79	91	19	75
Compressive strength 1% $\sigma_c$ (MPa)	22	19	25	4.5	23
Notched impact strength, charpy (kJ/m <sup>2</sup> )	4	7		Doesn't break	3
Ball indentation hardness (MPa)	170	155	216		170
Shore D hardness	83	75	86	62	80
Derived Hardness H (MPa)	12	9.9	12.9	73	11.2





PLA

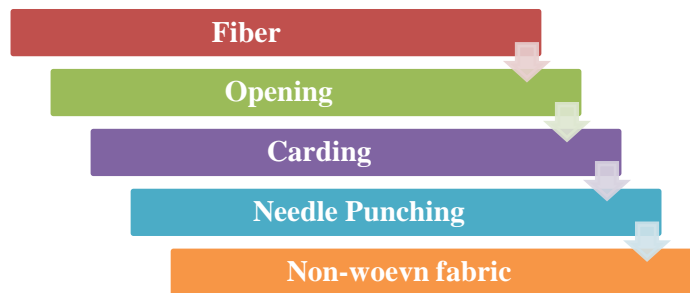


Cottonized hemp

Fig. 3.1. Fibers used in the fabrication of composite

#### Methods:

The hybrid non-woven composite, produced by needle punching, with 40 mass % hemp fibers and 60 mass % PLA with the following steps:



#### Opening:

Opening of the fibers was done with the LAROCHE opener. The fibers were placed in the opener and the attached Canvac EAN C140 vacuum was turned on to collect the opened fibers.

#### Carding:

The opened fibers then went to the carding process. For carding the Mesdan Lab 337A laboratory carding machine was used (Fig. 3.2). 80 grams of the opened fibers were placed on the belt of the carding machine. The carding was done twice to insure the homogeneity of obtained web.



Fig. 3.2. Carding machine (Boras University, Sweden)

Needle punching:

The bonding of webs is created by using a needle-punching technique (Fig. 3.3) where the fibers have been driven upward or downward by barbed needles. This needling action interlocks fibers and holds the structure together by friction forces, the weight of the non-woven fabric was 650 gr/m<sup>2</sup>.

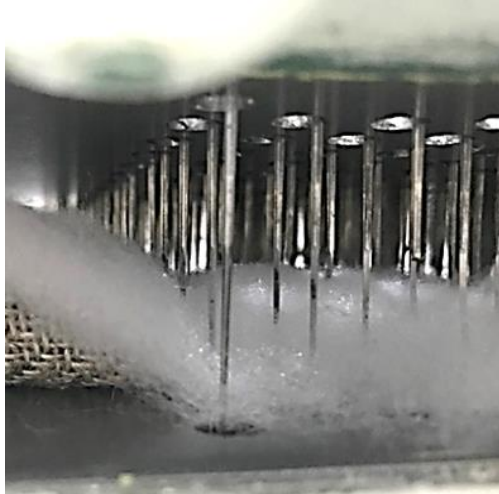


Fig. 3.3. Needle punching machine (Boras University, Sweden)

Fabrication of thermoplastic composites:

The composites were produced by compression molding. For each composite, 12 layers of hybrid (with 40 mass % hemp fibers and 60 mass % PLA) non-woven fabric (19×19 cm) in a 0/90-degree bidirectional lay-up were used. The fabric was put into an oven at 70 °C for 24 hours before processing.

The main parameters of the process of the fabrication of thermoplastic composite are:

- Pressures
- Temperature
- Processing time

The temperature should be high enough to decrease the viscosity of the molten thermoplastic, to ensure good impregnation of the PLA melted in the hemp. Simultaneously this temperature value should be lower than 190°C inside the specimen, as the hemp starts to degrade at this temperature.

The pressure needs to be sufficient to expel the air out of the specimen but should not be so high, as to push the fiber to the surface of the specimen, as this leads to stress concentration.

The processing time should be minimized but also have enough time to create a uniform temperature distribution in the specimen.

These parameters were optimized with the use of finite element calculation (Comsol Multi-physics software). The 3D geometry assembled, according to the composite lay-ups used in the production process (Fig. 3.4).

Table 3.2 shows the properties of fibers and PLA used.

Table 3.2. Properties of fibers and PLA used

Properties	PLA	Hemp
E (GPa)	2.91	14
Poisson's ratio	0.360	0.221
Density $\rho$ (g/cm <sup>3</sup> )	1.240	1.480
Heat capacity at constant pressure $C_p$ (J/(kg $\times$ $^{\circ}$ C))	2060	2000
Thermal conductivity $\lambda$ (W/(m $\times$ $^{\circ}$ C)) at 190 $^{\circ}$ C	0.195	0.04 (W/(m $\times$ K))
Coefficient of thermal expansion $\alpha$ (1/ $^{\circ}$ C)	$7.4\times 10^{-4}$	$10^{-6}$

The material's characteristics, which were used for calculation, are listed in Table 3.2.

For the optimization of pressure, Fig. 3.4 presents the final thickness (7 mm) for a part of the specimen under the optimized pressure.

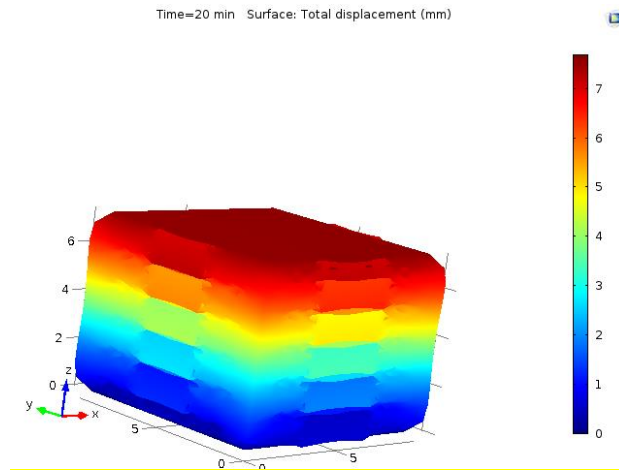


Fig. 3.4. Displacement of the composite with pressure (mm)

Finally, the simulation of the compression molding with the FEM, resulted with the processing parameters is illustrated in Fig. 3.5.

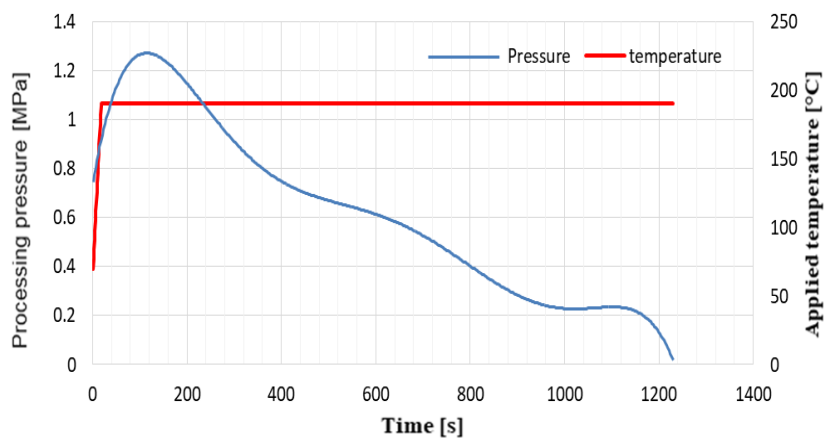


Fig. 3.5. Processing parameters

### 3. Materials and methods

A compression mould with a 20 tons manual bench press machine from Rondol Technology Ltd was used to produce the composites (Fig. 3.6). These composites were produced with the parameters from the finite element simulation (FEM).



Fig. 3.6. The manual bench press machine (Boras University, Sweden)

The results from the compression moulding were flat composite plates with smooth finished surfaces, and with dimensions of 361 cm<sup>2</sup> by a thickness of 6 mm, as shown in the Fig. 3.7.

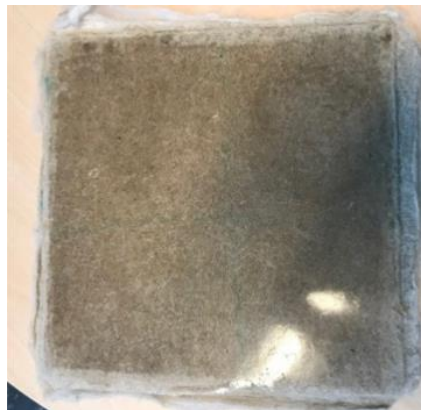


Fig. 3.7. Composite thermoplastic plate

The mechanical properties of this bio-composite material were tested (Fig. 3.8), and the properties are shown in Table 3.3.



Fig. 3.8. Measuring mechanical properties of the bio-composite material (MATE University, Hungary)

Table 3.3. The properties of the bio-composite material (PLA-HF)

Properties	PLA-HF
Composite density $\rho_c$ (g/cm <sup>3</sup> )	1.28
Fiber volume fraction $V_f$ (%)	34.62
Matrix volume fraction $V_m$ (%)	61.99
Porosity volume fraction $V_p$ (%)	3.39
Yield stress $\sigma_y$ (MPa)	58.2
Modulus of elasticity (tensile test) E (MPa)	32600
Elongation at break $\varepsilon_B$ (%)	0.6
Flexural strength $\sigma_F$ (MPa)	130.2
Tensile strength $\sigma_M$ (MPa)	58.2
Compressive strength 1% $\sigma_C$ (MPa)	0.737
Impact strength (KJ/m <sup>2</sup> )	24
Shore D hardness	82.3
Derived Hardness H (MPa)	11.8

Two test methods have been developed for a broad study about abrasion resistance of the selected engineering polymers and the bio-composite: an abrasive pin-on-plate and a slurry pot systems. Using abrasive pin-on-plate method micro- and macro cutting occur on the polymer surface due to the abrasive particles of the standardized commercial clothes, that are designed for surface cutting/polishing tool originally.

That phenomenon is reportedly dominant – as it is mentioned in the introduction – for tillage or cultivator elements (Kalácska et al., 2020) in the lower speed range ( $v = 0 - 10$  km/h).

The slurry pot model can perform abrasive erosion, which is common for the harvesters' parts, acting with wet, soil contaminated products (different plants e.g. potatoes, rice). Due to frequent abrasive erosion, surface fatigue and micro-cracks can be detected, as well as surface groove deformation, and wedge formation and cutting (Keresztes et al., 2008).

### 3.2. Test systems

#### 3.2.1. Abrasive pin-on-plate test system

The cylindrical polymer pin with a given normal load (N) slides (m/s) on the abrasive belt moving underneath. Meanwhile, the attached strain gauges measure the abrasion friction force (N), a sensor records the vertical displacement of the clamping head as wear (mm), and the thermocouple measures the temperature change (°C) in the polymer pin (Fig. 3.9).

The data acquisition system contains a Spider 8 A/D converter that passes the digitalized data to a computer system.

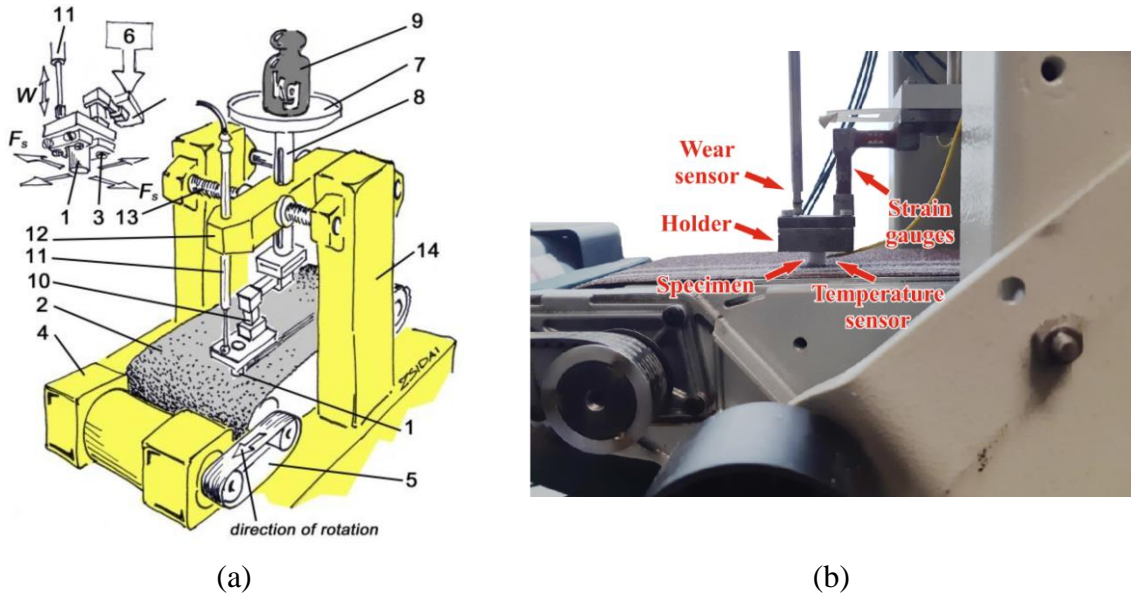


Fig. 3.9. Schematic figure (a) and a photo (b) about the abrasive pin-on-plate test system. (1) polymer specimen; (2) abrasive cloth; (3) nuts and clamp; (4) electrical motor; (5) twin roll driving system; (6) manual loading system; (7) plate; (8) vertical column; (9) dead loading weights; (10) strain gauges; (11) linear gauge (for vertical displacement as a result of wear); (12) console head unit; (13) spindle for cross movement (which was not used for these tests)

The sampling rate was 5 (1/s) while measuring. Testing time was set for 10 minutes as the base for the preliminary measurements, however, not for all the materials and  $p_v$  set (Table 3.4) could withstand this time limit due to severe wear ( $p_v$  - contact pressure x sliding speed ( $\text{MPa ms}^{-1}$ ), a feature of polymeric tribo systems). These cases are shown in later results.

For this test, the following variables were applied:

- Two types of wear interfaces: P60 and P150 standard abrasive clothes.
- Two sliding speeds: 0.031 m/s and 0.056 m/s (were controlled by the speed box)
- Three normal loads: 9.81 N, 29.43 N and 49.05 N

With these parameters there are 12 experimental cases. The test conditions for these cases are listed in Table 3.4. The extremes of the load and speed conditions on both types of abrasive clothing are highlighted. Testing time was 10 minutes with both speed settings (Table 3.4), except when the wear was extremely fast. When the material loss was between 6-8 mm, the measurements had to be stopped. The test runs were repeated three times for all 12 cases.

Table 3.4. Test cases for the abrasive pin-on-plate test device.

Test System No.		1	2	3	4	5	6	7	8	9	10	11	12
Test conditions	Load, $F_N$ (N)	9.81	29.43	49.05	9.81	29.43	49.05	9.81	29.43	49.05	9.81	29.43	49.05
	$v$ (m/s)	0.031	0.031	0.031	0.056	0.056	0.056	0.031	0.031	0.031	0.056	0.056	0.056
	Abrasive interface	P60	P60	P60	P60	P60	P60	P150	P150	P150	P150	P150	P150
	Calculated $p.v$ ( $\text{MPa} \cdot \text{m/s}$ )	0.0062	0.0185	0.0308	0.0109	0.0327	0.0544	0.0062	0.0185	0.0308	0.0109	0.0327	0.0544

In the on-line measured pin-on-plate test system: wear as vertical displacement of the specimen holder (mm), calculated specific wear (calculated wear volume under unit load and sliding distance) ( $\text{mm}^3/\text{N}\cdot\text{m}$ ), abrasive friction force (N) and friction temperature ( $^{\circ}\text{C}$ ) evolution, were registered for all 12 system conditions (Table 3.4) in the function of sliding distance,  $s$  (m).

For the evaluation of the 3D surface parameters of the tested polymers, before and after abrasion, a Taylor-Hobson white light microscopy was used, and the 3D parameters' values were evaluated by IBM SPSS 25 software. (Details later in 3.4.)

Specimens preparation:

For the abrasive pin-on-plate test system, polymer specimens were machined into cylindrical pins with an 8mm diameter and a 20 mm length.

The thermocouple sensor which measures the temperature change ( $^{\circ}\text{C}$ ) was placed inside the polymer pin at a distance of 8 mm from the contact zone (Fig. 3.10).

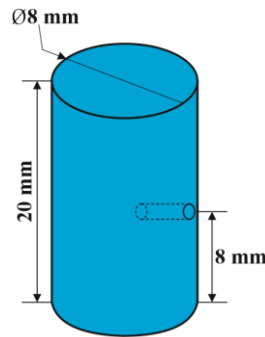


Fig. 3.10. Sample dimensions of abrasive pin-on-plate test system

For the PLA-HF, the sample has been placed in the sample holder where the sliding direction is at an angle of 30 degrees from the direction of the fibers, as shown in Fig. 3.11.

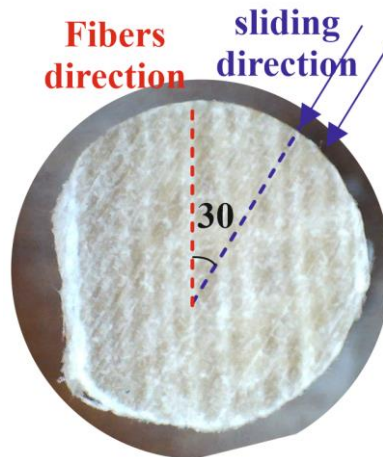


Fig. 3.11. The angel between sliding direction and the fibers direction for the PLA-HF (condition no.7, Table 3.4)

## 3.2.2. Slurry pot test system

Figs. 3.12 and 3.13 show the structure of the applied slurry-pot system.

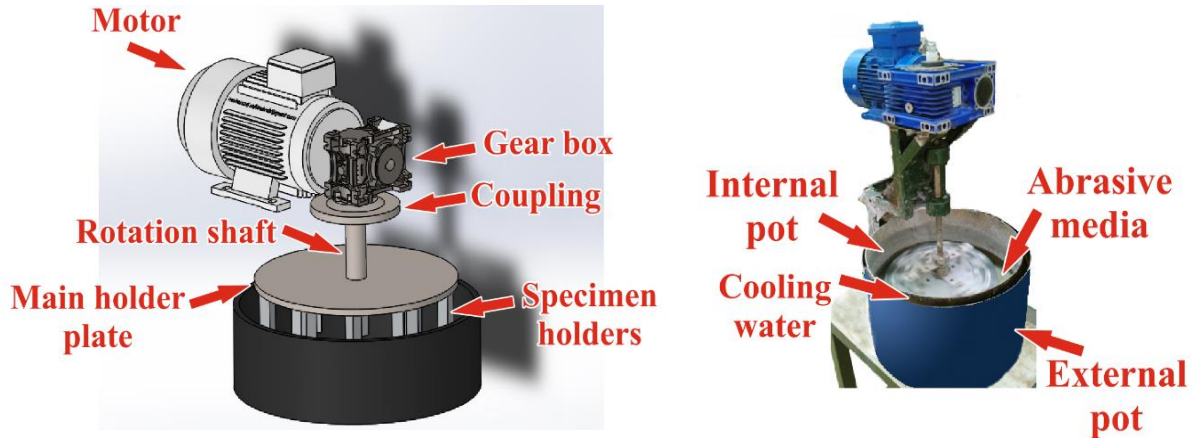


Fig. 3.12. Assembly of the slurry-pot test system

The electric motor drives a vertical shaft via a worm gear (1:10) and a clutch.

The main holder steel plate is fixed to the shaft. Twelve steel columns holding the polymer specimens are screwed into the disc from below, arranged on two radii ( $r_1$  and  $r_2$ ) for 6-6 splits of 60 degrees from each other (Fig. 3.13).

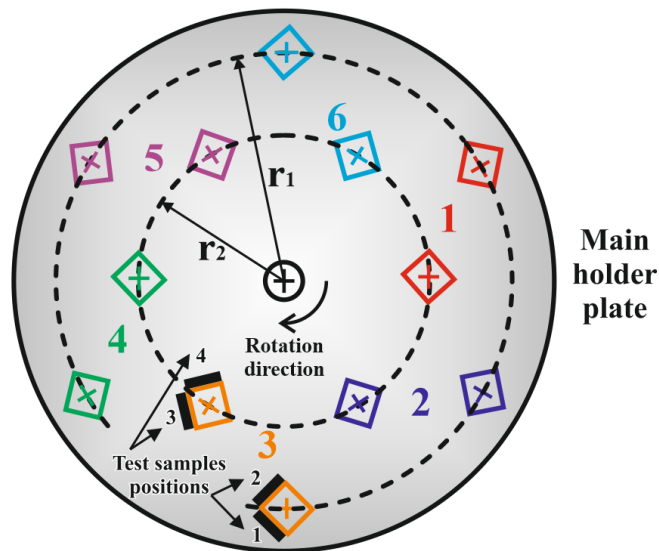


Fig. 3.13. Layout of the 12 holder columns on the main holder plate. Tangential and direct collision as well as the numbered polymer sample positions (1-4) are indicated

On the two radii, the columns are offset from each other. The polymer plates to be tested, which were machined to size, are fixed to the two sides of each specimen holder column (Fig. 3.14).



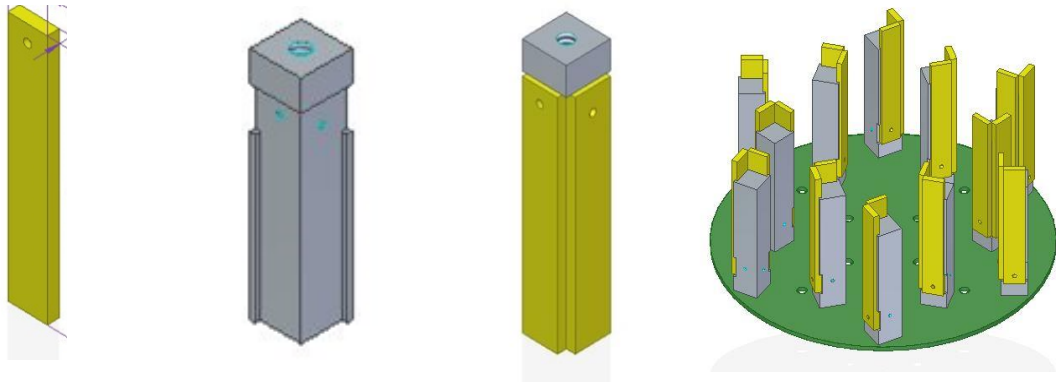


Fig. 3.14. Assembly line of the specimen system: polymer sample, steel holder column, samples placed on the column, and finally the holder unit in upside down position

The outer radius  $r_1 = 280$  mm and the inner radius  $r_2 = 200$  mm. The twelve holders were divided into six numbered groups as shown in Fig 3.13, one for each polymer type tested. Each group has an outer and an inner holder, creating the possibility to test and compare 6 types of materials with two mean circumferential speeds.

Based on the Eq. 3.1, the two mean speeds can be calculated.

$$v = \omega \cdot r \quad (3.1)$$

The first mean speed is  $2.038 m \cdot s^{-1}$  while the second one is  $1.456 m \cdot s^{-1}$ .

The entire assembled specimen holder unit is immersed in the abrasive medium and rotated therein (Fig. 3.12). Based on preliminary experiments, the rotating shaft was placed eccentrically in the pot, thus providing better mixing of the abrasive medium. (Diameter of the holder plate (320 mm), the diameter of the pot (380 mm) and the height of the pot (400mm), with an eccentricity between the rotating shaft and internal pot). During the rotational motion, the particles collide with the polymer plates to be tested.

Depending on the location of the polymer plates on the column, “tangential” and “direct” collisions can be distinguished (Fig. 3.15) in the system with different impact and mean velocity values (according to  $r_1$  and  $r_2$ ).

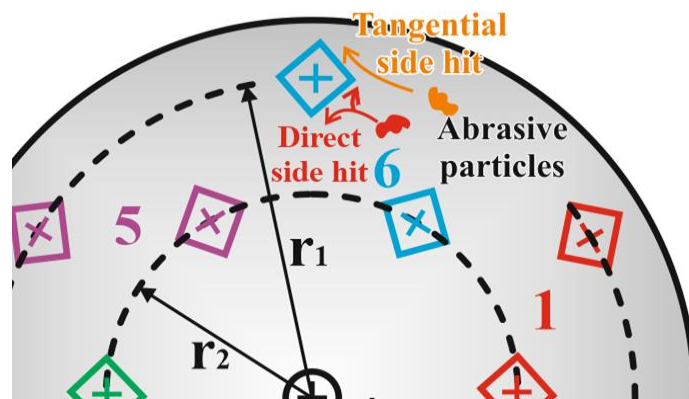


Fig. 3.15. The tangential and direct collisions of abrasive medium

For the temperature control of the slurry, double pots were used (the diameter of the external pot (400 mm) and the height of the external pot (400mm)) with cooling water in between. Thus, a

temperature of 30 °C could be set for the slurry during the tests. The slurry was consistently mixed in a 1:4 volume ratio of water to dry abrasive material.

The polymer samples were tested for five days. 22 working hours, with two hours for daily wear measurements (the duration was determined with preliminary tests to ascertain the limit of the sample's geometrical loss, without abrading the holders). The total abrasive testing time was 110 hours for one test series. In some cases, the samples could not withstand this time limit due to a given combination of speed, media and position.

The daily 22 working hours can be converted into a straight distance:

- Position 1 and 2 (Fig. 3.13): 22 (hours) \* 60 (mins) \* 60 (sec) \* 2.038 (m.s<sup>-1</sup>) = 161409.6 m
- Position 3 and 4 (Fig. 3.13): 22 (hours) \* 60 (mins) \* 60 (sec) \* 1.456 (m.s<sup>-1</sup>) = 115315.2 m

During the daily stopping hours, the wear was measured by the weight loss of the polymer specimens, and their dimensions were controlled.

For this test, the following variables were applied:

- Two speeds: 2.038m. s<sup>-1</sup> and 1.456 m. s<sup>-1</sup>
- Two types of collisions for the abrasive mediums (tangential and direct)
- Four abrasive mediums

In the slurry-pot system, the wear on the worn surface area (acting with the abrasive slurry to a different extent, depending on the position of the specimen) of the specimen was measured as a decrease in mass (g) after 22 hours of operation daily. The size of the worn surface was conventionally determined for each specimen position by preliminary experiments. Thus, the measured absolute weight loss had to be normalized according to the worn area depended on the position. Fig. 3.16. The measured absolute wear mass after the area normalization (g/mm<sup>2</sup>) was considered as “wear” for further calculation and comparison e.g. the daily change in %..

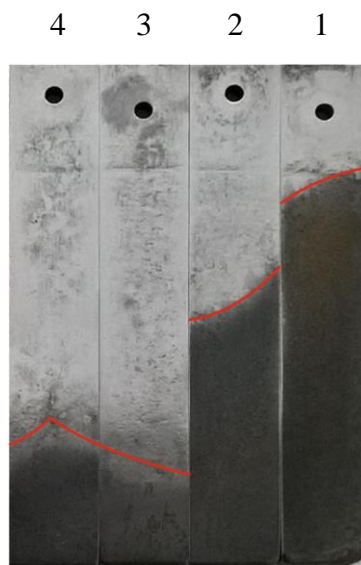


Fig. 3.16. Slurry-pot samples showing the agreed active worn areas according to the positions 1-2-3-4.  $A_1=1861.2 \text{ mm}^2$ ,  $A_2=1378.8 \text{ mm}^2$ ,  $A_3=512.4 \text{ mm}^2$ ,  $A_4=628.8 \text{ mm}^2$

The relative wear (%) was calculated as an actual (daily cumulative) weight loss in percentage of the active worn surfaces determined according to the Fig. 3.16, compared to the zero day weight

according to the four different positions. Furthermore, the relative wear normalized to km was, also defined. The results were compared in the dedicated collision angle and rotational speed (m/s). For the evaluation of the 3D surface parameters for the tested polymers, before and after abrasion, the same method was used as the pin-on-plate system.

The abrasive media:

Four abrasive media were selected for making slurry:

- Corundum ( $\text{Al}_2\text{O}_3$ ) as a reference
- Gravelly skeletal soil (gravel)
- Lime coated chernozem (loamy soil).
- Humic sand soil (Sandy soil)

\* Aluminum Oxide (Electro corundum) is a sharp, angular, long-lasting abrasive sandblast cutting medium that can be re-used many times for grit blasting. It is the most widely used abrasive in sandblast finishing and surface preparation, for all kinds of materials due to its cost, longevity and hardness. As an abrasive blasting medium, it is harder than most common dry abrasive blast media. It does not produce much dust, it is non toxic and it is not dangerous to health in any form. The quality of corundum depends on the share of  $\text{Al}_2\text{O}_3$  (Toplice, 2009).

Table 3.5 shows the properties of the corundum used.

Table 3.5. The properties of the corundum used (Accuratus, 2013)

Properties	Units of Measure	SI/Metric
Density	gm/cc (lb/ft <sup>3</sup> )	3.72
Porosity	% (%)	0
Color	—	white
Flexural Strength	MPa (lb/in <sup>2</sup> x103)	345
Elastic Modulus	GPa (lb/in <sup>2</sup> x106)	300
Shear Modulus	GPa (lb/in <sup>2</sup> x106)	124
Bulk Modulus	GPa (lb/in <sup>2</sup> x106)	172
Poisson's Ratio	—	0.21
Compressive Strength	MPa (lb/in <sup>2</sup> x103)	2100
Hardness	Kg/mm <sup>2</sup>	1100
Fracture Toughness KIC	MPa.m <sup>1/2</sup>	3.5
Maximum Use Temperature (no load)	°C (°F)	1700
Thermal Conductivity	W/m.°K (BTU.in/ft <sup>2</sup> .hr.°F)	25
Coefficient of Thermal Expansion	10 <sup>-6</sup> /°C (10 <sup>-6</sup> /°F)	8.2
Specific Heat	J/Kg.°K (Btu/lb.°F)	880
Dielectric Strength	ac-kv/mm (volts/mil)	14.6
Dielectric Constant	@ 1 MHz	9.0
Dissipation Factor	@ 1 kHz	0.0011
Loss Tangent	@ 1 kHz	—
Volume Resistivity	ohm.cm	>1014

\* The gravelly skeletal soil is considered a very abrasive one in the industry and one of the most aggressive on machine parts, as it is dominated by particles exceeding 2 mm. In some cases there is a significant percentage of clay. Land near Kiskunlacháza was chosen as a typical sampling site, though agro-topographic maps show different soil types here. There are a number of gravel quarries in this region.

In flood plains, terraces and rubble heaps of existing or former rivers, they have a high pebble content, which results in a poor water management regime.

Purely pebble and, clay and pebble layers, are often found in profiles, showing previous periods of inundation. The percentage of the earth content originating from the mud settling from the river or from settling dust dominates the characteristics of this type of soil and whether it is suitable for agriculture utilisation.

If the proportion of pebbles exceeds 80 %, soil formation does not reach a level where deeper soil layers could form.

\* The lime coated chernozem is the most widely cultivated soil type, owing to its excellent physical characteristics and with a nutrient management regime considered to be the most suitable for farming. The texture of the types of clay that have developed on loess is dominated by the percentage of dust. Mezőföld was chosen as a typical sampling point.

The main type of chernozem soils include the types of soils that are characterised by the accumulation of humic matter, the development of a favourable crumble structure and a two-way movement of soil moisture (saturated with calcium), resulting from soil developed beneath vegetation, which is dominated by grasses.

Lime coated chernozem soils constitute a characteristic type of chernozem soils. Their name is derived from the lime coating appearing at depths between 30 and 70 cm in general. The soil coating covers the structural elements in the form of a fine film that is similar to the hyphae of fungi.

This is a consequence of the special dynamic of this soil type, in which periods of leaching - dissolution of lime - and the generation of the coating, which is the precipitation of lime from the soil moisture, follow one another in an alternating process. Leaching occurs during the water intake between the autumn and the Spring, while the coating is produced as a consequence of drying out in the Summer, resulting in the increasing saturation of the soil moisture. The lime coated layer is light in colour - a greyish shade - crumbling very easily into its structural elements.

Chernozem soils are cultivated in most places thanks to their excellent physical and chemical features. The consequences of this are also reflected by the profile structures.

The ploughed layer ( $A_p$ ) is often of a degraded structure, consisting of very small crumbs, dusty and with a compacted layer at its bottom. Its chemical reaction is neutral or slightly alkaline, containing lower levels of lime, with 3-6 % humus content.

\* The Humic sand soil is not very suitable for farming. Its texture is dominated by sand, with a small dust percentage and less than 1% organic matter content. A sampling site was chosen near the village of Csemő.

Humic sand soils include soils containing a morphologically distinct humic layer without any other signs of soil developing processes. The degree of humification does not reach the lower limits for chernozem-sand soils. In general, the thickness of the humic layer does not exceed 40 cm, with humus content below 1 %.

Humic sand soils are more productive than wind-blown sand soils since they can retain more water. They do not dry as easily, thereby they are more resistant to deflation. Their nutrient supplying capacity is also better, yet they are not very suitable for farming. They would need regular nutrient supplies if they are to be farmed. The geotechnical properties of them can be found in Table 3.6.

Table 3.6. The properties of the soils used as abrasive media

<b>Geotechnical property</b>	<b>gravelly skeletal soil (gravel)</b>	<b>lime coated chernozem (loamy)</b>	<b>Humic sand soil (Sandy)</b>
Natural moisture content W (%)	12.00	26.02	26,41
Volumetric weight in the state of natural moisture content $v$ (kN/m <sup>3</sup> )	18.96	18.67	18,67
Specific gravity $v_s$ (kN/m <sup>3</sup> )	26.02	25.05	26,04
Volumetric weight in the dry state $v_d$ (kN/m <sup>3</sup> )	16.92	14.80	14,77
The lower limit of plasticity $W_p$ (%)	-	29.58	-
The upper limit of plasticity $W_L$ (%)	-	56.00	-
Consistency index $I_c$	-	1.13	-
Pore index $e$	0.53	0.69	0,76
Porosity $n$ (%)	65.60	40.74	43,27
Edometric deformation modulus $M$ (kPa)	12000	9558	10000
Linear deformation modulus $E$ (kPa)	12000	9558	10000
Internal friction angle $\Phi$ (°)	20	13	20
Cohesion $c$ (kPa)	25	100	25
Plasticity criterion $C_p$	-	26.00	-

Specimens preparation:

For the slurry-pot test system, the specimen holder has an exact dimension, shown in Fig. 3.17 a).

The specimens were machined into cuboid shape with 120 mm as length, 20 mm as width and 6 mm as thickness, these dimensions have been chosen to fit the holder. The samples are 5mm longer than the holders in order to protect them from any possible wear.

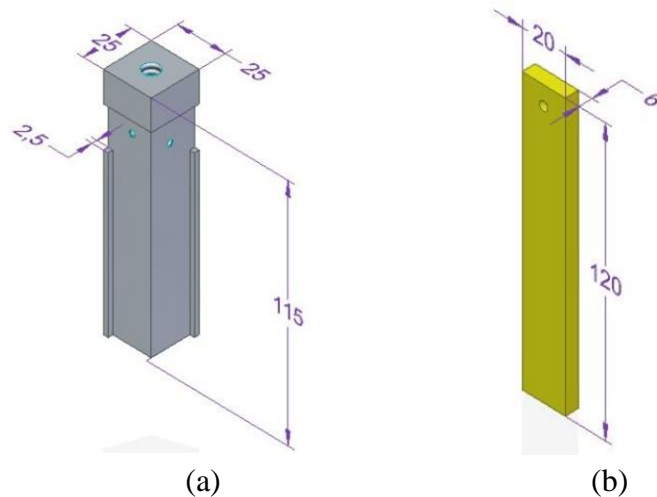


Fig. 3.17. Holder and Sample dimensions of slurry-pot test system

### 3.4. Topography

For both test systems the 3D polymer surface topography was evaluated before and after a given test. Several parameters were measured based on ISO 25178.

#### Root mean square height (Sq)

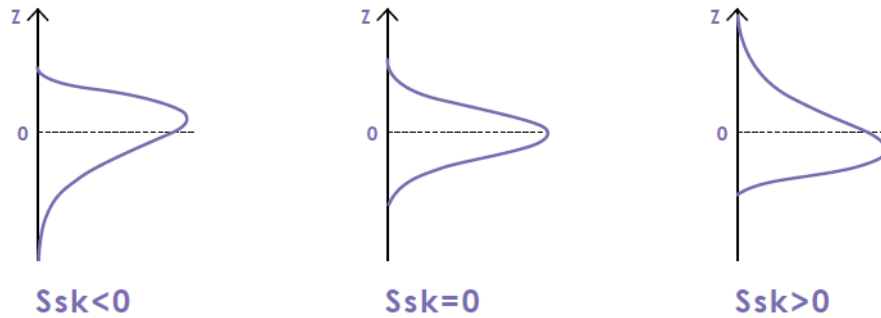
This parameter represents the root mean square value of ordinate values within the definition area. It is equivalent to the standard deviation of heights.

$$S_q = \sqrt{\frac{1}{A} \iint_A Z^2(x, y) dx dy} \quad (3.2)$$

#### Skewness (Ssk)

Ssk values represent the degree of bias of the roughness shape (asperity).

$$S_{sk} = \frac{1}{S_q^3} \left[ \iint_A Z^3(x, y) dx dy \right] \quad (3.3)$$

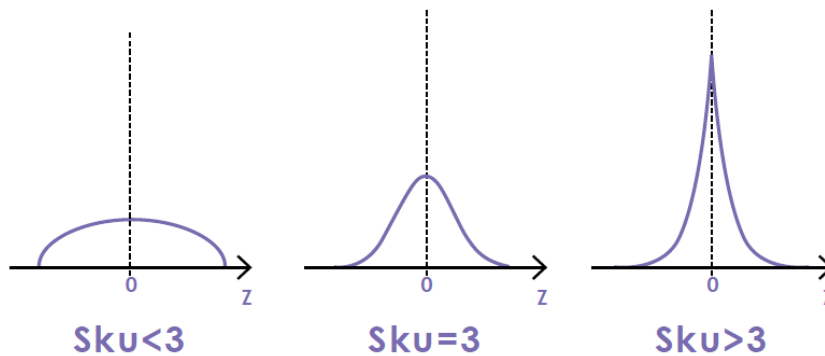


- Ssk < 0: Height distribution is skewed above the mean plane.
- Ssk = 0: Height distribution (peaks and pits) is symmetrical around the mean plane.
- Ssk > 0: Height distribution is skewed below the mean plane.

#### Kurtosis (Sku)

Sku value is a measure of the sharpness of the roughness profile.

$$S_{ku} = \frac{1}{S_q^4} \left[ \frac{1}{A} \iint_A Z^4(x, y) dx dy \right] \quad (3.4)$$



- $Sku < 3$ : Height distribution is skewed above the mean plane.
- $Sku = 3$ : Height distribution is normal distribution. (Sharp portions and indented portions co-exist.)
- $Sku > 3$ : Height distribution is spiked.

Maximum peak height ( $S_p$ )

This is the height of the highest peak within the defined area.

$$S_p = \max_A z(x, y) \quad (3.5)$$

Maximum pit height ( $S_v$ )

This is the absolute value of the height of the largest pit within the defined area.

$$S_v = \left| \min_A z(x, y) \right| \quad (3.6)$$

Maximum height ( $S_z$ )

This parameter is defined as the sum of the largest peak height value and the largest pit depth value within the defined area.

$$S_z = S_p + S_v \quad (3.7)$$

Arithmetical mean height ( $S_a$ )

This parameter is the mean of the absolute value of the height of points within the defined area.

$$S_a = \frac{1}{A} \iint_A |Z(x, y)| dx dy \quad (3.8)$$

The surface topography was evaluated from non-contact profilometry, using a 3D optical profilometer Coherence Correlation Interferometry (CCI) HD type (Taylor Hobson, Leicester, England, the equipment is available at Soete Laboratory, Ghent University), Fig. 3.18, with an ultra-high precision closed loop piezoless z-scanner having a resolution in z-direction of 0.1 Å.

The white light illumination was produced from a fiber lite DC-950 source and measurements were made at 50% light intensity. A surface area of  $330 \times 330 \mu\text{m}^2$  was imaged by vertical scanning interferometry, with an objective lens at magnification 50X and numerical aperture= 0.55.

The scanning arrays contained  $2048 \times 2048$  pixels with a field-of-view= 330  $\mu\text{m}$ , corresponding to a pixel size of 0.165  $\mu\text{m}$ . The images were processed by Talymap software (Digiserve) to calculate the 3D surface roughness parameters according to ISO 25178, including  $S_a$  (average roughness),  $S_z$  (maximum height),  $Sku$  (kurtosis), and  $Ssk$  (skewness) (Deltombe et al., 2014). The roughness values were determined by taking an average of three measurements at independent surface locations, with repeatability  $S_a < 0.2 \text{ \AA}$ . More details about (CCI) theory and measurements in (Kaplonek and Lukianowicz, 2012).



Fig. 3.18. 3D optical profilometer, Taylor Hobson CCI HD device

This device has several features like:

- Reduced inaccuracy and noise compared to 2D
- High resolution, precise results
- Data extraction from the whole 3D surface

Moreover, during the measurement, the used settings are:

- 50X lens
- Scanning speed: x1, 4m mode, filter 2, rough surface

### 3.5. Dimensionless numbers

All the measured data was evaluated from the function of mechanical properties (Table 3.1 and 3.3) and from the dimensionless numbers formed from them. A similar method was used for the friction analysis of numerous polymers in adhesive systems (Kalacska, 2013).

The hardness values in (MPa) used for further combined calculations with other material properties were derived from Shore D dimensionless values. The derived values in MPa give the same order of material hardness as Shore D.

The combined dimensionless numbers are:

- $\frac{H}{E}$  the ratio between: hardness and elasticity modulus
- $\frac{\sigma_y E}{\sigma_M H}$  the ratio between: combined tensile performance / combined bulk-surface stiffness
- $\frac{\sigma_y H}{\sigma_M E}$  the ratio between: combined surface strength / combined strength-stiffness
- $\frac{\sigma_F \sigma_y}{\sigma_M H}$  the ratio between: combined tensile-flexural strength / combined strength-hardness
- $\frac{E}{\sigma_C}$  the ratio between: elasticity modulus / compression strength



- $\frac{\sigma_F}{\sigma_C}$  the ratio between: flexural strength / compression strength
- $\frac{H\varepsilon_B}{\sigma_y}$  the ratio between: combined Hardness-strain capability / Yield strength
- $\frac{\sigma_C\varepsilon_B}{\sigma_M}$  the ratio between: combined compression - strain capability / tensile strength
- $\frac{\sigma_y}{\sigma_C\varepsilon_B}$  the ratio between: Yield strength / combined compression - strain capability
- $\frac{\sigma_F H}{\sigma_M E}$  the ratio between: combined Flexural performance / combined bulk-surface stiffness

### 3.6. Statistical analysis

For the statistical analysis, multiple linear regression models were developed using IBM SPSS 25 software. To examine how a dependent variable depends on several independent (or explanatory) variables which are all measured on scales, the main tool is multiple regression. In this paper it is verified that the functions of several variables which describes this dependence is approximately linear, that is for a dependent variable:

$$Y = a_0 + a_1X_1 + a_2X_2 + \dots + a_nX_n, \quad (3.9)$$

where  $n$  is the number of independent variables and  $X_1, X_2, \dots, X_n$  are the independent variables.

The method of least squares is the most common way to fit such a model to the measured data. First, always an  $F$  test is carried out to see whether the corresponding model is relevant.

If the  $p$ -value is less than 0.05, that is, it is significant, then the model is relevant, otherwise it is not. Usually, the  $R^2$  value measures the aptness of such a linear model, it shows what portion of the variance of the dependent variable is explained by the independent variables. If for a coefficient  $a_k (k \in \{0, 1, \dots, n\}) p < 0.05$  holds, then it means it is statistically different from 0, thus the corresponding independent variable  $X_k$  indeed plays a role in describing the dependence of  $Y$ .

In the discussed models only those explanatory variables are included for which their associated coefficient turned out to be significant. To see which independent variable has the greater effect on  $Y$ , one must consider the absolute value of the standardized (or beta) coefficients of the significant independent variables, the higher this value is, the higher the effect is.

Among the possible methods of entering variables into a linear regression model the stepwise method was used. It means that at each step of the model building algorithm among the possible, significant independent variables the one is entered which causes the highest change in  $R^2$ . The algorithm ends when there is no new independent variable to enter. In some cases of the models presented below, not all significant variables were included: the ones causing very low change in  $R^2$  are neglected.

It is important to mention that one of the assumptions of the applicability of multiple linear regression is that the independent variables are not collinear. Since many of the parameters of the studied materials have high correlation coefficients with an another parameter, therefore not all of them were used in the models at the same time.

## 4. RESULTS

This chapter presents the results that were achieved and discusses them in regard to the scientific findings established.

### 4.1. Pin-on-plate system

As it was introduced in detail in 3.2.1 chapter that two types of wear interfaces (P60 and P150 standard abrasive clothes), two sliding speeds (0.031 m/s and 0.056 m/s) and three normal loads (9.81 N, 29.43 N and 49.05 N) were applied. The twelve system cases can be reviewed in Table 3.4. The following sub-chapters (4.1.1 – 4.1.3) show some typical wear curves about the effects of the modification of normal load, sliding speed and abrasive particles, indicating the actual number of the system conditions (Table 3.4).

#### 4.1.1. The effect of the load

Figs. (4.1 – 4.6) represent the experimental relation between the wear (mm) and sliding distance (m) for the materials used, with a constant speed and using the same wear interface. The speed was 0.031 (m/s) and the abrasive clothes were P60, which refer the systems no. 1, 2 and 3 in Table 3.4.

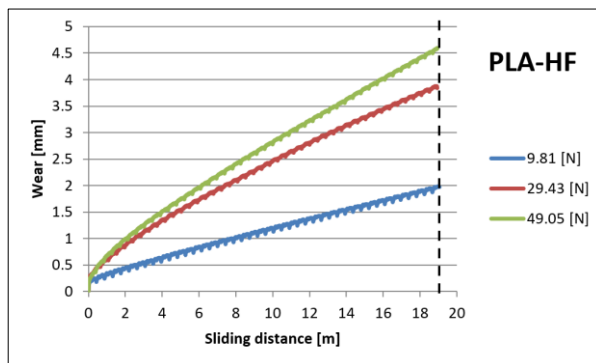


Fig. 4.1. The experimental relation between the wear and sliding distance for PLA-hemp with the three used loads

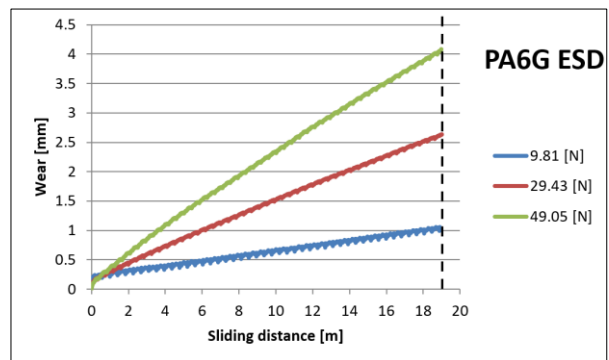


Fig. 4.2. The experimental relation between the wear and sliding distance for PA6G ESD with the three used loads

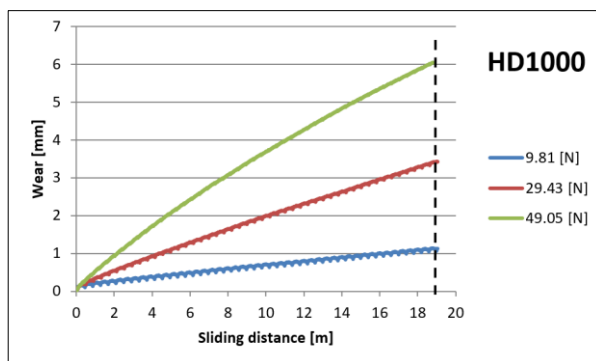


Fig. 4.3. The experimental relation between the wear and sliding distance for HD1000 with the three used loads

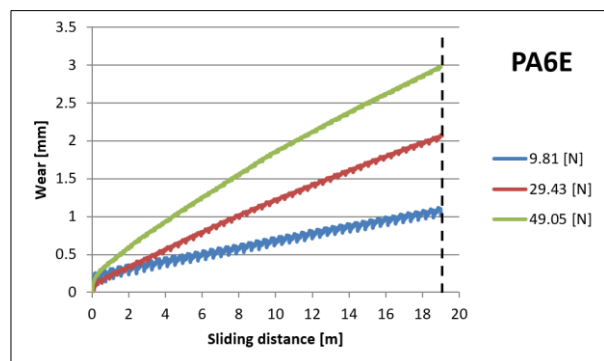


Fig. 4.4. The experimental relation between the wear and sliding distance PA6E with the three used loads

## 4. Results

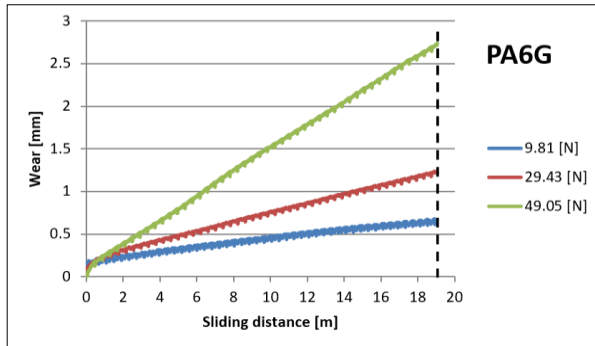


Fig. 4.5. The experimental relation between the wear and sliding distance for PA6G with the three used loads

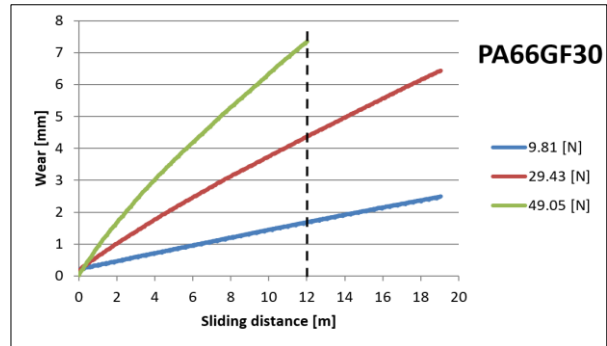


Fig. 4.6. The experimental relation between the wear and sliding distance for PA66GF30 with the three used loads

As a result, under a constant speed value and with same abrasive clothes, the wear values increased by increasing the load.

By considering the wear of 9.81(N) as a reference point, the increasing percentages of using 29.43 (N) and 49.05 (N) are shown in Table 4.1 using the last comparable measured wear values shown with dotted lines in Figs. (4.1 – 4.6).

Table 4.1. The wear values at the used loads and the increasing percentages

Material	Wear (mm) at load 9.81 (N)	Wear (mm) at load 29.43 (N)	Increasing percentages	Wear (mm) at load 49.05 (N)	Increasing percentages
PA66GF30	1.675	4.35	159.7%	7.35	338.8%
PA6G ESD	1.056	2.631	149.1%	4.082	286.5%
PA6E	1.1	2.075	88.6%	2.981	171%
PA6G	0.681	1.238	81.7%	2.738	302%
PLA-HF	1.988	3.875	94.9%	4.594	131%
HD1000	1.156	3.425	196.2%	6.05	423.3%

For better visualisation of the data in Table 4.1, Fig. 4.7 shows them in columns.

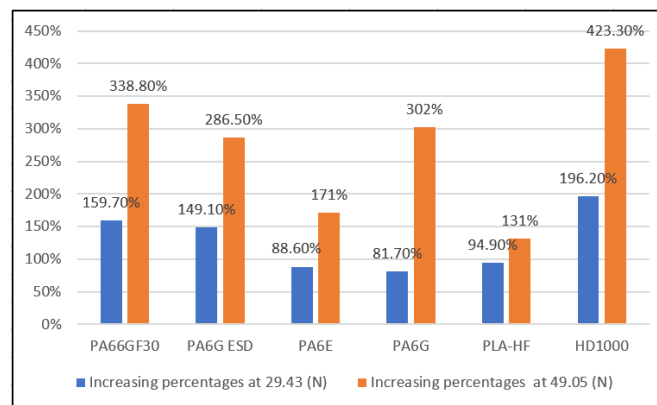


Fig. 4.7. The increasing percentages of the materials tested by increasing the load

From the table, both of PA66GF30 and HD1000 were the most sensitive materials to the changing loads. PA6E performed as a less sensitive one to the increasing loads.

The measured on-line wear points of these conditions were approached by linear fit similarly to the speed analyses. The slope values “a” of the linear regression ( $y = ax + b$ ) are summarized in Table 4.2.

Table 4.2. The “a” values at the three used loads

Material	“a” values at load 9.81 (N)	“a” values at load 29.43 (N)	“a” values at load 49.05 (N)
PA66GF30	0.1198	0.3226	0.5914
PA6G ESD	0.0433	0.1295	0.2064
PA6E	0.0457	0.1031	0.1437
PA6G	0.0258	0.055	0.1387
PLA-HF	0.0913	0.1822	0.2166
HD1000	0.0508	0.1709	0.3115

#### 4.1.2. The effect of the speed

Figs. (4.8 – 4.13) represent the relation between the wear (mm) and sliding distance (m) for the materials used, with an exact load and using the same wear interface. The load was 49.05 (N) and the abrasive clothes were P60, which refer the systems no.3 and 6 in Table 3.4.

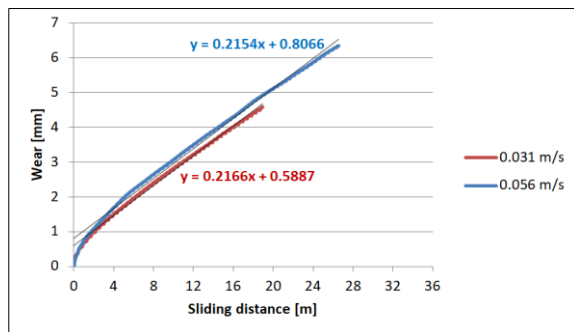


Fig. 4.8. The relation between the wear and sliding distance for PLA-hemp with the two speeds

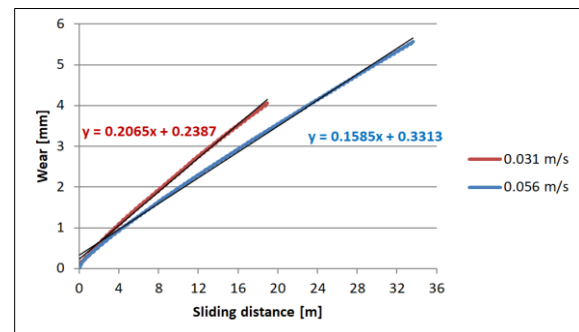


Fig. 4.9. The relation between the wear and sliding distance for PA6G ESD with the two speeds

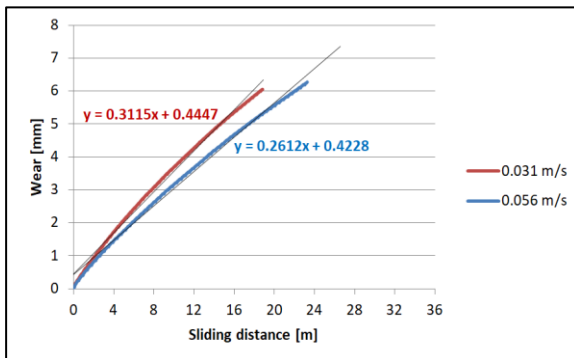


Fig. 4.10. The relation between the wear and sliding distance for HD1000 with the two speeds

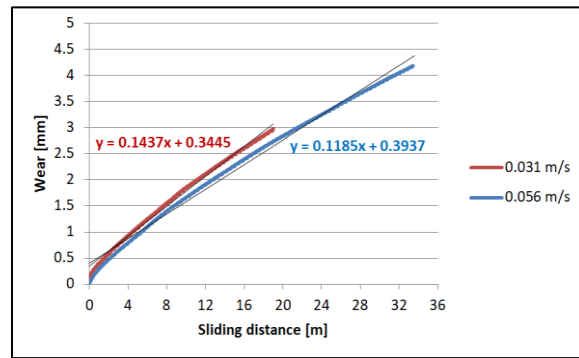


Fig. 4.11. The relation between the wear and sliding distance PA6E with the two speeds

## 4. Results

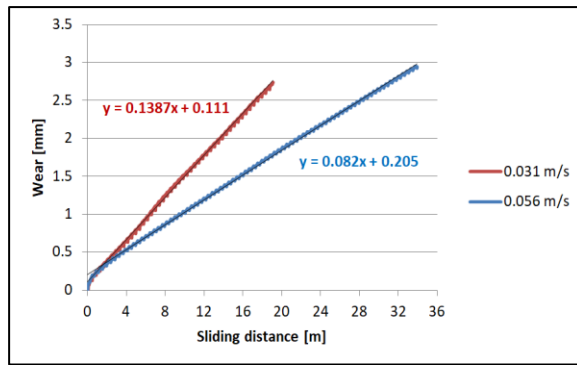


Fig. 4.12. The relation between the wear and sliding distance for PA6G with the two speeds

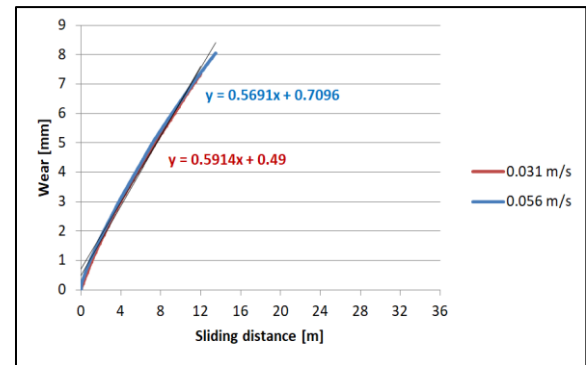


Fig. 4.13. The relation between the wear and sliding distance for PA66GF30 with the two speeds

As a result, under the same load value and with same abrasive clothes, the wear values increased by increasing the speed.

The measured on-line wear points of these conditions were approached by linear fit. The slope values “a” of the linear regression ( $y = ax + b$ ) are summarized in Table 4.3 which can help to compare the wear speeds.

Table 4.3. The “a” values at the two used speeds

Material	“a” values at v=0.031 m/s	“a” values at v=0.056 m/s
PA66GF30	0.5914	0.5691
PA6G ESD	0.2065	0.1585
PA6E	0.1437	0.1184
PA6G	0.1337	0.082
PLA-HF	0.2166	0.2154
HD1000	0.3115	0.2609

The table shows that the wear speeds under 0.031 m/s sliding velocity are higher than the wear speed under 0.056 m/s sliding. As a result, increasing the sliding velocity the wear speed will be lower, except the PLA-HF.

### 4.1.3. The effect of the wear interface

Figs. (4.14 - 4.19) represent the relation between the wear (mm) and sliding distance (m) for the materials used, with an exact load and at the same speed. The speed was 0.031 (m/s) and the load 9.81 (N). The lines represent P60 and P150 abrasive surfaces, which refer the systems no. 1 and 7 in Table 3.4.

## 4. Results

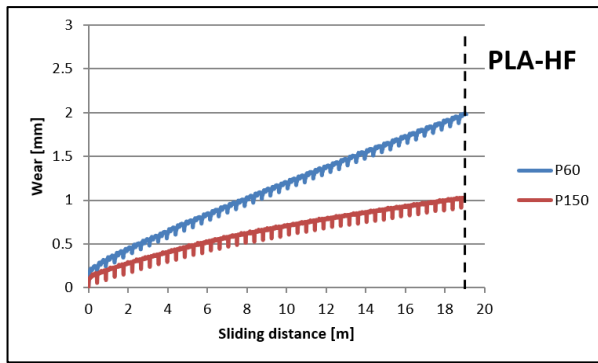


Fig. 4.14. The relation between the wear and sliding distance for PLA-hemp with the two abrasive clothes

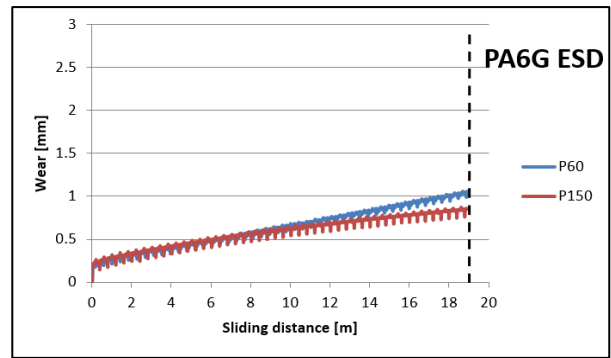


Fig. 4.15. The relation between the wear and sliding distance for PA6G ESD with the two abrasive clothes

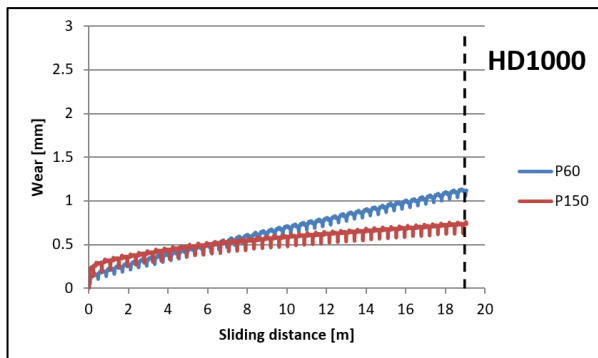


Fig. 4.16. The relation between the wear and sliding distance for HD1000 with the two abrasive clothes

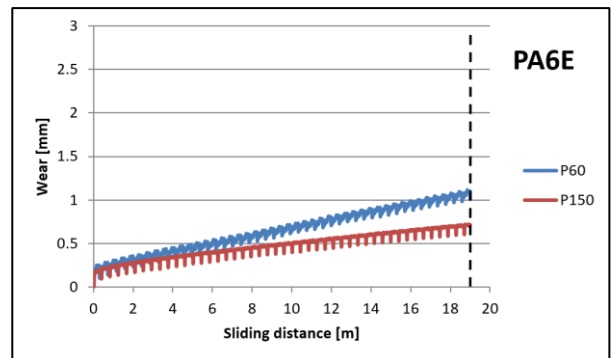


Fig. 4.17. The relation between the wear and sliding distance PA6E with the two abrasive clothes

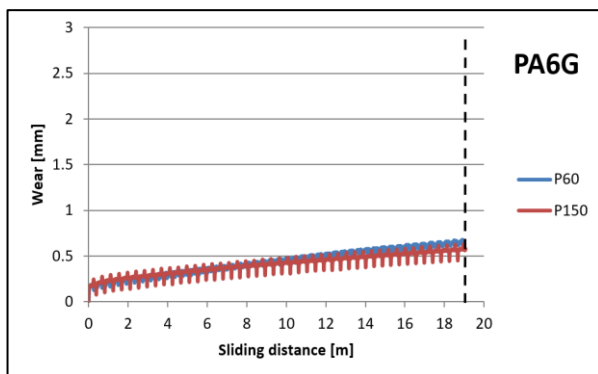


Fig. 4.18. The relation between the wear and sliding distance for PA6G with the two abrasive clothes

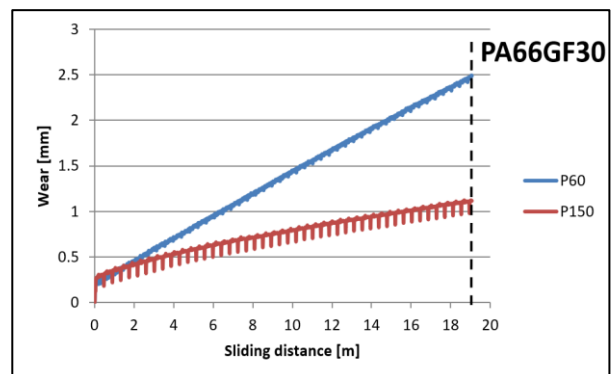


Fig. 4.19. The relation between the wear and sliding distance for PA66GF30 with the two abrasive clothes

As a result, under a constant speed value and with same load, the wear values for P60 were higher than the P150 values, since P60 have bigger and tougher grit than the P150.

By considering the wear of P150 as a reference point, the percentage increase of using P60 are as in Table 4.4. The wear values refer to 19 m (before stopping the measurements) sliding distance indicated with dotted lines in Figs. (4.14 – 4.19).

Table 4.4. The wear values at the two used wear interfaces and the increasing percentages

Material	P150 wear (mm)	P60 wear (mm)	Increasing percentages
PA66GF30	1.131	2.494	120.5%
PA6G ESD	0.863	1.056	22.3%
PA6E	0.725	1.1	51.7%
PA6G	0.581	0.681	17.2%
PLA-HF	1.025	1.988	93.2%
HD1000	0.756	1.156	52.9%

From the Table 4.4., PA66GF30 were the most sensitive one, while PA6G is almost insensitive to the change of abrasive surface morphology.

As shown in the Figs. (4.14 - 4.19), there is a repeated drop every few seconds because of the welding point between the two ends of the belt. This will lead to a disruption on the wear lines. Fig. 4.20 shows that clearly by zooming in on the lines.

Fig. 4.20 shows the relation between the wear and sliding distance, for PA66GF30 with the two abrasive clothes before using the “moving average” analysis tools.

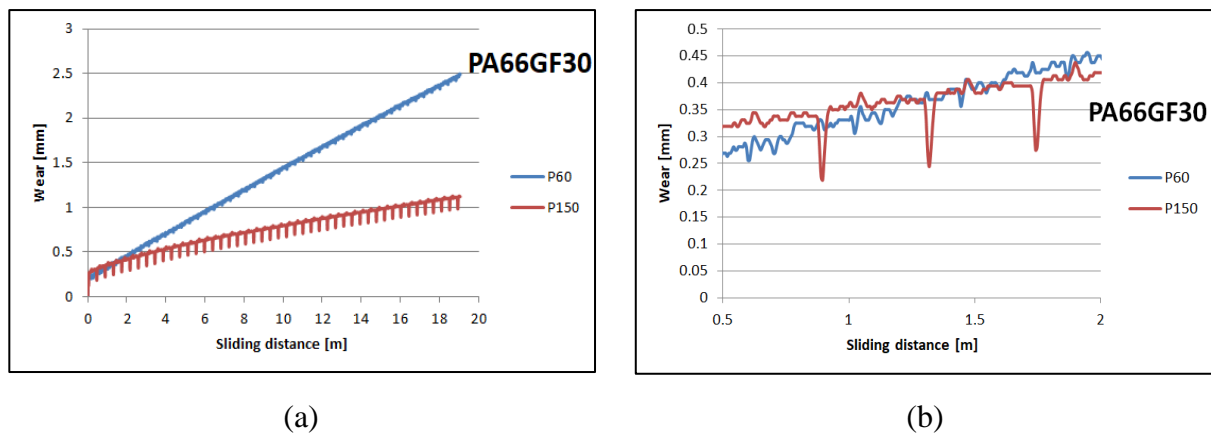


Fig. 4.20. The relation between the wear and sliding distance for PA66GF30 with the two abrasive clothes before using the moving average, a) without zoom, b) with zoom

To negate the effect of the welding point between the two ends of the belt, the “moving average” analysis tool was used with an interval of ‘10’ to make corrections for these lines to negate the disruption, as much as possible, without changing the wear behavior of the materials.

#### 4.1.4. Comparing the materials for wear

Concerning the large on-line registered database, the extremes of test conditions (maximum and minimum loads and speeds, numbered as 1, 6, 7, 12 in Table 3.4) on two types of abrasive clothes are shown in the Figs. (4.21 and 4.22). The other cases will be shown in the Appendix 3.

Fig. 4.21 shows the P60 results: wear in the function of sliding distance with linear approach.

#### 4. Results

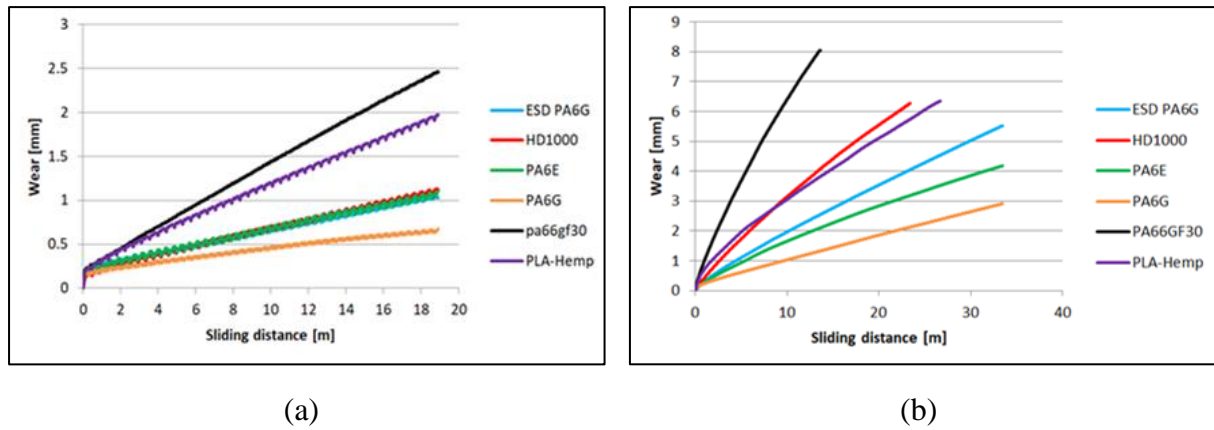


Fig. 4.21. The relation between the wear and sliding distance for several polymer types on P60 abrasive clothing. (a) lowest applied  $pv$ , (b) highest applied  $pv$

Fig. 4.21 a) refers to No.1 test condition (Table 3.4) having the lowest speed and load (lowest  $pv$ ), where all the materials could slide the same distance. Cast polyamide 6 performed the best while PA66GF30 the worst.

When tested at the top speed and load, which is the highest  $pv$ , (Table 3.4, No. 6 test condition) different sliding distances can be seen (Fig. 4.21 b)) according to the limit of fast wear and specimen dimensions, PA6G offered the best wear resistance.

Fig. 4.22 shows the P150 results: wear in the function of sliding distance.

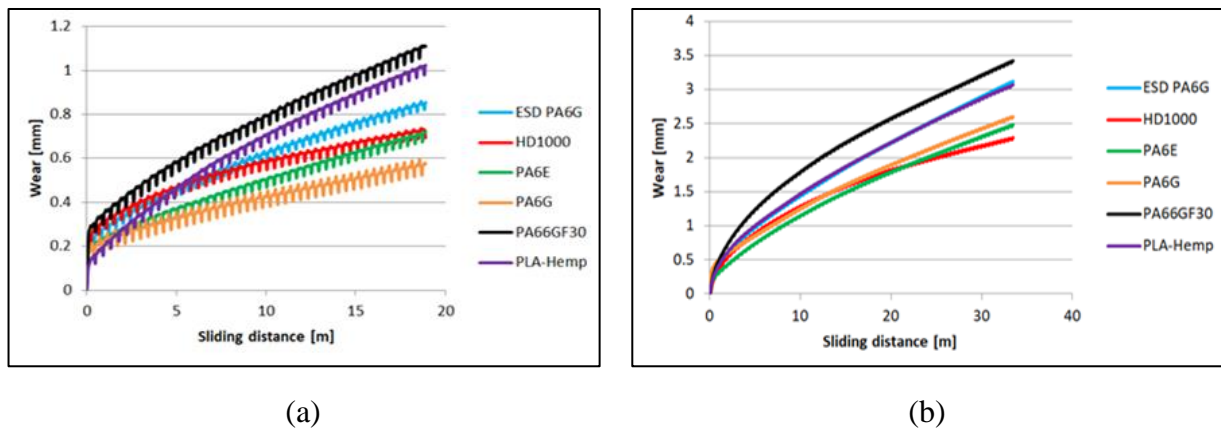


Fig. 4.22. The relation between the wear and sliding distance for several polymer types on P150 abrasive clothing. a) lowest applied  $pv$ , b) highest applied  $pv$

Fig. 4.22 a) refers to No.7 test condition (Table 3.4) having lowest speed and load (lowest  $pv$ ), were all the materials could slide the same distance. Cast polyamide 6 performed the best while PA66GF30 the worst.

When tested at the top speed and load, which is the highest  $pv$  using P150 abrasive clothes, (Table 3.4, No. 12 test condition) the PA6E (extruded polyamide 6), PA6G (cast polyamide 6) and UHMW-PE HD1000 offered the best wear resistances in high  $pv$  conditions (Fig. 4.22 b)).



#### 4. Results

The measured on-line wear points of the twelve system conditions (Table 3.4) were approached by linear fit. The wear line equation and the slope values are shown in Appendix 4.

The summary of the slope values “a” of the linear regression ( $y = ax + b$ ) are summarized in Table 4.5 and Fig. 4.23, which can help to compare the wear speeds.

Table 4.5. The slope values (speed of wear) of linear regression in all the 12 test conditions

Material	1	2	3	4	5	6	7	8	9	10	11	12
PA66GF30	0.1198	0.323	0.5907	0.108	0.3457	0.5676	0.0422	0.0808	0.1053	0.0355	0.0632	0.0838
PA6G ESD	0.0433	0.1296	0.2065	0.0415	0.1036	0.1586	0.032	0.0643	0.0918	0.0255	0.0555	0.0794
PA6E	0.0457	0.1032	0.1439	0.0343	0.0898	0.1184	0.0269	0.0563	0.0757	0.0198	0.0485	0.0648
PA6G	0.0258	0.0549	0.1338	0.016	0.0669	0.082	0.0192	0.0523	0.0753	0.0186	0.048	0.0641
PLA-HF	0.0912	0.1821	0.2165	0.0551	0.1292	0.2151	0.0455	0.0759	0.1036	0.0355	0.056	0.078
HD1000	0.0508	0.171	0.3112	0.0578	0.1598	0.2609	0.0228	0.0228	0.0702	0.0211	0.0428	0.0552

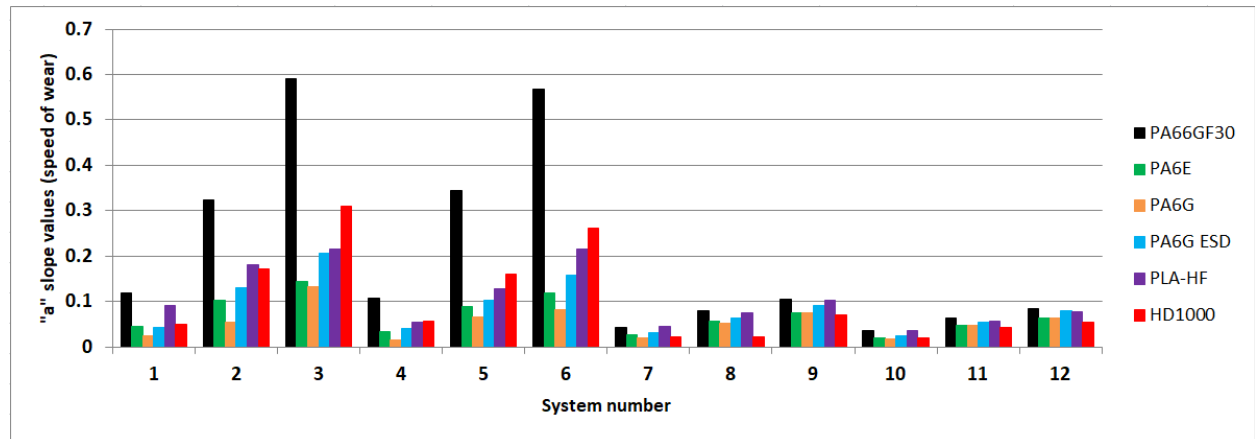


Fig. 4.23. The slope values (speed of wear) of linear regression in all the 12 test conditions

It is clear that PLA-HF bio-composite was not worse than the average of the tested engineering polymers, in this pin-on-plate system, while PA66GF30 had the highest slope values and it was subjected to the highest wear rate.

In the first six test conditions, (Cast polyamide 6) PA6G had the lowest values, while in the second six test conditions UHMW-PE HD1000 had the lowest. In other words, PA6G behaved better against the medium abrasive particle size (P60), while UHMW-PE HD1000 behaved better against the small abrasive particle size (P150).

Table 4.6 and Fig. 4.24 show the highest comparable wear values (mm) for all 12 systems conditions.

#### 4. Results

Table 4.6. The highest comparable wear values (mm) for all 12 systems conditions, indicating the actual sliding distance belonging to the wear values

System number	1	2	3	4	5	6	7	8	9	10	11	12
sliding distance (m)	18	18	12.01	36	22.14	13.52	18	18	18	36	36	36
PA66GF30	2.475	6.413	7.350	3.663	7.831	8.044	1.106	1.963	2.525	1.338	2.656	3.431
PA6E	1.088	2.038	2.113	1.263	2.338	2.094	0.725	1.288	1.706	0.813	1.819	2.488
PA6G	0.613	1.225	1.781	0.663	1.606	1.325	0.575	1.213	1.631	0.794	1.775	2.606
PA6G ESD	1.031	2.619	2.763	1.500	2.513	2.550	0.863	1.575	2.000	1.006	2.044	3.125
PLA-Hemp	1.981	3.838	3.225	2.013	3.744	3.813	1.025	1.688	2.369	1.431	2.3	3.019
HD1000	1.113	3.4	4.275	2.125	3.925	4.081	0.731	0.731	1.625	0.938	2.050	2.294

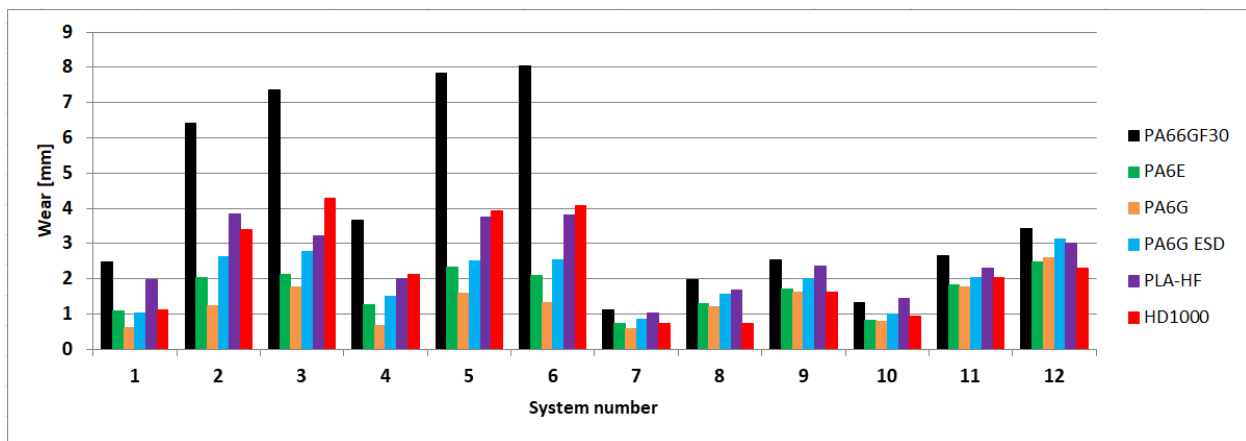


Fig. 4.24. The highest comparable wear values (mm) for all 12 systems conditions

Based on the vertical wear values (mm), the area of the cross section of the sample with 8 mm as diameter, the applied load on the specimen (N), and the sliding distance (m), the *specific wear* has been calculated for each test as ( $m^3/N.m$ )

Concerning the large on-line registered database, under the extremes of test conditions (maximum and minimum loads and speeds, numbered as 1, 6, 7, 12 in Table 3.4) the specific wear on two types of abrasive clothes are shown in Figs. (4.25 and 4.26). The other cases will be in the Appendix 5.

The initial part of the specific wear curves calculated for the same cases and materials are shown in Figs. (4.25 and 4.26), they focus on the running-in phases of the tests, where the starting sensitivity and differences can be expressed.

The first half meter of sliding is critical from the point of specific wear, that dictates the slopes (Table 4.5) and positions of the wear lines even further (Figs. 4.25 and 4.26).

## 4. Results

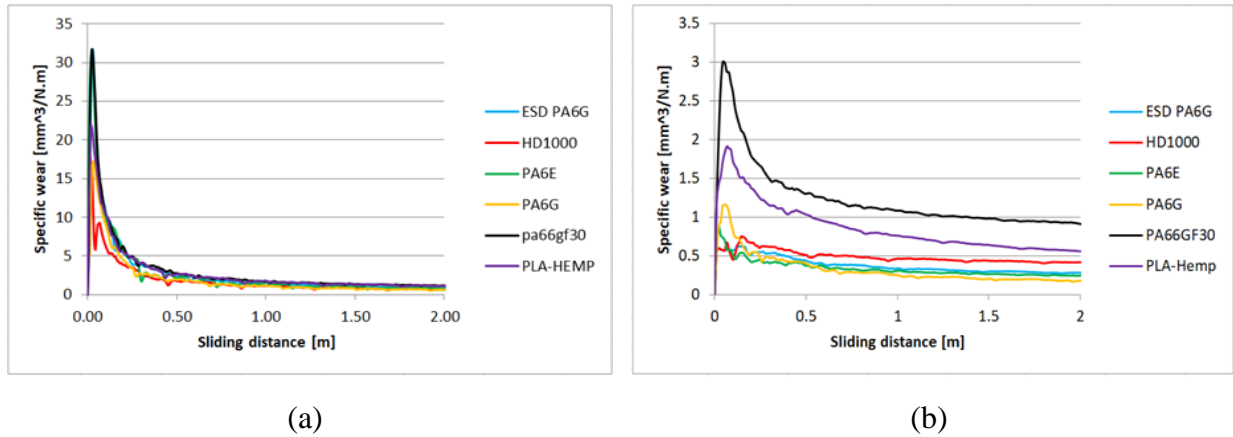


Fig. 4.25. The relation between the specific wear and sliding distance for several polymers types on P60 abrasive clothing. (a) lowest applied  $pv$ , (b) highest applied  $pv$  (Table 3.4)

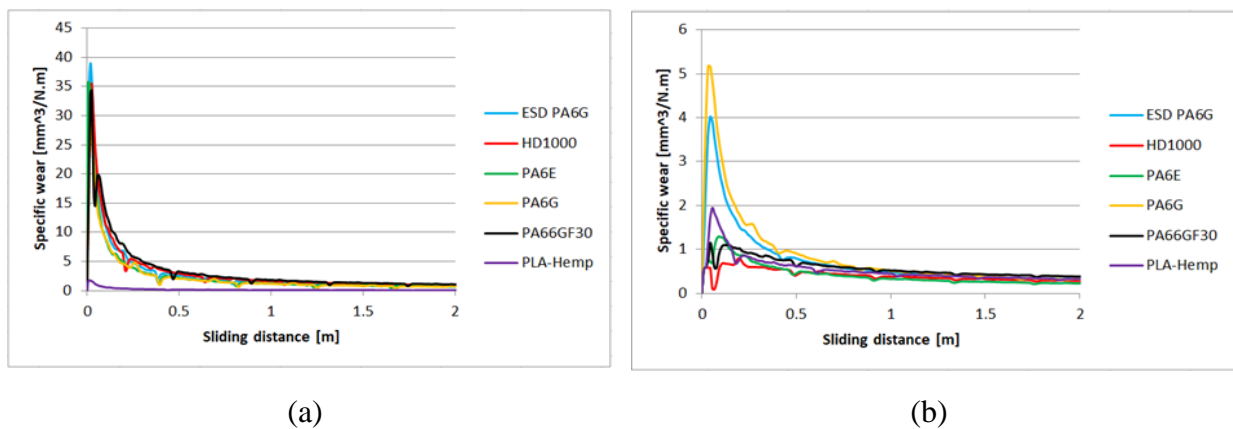


Fig. 4.26. The relation between the specific wear and sliding distance for several polymers types on P150 abrasive clothing. (a) lowest applied  $pv$ , (b) highest applied  $pv$

From Figs. (4.25 and 4.26) it can also be concluded that the specific wear during running-in for PLA-HF bio-composite was not worse than the average of the tested engineering polymers in this pin-on-plate system. On both P60 and P150 abrasive surfaces, it can be ranked as 4–5th in terms of wear resistance, i.e., similar to UHMW-PE or PA6 ESD, according to the  $pv$ .

To compare the specific wear values for the whole measurements, Table 4.7 contains the highest (top) and end point calculated specific wear values.

Finally, based on the Table 4.6, the following can be stated about the wear of polyamides types:

- In all cases PA66GF30 had the highest wear values
- In all cases PA6G had the lowest wear values (except test number 12), this result represented 91.67% of the test
- In all cases PA6G ESD had the second highest wear values after PA66GF30 (except test number 1), this result represented 91.67% of the test
- In all cases PA6E had the second lowest wear values after PA6G (except test number 12), this result represented 91.67% of the test

According to these 4 points, it is clear that the wear order of the polyamide family went, according to the following sequence:

## 4. Results

- PA66GF30 (the highest wear)
- PA6G ESD
- PA6E
- PA6G (the lowest wear)

Parallel with the wear curves, the arising friction force and temperature change in the plastic pin, were recorded on-line too.

Table 4.7. The highest and last values of the specific wear ( $m^3/N \cdot m$ ) of the materials used in 12 system conditions

	PA66GF30		PA6E		PA6G		PLA-Hemp		HD1000		PA6G ESD	
	Top	End	Top	End	Top	End	Top	End	Top	End	Top	End
<b>1</b>	31.671	0.670	31.671	0.295	17.216	0.166	21.926	0.536	17.865	0.301	31.671	0.279
<b>2</b>	9.565	0.579	2.572	0.184	4.263	0.111	11.857	0.347	3.384	0.307	6.767	0.236
<b>3</b>	1.316	0.627 (12.01 m)	2.631	0.160	0.975	0.147	5.685	0.248	2.111	0.329	1.462	0.220
<b>4</b>	4.363	0.561	9.644	0.193	9.299	0.101	11.481	0.308	13.225	0.325	6.199	0.230
<b>5</b>	1.760	0.604 (22.14m)	2.641	0.165	0.957	0.119	7.654	0.253	1.308	0.281	1.276	0.185
<b>6</b>	3.008	0.610 (13.52m)	0.873	0.128	1.157	0.089	1.913	0.245 (26.57m)	0.749	0.276 (23.28m)	0.622	0.169
<b>7</b>	34.310	0.299	35.731	0.194	28.693	0.155	1.786	0.027	35.528	0.197	38.980	0.233
<b>8</b>	11.436	0.177	6.767	0.116	3.428	0.109	2.255	0.152	3.428	0.106	13.128	0.142
<b>9</b>	4.588	0.137	3.816	0.092	1.353	0.088	3.735	0.128	1.055	0.088	2.558	0.108
<b>10</b>	7.233	0.205	10.562	0.124	10.378	0.122	9.299	0.219	12.169	0.144	9.644	0.154
<b>11</b>	8.317	0.136	1.684	0.093	1.714	0.091	4.784	0.117	7.016	0.105	0.995	0.104
<b>12</b>	1.148	0.105	1.297	0.076	5.166	0.080	1.947	0.092	0.796	0.070	4.018	0.096

### 4.1.5. Comparing the materials for friction temperature evolution

Similarly to the wear evaluation, the extremes of the test conditions (maximum and minimum loads and speeds, numbered as 1, 6, 7, 12 in Table 3.4) on two types of abrasive clothes are shown in Figs. (4.27 and 4.28), for the temperature evaluation. The other cases will be shown in the Appendix 6.

Fig. 4.27 shows the P60 results: for temperature evaluation in the function of sliding distance of the materials used.

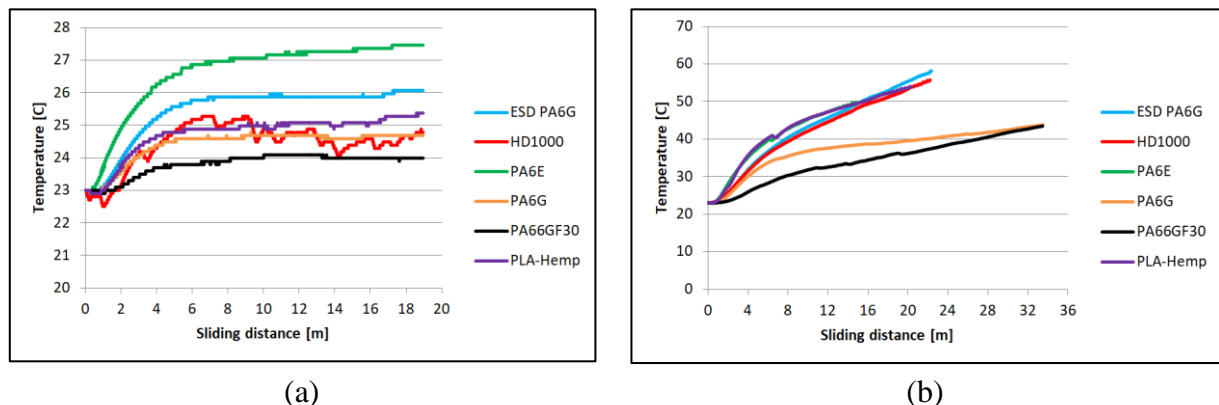


Fig. 4.27. The relation between the temperature evolution and sliding distance for several polymer types on P60 abrasive clothing. (a) lowest applied pv, (b) highest applied pv

#### 4. Results

Fig. 4.28 shows the P150 results: for temperature evaluation in the function of sliding distance of the materials used.

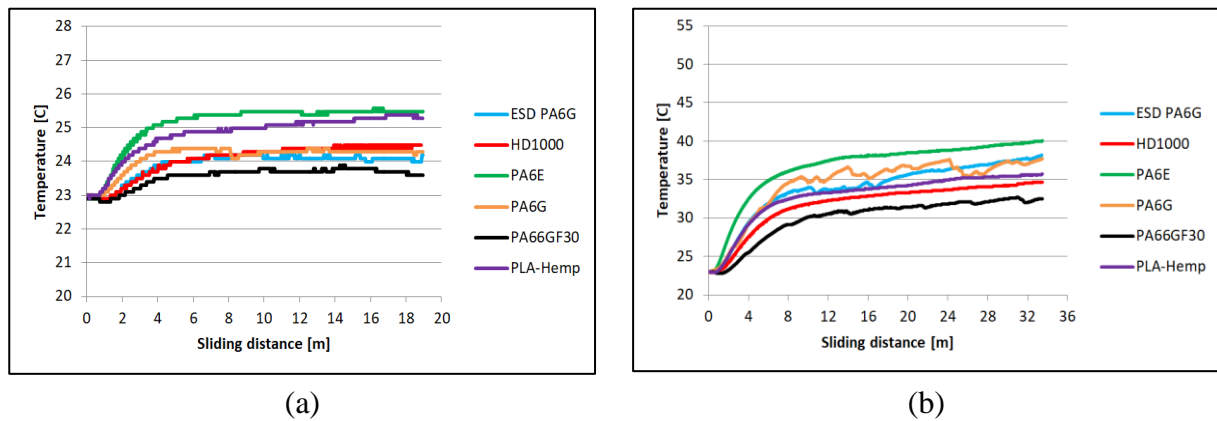


Fig. 4.28. The relation between the temperature and sliding distance for several polymer types on P150 abrasive clothing. a) lowest applied pv, b) highest applied pv

Table 4.8. The thermal properties of the materials used

	PA6E	PA6G ESD	PA6G	HD1000	PA66GF30
Thermal conductivity (W/ (K.m))	0.37	0.29	0.38	0.41	0.39
Melting temperature (°C)	220	216	216	135	260
Glass transition temperature (°C)	45		40		48
Specific heat (J/(g.K))	1.7		1.7	1,9	1.2
Coefficient of linear thermal expansion (CLTE): 23 - 60°C (m/(m.K)x10 <sup>-5</sup> )	12		12	150	5
Coefficient of linear thermal expansion (CLTE): 23 - 100°C (m/(m.K)x10 <sup>-5</sup> )	13		12	230	5
Max. allowable service temperature in air, short term (°C)	160	170	170	130	170
Max. allowable service temperature in air, long term (°C)	100	110	100	80	110
Min. allowable service temperature in air, long term (°C)	- 40	-40	- 40	- 250	- 20
Heat deflection temperature (°C)	75	100	95	80	150

As shown in the Figs. 4.27 and 4.28, PA6E recorded the highest temperatures, while PA66GF30 the lowest temperature, which can not be explained by the similar thermal properties shown in Table 4.8. However, it is a fact that PA6E has the lowest heat deflection temperature, high specific heat. The resulted temperature evolution a much more complex phenomenon in accordance with Archard's friction theory, the transformation of energy dissipated in the contact zone, where the shear of adhesion at actual contact and the viscoelastic behavior of microgeometric deformation together result in the generation of heat. The slightly different thermal conductivity of the polymers then affects the value of the temperature curves determined by the measurement.

#### 4.1.6. Comparing the materials for friction force

The extremes of test conditions (maximum and minimum loads and speeds, numbered as 1, 6, 7, 12 in Table 3.4) on two types of abrasive clothes are shown in Figs. 4.29 and 4.30 for the friction force. The other cases will be shown in the Appendix 7.

Fig. 4.29 shows the P60 results: for friction force in the function of sliding distance of the materials used.

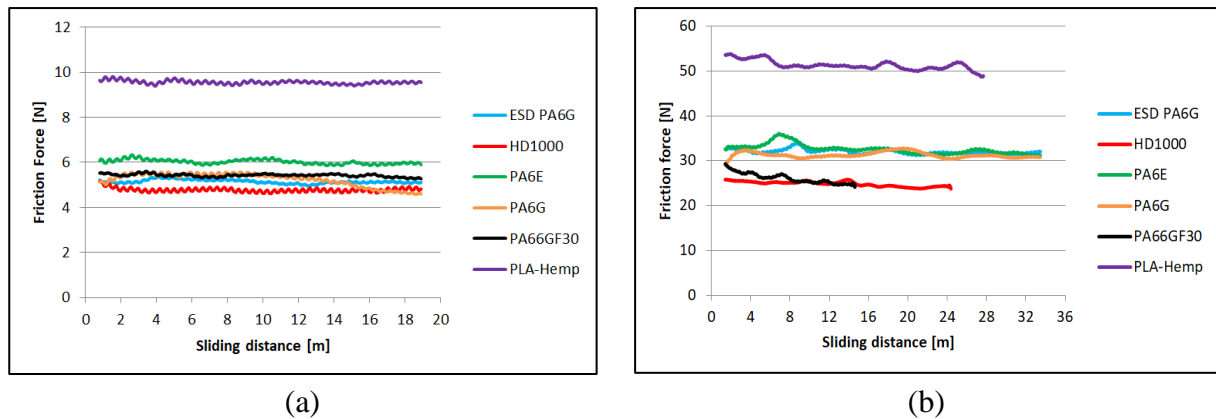


Fig. 4.29. The relation between the friction force and sliding distance for several polymer types on P60 abrasive clothing. a) lowest applied pv, b) highest applied pv

Fig. 4.30 shows the P150 results: for friction force in the function of sliding distance for the materials used.

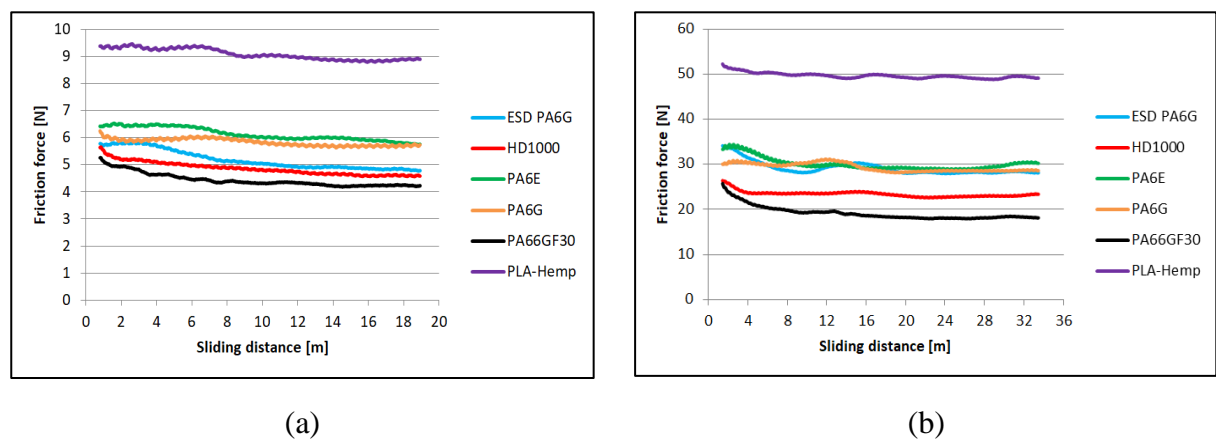


Fig. 4.30. The relation between the friction force and sliding distance for several polymer types on P150 abrasive clothing. a) lowest applied pv, b) highest applied pv

In general it is clear that, the friction force of the engineering plastics were almost close to each other, the bio-composite material (PLA-HF) had higher friction resistance continuously during the measurements. The main reason of this behavior is due to hemp fibres (Fig. 4.31) arising on the cut contact zone resulting an extra force for cutting effects.

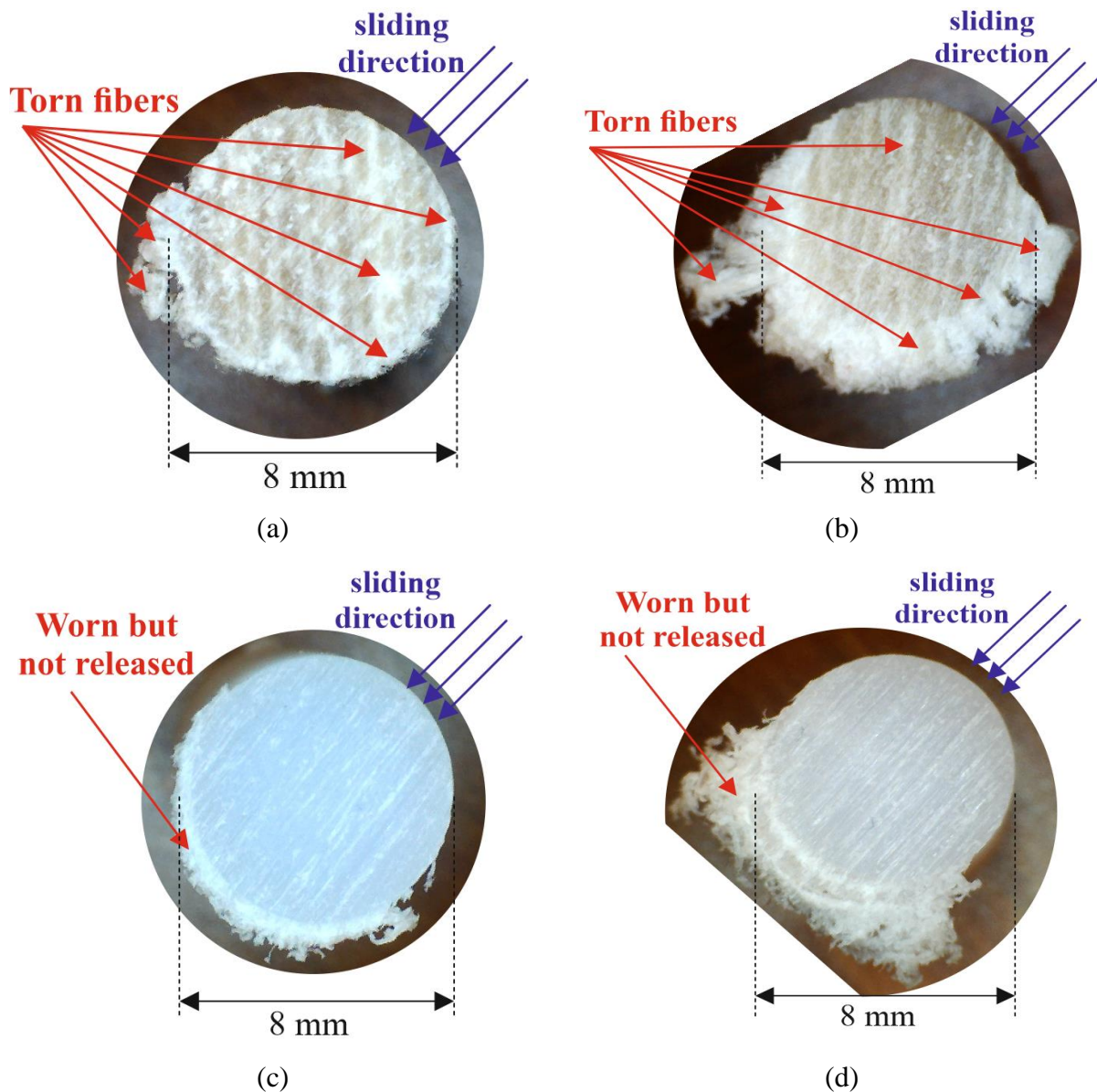


Fig. 4.31. A zoom photo on the worn surfaces for the PLA-HF and UHMW-PE HD1000  
 a) PLA-HF (condition no. 1) , b) PLA-HF (condition no. 6)  
 c) UHMW-PE HD1000 (condition no. 1) , d) UHMW-PE HD1000 (condition no. 6 Table 3.4.)

#### 4.1.7. Abrasive wear against dimensionless parameters of mechanical properties

Based on the mechanical properties of the materials used (Tables 3.1 and 3.3), ten dimensionless numbers were derived, which can characterize each polymers. Taken the wear values of on-line wear curves (obtained at the last measurable point in all test systems for all materials) summarized in Table 4.6, the connection with the dimensionless numbers can be investigated. However, the whole project focuses on 6 selected polymers, it is clear that the 4 polyamide types can perform clear trends at this type of evaluation and many new results were thus revealed.

The wear values taken from the end region of the tests, that were plotted against the dimensionless numbers of the materials, can offer connections within the polyamide family, regardless of whether they are natural or composite. Typical trends are shown in Figs. (4.32 – 4.41) based on the wear values taken from test system no. 7.

## 4. Results

### 1. Wear evaluation against $H/E$

The calculated quotients (*hardness / elasticity modulus*) are in Table 4.9.

Table 4.9. The H/E values for the materials used

The dimensionless number	PA6G	PA6E	PA66GF30	UHMW-PE HD1000	PA6G ESD	PLA-HF
$\frac{H}{E}$	0.0034	0.0030	0.0023	0.0100	0.0028	0.0004

Focusing on the polyamides in Table 4.9 the decreasing order of  $\frac{H}{E}$  values were as follows (PA6G - PA6E - PA6G ESD - PA66GF30), this order is the exact opposite order of the highest wear values that were shown in 4.1.4. As a result, there is an inverse relation between H/E and the wear. By increasing the values of H/E the wear is increasing.

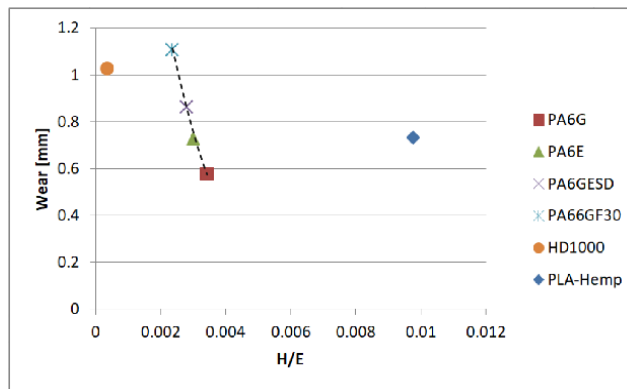


Fig. 4.32. Typical relation between wear at the last measurable point of test and  $\frac{H}{E}$  dimensionless number combined from mechanical properties

Fig. 4.32 shows that the polyamide family performed a decreasing trend as a relation with  $\frac{H}{E}$ , while both the PLA-HP and UHMW-PE HD1000 were out of this trend.

### 2. Wear evaluation against $\frac{\sigma_y E}{\sigma_M H}$

The calculated quotients (*combined tensile performance / combined bulk-surface stiffness*) are in Table 4.10.

Table 4.10. The  $\frac{\sigma_y E}{\sigma_M H}$  values for the materials used

The dimensionless number	PA6G	PA6E	PA66GF30	UHMW-PE HD1000	PA6G ESD	PLA-HF
$\frac{\sigma_y E}{\sigma_M H}$	281	327.5	427.0083	102.3474	357.58	2758.97

From the Table 4.10, the order of  $\frac{\sigma_y E}{\sigma_M H}$  values were as follows (PA66GF30 - PA6G ESD - PA6E - PA6G), this order is the exact same order of the highest wear values that were shown in 4.1.4.



## 4. Results

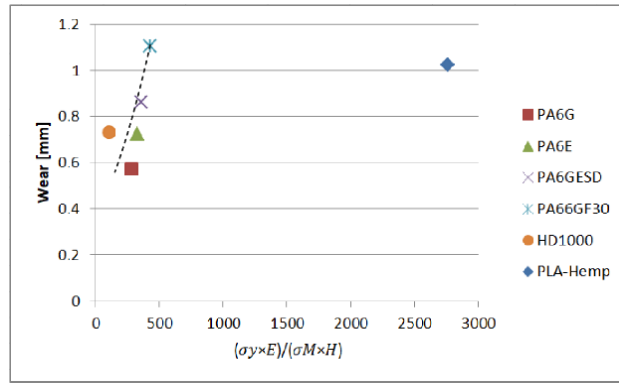


Fig. 4.33. Typical relation between wear at the last measurable point of test and  $\frac{\sigma_y E}{\sigma_M H}$  dimensionless number combined from mechanical properties

Fig. 4.33 shows that the polyamide family and UHMW-PE HD1000 performed an increasing trend as a relation with  $\frac{\sigma_y E}{\sigma_M H}$ , while PLA-HP was out of this trend.

### 3. Wear evaluation against $\sigma_y H / \sigma_M E$

The calculated quotients (*combined surface strength / combined strength-stiffness*), which contain the same material properties like in no. 2 are in Table 4.11. This type of combination  $\frac{\sigma_y H}{\sigma_M E}$  better shows the trend of the polyamides and the differences between the tested materials (Fig. 4.34). The polyamides' values order follows (PA6G - PA6E - PA6G ESD - PA66GF30) the exact invers proportionality with the wear. By increasing the values of  $\frac{\sigma_y H}{\sigma_M E}$  the wear will be lower.

Table 4.11. The  $\frac{\sigma_y H}{\sigma_M E}$  values for the materials used

The dimensionless number	PA6G	PA6E	PA66GF30	UHMW-PE HD1000	PA6G ESD	PLA-HF
$\frac{\sigma_y H}{\sigma_M E}$	0.003306	0.002976	0.002342	0.009771	0.002797	0.000362

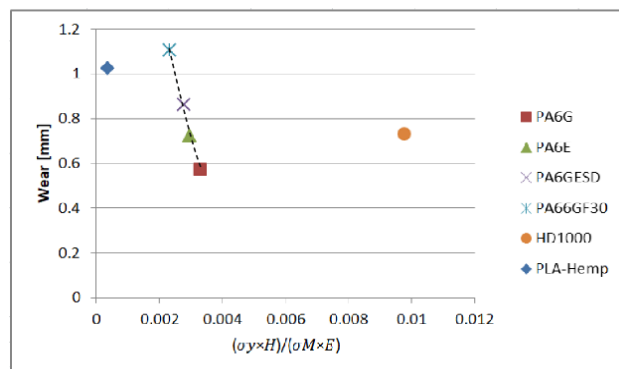


Fig. 4.34. Typical relation between wear at the last measurable point of test and  $\frac{\sigma_y H}{\sigma_M E}$  dimensionless number combined from mechanical properties

Fig. 4.34 shows that the polyamide family performed a decreasing trend for wear with increasing  $\frac{\sigma_y H}{\sigma_M E}$ , while both the PLA-HP and UHMW-PE HD1000 were out of this type of plotted trend.

4. Wear evaluation against  $\sigma_F \cdot \sigma_y / \sigma_M \cdot H$

$\frac{\sigma_F \sigma_y}{\sigma_M H}$  is the ratio between: *combined tensile-flexural strength / combined strength-hardnes*, Calculated values are put in Table 4.12.

Table 4.12. The  $\frac{\sigma_F \sigma_y}{\sigma_M H}$  values for the materials used

The dimensionless number	PA6G	PA6E	PA66GF30	UHMW-PE HD1000	PA6G ESD	PLA-HF
$\frac{\sigma_F \sigma_y}{\sigma_M H}$	8.752	9.927	10.481	2.866	9.118	11.019

From the Table 4.12, the order of  $\frac{\sigma_F \sigma_y}{\sigma_M H}$  values show that only three polyamides (PA66GF30 - PA6E - PA6G) followed the normal wear order (4.1.4), however, linear approach can be applied for all polyamides and for the PLA-HF as well

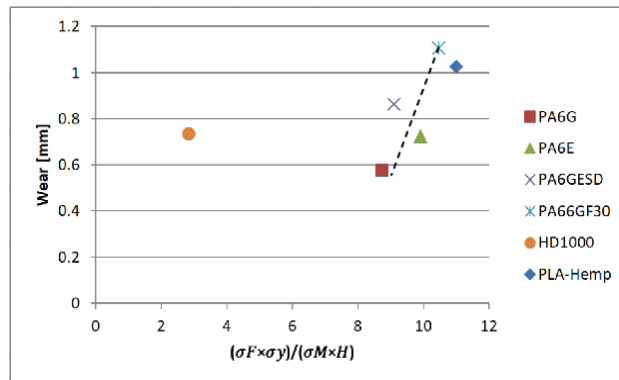


Fig. 4.35. Typical relation between wear at the last measurable point of test and  $\frac{\sigma_F \sigma_y}{\sigma_M H}$  dimensionless number combined from mechanical properties

Fig. 4.35 shows that the polyamide family and PLA-HF showed an increasing trend as a relation with  $\frac{\sigma_F \sigma_y}{\sigma_M H}$ , while UHMW-PE HD1000 was out of this trend.

5. Wear evaluation against  $E / \sigma_C$

$\frac{E}{\sigma_C}$  is the ratio between: *elasticity modulus / compression strength*. Calculated values are put in Table 4.13.

Table 4.13. The  $\frac{E}{\sigma_C}$  values for the materials used

The dimensionless number	PA6G	PA6E	PA66GF30	UHMW-PE HD1000	PA6G ESD	PLA-HF
$\frac{E}{\sigma_C}$	159.091	173.684	220.000	166.667	173.913	44233.38

From the Table 4.13, the order of  $\frac{E}{\sigma_C}$  values of polyamides were as follows (PA66GF30 - PA6G ESD - PA6E - PA6G), this order is exactly the same order of the highest wear values that were shown in 4.1.4.

## 4. Results

As a result, there is proportional relation between  $\frac{E}{\sigma_C}$  and the wear. By increasing the values of  $\frac{E}{\sigma_C}$  the wear is also increasing.

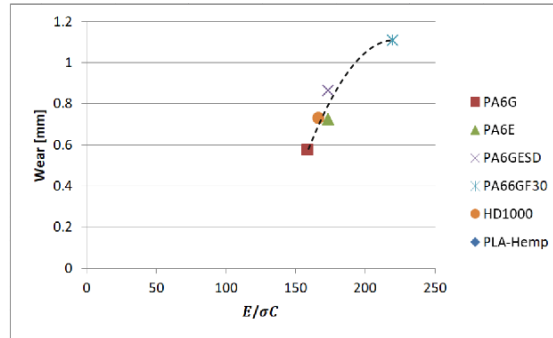


Fig. 4.36. Typical relation between wear at the last measurable point of test and  $\frac{E}{\sigma_C}$  dimensionless number combined from mechanical properties

Fig. 4.36 shows that the polyamide family and UHMW-PE HD1000 offered the increasing trend as a relation with  $\frac{E}{\sigma_C}$ , while PLA-HP was completely out and faraway of this trend.

### 6. Wear evaluation against $\sigma_F/\sigma_C$

$\frac{\sigma_F}{\sigma_C}$  is the ratio between: *flexural strength / compression strength*. Calculated values are put in Table 4.14.

Table 4.14. The  $\frac{\sigma_F}{\sigma_C}$  values for the materials used

The dimensionless number	PA6G	PA6E	PA66GF30	UHMW-PE HD1000	PA6G ESD	PLA-HF
$\frac{\sigma_F}{\sigma_C}$	4.955	5.263	5.400	4.667	4.435	176.662

From the Table 4.14, the order of  $\frac{\sigma_F}{\sigma_C}$  values show that only three polyamides (PA66GF30 - PA6E - PA6G, just like in no. 4) followed the normal wear order (4.1.4), however, the PA6G ESD is exception.

As a result, there is proportional relation between  $\frac{\sigma_F}{\sigma_C}$  and the wear. In another words, by increasing the values of  $\frac{\sigma_F}{\sigma_C}$  the wear can increase.

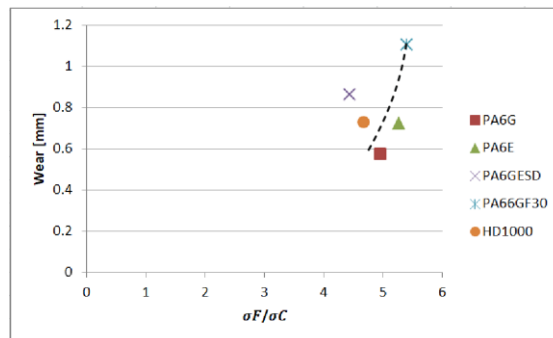


Fig. 4.37. Typical relation between wear at the last measurable point of test and  $\frac{\sigma_F}{\sigma_C}$  dimensionless number combined from mechanical properties

Fig. 4.37 shows that the mentioned three polyamides and UHMW-PE HD1000 followed an increasing trend as a relation with  $\frac{\sigma_F}{\sigma_C}$ , while PLA-HF was completely out and faraway of this trend.

7. Wear evaluation against  $H\varepsilon_B/\sigma_y$

$\frac{H\varepsilon_B}{\sigma_y}$  the ratio between: *combined Hardness-strain capability / Yield strength* Calculated values are put in Table 4.15.

Table 4.15. The  $\frac{H\varepsilon_B}{\sigma_y}$  values for the materials used

The dimensionless number	PA6G	PA6E	PA66GF30	UHMW-PE HD1000	PA6G ESD	PLA-HF
$\frac{H\varepsilon_B}{\sigma_y}$	19.50	16.57	1.840	58.62	0.746	0.122

From the Table 4.15, the order of  $\frac{H\varepsilon_B}{\sigma_y}$  values were as follows (PA6G - PA6E - PA6G ESD), this order is the exact opposite order of the highest wear values that were shown in 4.1.4.

As a result, there is an inverse relation between  $\frac{H\varepsilon_B}{\sigma_y}$  and the wear. By increasing the values of  $\frac{H\varepsilon_B}{\sigma_y}$  the wear will decrease.

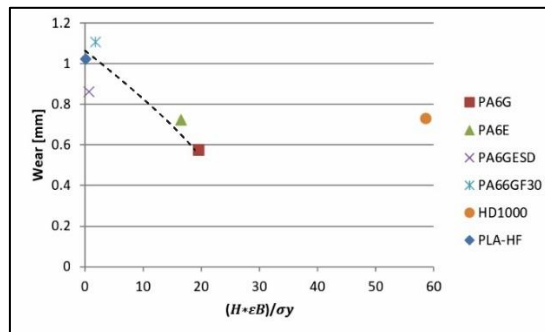


Fig. 4.38. Typical relation between wear at the last measurable point of test and  $\frac{H\varepsilon_B}{\sigma_y}$  dimensionless number combined from mechanical properties

Fig. 4.38 shows that the polyamide family (except PA6G ESD) and PLA-HF showed a decreasing trend as a relation with  $\frac{H\varepsilon_B}{\sigma_y}$ , while UHMW-PE HD1000 is out of that.

8. Wear evaluation against  $\sigma_C\varepsilon_B/\sigma_M$

$\frac{\sigma_C\varepsilon_B}{\sigma_M}$  the ratio between: *combined compression - strain capability / tensile strength*. Calculated values are put in Table 4.156.

Table 4.16. The  $\frac{\sigma_C\varepsilon_B}{\sigma_M}$  values for the materials used

The dimensionless number	PA6G	PA6E	PA66GF30	UHMW-PE HD1000	PA6G ESD	PLA-HF
$\frac{\sigma_C\varepsilon_B}{\sigma_M}$	34.458	31.266	3.571	36	1.533	0.008

## 4. Results

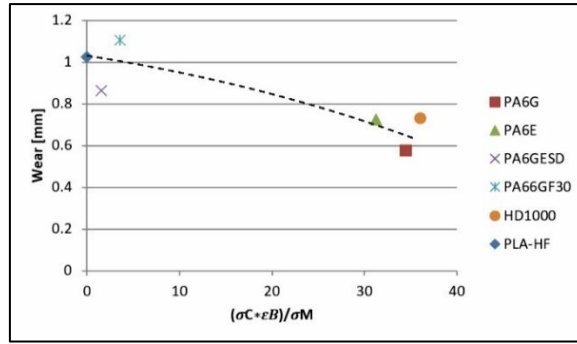


Fig. 4.39. Typical relation between wear at the last measurable point of test and  $\frac{\sigma_C \epsilon_B}{\sigma_M}$  dimensionless number combined from mechanical properties

From the Table 4.16, the order of  $\frac{\sigma_C \epsilon_B}{\sigma_M}$  values were as follows (PA6G - PA6E - PA6G ESD) for polyamides, this order is the exact opposite order of the highest wear values that were shown in 4.1.4.

Fig. 4.39 shows a loosen trend for all the examined polymers where the increasing  $\frac{\sigma_C \epsilon_B}{\sigma_M}$  can result lower wear.

### 9. Wear evaluation against $\sigma_y / \sigma_C \epsilon_B$

$\frac{\sigma_y}{\sigma_C \epsilon_B}$  the ratio between: *yield strength / combined compression - strain capability* Calculated values are put in Table 4.17.

Table 4.17. The  $\frac{\sigma_y}{\sigma_C \epsilon_B}$  values for the materials used

The dimensionless number	PA6G	PA6E	PA66GF30	UHMW-PE HD1000	PA6G ESD	PLA-HF
$\frac{\sigma_y}{\sigma_C \epsilon_B}$	0.028	0.032	0.280	0.0278	0.652	131.615

From the Table 4.17, the order of  $\frac{\sigma_y}{\sigma_C \epsilon_B}$  values among the polyamides were as follows (PA6G ESD - PA6E - PA6G), this is exactly the same order like the wear values shown in 4.1.4.

As a result, there is proportional relation between  $\frac{\sigma_y}{\sigma_C \epsilon_B}$  and the wear. By increasing the values of  $\frac{\sigma_y}{\sigma_C \epsilon_B}$  the wear is also higher.

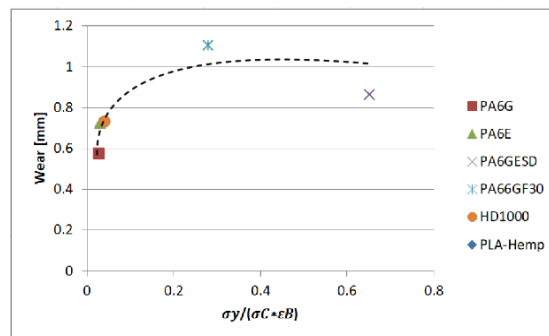


Fig. 4.40. Typical relation between wear at the last measurable point of test and  $\frac{\sigma_y}{\sigma_C \epsilon_B}$  dimensionless number combined from mechanical properties

Fig. 4.40 shows a trend where beside the polyamides the UHMW-PE HD1000 followed a saturation-type curve. The PLA-HF is out of that plot.

#### 10. Wear evaluation against $\sigma_F H / \sigma_M E$

$\frac{\sigma_F H}{\sigma_M E}$  the ratio between: *combined Flexural performance / combined bulk-surface stiffness*.

Calculated values are put in Table 4.18.

Table 4.18. The  $\frac{\sigma_F H}{\sigma_M E}$  values for the used materials

The dimensionless number	PA6G	PA6E	PA66GF30	UHMW-PE HD1000	PA6G ESD	PLA-HF
$\frac{\sigma_F H}{\sigma_M E}$	0.00450	0.00382	0.00347	0.01080	0.00380	0.00081

From the Table 4.18, the order of  $\frac{\sigma_F H}{\sigma_M E}$  values among the polyamides were as follows (PA6G - PA6E - PA6G ESD - PA66GF30), this order is the exact opposite order of the wear trend shown in 4.1.4.

As a result, there is an inverse relation between  $\frac{\sigma_F H}{\sigma_M E}$  and the wear. By increasing the values of  $\frac{\sigma_F H}{\sigma_M E}$  the wear is decreasing.

Fig. 4.41 shows that the polyamide family followed a decreasing trend as a relation with  $\frac{H}{E}$ , while both of PLA-HP and UHMW-PE HD1000 were out of this trend.

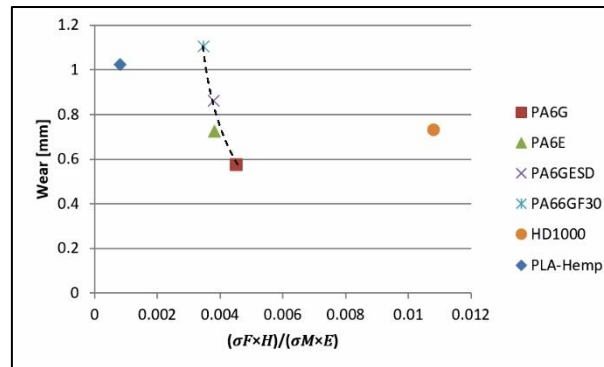


Fig. 4.41. Typical relation between wear at the last measurable point of test and  $\frac{\sigma_F H}{\sigma_M E}$  dimensionless number combined from mechanical properties

From Figs. (4.32 - 4.41) it can be concluded, that the wear resistance order for polyamides described in 4.1.4 can be well approached with the combined dimensionless numbers, at some cases the UHMW-PE HD1000 and PLA-HF could be involved into the same evaluating trends as written in the following:

<b>Proportional relation</b>	<ul style="list-style-type: none"> <li>• There are proportional relations between the wear values of all the tested polyamide types (PA66GF30, PA6G ESD, PA6G and PA6E) and <math>\frac{\sigma_y E}{\sigma_M H}</math>, as well as <math>\frac{\sigma_y}{\sigma_C \varepsilon_B}</math>. By increasing dimensionless number values a higher wear value was measured.</li> <li>• In case of <math>\frac{E}{\sigma_C}</math> there is proportional relation with wear values concerning all the polyamides and UHMW-PE HD1000 together.</li> <li>• Also there are proportional relations between the wear values of three polyamides (PA66GF30, PA6G and PA6E) and <math>\frac{\sigma_F}{\sigma_C}</math>. The trend is followed by the UHMW-PE HD1000, too.</li> <li>• <math>\frac{\sigma_F \sigma_y}{\sigma_M H}</math> offers such a proportional relation with wear, where 5 materials follow the trend-line except for UHMW-PE HD100.</li> </ul>
<b>Inverse relation</b>	<ul style="list-style-type: none"> <li>• There are inverse relations between values <math>\frac{H}{E}</math>, <math>\frac{\sigma_y H}{\sigma_M E}</math>, <math>\frac{\sigma_F H}{\sigma_M E}</math> and the wear of polyamides (PA66GF30, PA6G ESD, PA6G and PA6E). By increasing dimensionless number values a lower wear value was measured.</li> <li>• There are inverse relations between values <math>\frac{H \varepsilon_B}{\sigma_y}</math> and the wear of three polyamides (PA6G, PA6E and PA6G ESD), the trend was followed by PLA-HF, too. By increasing the dimensionless number value, a lower wear value was measured.</li> <li>• Calculating <math>\frac{\sigma_C \varepsilon_B}{\sigma_M}</math>, loosen inverse relation was found concerning all the tested six polymers.</li> </ul>

These findings are in accordance with the previous publications (Rajesh et al., 2001, 2002; Kumar and Panneerselvam, 2016) of the main mechanical properties. However, the combined dimensionless numbers analyzed above, were not studied in such details, and even the new findings between wear and combined properties valid for polyamides and UHMW-PE together, have not been published yet.

#### 4.1.8. Multiple linear regression analysis

As it is introduced in 3.6. large amount of data was evaluated with the statistical models developed. Multiple linear regression models analyzed the impact of material properties and test system characteristics on wear, friction force, heat generation and change of 3D topography, on both P60 and P150 abrasive surfaces. In the test systems the sliding distance “s”, the load “ $F_N$ ”, and the sliding velocity “v”, were considered as independent variables, as well as the material properties and the indicators formed from them. According to the following:

##### Wear, using P60 abrasive

The best fitting model was Eq. 4.1:

$$\text{wear} = a_0 + a_1 s + a_2 F_N + a_3 \cdot \frac{\sigma_y}{\sigma_C \varepsilon_B} + a_4 H \quad (4.1)$$

The  $F$ -value of the model was  $9.619 \cdot 10^4$  and  $p < 0.001$ , thus this model is relevant. The coefficients of the model are summarized in Table 4.19. For this model, the goodness-of-fit is

$R^2 = 0.831$ . The duration of the experiment has the biggest effect on the wear of the test sample, while the material parameters e.g.  $\frac{\sigma_y}{\sigma_c \varepsilon_B}$  have some effect.

Table 4.19. Coefficients of the regression model with P60 abrasive

Model	coefficient	Standardized regression coefficient, Beta	t	p
Constant	-0.387		-33	<0.001
$s$	0.125	0.707	539	<0.001
$F_N$	0.501	0.599	457	<0.001
$\frac{\sigma_y}{\sigma_c \varepsilon_B}$	0.010	0.341	239	<0.001
$H$	-0.066	-0.092	-65	<0.001

#### Wear, using P150 abrasive

The best fitting model was Eq. 4.2:

$$\text{wear} = a_0 + a_1 s + a_2 F_N + a_3 v + a_4 \cdot \frac{\sigma_y}{\sigma_c \varepsilon_B} \quad (4.2)$$

the  $F$ -value of the model was  $2.112 \cdot 10^5$  and  $p < 0.001$ , thus this model is relevant. The coefficients of the model are summarized in Table 4.20.

Table 4.20. Coefficients of the regression model with P150 abrasive

Model	coefficient	Standardized regression coefficient, Beta	t	p
Constant	-0.157		6	<0.001
$s$	0.063	0.756	23	<0.001
$F_N$	0.260	0.598	-4	<0.001
$v$	-5.987	-0.105	-9	<0.001
$\frac{\sigma_y}{\sigma_c \varepsilon_B}$	0.003	0.176	-5	<0.001

For this model the goodness-of-fit is  $R^2 = 0.890$ . The duration of the experiment has the biggest effect on the wear of the test body, while the material parameters  $\frac{\sigma_y}{\sigma_c \varepsilon_B}$  have some effect.

#### Abrasive friction force, P60

Without the table of coefficients of the regression model, in case of P60 abrasive (4.3): the best fitting model was Eq. 4.3:

$$F_f = -1.427 + 10.351 F_N - 0.022 \varepsilon_B + 0.243 \cdot \frac{\sigma_c}{\sigma_y \varepsilon_B} \quad (4.3)$$

The  $F$ -value of the model is  $3.370 \cdot 10^6$  and  $p < 0.001$ , thus the model is relevant. For this model the goodness-of-fit is  $R^2 = 0.99$ . The load has the biggest effect on the resultant friction force, while the material parameters  $\frac{\sigma_F \sigma_y}{\sigma_M H}$  and  $H$  minor effects.



Abrasive friction force, P150

With P150 abrasive, the best fitting model was Eq. 4.4

$$F_f = -4.951 - 0.084s + 9.051F_N + 1.424H - 1.133 \cdot \frac{\sigma_F \sigma_y}{\sigma_M H} \quad (4.4)$$

the  $F$ -value of the model is  $5.207 \cdot 10^4$  and  $p < 0.001$ , thus the model is relevant. For this model the goodness-of-fit is  $R^2 = 0.983$ . The load has the biggest effect on the resultant friction force, while the material parameters  $\frac{\sigma_F \sigma_y}{\sigma_M H}$  and  $H$  have some effect.

Friction heat change, P60

Concerning the friction heat evolution on P60 abrasive clothes measured close to contact inside the polymer pin, the best fitting model was Eq. 4.5:

$$\Delta T = 17.502 + 0.349s + 2.618F_N + 107.796v + 0.229H - 0.163\sigma_F - 1205.488 \cdot \frac{\sigma_F H}{\sigma_M E} - 0.108 \cdot \frac{H \epsilon_B}{\sigma_y} \quad (4.5)$$

the  $F$ -value of the model was 3654 and  $p < 0.001$ , thus the model is relevant. For this model the the goodness-of-fit is  $R^2 = 0.728$ .  $\sigma_F$  has a very big effect, while the load, distancia and  $\frac{\sigma_F H}{\sigma_M E}$  has a moderate effect on the temperature increase, during sliding.

Friction heat change, P150

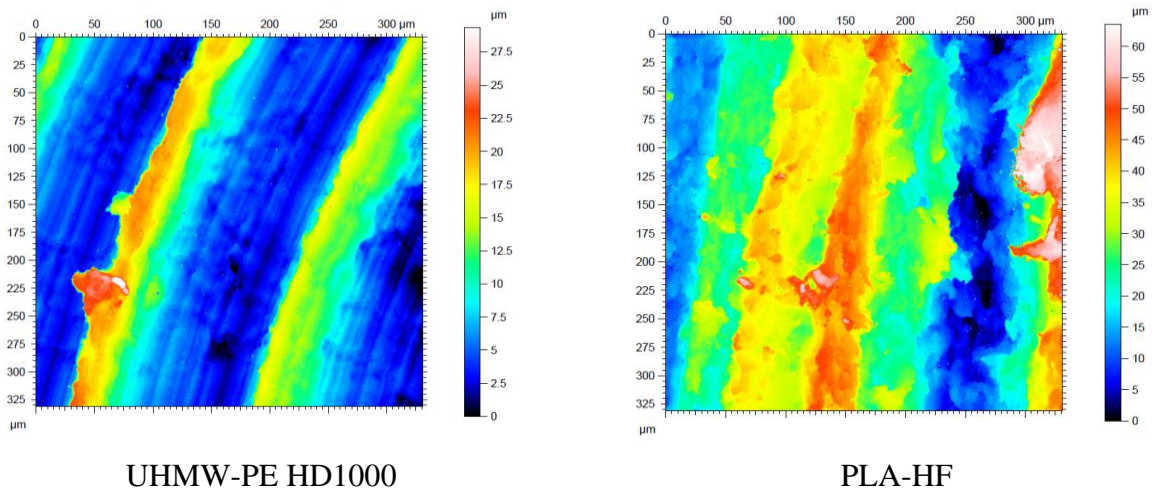
With P150 abrasive, the heat generation is approximated as Eq. 4.6:

$$\Delta T = 8.787 + 0.158s + 1.535F_N + 70.251v + 0.011\epsilon_B - 1.009H - 723.359 \cdot \frac{\sigma_F H}{\sigma_M E} \quad (4.6)$$

the  $F$ -value of the model was  $6.797 \cdot 10^4$  and  $p < 0.001$ , thus the model is relevant. For this model the goodness-of-fit is  $R^2 = 0.794$ . The load,  $H$  and  $\frac{\sigma_F H}{\sigma_M E}$  have the biggest effect on the temperature change, that was measured.

*4.1.9. 3D microscopy results and regression models*

Concerning the change of the polymer surfaces, white light 3D microscopy was used as detailed in 3.4. Table 4.21 gives a summary of the original 3D surface characteristics and Fig. 4.42 shows the surface 3D topography of the materials before testing.



## 4. Results

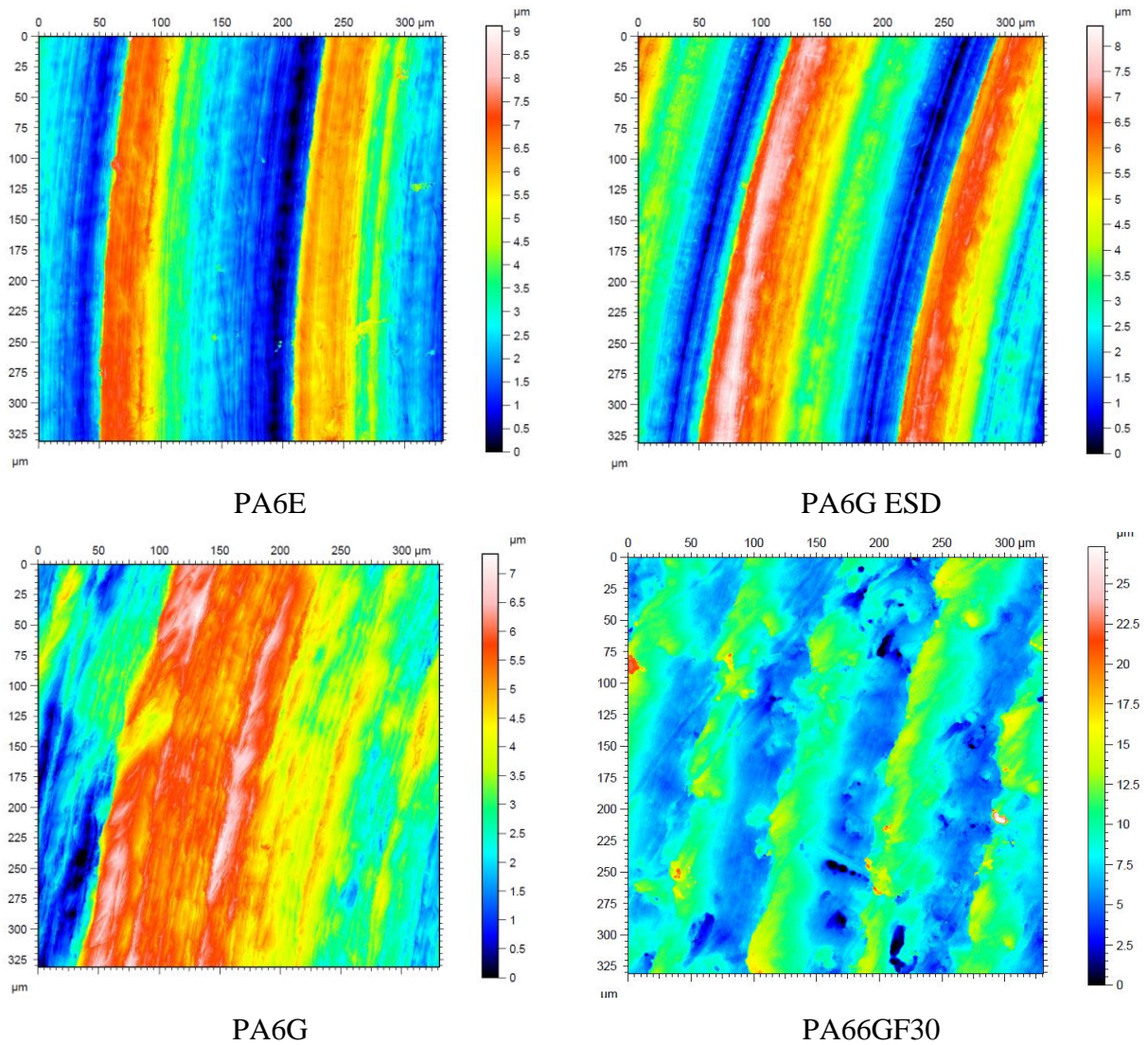


Fig. 4.42. Microscopic visualization of the surface 3D topography of the materials before testing

Table 4.21. Original surface characteristics of the polymers tested

	<b>HD1000</b>	<b>PLA-HF</b>	<b>PA6E</b>	<b>PA6G ESD</b>	<b>PA6G</b>	<b>PA66GF30</b>
Sq (μm)	5.3	13.1	1.9	1.9	1.5	2.6
Ssk	1.0	0.1	0.4	0.2	-0.2	0.5
Sku	3.0	2.3	1.9	1.9	2.0	4.1
Sp (μm)	21.6	36.0	5.7	4.6	3.4	18.9
Sv (μm)	7.6	27.4	3.3	3.7	3.9	8.3
Sz (μm)	29.3	63.5	9.1	8.3	7.3	27.2
Sa (μm)	4.4	10.8	1.6	1.7	1.3	2.1

Figs. 4.43 and 4.44 show the microscopic visualization of the change in the surface 3D topography of the tested materials on P60 and P150 abrasive, when applying the top speed and load (No. 6 and 12 conditions, Table 3.4). Other highlighted cases will be shown in the Appendix 8.

## 4. Results

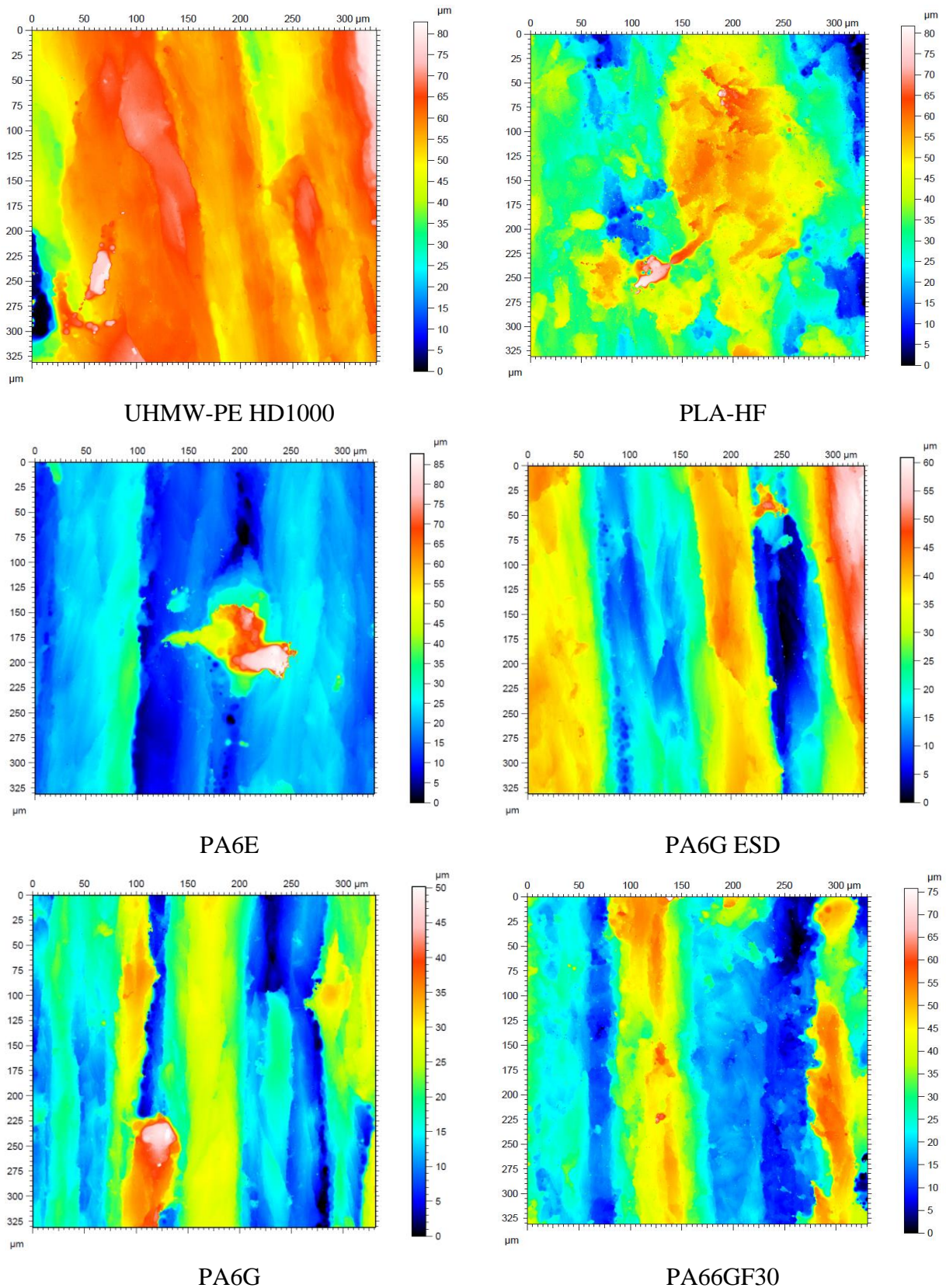


Fig. 4.43. Microscopic visualization of the change in the surface 3D topography of the tested materials on P60 abrasive, when applying the top speed and load (No. 6 condition, Table 3.4)

In Fig. 4.43 it is clearly seen that the tough HD1000 suffered essential deformation, new hills on the surfaces, while the less tough PA66GF30 really presented new, deep and wide grooves. That appearance is in accordance with the deformation capability of the materials.

## 4. Results

Comparing Figs. 4.42 and 4.43 and the characteristics of the parameters, it is clear that by the end of the pin-on-plate test, the original machining marks of the surfaces had completely disappeared. For all cases, the results are the deformed-, cut and polished surfaces of differing degrees, with moderate hills and valleys.

Fig. 4.44 shows the microscopic visualization of the change in the surface 3D topography of the tested materials on P150 abrasive, when applying the top speed and load (No. 12 condition, Table 3.4)

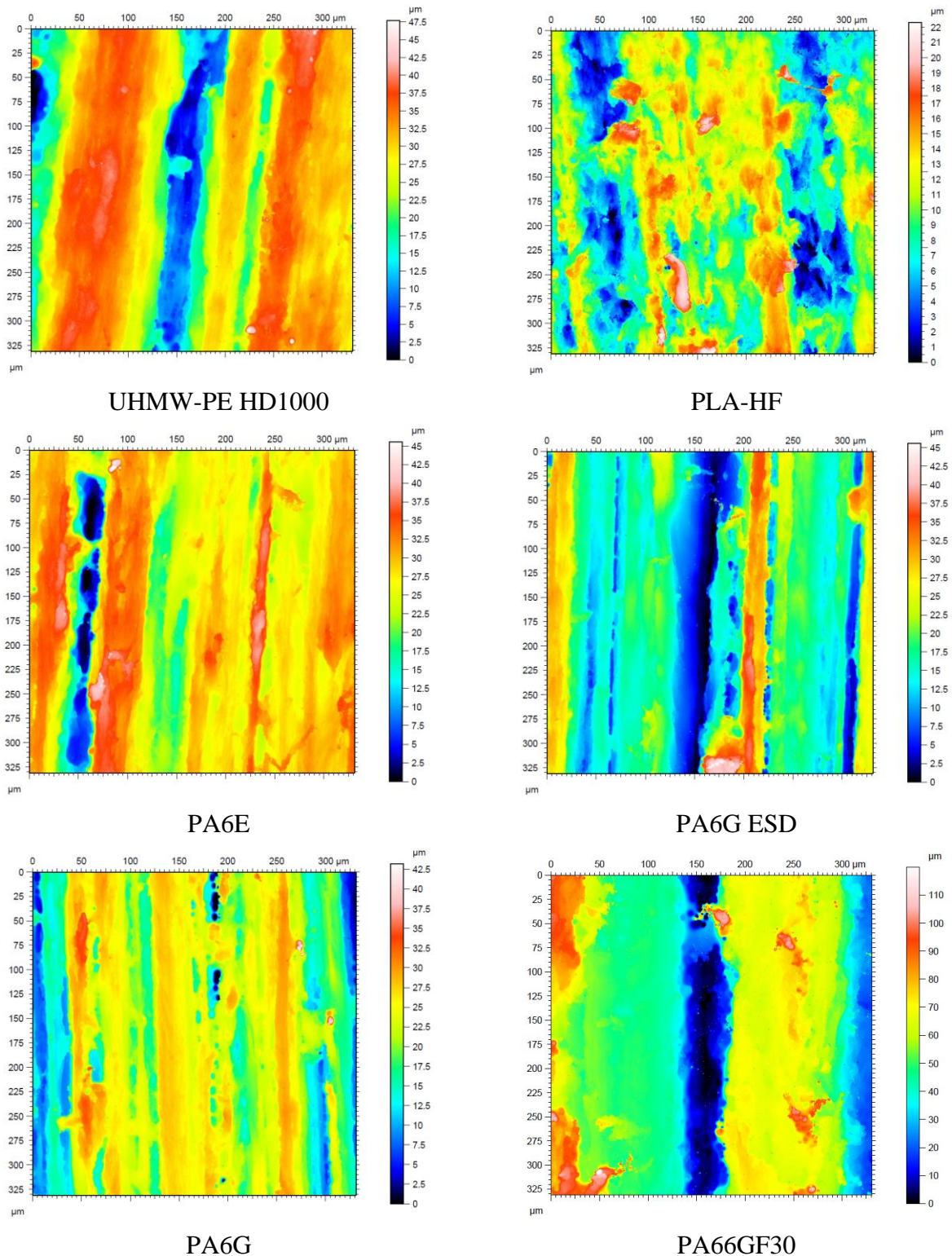


Fig. 4.44. Microscopic visualization of the change in the surface 3D topography of the tested materials on P150 abrasive, when applying the top speed and load (No. 12 condition, Table 3.4)

#### 4. Results

In Fig. 4.44 it is clear that similarly to the P60 results, the tough HD1000 and PA6E suffered essential deformation, new hills on the surfaces, while the less tough PA66GF30 and PA6G ESD really presented missing materials with new and deep, wide grooves.

Comparing Figs. 4.43 and 4.44 one can conclude that the visualization of the damage is similar, however in different extent. The differences can be expressed in percentage on the base of 3D surface parameters. The change of the surface parameters were systematically measured and evaluated for the selected test conditions (extremes cases, shown in Table 3.4), and the data was analyzed by the multiple regression models. The change of the parameters in the system condition No. 6 can be seen in Table 4.22.

Table 4.22. Surface characteristics after the tests and the percentage change (%) (test condition No. 6)

	<b>HD1000</b>	<b>PLA-HF</b>	<b>PA6E</b>	<b>PA6G ESD</b>	<b>PA6G</b>	<b>PA66GF30</b>
<b>after the test</b>						
Sq ( $\mu\text{m}$ )	9.5	12.6	9.4	12.7	8.2	13.2
Ssk	-2.1	0.01	0.2	-0.004	0.3	0.5
Sku	12.4	2.8	3.6	2.1	2.8	2.2
Sp ( $\mu\text{m}$ )	25.9	45.4	27.9	33.5	31.5	49.1
Sv ( $\mu\text{m}$ )	56.8	36.2	30.6	27.3	18.6	26.5
Sz ( $\mu\text{m}$ )	82.7	81.6	58.5	60.8	50.1	75.7
Sa ( $\mu\text{m}$ )	6.3	10.1	7.0	11.1	6.7	11.1
<b>Change in %</b>						
Sq ( $\mu\text{m}$ )	80%	-4%	384%	540%	436%	396%
Ssk	-309%	-92%	-50%	-102%	-260%	0.22%
Sku	309%	17%	91%	13%	37%	-45%
Sp ( $\mu\text{m}$ )	20%	26%	385%	624%	827%	159%
Sv ( $\mu\text{m}$ )	644%	32%	813%	627%	373%	220%
Sz ( $\mu\text{m}$ )	182%	29%	542%	625%	583%	177%
Sa ( $\mu\text{m}$ )	43%	-6%	316%	552%	413%	408%

The above concluded visualization is supported by the numbers in Table 4.22. The tough UHMW-PE HD1000 and PA6E material performed essential deformation with increased parameters (Sp, Sv, Sz, Sa) beside decreased Skewness (Ssk) -meaning that the asperities, the surface material is elevated and deformed above the mean plane – and increased Kurtosis (Sku) meaning that the height distribution is more spiked due to the cutting effect. On the contrary, the more rigid PA66GF30 due to the cutting effects performed increased Skewness – the height distribution is skewed below the mean plane meaning essential wear – and decreased Kurtosis (Sku) resulting more indented portion on the surface. Very similar tendencies can be stated for the case of No. 12 test condition shown in Table 4.23. Other test cases results are summarized in Appendix 8.

#### 4. Results

The change of the parameters in the system condition No.12 can be seen in Table 4.23.

Table 4.23. Surface characteristics after the tests and the percentage change (%) in test condition No. 12

	<b>HD1000</b>	<b>PLA-HF</b>	<b>PA6E</b>	<b>PA6G ESD</b>	<b>PA6G</b>	<b>PA66GF30</b>
<b>after the test</b>						
Sq (μm)	8.8	3.9	6.7	7.8	6.1	6.1
Ssk	-1.1	-0.1	-1.5	0.3	-0.7	-0.7
Sku	3.3	2.6	6.4	3.1	3.0	3.0
Sp (μm)	20.1	12.5	18.4	28.3	21.9	21.9
Sv (μm)	27.6	9.8	27.2	17.3	21.3	21.3
Sz (μm)	47.7	22.3	45.5	45.6	43.2	43.2
Sa (μm)	7.0	3.2	4.7	5.9	5.0	5.0
<b>Change in %</b>						
Sq (μm)	66%	-70%	243%	290%	298%	129%
Ssk	-205%	-158%	-412%	26%	223%	-241%
Sku	9%	10%	232%	59%	42%	-28%
Sp (μm)	-7%	-65%	219%	511%	545%	16%
Sv (μm)	261%	-64%	709%	360%	440%	156%
Sz (μm)	63%	-65%	399%	443%	489%	58%
Sa (μm)	59%	-71%	176%	245%	282%	130%

The 3D surface data were analyzed by multiple linear regression models, too. The dependent variables were the 3D surface parameters, while the independent variables were the sliding distance, load, the calculated  $pv$ , the sliding velocity, the material properties and the derived dimensionless numbers from them. Concerning the results, in general, it can be said that for wear interface P60 the suitability varied between 0.25 and 0.47 and usually the only explanatory variable was the sliding distance, except in the case of Ssk, where instead of  $s$ ,  $\sigma_F$  appeared. It is important to note that for Sku there wasn't any suitable linear model for the process. This is mainly due to the high deviation of this parameter in the examined materials. The P60 abrasive surface acted as a real cutting one in almost mm scale, where the measurements of the standard parameters may start to fail. Regarding the case of the much smoother wear interface P150 for the 3D parameters Ssk, Sku and Sp the goodness-of-fit was low (0.2-0.4), but for the other ones it ranges from the mid to high domain, therefore the obtained models are presented below in detail.

#### Sq, P150

For Sq, the best fitting model among the possible ones is as Eq. 4.7.

$$Sq = 6.057 + 0.052s - 0.00014E \quad (4.7)$$

the  $F$ -value of the model was 15.989 and  $p = 0.001$ , thus the model is relevant. For this model the goodness-of-fit is  $R^2 = 0.804$ ,  $E$  has the highest effect on Sq.

#### Sv, P150

For Sv, the best fitting model among the possible ones is as Eq. 4.8.

$$Sv = 12.790 + 0.036s - 0.0003302E \quad (4.8)$$

the  $F$ -value of the model was 54.157 and  $p < 0.001$ , thus the model is relevant. For this model the goodness-of-fit is  $R^2 = 0.861$ ,  $E$  has a high effect on Sv.

#### Sz, P150

For Sz, the best fitting model among the possible ones is as Eq. 4.9.

$$Sz = 2.908 + 0.142s + 0.031 \cdot \frac{\sigma_F}{\sigma_c} \quad (4.9)$$

the  $F$ -value of the model was 12.960 and  $p < 0.001$ , thus the model is relevant. For this model the goodness-of-fit is  $R^2 = 0.552$ ,  $\frac{\sigma_F}{\sigma_c}$  has a highest effect on Sv.

#### Sa, P150

For Sa, the best fitting model among the possible ones is as Eq. 4.10.

$$Sa = 5.018 + 0.032s - 0.0001164E \quad (4.10)$$

the  $F$ -value of the model was 38.520 and  $p < 0.001$ , thus the model is relevant. For this model the goodness-of-fit is  $R^2 = 0.786$ ,  $E$  has the highest effect on Sa.

According to the results presented above, one can see that the elasticity modulus, and flexural and compressive strength, play a role in the change of the surface parameters under a much smoother P150 abrasive condition, compared to P60.

These findings are in accordance with the effects of contact loads on the micro-geometry. The micro-geometry of the moving polymer surfaces under a given normal load suffer shear, bending and compressive effects mainly. These effects can cause the appearance of deformation, wedge formation and micro-cutting (Bhushan, 2000; Stachowiak and Batchelor, 2013). According to the shear, bending and compressive loads, the models proved the role of  $\sigma_F$  and  $\sigma_c$  in tandem with the Young modulus. Other tensile values did not play significant role.

#### *4.1.10. Abrasive sensitivity of the tested materials with the pin-on-plate system*


In the final statistical evaluation of the pin-on-plate test results, many novel research results are summarized:

- Introducing the abrasive sensitivity of the tested materials based on the standardized coefficients of multiple regression models,
- Ranking the abrasive sensitivity of the materials according to the independent variables of the test systems.

#### 4. Results

Consider a dependent variable (e.g. wear, etc.) and those material properties and indicators formed from them which has a significant affect on it. The abrasive sensitivity, is the extent of how the independent variables affect it, which is related to the standardized regression coefficients. Therefore, the higher the absolute value of the corresponding standardized regression coefficient is, the higher the abrasive sensitivity of the dependent variable (wear, friction, temperature, surface 3D properties) is, in respect to the independent variable. The sensitivity can be visualized in 2D map constructed for Table 4.24. showing the abrasive sensitivity for wear, abrasive friction force, heat generation and the 3D parameters. The factors are in an increasing order of affect.

Table 4.24. 2D map of abrasive sensitivity in pin-on-plate system (ranking the sensitivity to systems' features)

<b>factors in increasing abrasive sensitivity to system variables</b>				
<b>less dominant</b>		<b>more dominant</b>		
				
Wear, P60	$H$	$\frac{\sigma_y}{\sigma_c \varepsilon_B}$		
Wear, P150	$\frac{\sigma_y}{\sigma_c \varepsilon_B}$			
$F_f$ , P60	$\varepsilon_B$	$\frac{\sigma_c}{\sigma_y \varepsilon_B}$		
$F_f$ , P150	$H$	$\frac{\sigma_F \sigma_y}{\sigma_M H}$		
$\Delta T$ , P60	$H$	$\frac{H \varepsilon_B}{\sigma_y}$	$\frac{\sigma_F H}{\sigma_M E}$	$\sigma_F$
$\Delta T$ , P150	$\varepsilon_B$	$H$	$\frac{\sigma_F H}{\sigma_M E}$	
Sq, P150	$E$			
Ssk, P60	$\sigma_F$			
Ssk, P150	$H$			
Skv, P150	$E$			
Sp, P150	$\frac{\sigma_y}{\sigma_c \varepsilon_B}$			
Sv, P150	$E$			
Sz, P150	$\frac{\sigma_F}{\sigma_c}$			
Sa, P150	$E$			



## 4.2. Slurry-pot system

As introduced in detail at 3.2.2., in the slurry-pot system, the sample materials moving in a slurry medium at two circumferential speeds and at two angles of impact, experience abrasive erosion on their surface.

As previous tests have proven, on the surfaces of many structural materials and coatings, micro-cutting-, polishing and pitting (surface fatigue due to particle impact) can occur in the function of the applied slurry-pot system features (Szabadi, 2011).

In the following cases, where Corundum ( $\text{Al}_2\text{O}_3$ ), gravelly skeletal soil, loamy soil, and sand soil were used as abrasive media against polymer materials, the micro-cutting and polishing as dominant effects caused continuous material loss leaving grooves on the partly polished surfaces. It is important to emphasize that the material loss visualized as cut grooves or multi-directional polished marks is different from the abrasive cutting system described in chapter 4.1 due to the impact energy of the free-moving particles, which generates different deformation capability and fatigue in the surface zone of plastics, influencing the wear groove formation.

As it was detailed in chapter 3.2.2 the relative wear (%) was calculated as an actual (daily cumulative) weight loss in percentage of the active worn surfaces determined according to Fig. 3.16, compared to the zero day weight according to the dedicated four different positions. Furthermore, the relative wear plotted against the wearing distance in *km* was also defined. The results were compared in the dedicated collision angles and rotational speeds (m/s).

### 4.2.1. The effect of the speed

Figs. (4.45 – 4.50) present typical relations between the relative wear as a percentage (%) and the running distance (km) for the materials used. They used the same type of abrasive collision wearing medium. The type of collision was tangential and the wear medium was gravelly soil (gravel).

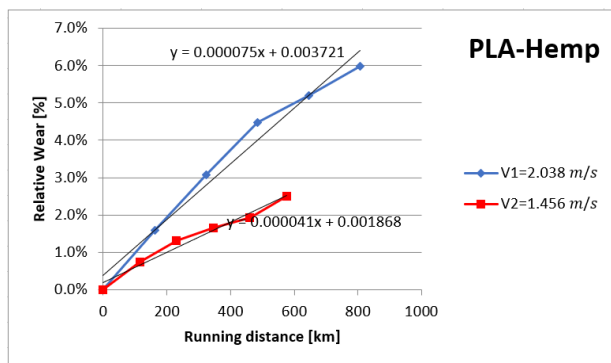


Fig. 4.45. The relation between the relative wear and sliding distance for PLA-hemp with two speeds (tangential collision in gravel)

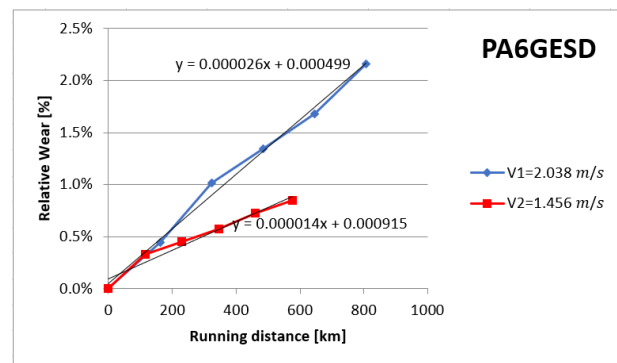


Fig. 4.46. The relation between the relative wear and sliding distance for PA6G ESD with two speeds (tangential collision in gravel)

## 4. Results

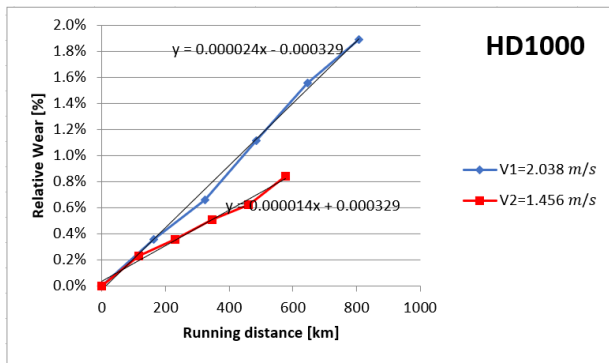


Fig. 4.47. The relation between the relative wear and sliding distance for HD1000 with two speeds (tangential collision in gravel)

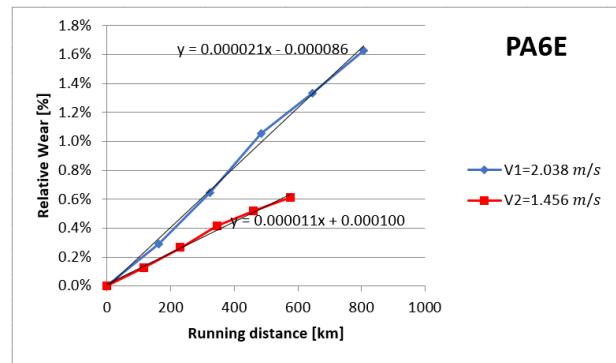


Fig. 4.48. The relation between the relative wear and sliding distance PA6E with two speeds (tangential collision in gravel)

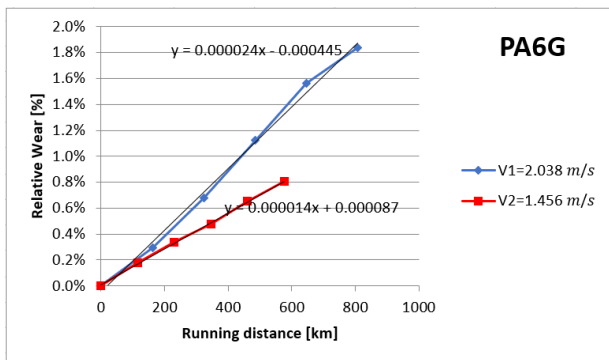


Fig. 4.49. The relation between the relative wear and sliding distance for PA6G with two speeds (tangential collision in gravel)

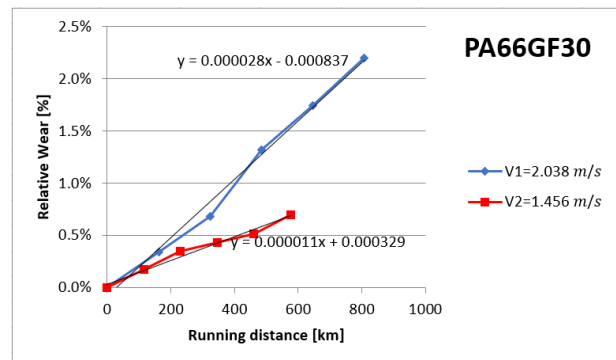


Fig. 4.50. The relation between the relative wear and sliding distance for PA66GF30 with two speeds (tangential collision in gravel)

As a result, with the collision type and with the same abrasive medium, the relative wear values increased by increasing the speed.

The measured on-line wear points of these conditions were approached by linear fit. The slope values “a” of the linear regression ( $y = ax + b$ ) are summarized in Table 4.25, which show the comparison between the wear speeds.

Table 4.25. Comparison between the two wear speeds and the increasing percentage in “a” values

Material	Wear speed at $v=1.456$ m/s	Wear speed at $v=2.038$ m/s	Increasing percentages in “a” values, %
PA66GF30	0.000011	0.000028	254.54%
PA6G ESD	0.000014	0.000026	185.71%
PA6E	0.000011	0.000021	190.09%
PA6G	0.000014	0.000024	171.42%
PLA-HF	0.000041	0.000075	182.92%
HD1000	0.000014	0.000024	171.42%

The table shows that under tangential collision in gravel the wear speeds of 2.038 m/s are higher than that of 1.456 m/s, which is the opposite appearance of the pin-on-plate case. Considering the differences of wear speeds shown in Table 4.25 the less sensitive materials against increased speed

in gravel slurry were cast polyamide 6 and UHMW-PE HD1000, while PA66GF30 was the most sensitive. The PLA-HF was ranked in the second best position in that system.

In general it was found that increasing the slurry abrasive speed higher relative wear occurred in different distinct according to the applied slurry system.

#### 4.2.2. The effect of the collision

Figs. (4.51 – 4.56) show the relation between the relative wear (%) against running distance (km) for the materials used, with same speed and same wear medium. The mean speed  $v_1$  was 2.038 m/s and the wear medium was gravelly soil (gravel).

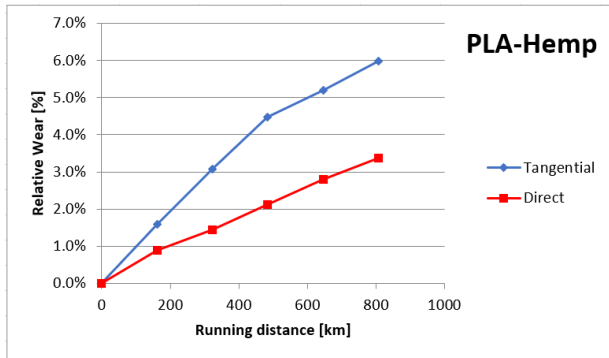


Fig. 4.51. The relation between the relative wear and sliding distance for PLA-hemp with two collision types (in gravel,  $v_1=2.038$  m/s)

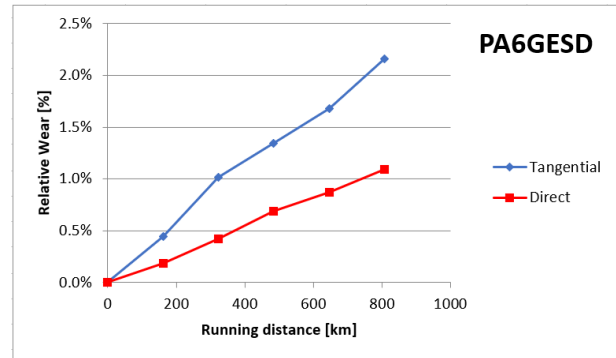


Fig. 4.52. The relation between the relative wear and sliding distance for PA6G ESD with two collision types (in gravel,  $v_1=2.038$  m/s)

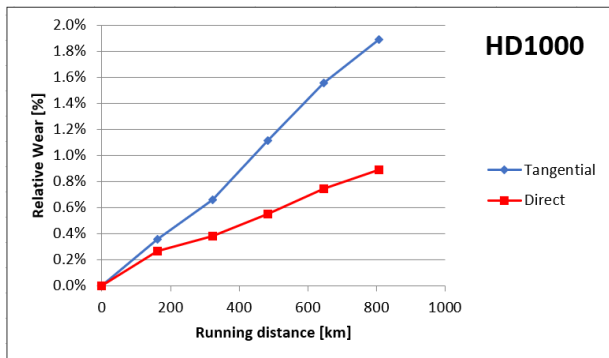


Fig. 4.53. The relation between the relative wear and sliding distance for HD1000 with two collision types (in gravel,  $v_1=2.038$  m/s)

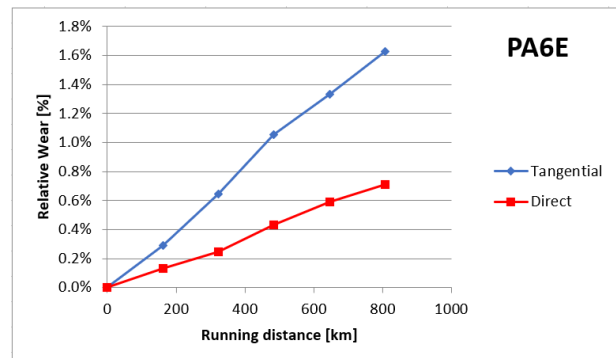


Fig. 4.54. The relation between the relative wear and sliding distance PA6E with two collision types (in gravel,  $v_1=2.038$  m/s)

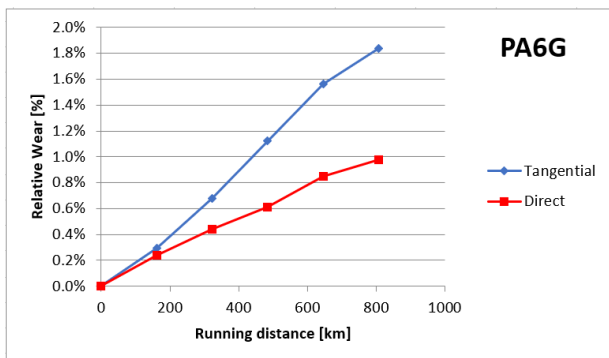


Fig. 4.55. The relation between the relative wear and sliding distance for PA6G with two collision types (in gravel,  $v_1=2.038$  m/s)

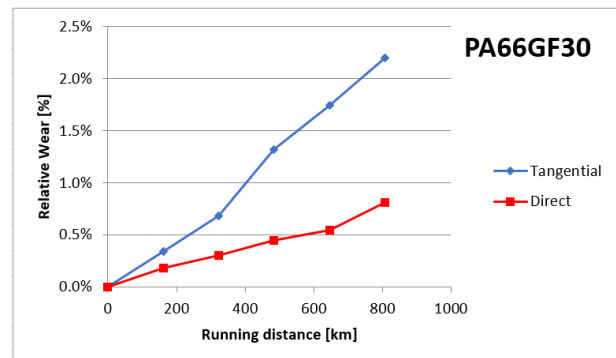


Fig. 4.56. The relation between the relative wear and sliding distance for PA66GF30 with two collision types (in gravel,  $v_1=2.038$  m/s)

### 4.2.3. Evaluation of the relative wear

The relative wear of the different polymer samples - daily cumulative of the weight loss as a percentage (%) compared to the zero day weight – is evaluated for the applied slurry materials. The reference was the most abrasive Corundum.

#### Corundum ( $Al_2O_3$ )

Fig. 4.57 shows the relative wear according to the four different positions (Fig. 3.13) in the case of a corundum medium. Fig. 4.57 (a) and (b) shows a longer distance daily for the  $r_1$  radius positions 1 and 2, (Fig. 3.13) due to higher speed.

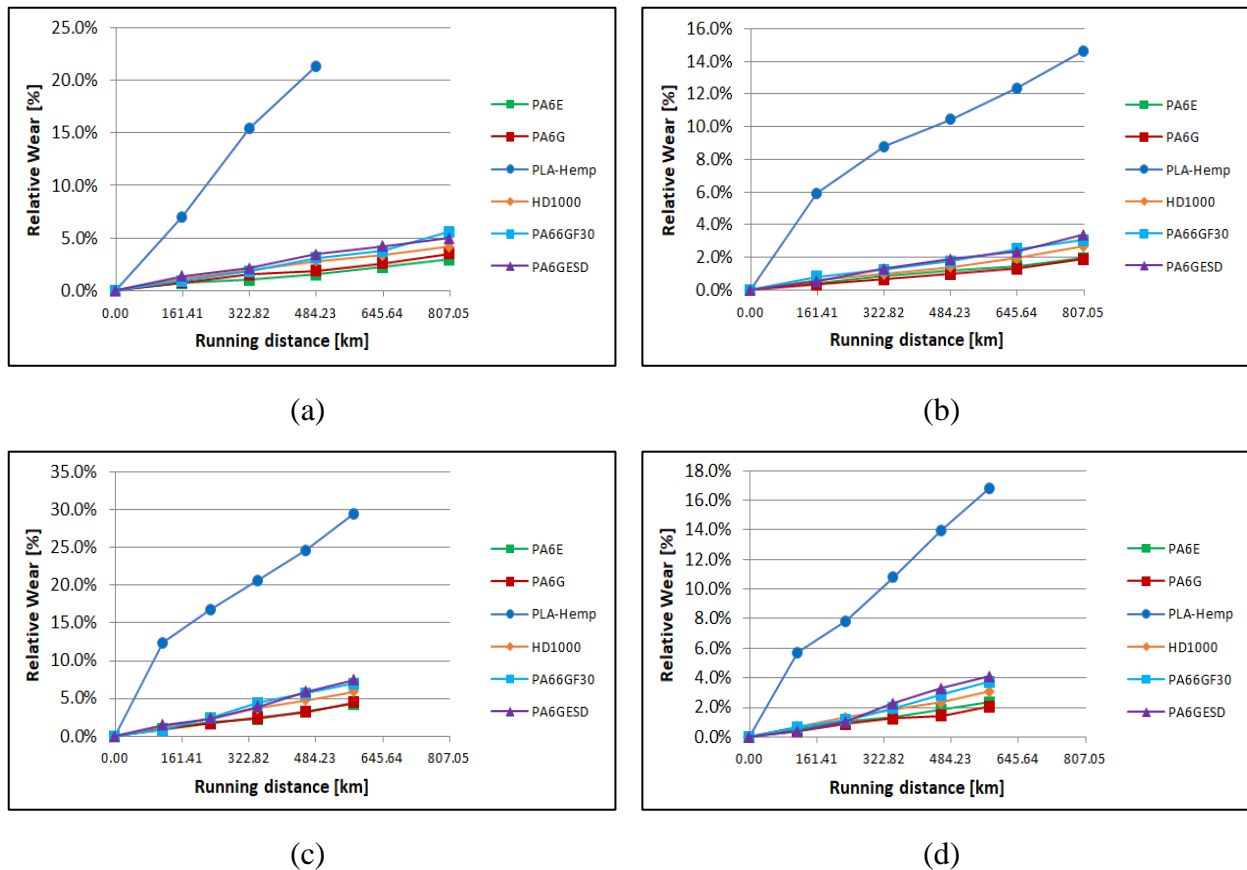


Fig. 4.57. The relative wear of the tested materials in corundum slurry (a) position 1, (b) position 2, (c) position 3, (d) position 4 (Fig. 3.13)

It is clear, that PLA-HF composites were more sensitive for the slurry-pot conditions, than for the pin-on-plate abrasive dry cutting. While on the dry pin-on-plate system the bio-degradable composite had an average wear resistance among the engineered plastics, in the corundum slurry system the PLA-HF suffered a severe material loss and was not comparable with the engineered polymers. As it can be seen in Fig. 4.54(a) the bio-composite could not survive the whole testing period in position 1 with  $v_1$  mean speed. The measurements had to be stopped, since the sample became shorter than the holder (to protect the holder from getting worn).

#### Gravelly skeletal soil (gravel)

Similarly to the corundum cases, Figure 4.58 shows the relative wear in gravelly skeletal soil (which is considered as possibly the most abrasive soil). Fig. 4.58 (a) and (b) shows a longer distance daily for the  $r_1$  radius positions 1 and 2 (Fig. 3.13) due to higher speed.

## 4. Results

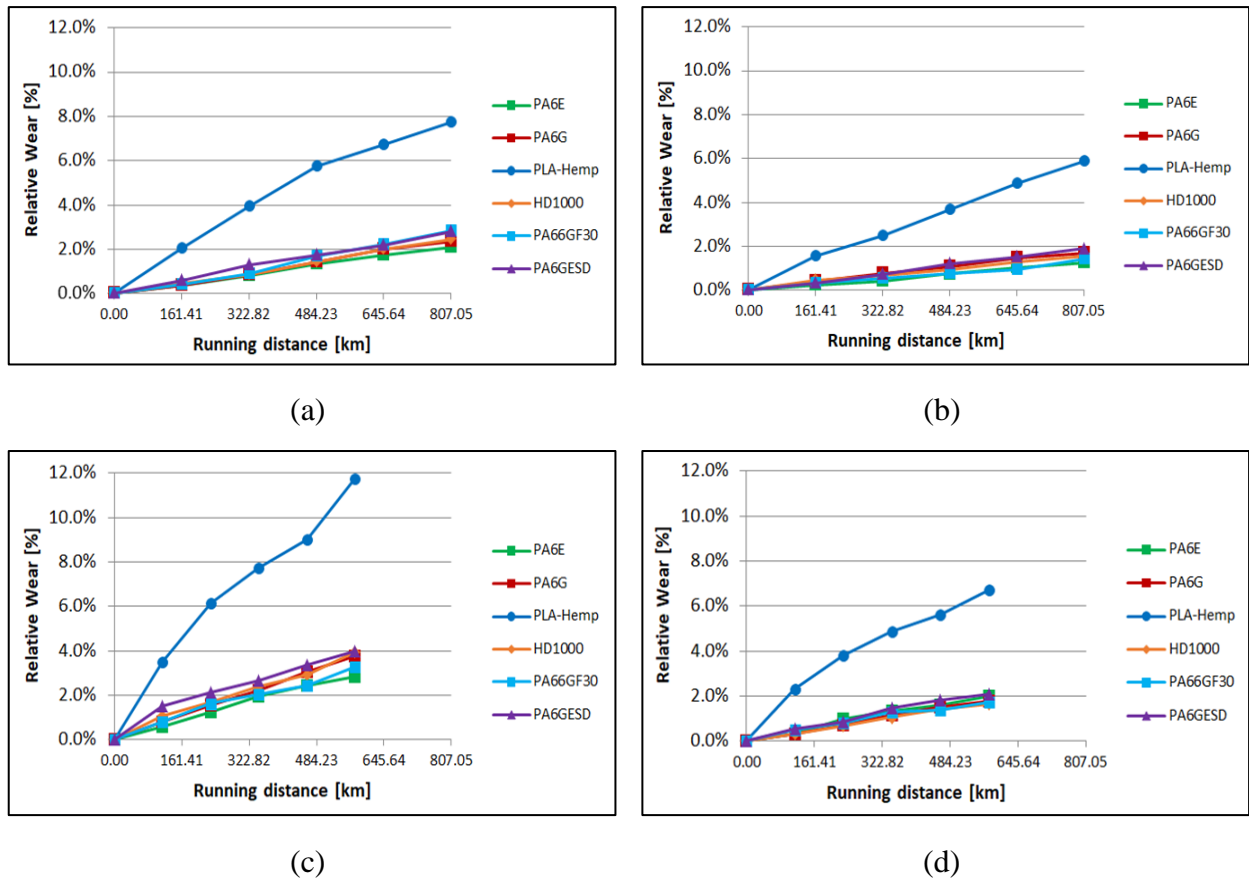


Fig. 4.58. The relative wear of the tested materials in gravelly skeletal soil based slurry (a) position 1, (b) position 2, (c) position 3, (d) position 4 (Fig. 3.13)

Comparing the wear curves (Fig.4.58) to the reference corundum (Fig. 4.57) results it can be stated that the gravel was not so abrasive and erosive as the corundum. It is clear, that PLA-HF still remained more sensitive in gravel slurry conditions and performed faster wear comparing to the engineering plastics, however the gravel did not killed the PLA-HF samples as fast as corundum did and the measurements could run to the end with PLA-HF in all system cases. Against the tangential load in positions 1 and 3 the PA6E had performed the best wear resistance. In general, the engineering polymers suffered very similar abrasive erosion in gravel slurry.

### Lime coated chernozem (Loamy soil):

Testing with this medium is of greater practical significance than with corundum and skeletal soil. As it is introduced in chapter 3.2.2 the chernozem soils are cultivated in most places due to their excellent physical and chemical features. The ploughed or cultivated layer is often of a degraded structure, consisting of very small crumbs, dusty and with a compacted layer at its bottom. Its chemical reaction is neutral or slightly alkaline, containing lower levels of lime, with 3-6 % humus content. Its actual physical fractions with the humus content resulted differing wear curves even for the engineering polymers, too. Fig. 4.59 shows the relative wear evaluation.

In the case of a good quality loamy soil, for growing cereals, the abrasive erosion resulted in less contrast between PLA-HF and engineering polymers. Still the bio-composite had the biggest wear but not so differently than with gravels and corundum. Also, a difference among the engineering polymers can be seen with the loamy soil. With the loamy slurry media, the PA6G was the best.

## 4. Results

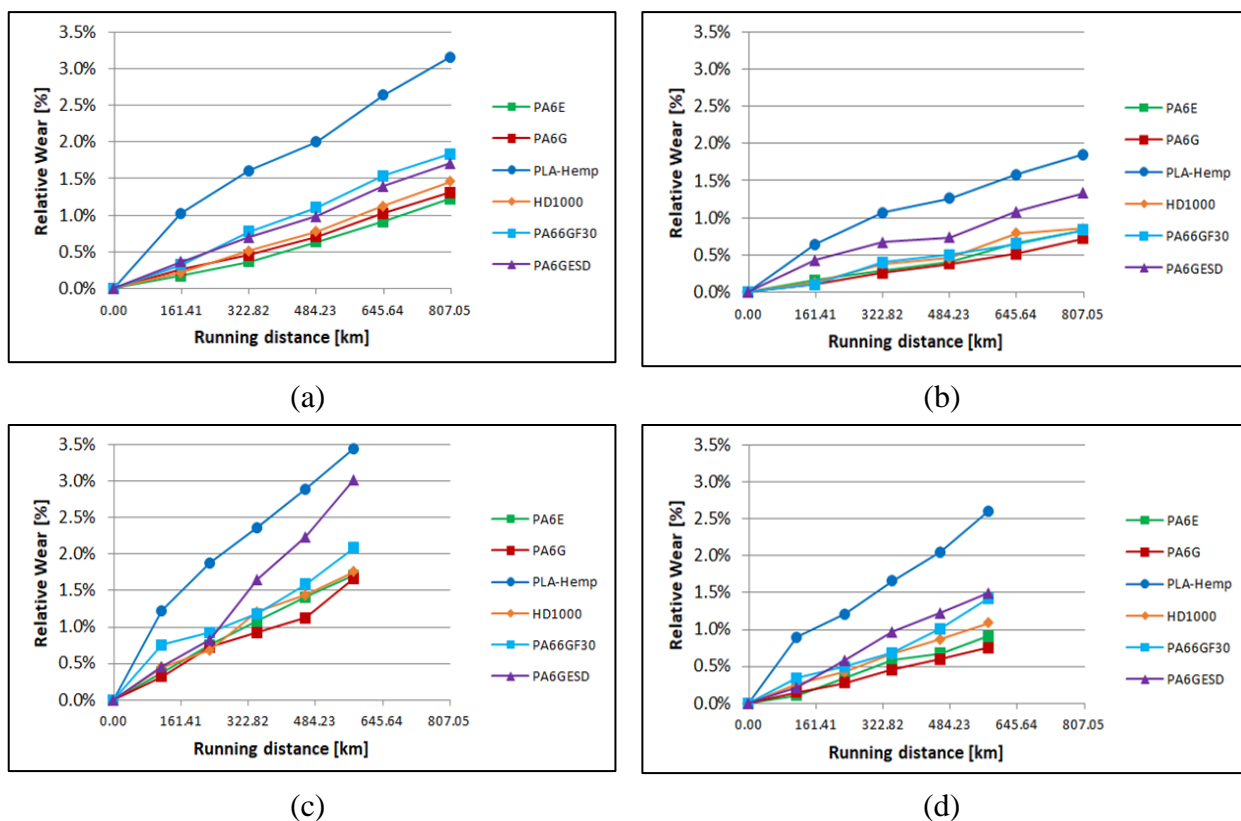


Fig. 4.59. The relative wear of the tested materials in loamy soil based slurry (a) position 1, (b) position 2, (c) position 3, (d) position 4 (Fig. 3.13)

Humic sand soil (Sandy soil):

Fig. 4.60 shows the relative wear evaluation.

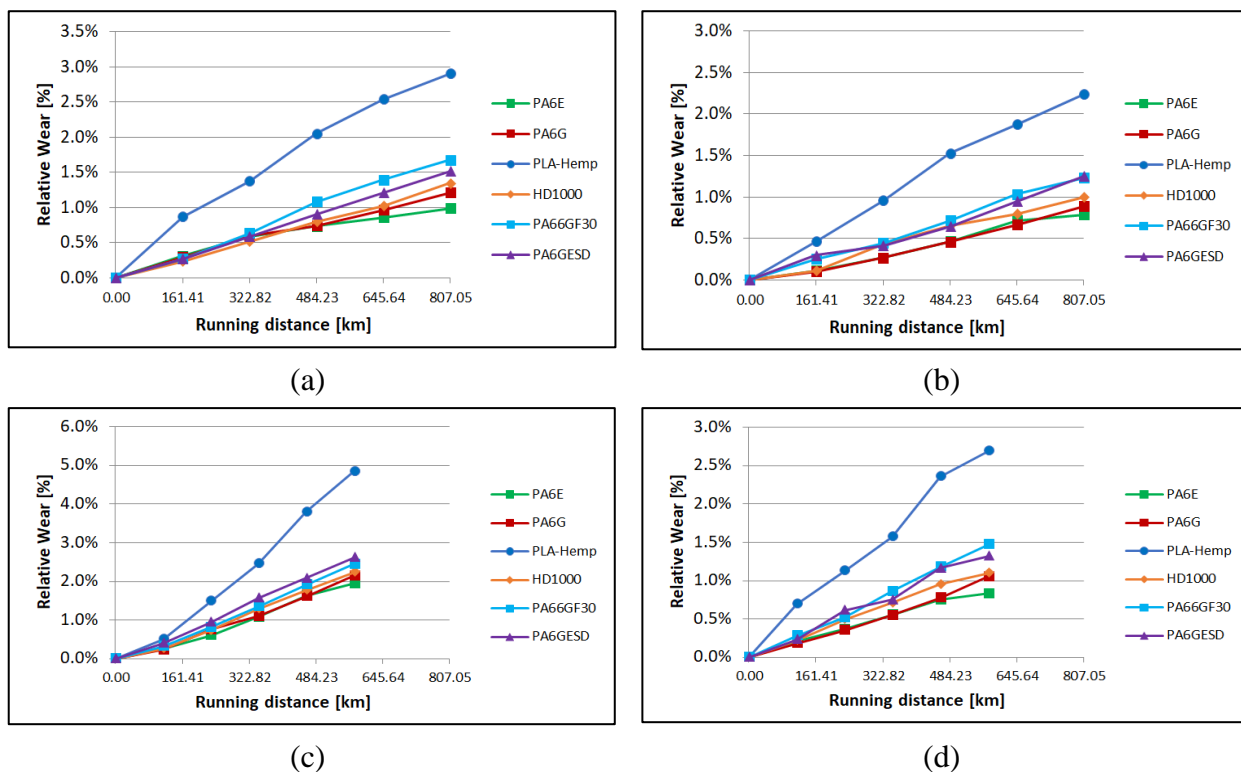


Fig. 4.60. The relative wear of the tested materials in sandy soil based slurry (a) position 1, (b) position 2, (c) position 3, (d) position 4 (Fig. 3.13)

#### 4. Results

It is clear, that PLA-HF composites were more sensitive for this type of slurry than the engineering polymers. Among those materials a slight difference can be seen even position 1 and 4, but they performed better abrasion and erosion resistance than PLA-HF. By the end of the measurements, the PA6E suffered the least wear in the sandy system.

Taking the 5<sup>th</sup> testing day (or last measurable point) wear results into consideration the Table 4.26 gives an overview about the experienced relative wear (%) results according to the applied slurry medium and material samples' position in the system (the full measurements results for all the used materials and all mediums are shown in Appendix 9). It is clear that beside the sandy soil the most commonly cultivated chernozem (loamy) was less aggressive and resulted moderate material loss under the slurry tests. As it was experienced in Fig. 4.59 the loamy soil caused even distribution of wear trends between the materials and PLA-HF even though it was weaker but was comparable with engineering materials.

Table 4.26. Relative wear values (%) at the end of measurements

		Corundum	Gravel	Loamy soil	Sandy soil
position 1	PLA-HF	-	7.72%	3.16%	2.90%
	PA6G	3.53%	2.37%	1.31%	1.22%
	PA6E	2.96%	2.10%	1.23%	0.99%
	PA66GF30	5.62%	2.84%	1.84%	1.67%
	PA6G ESD	5.00%	2.78%	1.71%	1.52%
	UHMW-PE HD1000	4.19%	2.44%	1.46%	1.35%
position 2	PLA-HF	14.64%	5.88%	1.85%	2.24%
	PA6G	1.91%	1.70%	0.72%	0.89%
	PA6E	1.99%	1.24%	0.83%	0.78%
	PA66GF30	3.09%	1.42%	0.84%	1.23%
	PA6G ESD	3.38%	1.90%	1.34%	1.25%
	UHMW-PE HD1000	2.70%	1.55%	0.85%	1.00%
position 3	PLA-HF	29.43%	11.73%	3.45%	4.85%
	PA6G	4.52%	3.76%	1.67%	2.14%
	PA6E	4.26%	2.86%	1.71%	1.94%
	PA66GF30	7.03%	3.28%	2.09%	2.45%
	PA6G ESD	7.50%	3.98%	3.02%	2.62%
	UHMW-PE HD1000	5.95%	3.93%	1.76%	2.24%
position 4	PLA-HF	16.84%	6.71%	2.60%	2.69%
	PA6G	2.05%	1.80%	0.75%	1.05%
	PA6E	2.35%	1.99%	0.91%	0.83%
	PA66GF30	3.73%	1.73%	1.42%	1.47%
	PA6G ESD	4.13%	2.11%	1.50%	1.32%
	UHMW-PE HD1000	3.09%	1.66%	1.09%	1.10%

#### 4.2.4. The daily relative wear

Beside the relative wear (%) introduced in 4.2.3 the daily relative wear of the weight loss as a percentage (%), compared to the previous day's weight was also determined. This type of plot gives a better view about the wear speed during the process and at the same time as the material wears, the possible effect of the changing material structure/property is more detectable. According to this, the speed of wear between the days can vary. Fig. 4.61 shows an example for the position 1 results, with four types of slurry. Other positions of the materials with the different medium are summarized in Appendix 10.

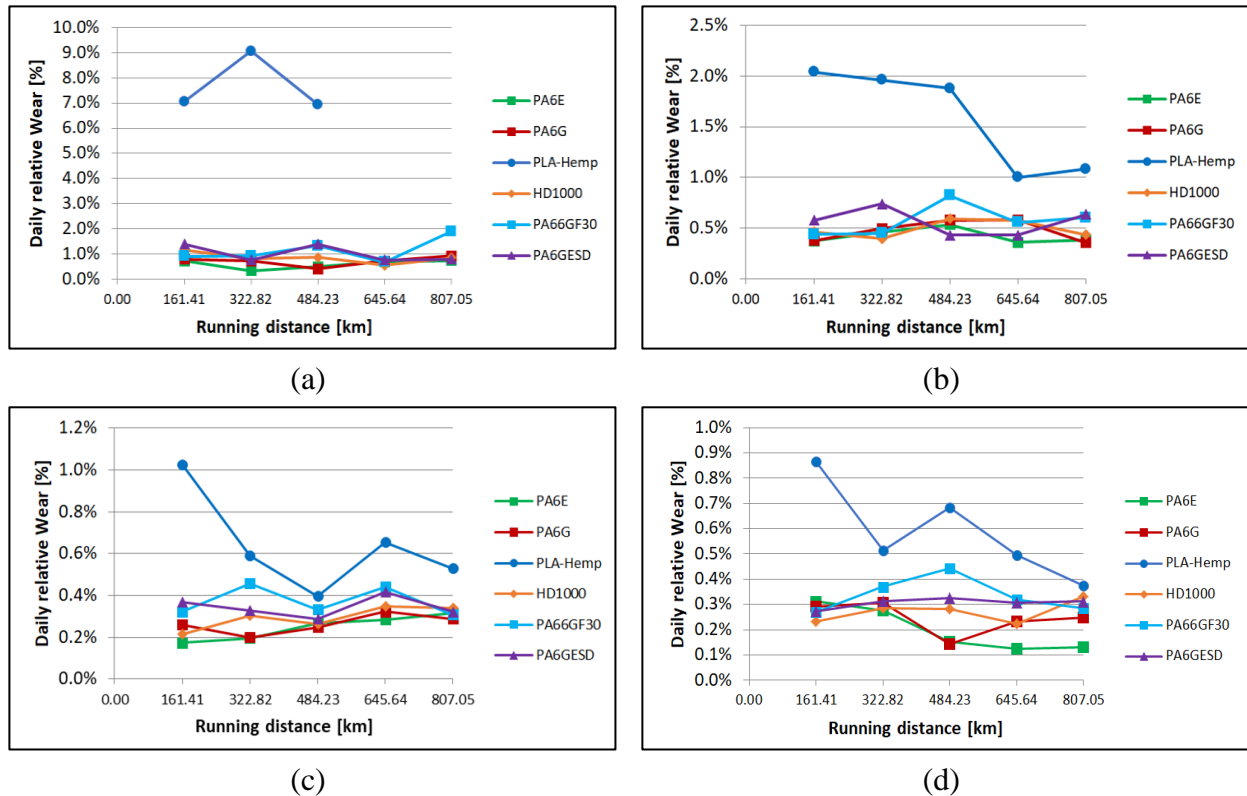


Fig. 4.61. Daily relative wear in position 1 (Fig. 3.13) with (a) corundum medium (b) gravel skeletal soil (c) loamy soil based slurry, and (d) sandy soil

It is clear, that the PLA-HF had a running-in like effect during the first two to three days, which was caused by the fast wear of the coating layer of the composites. Later, the fibers of the bulk experienced a lower daily wear. Concerning the engineered polymers, the virgin PA6E, PA6G and UHMW-PE HD1000 showed less fluctuation in daily wear than the composite PA66GF30 and PA6G ESD, where differing material structure of skin and bulk regions can not be ruled out.

This observation is in accordance with the previous studies of composite materials in abrasive systems (Rajesh et al., 2001, 2002) since the reinforcements – beside the general positive effect on mechanical properties - can cause uneven internal stresses that influence the wear behavior, too.

#### 4.2.5. The statistical analysis of the wear results

Multiple linear regression models were applied to investigate statistically, the sensitivity of material properties on the experienced relative wear (%) under the four slurry types. In the test systems the duration of the test  $t$  (measured in days), the tangential velocity  $v$  of the test specimen and the contact angle were considered as independent variables, as were the material properties and the dimensionless numbers formed from them. It is important to mention that the contact angle



was dealt as a dummy variable in the models, that is, it was defined as 1 if its position was direct and as 0 if its position was tangential (Fig. 3.15). As shown below, the notation  $ca$  was used as the “contact angle”. The following models were obtained for the four types of slurry.

Wear, Corundum:

The best fitting model is as Eq. 4.11;

$$\text{wear} = -0.234 + 1.246t - 1.931 ca + 0.76 \cdot \frac{\sigma_y}{\sigma_c \varepsilon_B} \quad (4.11)$$

The  $F$ -value of the model is 119.6 and  $p < 0.001$ , thus the model is relevant. For this model the goodness-of-fit is  $R^2 = 0.722$ . Among the material properties  $\frac{\sigma_y}{\sigma_c \varepsilon_B}$  has the biggest effect on wear.

Table 4.27 shows the regression model with a corundum abrasive medium.

Table 4.27. Coefficients of the regression model with a corundum abrasive medium

Model	coefficient	Standardized regression coefficient, Beta	t	p
Constant	-0.234		-0.5	
t	1.246	0.430	9.5	<0.001
ca	-1.931	0.599	-4.3	<0.001
$\frac{\sigma_y}{\sigma_c \varepsilon_B}$	0.76	0.732	16.2	<0.001

Wear, gravel:

Without presenting all the details of the fitted model, the best fitting one is as Eq. 4.12;

$$\text{wear} = 0.018 + 0.007t - 0.010v - 0.009ca + 0.0002434 \cdot \frac{\sigma_y}{\sigma_c \varepsilon_B} \quad (4.12)$$

The  $F$ -value of the model is 131.8 and  $p < 0.001$ , thus the model is relevant. For this model the goodness-of-fit is  $R^2 = 0.791$ .  $\frac{\sigma_y}{\sigma_c \varepsilon_B}$  and the length of time of the experiment has the biggest effect on the wear.

Table 4.28 shows the regression model with a gravelly soil abrasive medium.

Table 4.28. Coefficients of the regression model with a gravelly soil abrasive medium

Model	coefficient	Standardized regression coefficient, Beta	t	p
Constant	0.011		3.7	<0.001
t	+0.007	0.577	14.8	<0.001
v	-0.010	-0.151	-3.8	<0.001
ca	-0.009	-0.228	-5.8	<0.001
$\frac{\sigma_y}{\sigma_c \varepsilon_B}$	0.0002434	0.620	15.9	<0.001

Wear, loamy soil:

The best fitting model is as Eq. 4.13;

$$\text{wear} = 0.011 + 0.003t - 0.004v - 0.004ca - 0.0000260\varepsilon_B - 0.0000255\sigma_F + 0.0000033 \cdot \frac{\sigma_y E}{\sigma_M H} \quad (4.13)$$

The  $F$ -value of the model is 145.7 and  $p < 0.001$ , thus the model is relevant. For this model the goodness-of-fit is  $R^2 = 0.865$ . Among the material properties  $\frac{\sigma_y E}{\sigma_M H}$  has the biggest effect on wear but overall it's extent is mediocre. Table 4.29 shows the regression model with a loamy soil medium.

Table 4.29. Coefficients of the regression model with a loamy soil abrasive medium

Model	coefficient	Standardized regression coefficient, Beta	t	p
Constant	0.011		5.9	<0.001
$t$	+0.003	0.740	23.5	<0.001
$v$	-0.004	-0.140	-4.4	<0.001
$ca$	-0.004	-0.278	-8.8	<0.001
$\varepsilon_B$	-0.000026	-0.226	-5.1	<0.001
$\sigma_F$	-0.0000255	-0.131	-3.1	<0.005
$\frac{\sigma_y E}{\sigma_M H}$	0.0000033	0.375	9.7	<0.001

Wear, Sandy soil:

The best fitting model is as Eq. 4.14;

$$\text{wear} = 0.696 + 0.354t - 0.386ca - 0.447v + 0.0000304E \quad (4.14)$$

The  $F$ -value of the model is 150.5 and  $p < 0.001$ , thus the model is relevant. For this model the goodness-of-fit is  $R^2 = 0.812$ . Among the material properties  $t$  and  $E$  have the biggest effects on wear. Table 4.30 shows the regression model with a sandy soil abrasive medium.

Table 4.30. Coefficients of the regression model with a sandy soil abrasive medium

Model	coefficient	Standardized regression coefficient, Beta	t	p
Constant	0.696		3.6	<0.001
$t$	0.354	0.748	20.3	<0.001
$ca$	-0.386	-0.239	-6.5	<0.001
$v$	-0.447	-0.161	-4.3	<0.001
$E$	0.0000304	0.412	11.2	<0.001

#### 4.2.6. 3D surface microscopy results

The evaluation of the 3D surface topographic changes were similar to those already presented in the pin-on-plate system. For all slurry abrasive media, the state before and after measurement was compared according to the four positions (Fig. 3.13) for each polymer.

## 4. Results

Fig. 4.62 shows the microscopic visualization of the polymer surfaces in the initial states of the tested materials in position 1. The measured values of the surface parameters are summarized in Table 4.31.

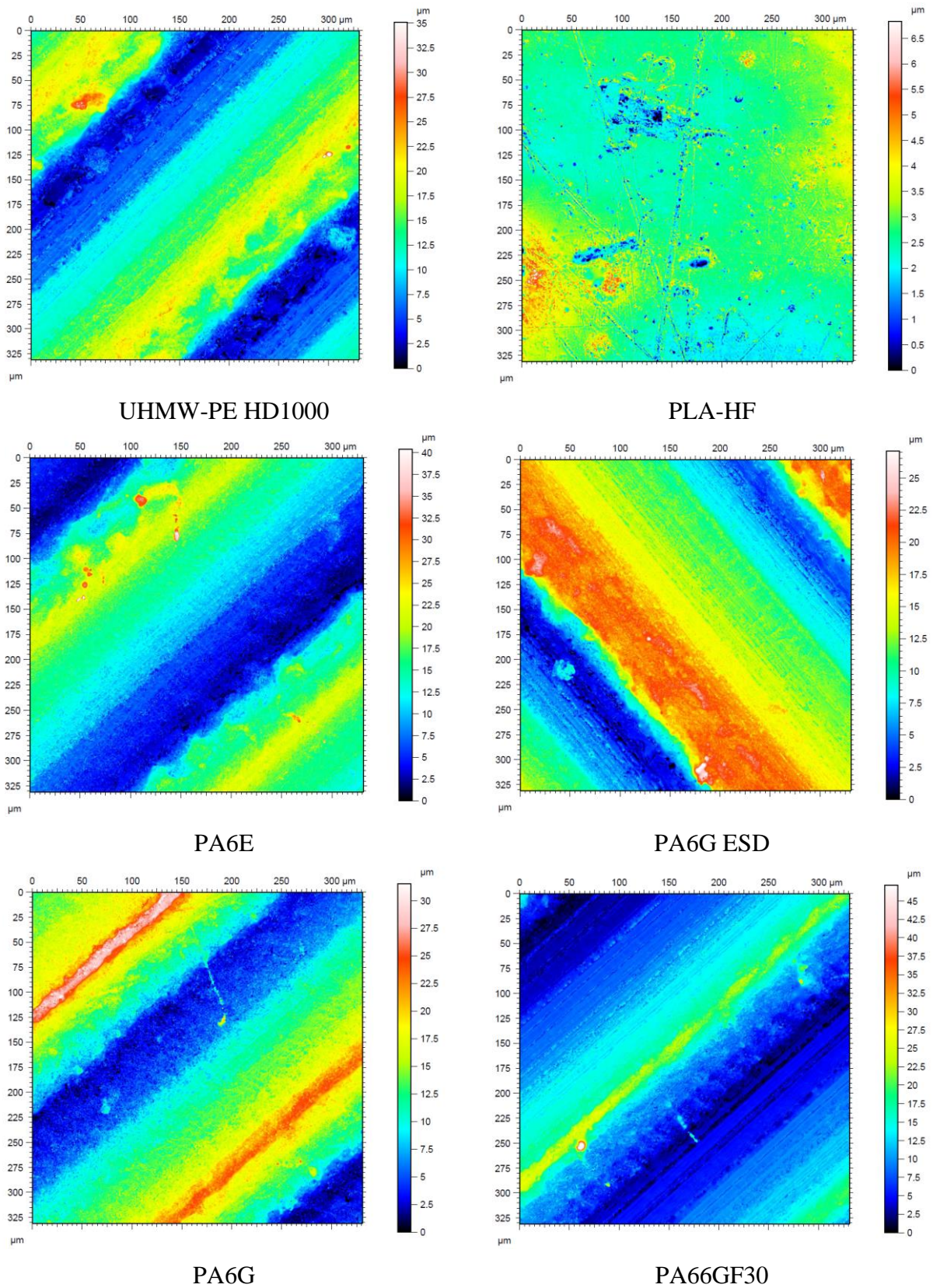


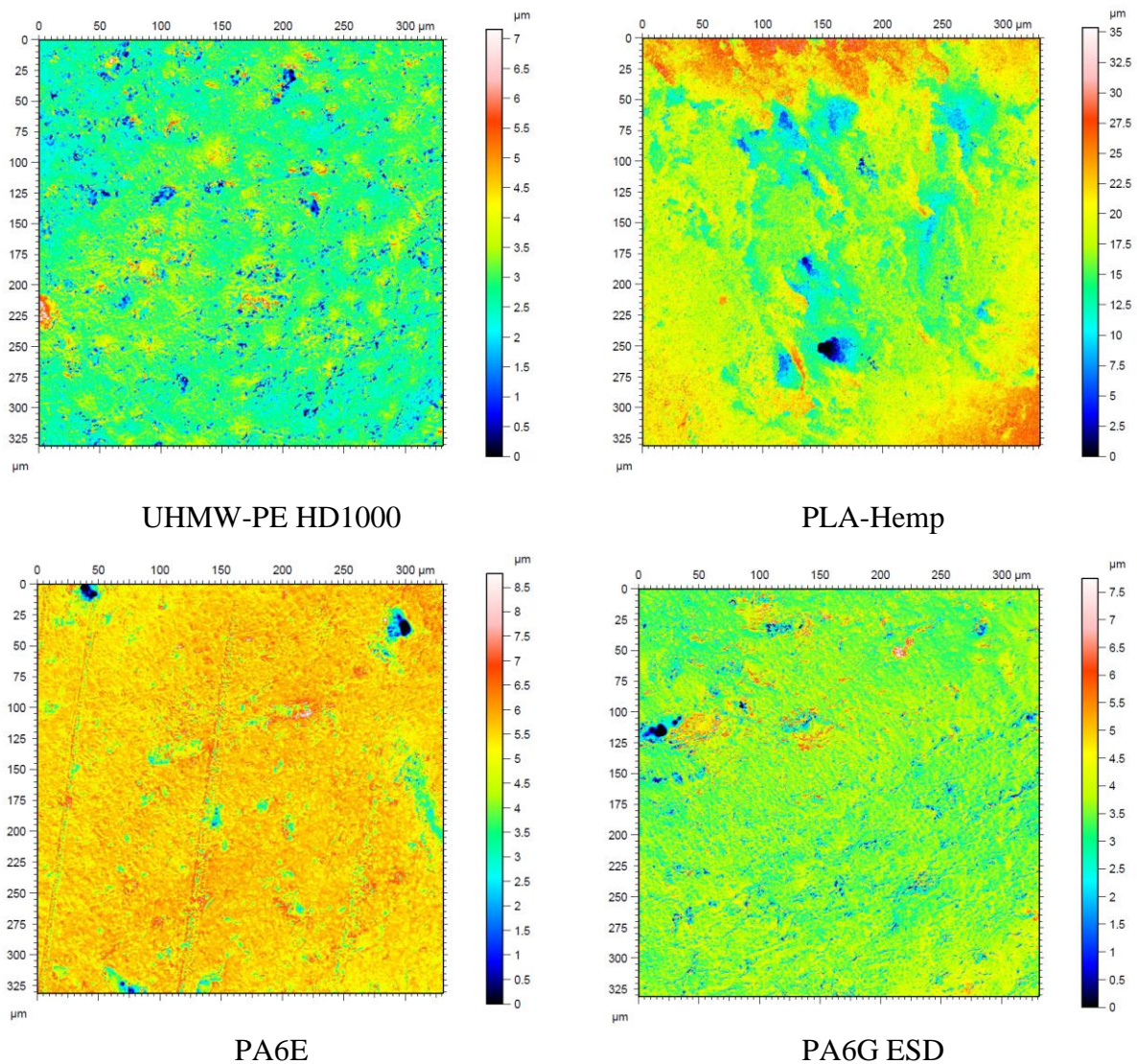
Fig. 4.62. The tested polymer surfaces before measurements: PLA-HF is pressed, while the others are machined surfaces

Table 4.31. 3D surface characteristics before testing

	<b>HD1000</b>	<b>PLA-HF</b>	<b>PA6E</b>	<b>PA6G ESD</b>	<b>PA6G</b>	<b>PA66GF30</b>
Sq ( $\mu\text{m}$ )	5.5	0.6	5.9	5.6	6.1	5.3
Ssk	0.02	0.5	0.04	-0.1	0.2	0.6
Sku	2.0	5.6	2.2	1.9	2.5	3.5
Sp ( $\mu\text{m}$ )	23.6	4.1	28.5	14.5	19.7	37.3
Sv ( $\mu\text{m}$ )	11.4	2.7	11.7	12.5	11.7	9.7
Sz ( $\mu\text{m}$ )	35.09	6.8	40.3	27.07	31.5	47.1
Sa ( $\mu\text{m}$ )	4.6	0.4	5.0	4.7	5.0	4.3

Corundum:

Fig. 4.63 shows the microscopic visualization of the polymer surfaces in the final states with the corundum medium in position 1. The measured values of the surface parameters and the changes to the starting condition are shown in Table 4.32. The other position results are summarized in Appendix 11.



## 4. Results

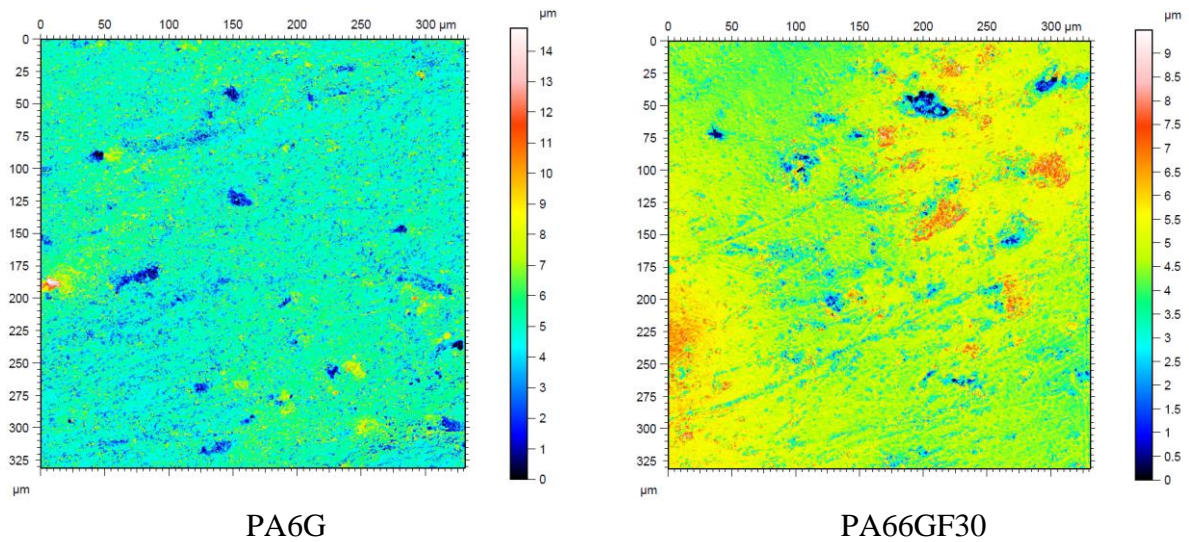


Fig. 4.63. Microscopic visualization of the change in the surface 3D topography of the tested materials on corundum slurry in position 1 (Fig. 3.13)

Table 4.32. Surface characteristics after the tests and the change as a percentage (%)

	<b>HD1000</b>	<b>PLA-HF</b>	<b>PA6E</b>	<b>PA6G ESD</b>	<b>PA6G</b>	<b>PA66GF30</b>
	<b>after the test</b>					
Sq ( $\mu\text{m}$ )	0.63	3.87	0.63	0.65	1.12	0.88
Ssk	-0.04	-0.25	-2.44	-0.32	0.08	-0.61
Sku	7.25	4.14	17.39	8.75	6.49	6.68
Sp ( $\mu\text{m}$ )	4.31	17.46	3.29	4.18	9.76	4.79
Sv ( $\mu\text{m}$ )	2.84	17.89	5.49	3.56	4.99	4.70
Sz ( $\mu\text{m}$ )	7.15	35.35	8.78	7.75	14.74	9.49
Sa ( $\mu\text{m}$ )	0.44	2.95	0.39	0.42	0.81	0.62
	<b>Change in %</b>					
Sq ( $\mu\text{m}$ )	-88.56%	511.10%	-89.38%	-88.55%	-81.57%	-83.45%
Ssk	-291.37%	-149.70%	-5324.69%	129.58%	-72.10%	-192.68%
Sku	250.91%	-27.37%	676.54%	346.14%	155.32%	87.59%
Sp ( $\mu\text{m}$ )	-81.76%	324.56%	-88.50%	-71.29%	-50.54%	-87.20%
Sv ( $\mu\text{m}$ )	-75.23%	558.74%	-53.42%	-71.52%	-57.69%	-51.69%
Sz ( $\mu\text{m}$ )	-79.63%	417.67%	-78.26%	-71.40%	-53.21%	-79.86%
Sa ( $\mu\text{m}$ )	-90.63%	541.97%	-92.26%	-91.19%	-83.84%	-85.71%

Comparing Figs. 4.62 and 4.63, it is clear that by the end of the slurry abrasive erosion, the original machining marks of the surfaces have completely disappeared due to the swirling slurry. For all cases, the results are completely converted surfaces to differing degrees, while PLA-HF - beside the surface change - suffered essential deformation due to the internal stress release. The worn surface can be characterized with moderate hills and valleys partly interrupted by micro-grooves for all tested samples. In Figure 4.63 the dark blue dots of the images indicates the complexity of the load and the material response. The continuous collision with the abrading particles could cause a small craters on the surfaces, which reminds the typical appearance of pitting as a result of surface fatigue. The above concluded visualization is supported by the numbers in Table 4.32. The engineering polymers became polished with decreased Sp, Sv, Sz, Sa but for the PLA-HF, where the layered structure came up to the surface and the torn hemp fibers caused increased

surface parameters. The decreased Skewness (Ssk) for Hemp-HF also prove the findings meaning that the asperities, the surface material is elevated and deformed above the mean plane.

#### Gravel soil:

Fig. 4.64. shows the microscopic visualization of the polymer surfaces in their final states with the gravel medium in position 1. The measured values of the surface parameters and the changes to the starting condition are shown in Table 4.33. The other position results are summarized in Appendix 12.

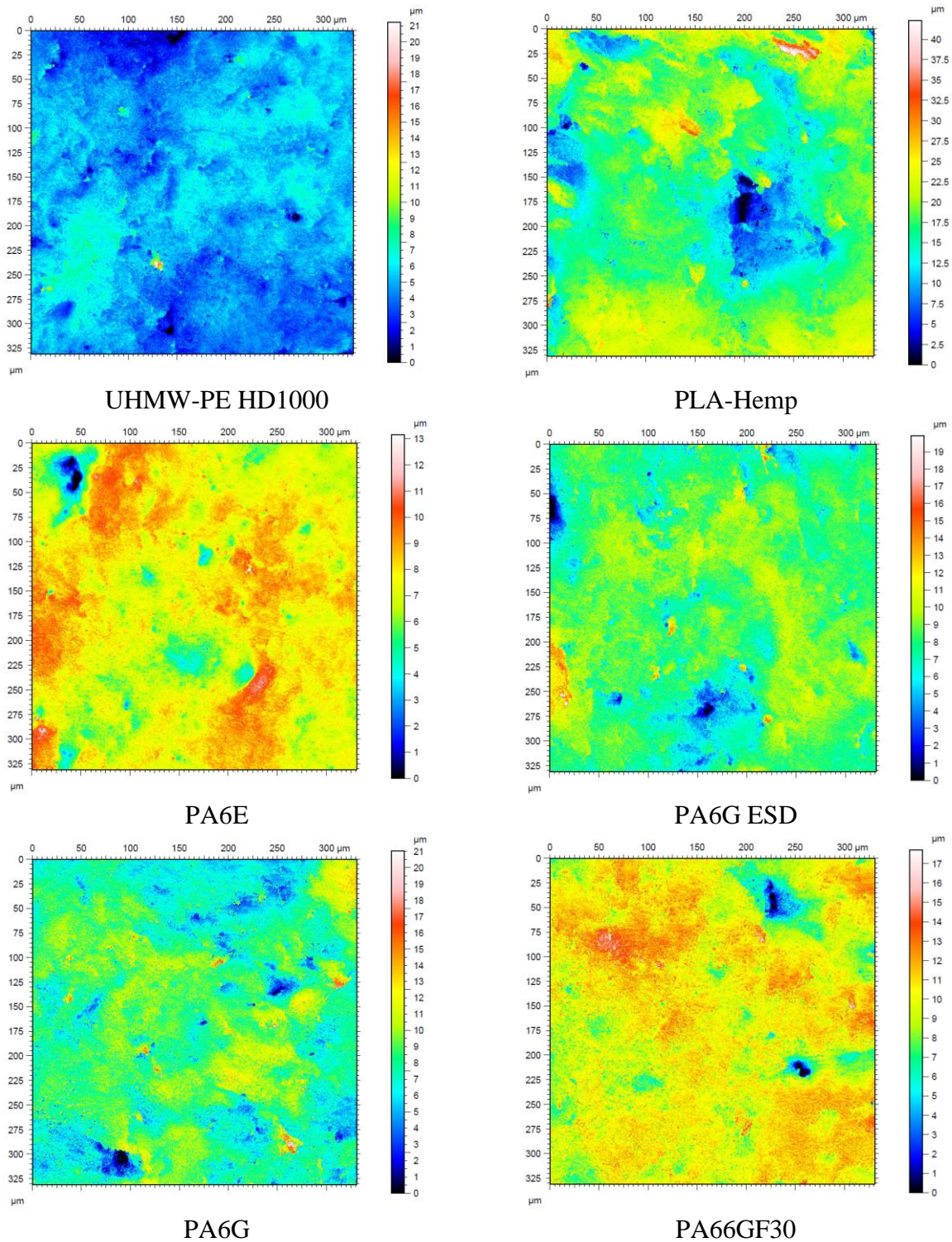


Fig. 4.64. Microscopic visualization of the change in the surface 3D topography of the tested materials on gravel slurry in position 1 (Fig. 3.13)

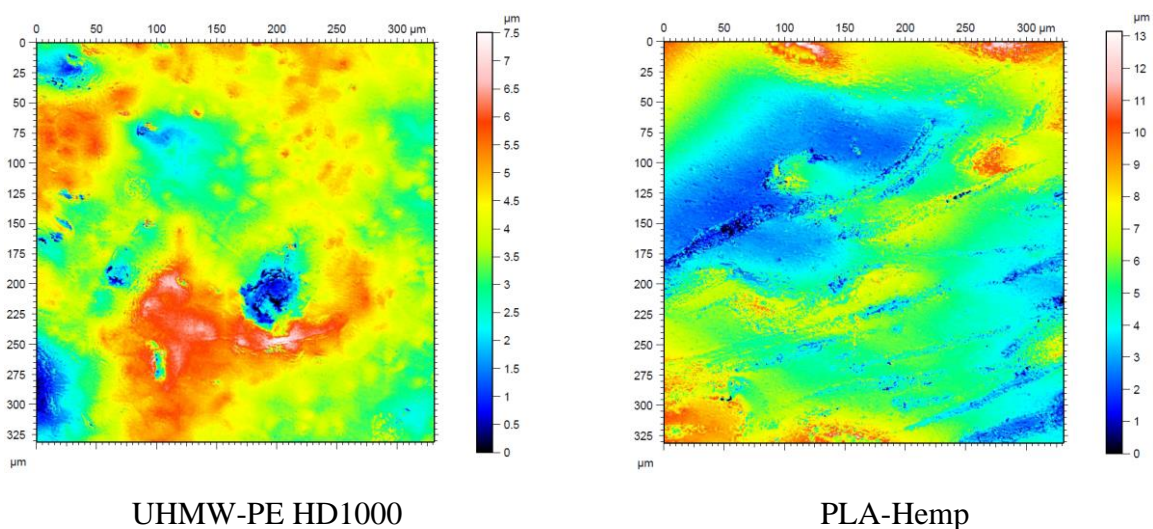
Table 4.33. Surface characteristics after the tests and the change as a percentage (%)

	HD1000	PLA-HF	PA6E	PA6G ESD	PA6G	PA66GF30
	after the test					
Sq ( $\mu\text{m}$ )	1.24	4.58	1.26	1.59	1.97	1.73
Ssk	0.43	-0.25	-0.93	-0.46	0.02	-1.03
Sku	11.33	4.53	6.59	6.16	4.44	6.83
Sp ( $\mu\text{m}$ )	16.37	25.00	5.55	11.71	12.93	7.59
Sv ( $\mu\text{m}$ )	4.85	17.31	7.60	8.20	8.08	10.11
Sz ( $\mu\text{m}$ )	21.22	42.32	13.15	19.91	21.01	17.70
Sa ( $\mu\text{m}$ )	0.94	3.49	0.93	1.16	1.52	1.26
	Change in %					
Sq ( $\mu\text{m}$ )	-77.57%	622.75%	-78.95%	-71.89%	-67.73%	-67.55%
Ssk	1796.28%	-148.57%	-2088.16%	237.37%	-91.08%	-255.53%
Sku	448.19%	-20.51%	194.21%	213.85%	74.80%	91.78%
Sp ( $\mu\text{m}$ )	-30.72%	507.86%	-80.59%	-19.61%	-34.42%	-79.70%
Sv ( $\mu\text{m}$ )	-57.72%	537.67%	-35.48%	-34.48%	-31.49%	3.87%
Sz ( $\mu\text{m}$ )	-39.54%	519.71%	-67.43%	-26.48%	-33.32%	-62.43%
Sa ( $\mu\text{m}$ )	-79.88%	659.34%	-81.64%	-75.61%	-69.69%	-70.67%

By the end of the slurry abrasive erosion (Fig. 4.64), the original machining marks of the surfaces have completely disappeared due to the swirling slurry, similarly to the corundum case. However, the wear volume with gravel was smaller than with corundum, the same polishing effect of the engineering polymers can be realized with the decreased Sq, Sp, Sv, Sz, Sa. The PLA-HF showed torn fibers and increased roughness with elevated mean plane as expressed with the decreased Ssk. The collision of the particles causing pits are moderate with gravel comparing to the effect of hard and sharp corundum's effect.

#### Loamy soil:

Fig. 4.65 shows the microscopic visualization of the polymer surfaces in their final states with the Loamy medium in position 1. The measured values of the surface parameters changes are shown in Table 4.34. The other position results are summarized in Appendix 13.



#### 4. Results

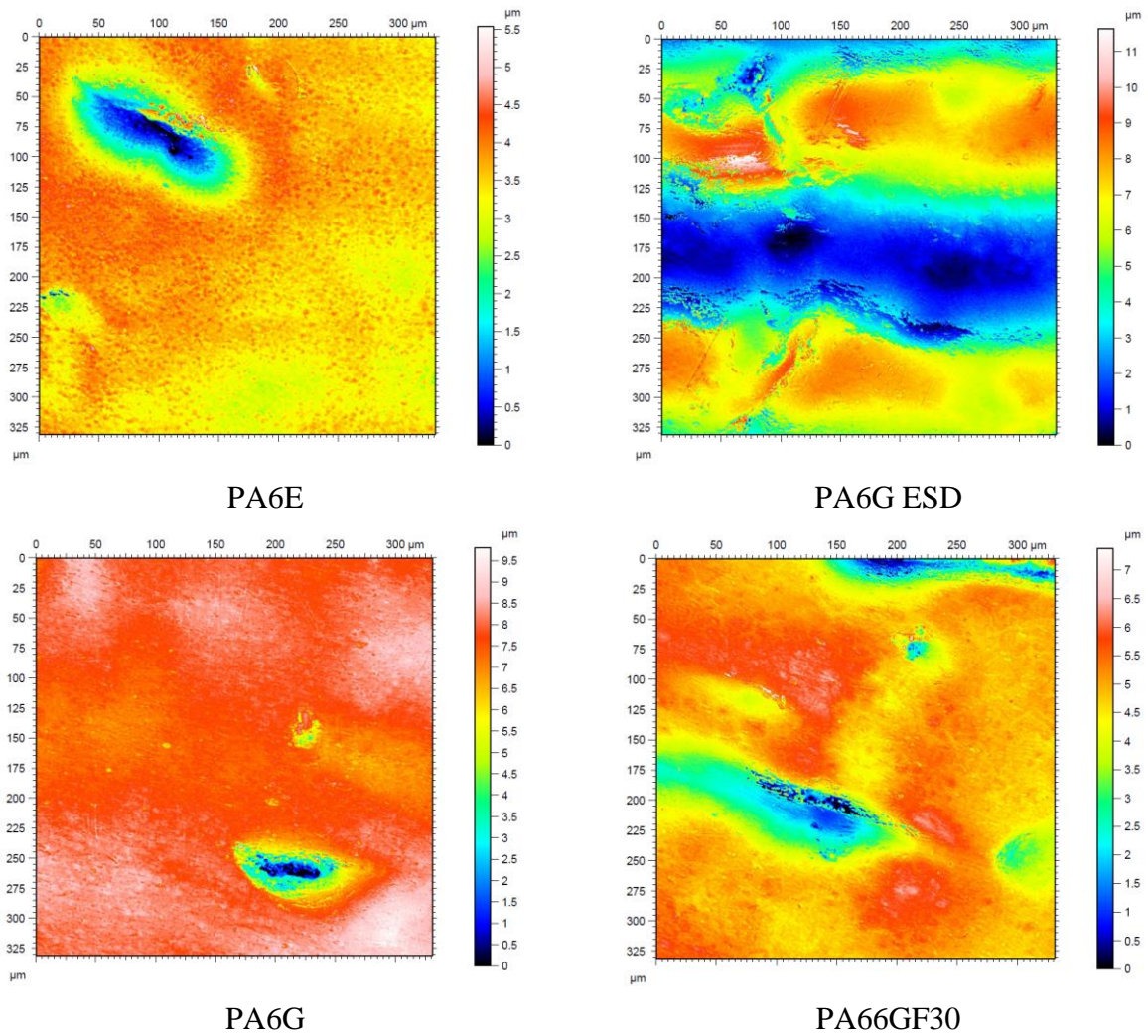


Fig. 4.65. Microscopic visualization of the change in the surface 3D topography of the tested materials on loamy slurry in position 1 (Fig. 3.13)

Table 4.34. Surface characteristics after the tests and the change as a percentage (%)

	<b>HD1000</b>	<b>PLA-HF</b>	<b>PA6E</b>	<b>PA6G ESD</b>	<b>PA6G</b>	<b>PA66GF30</b>
	after the test					
Sq (μm)	1.04	1.85	0.62	2.53	0.87	0.98
Ssk	-0.30	0.42	-2.35	-0.14	-3.89	-1.73
Sku	3.61	3.17	10.96	1.77	27.16	6.50
Sp (μm)	3.54	7.96	2.07	6.77	2.07	2.66
Sv (μm)	3.97	5.19	3.46	4.86	7.72	4.71
Sz (μm)	7.51	13.15	5.53	11.63	9.79	7.38
Sa (μm)	0.81	1.48	0.40	2.24	0.51	0.67
	Change in %					
Sq (μm)	-81.12%	192.38%	-89.68%	-55.35%	-85.67%	-81.52%
Ssk	-1439.16%	-17.49%	-5137.63%	-0.86%	-1502.96%	-361.16%
Sku	74.43%	-44.26%	389.39%	-9.64%	969.08%	82.35%
Sp (μm)	-85.01%	93.46%	-92.75%	-53.53%	-89.49%	-92.88%
Sv (μm)	-65.43%	91.13%	-70.61%	-61.16%	-34.51%	-51.59%
Sz (μm)	-78.61%	92.53%	-86.29%	-57.06%	-68.92%	-84.35%
Sa (μm)	-82.65%	221.48%	-92.18%	-53.19%	-89.94%	-84.38%

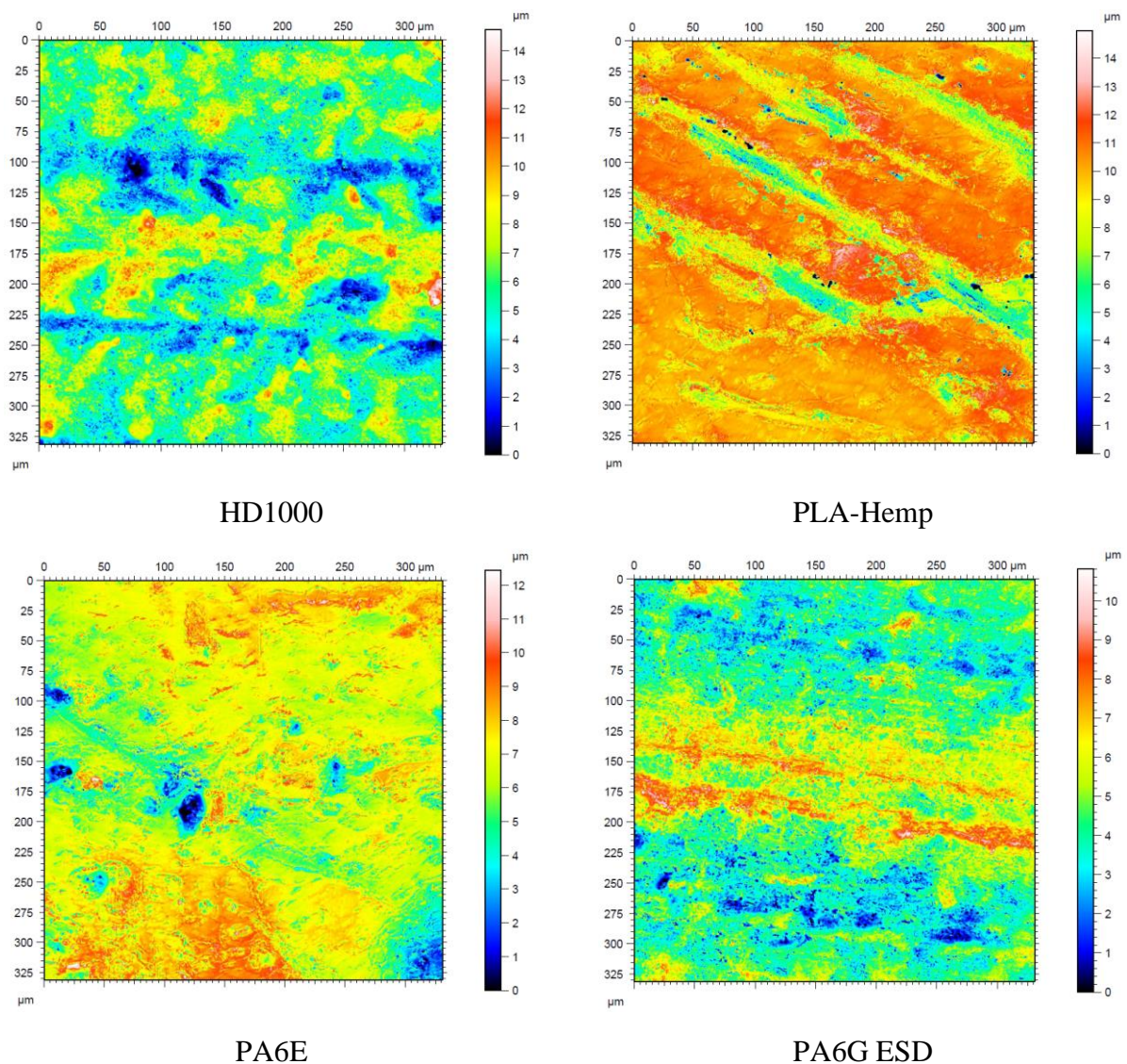


## 4. Results

Using loamy soil for slurry, even polishing effect can be detected, both on the photos (Fig. 4.65) and the surface characteristics (Table 4.34) for the tested engineering polymers. Sq, Sp, Sy, Sv, Sz, Sa decreased accordingly. The exception - similarly to the introduced corundum and gravel results – is the PLA-HF. The opposite trend is again the increased surface roughness and mean plane. In the loamy slurry the sharp impact of the particles may decreased causing much less small pits and craters on the surfaces as it can be experienced with the photos (Figure 4.65). A new form of surface damage occurred: larger but shallow surface flake detachments, indentations, pools appeared.

### Sandy soil:

Fig. 4.66 shows the microscopic visualization of the polymer surfaces in the final states with the Sandy medium at position 1. The measured values of the surface parameters changes are shown in Table 4.35. The other position results are summarized in Appendix 14.



#### 4. Results

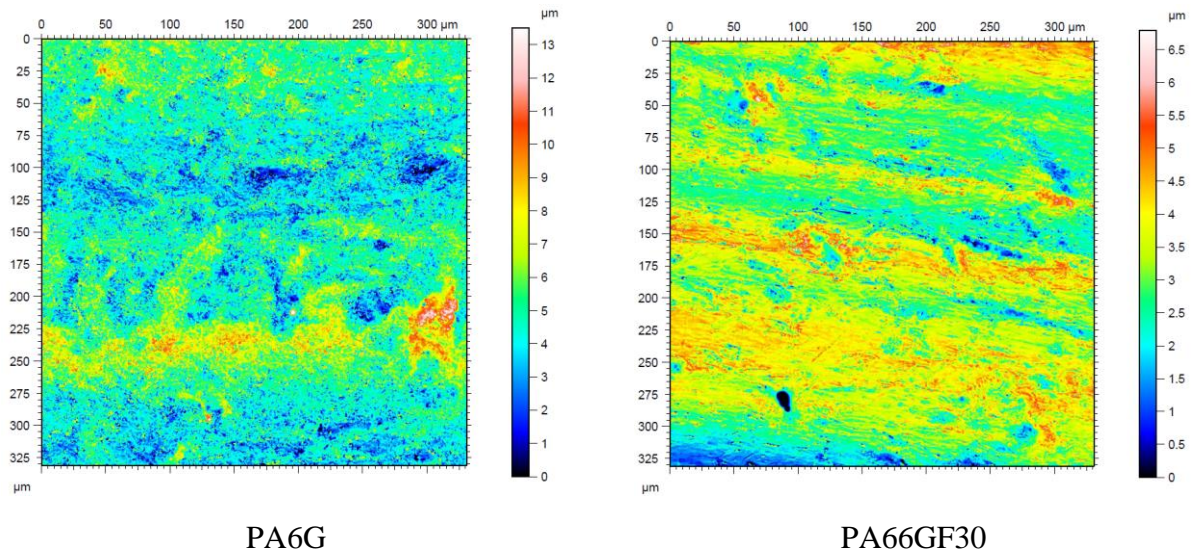


Fig. 4.66. Microscopic visualization of the change in the surface 3D topography of the tested materials on sandy slurry in position 1 (Fig. 3.13)

Table 4.35. Surface characteristics after the tests and the change as a percentage (%)

	<b>HD1000</b>	<b>PLA-HF</b>	<b>PA6E</b>	<b>PA6G ESD</b>	<b>PA6G</b>	<b>PA66GF30</b>
	after the test					
Sq ( $\mu\text{m}$ )	1.86	1.70	1.43	1.52	1.60	0.86
Ssk	0.02	-1.55	-0.77	0.30	0.51	-0.16
Sku	3.25	6.73	5.14	3.25	4.24	3.30
Sp ( $\mu\text{m}$ )	8.84	5.17	5.75	6.24	8.72	3.55
Sv ( $\mu\text{m}$ )	5.90	9.80	6.69	4.57	4.78	3.24
Sz ( $\mu\text{m}$ )	14.74	14.97	12.44	10.81	13.51	6.79
Sa ( $\mu\text{m}$ )	1.48	1.22	1.05	1.20	1.22	0.68
	Change in %					
Sq ( $\mu\text{m}$ )	-66.27%	167.95%	-76.03%	-73.17%	-73.82%	-83.92%
Ssk	7.26%	-404.16%	-1757.01%	-321.10%	84.83%	-124.58%
Sku	57.10%	18.28%	129.61%	65.78%	67.05%	-7.42%
Sp ( $\mu\text{m}$ )	-62.58%	25.69%	-79.90%	-57.14%	-55.77%	-90.50%
Sv ( $\mu\text{m}$ )	-48.59%	260.86%	-43.20%	-63.49%	-59.44%	-66.75%
Sz ( $\mu\text{m}$ )	-58.01%	119.19%	-69.19%	-60.07%	-57.14%	-85.59%
Sa ( $\mu\text{m}$ )	-68.37%	166.37%	-79.39%	-74.94%	-75.69%	-84.25%

The hit of sandy particles could result many small fatigue type pits on the surfaces, which are visible for not only the engineering materials, but for the PLA-HF as well. The decreased surface characteristics - Sq, Sp, Sy, Sv, Sz, Sa - of the engineering polymers confirm the polishing effects just like with the other slurry medium the materials. The exception is again the PLA-HF, where the roughness increased with elevated mean surface as the increased Ssk indicates.

#### 4.2.7. Statistical evaluation of the 3D surface parameters

The complete surface topographic database of slurry measurements is analyzed in detail with the regression modeling (which has been explained already).

To examine the dependence of the 3D surface parameters for the duration of the test, the tangential velocity of the test specimen, the contact angle and the material properties were all used to construct multiple linear regression models.

##### Corundum:

Unfortunately, for the corundum medium, due to the high deviation of the 3D parameters of the examined materials for Sv and Sz models, the goodness-of-fit was lower than 0.5 and usually the only explanatory variable was the duration of the experiment.

##### Sq, Corundum:

For Sq the best fitting model among the possible ones is shown in Eq. 4.15;

$$Sq = 4.870 - 0.762t \quad (4.15)$$

the  $F$ -value of the model was 53.294 and  $p < 0.001$ , thus the model is relevant. For this model the goodness-of-fit is  $R^2 = 0.611$ ,  $t$  has a mediocre effect on Sq.

##### Ssk, Corundum:

For Ssk the best fitting model among the possible ones is shown in Eq. 4.16;

$$Ssk = 0.230 - 0.198 t \quad (4.16)$$

the  $F$ -value of the model was 40.828 and  $p < 0.001$ , thus the model is relevant. For this model the goodness-of-fit is  $R^2 = 0.546$ ,  $t$  has a mediocre effect on Ssk.

##### Sku, Corundum:

For Sku the best fitting model among the possible ones is shown in Eq. 4.17;

$$Sku = 3.011 + 0.961 t \quad (4.17)$$

the  $F$ -value of the model was 38.558 and  $p < 0.001$ , thus the model is relevant. For this model the goodness-of-fit is  $R^2 = 0.531$ ,  $t$  has a mediocre effect on Sku.

##### Sp, Corundum:

For Sp the best fitting model among the possible ones is shown in Eq. 4.18;

$$Sp = 21.335 - 3.195t \quad (4.18)$$

the  $F$ -value of the model was 35.047 and  $p < 0.001$ , thus the model is relevant. For this model the goodness-of-fit is  $R^2 = 0.508$ ,  $t$  has a mediocre effect on Sp.

##### Sa, Corundum:

For Sa the best fitting model among the possible ones is shown in Eq. 4.19;

$$Sa = 4.260 - 0.659t - 0.009 \frac{\sigma_y}{\sigma_c \cdot \varepsilon_B} \quad (4.19)$$

the  $F$ -value of the model was 34.290 and  $p < 0.05$ , thus the model is relevant. For this model the goodness-of-fit is  $R^2 = 0.675$ ,  $t$  and  $\frac{\sigma_y}{\sigma_{c.\varepsilon_B}}$  have an effect on Sa.

#### Gravel:

Unfortunately, for a gravelly type slurry, due to the high deviation of the 3D parameters of the examined materials for Sq, Ssk, Sp, Sa and Sz models, the goodness-of-fit was lower than 0.5 and usually the only explanatory variable was the duration of the experiment.

The only mentionable model was for Ssk, where  $R^2 = 0.449$ , although  $E$  and  $\frac{\sigma_y E}{\sigma_{MH}}$  appeared as explanatory variables.

#### Loamy:

For the loamy type slurry, due to the high deviation of the 3D parameters of the examined materials for Sku, Sp, Sv and Sz models, the goodness-of-fit was lower than 0.5 and usually the only explanatory variable was the duration of the experiment.

#### Sq, Loamy:

For Sq the best fitting model among the possible ones is shown in Eq. 4.20;

$$Sq = 5.320 - 0.674t - 0.0000543E, \quad (4.20)$$

the  $F$ -value of the model was 25.195 and  $p < 0.001$ , thus the model is relevant. For this model the goodness-of-fit is  $R^2 = 0.604$ ,  $t$  has the biggest effect on Sq, while  $E$  has a mediocre effect on Sq.

#### Sa, Loamy:

For Sa the best fitting model among the possible ones is shown in Eq. 4.21;

$$Sa = 4.473 - 0.581t - 0.0000504E, \quad (4.21)$$

the  $F$ -value of the model was 28.955 and  $p < 0.001$ , thus the model is relevant. For this model the goodness-of-fit is  $R^2 = 0.637$ ,  $E$  has a mediocre effect on Sa.

#### Sandy:

For the Sandy type of slurry, due to the high deviation of the 3D parameters of the examined materials for Ssk models, the goodness-of-fit varied between 0.12 and 0.4 and usually the only explanatory variable was the duration of the experiment

#### Sq, Sandy:

For Sq the best fitting model among the possible ones is shown in Eq. 4.22;

$$Sq = 5.691 - 0.629t - 0.0000993E \quad (4.22)$$

the  $F$ -value of the model was 55.998 and  $p < 0.001$ , thus the model is relevant. For this model the goodness-of-fit is  $R^2 = 0.772$ ,  $t$  has the biggest effect on Sq, while  $E$  have mediocre effects on Sq.

Sku, Sandy:

For Sku the best fitting model among the possible ones is shown in Eq. 4.23;

$$Sku = 1.138 + 0.0001627E + 0.497t + 1.580 ca \quad (4.23)$$

the  $F$ -value of the model was 17.858 and  $p < 0.001$ , thus the model is relevant. For this model the goodness-of-fit is  $R^2 = 0.626$ ,  $E$  has the biggest effect on Sku and  $t$  has mediocre effects on Sku.

Sp, Sandy:

For Sp the best fitting model among the possible ones is shown in Eq. 4.24;

$$Sp = 23.407 - 2.409t - 0.094 \frac{\sigma_y}{\sigma_c \cdot \varepsilon_B} \quad (4.24)$$

the  $F$ -value of the model was 19.979 and  $p < 0.001$ , thus the model is relevant. For this model the goodness-of-fit is  $R^2 = 0.548$ ,  $t$  has the biggest effect on Sp, and  $\frac{\sigma_y}{\sigma_c \cdot \varepsilon_B}$  has a low effect on Sp.

Sv, Sandy:

For Sv the best fitting model among the possible ones is shown in Eq. 4.25;

$$Sv = 11.019 - 0.861t - 0.000123E \quad (4.25)$$

the  $F$ -value of the model was 18.570 and  $p < 0.005$ , thus the model is relevant. For this model the goodness-of-fit is  $R^2 = 0.530$ ,  $t$  and  $E$  has a mediocre effect on Sv.

Sz, Sandy:

For Sz the best fitting model among the possible ones is shown in Eq. 4.26;

$$Sz = 33.988 - 3.351t - 0.120 \frac{\sigma_y}{\sigma_c \cdot \varepsilon_B} \quad (4.26)$$

the  $F$ -value of the model was 25.895 and  $p < 0.001$ , thus the model is relevant. For this model the goodness-of-fit is  $R^2 = 0.611$ ,  $t$  and  $\frac{\sigma_y}{\sigma_c \cdot \varepsilon_B}$  have a mediocre effect on Sz.

Sa, Sandy:


For Sa the best fitting model among the possible ones is shown in Eq. 4.27;

$$Sa = 4.762 - 0.545t - 0.0000853E \quad (4.27)$$

the  $F$ -value of the model was 62.254 and  $p < 0.001$ , thus the model is relevant. For this model the goodness-of-fit is  $R^2 = 0.790$ ,  $t$  and  $E$  have a mediocre effect on Sa.

Similarly to the abrasive sensitivity of the pin-on-plate system, the same concept can be introduced for the slurry-pot systems as well. The results, which are based again, on the standardized regression coefficients of the corresponding models, are summarized in Table 4.36.

Table 4.36. Ranking the abrasive sensitivity to slurry systems' features

<b>factors in increasing abrasive sensitivity to system variables</b>				
<b>less dominant</b>		<b>more dominant</b>		
				
Wear, corundum	$\frac{\sigma_y}{\sigma_c \cdot \epsilon_B}$			
Wear, gravel soil	$\frac{\sigma_y}{\sigma_c \cdot \epsilon_B}$			
Wear, loamy soil	$\sigma_F$	$\epsilon_B$	$\frac{\sigma_y E}{\sigma_M H}$	
Wear, Sandy soil	$E$			
Sa, Corundum	$\frac{\sigma_y}{\sigma_c \cdot \epsilon_B}$			
Ssk, gravel	$\frac{\sigma_y E}{\sigma_M H}$	$E$		
Sq, loamy soil	$E$			
Sa, loamy soil	$E$			
Sq, sandy soil	$E$			
Sku, sandy soil	$E$			
Sp, sandy soil	$\frac{\sigma_y}{\sigma_c \cdot \epsilon_B}$			
Sv, sandy soil	$E$			
Sz, sandy soil	$\frac{\sigma_y}{\sigma_c \cdot \epsilon_B}$			
Sa, sandy soil	$E$			

### 4.3. New scientific results

For the investigated engineering plastics (extruded polyamide 6 (PA6E), cast polyamide 6 (PA6G), electrostatic dissipative cast polyamide 6 composite (PA6G-ESD), extruded polyamide 66 composite reinforced with 30% glass fibre (PA66GF30), ultrahigh molecular weight polyethylene, high density grade “1000” (UHMW-PE HD1000)) and one kind of bio-composite materials (PLA reinforced by hemp fibres, PLA-HF) I made the following statements under broad system conditions, in relation to tribological system results and material properties and the dimensionless characteristic numbers formed from them.

#### 1. Abrasive wear in pin-on-plate

Concerning the tested materials I found that there is proportional relation between wear and dimensionless numbers, in different areas of validity. Wear of polyamides (PA66GF30, PA6G ESD, PA6G and PA6E) all correlated with  $\frac{\sigma_y E}{\sigma_M H}$ , and  $\frac{\sigma_y}{\sigma_c \epsilon_B}$ . All engineering plastics (polyamides and UHMW-PE HD 1000) correlated with  $\frac{E}{\sigma_c}$ , furthermore polyamides and bio-composites with  $\frac{\sigma_F \sigma_y}{\sigma_M H}$ . There was no dimensionless parameter proportional to the wear of all engineering plastics and bio-composites.

I found that the areas of validity of the inverse proportionality between wear and dimensionless numbers differ from the validity of direct proportionality. Wear of polyamides (PA66GF30, PA6G ESD, PA6G and PA6E) correlated with  $\frac{H}{E}, \frac{\sigma_y H}{\sigma_M E}, \frac{\sigma_F H}{\sigma_M E}$  and three polyamides (PA6G, PA6E and PA6G ESD) and the bio-composite (PLA-HF) with  $\frac{H \epsilon_B}{\sigma_y}$ . Calculating  $\frac{\sigma_C \epsilon_B}{\sigma_M}$ , loosen inverse relation was found concerning all the tested six polymers.

## 2. Abrasive friction force in pin-on-plate

I found that the abrasive friction resistance of the PLA-HF material is 80-90% higher compared to the five engineering polymers tested. I proved by microscopic images that the main reason for this is the continuous tearing and shearing of the HF fibres on the surface of the PLA-HF during sliding.

## 3. 3D surface topography in pin-on-plate and slurry systems

I concluded that in parallel with the abrasive wear process, the transformation of the surface geometry is bi-directional. I proved with 3D surface topography analyses that in the case of the tough, highly deformable UHMW-PE HD1000 and PA6E, the deformations occur in a larger material cross-section, the micro-geometric parameters (Sp, Sv, Sz, Sa) increased beside decreased Skewness (Ssk) -meaning that the asperities, the surface material is elevated and deformed above the mean plane – and increased Kurtosis (Sku) meaning that the height distribution is more spiked due to the cutting effect. On the contrary, the more rigid PA66GF30 due to the cutting effects performed increased Skewness – the height distribution is skewed below the mean plane in accordance with the experienced wear values – and decreased Kurtosis (Sku) resulting more indented portion on the surface.

## 4. Abrasive sensitivity as system approach method for both test systems

I introduced the abrasive sensitivity analyses as a system approach method. The abrasive sensitivity is the extent of how the independent variables - the sliding distance “s”, the load “ $F_N$ ”, the sliding velocity “v”, the material properties and the dimensionless numbers formed from them - affect the tribo results (wear, friction force, heat generation and change of 3D topography), which is related to the standardized regression coefficients of the models developed. The higher the absolute value of the corresponding standardized regression coefficient is, the higher the abrasive sensitivity of the dependent variable (wear, friction, temperature, surface 3D properties). I worked out such a 2D map visualization of the abrasive sensitivity, where the rank of all impacting factors on the all examined dependent variables are highlighted.

## 5. The change of the polymers' 3D surface characteristics

By means of IBM SPSS 25 software I developed multiple linear regression models and stated for the slurry test systems that wear and the change of the polymers' 3D surface characteristics are sensitive mainly for the tensile features e.g.  $\frac{\sigma_y E}{\sigma_M H}$ ,  $E$  and  $\epsilon_B$ , while the compressive and flexural properties, unlike the pin-on-plate system, played a lesser role. I concluded that some parameters appear in both test system's sensitivity analyses. Wear with P60, P150 pin-on-plate and with gravelly skeletal soil slurry, the  $\frac{\sigma_y}{\sigma_C \epsilon_B}$  is important among the material characteristics. The appearance of the compressive strength is in accordance with the mode of the complex load of micro-geometries. In both test systems,  $E$  is important for the change of 3D surface parameters. This reflects on the role of deformation capability of the surface micro-geometry.

## 5. CONCLUSIONS AND SUGGESTIONS

Abrasive pin-on-plate and slurry-pot systems were applied to study the abrasive behaviour of five engineered polymers and a bio degradable composite. The measured friction, wear and heat generation and 3D surface change, were analysed in conventional ways (graphs, microscopic photos), and furthermore, by means of multiple linear regression models, developed using IBM SPSS 25 software.

Concerning the tested materials, the “sensitivity to abrasion” was introduced, based on the multiple linear regression models, taking the standardized beta regression coefficients into account.

In abrasive pin-on-plate systems (on P60 and P150 particles), where the cutting effect is dominant: PA6G offered the best abrasive resistance while PA66GF30 the worst. The bio-polymer (PLA-HF) was average among the engineered polymers. There are proportional relations between the wear values of the polyamides (PA66GF30, PA6G ESD, PA6G and PA6E) and  $\frac{\sigma_y E}{\sigma_M H}$ , as well as  $\frac{\sigma_y}{\sigma_C \epsilon_B}$ . A similar trend is valid for the polyamides and UHMW-PE HD1000 in the case of  $\frac{E}{\sigma_C}$ .

There are reciprocal relations between values  $\frac{H}{E}$ ,  $\frac{\sigma_F H}{\sigma_M E}$  and the wear of polyamides (PA66GF30, PA6G ESD, PA6G and PA6E).

$\frac{\sigma_F \sigma_y}{\sigma_M H}$  offers such a proportional relation with wear, that 5 materials follow the trend-line except UHMW-PE HD1000.

Despite the different abrasive surfaces, similar material characteristics affected the  $\Delta T$ .  $\sigma_F$  and  $\frac{\sigma_F H}{\sigma_M E}$  are dominant parameters, which reflected on the accumulated work of the micro-geometrical deformation, which was partly converted to heat generation. The multiple regression models proved a high sensitivity and relation with  $\sigma_F$ ,  $\sigma_C$  alone, and in derived dimensionless forms. The change in the surface 3D parameters correlated mainly with E and  $\sigma_F$ ,  $\sigma_C$ .

In slurry-pot systems:

PLA-HF had the worst abrasive resistance, while the engineered polymers offered similar wear trends, the PAE and PA6G being the best ones.

Concerning the wear speed on a daily base, the PLA-HF had a running-in like effect during the first period of testing, which was caused by the fast wear of the coating layer of the composites.

The sensitivity analyses in the abrasive erosion systems enhanced the primary role of the tensile features e.g.  $\frac{\sigma_y E}{\sigma_M H}$ , E and  $\epsilon_B$ .

Sensitivity analyses proved that the varying abrasive load conditions bring different material characteristic groups (e.g. tensile, compressive, flexural) to the fore. Some parameters appear in other system conditions:

Wear P60, P150 and gravel:  $\frac{\sigma_y}{\sigma_C \epsilon_B}$  is important among the material characteristics.

In slurry-pot and pin-on-plate, E is important for the change of 3D surface parameters.

As a follow up to this research, further investigations and activities may be required to cover the most critical effects on both of the engineered polymers and bio-composite material’s tribology. I suggest the following key points:

Improving the performance of the bio-composite materials by using a high wear resistant coating layer.

Testing several types of bio-composite materials.

Studying other surface parameters like, functional parameters (volume) and amplitude parameters.

Initiate real field trials of these used materials and see how other parameters could affect the wear performance like the dynamic load, changing ambient temperature and humidity.



## 6. SUMMARY

To summarize, two different test systems were designed to evaluate the tribological behavior of 5 engineering plastics (PA6E, PA6G, PA66GF30, PA6GESD and UHMW-PE HD1000) and a fully degradable bio-composite (PLA-hemp fiber), targeted for agricultural machinery's abrasive conditions.

The first test system was constructed as a an abrasive pin-on-plate system, which was performed with different loads, sliding velocity on two different standardized abrasive surfaces. For the on-line wear, abrasive friction force and friction temperature change evolution are recorded, which allows specific wear curves to be calculated. The abrasive wear, the friction force and contact temperature evolution were also analyzed as a function of the materials' mechanical properties and the dimensionless numbers derived from them.

The material's response was further investigated in a slurry-pot abrasive test system (which is the second test system) with different sliding velocities and distances. Four different abrasive media compositions were applied while the tested material samples faced to two impact angles. The relative wear of the weight loss percentage (%), compared to the zero day weight, and the daily relative wear of the weight loss percentage (%) compared to the previous day's weight were calculated.

For both test systems, the 3D polymer surface topography was evaluated before and after a given test by using a Taylor-Hobson white light microscope.

All the results and the 3D parameters' values were evaluated and analyzed statistically using IBM SPSS 25 software by developing multiple linear regression models. To examine how a dependent variable depends on several independent (or explanatory) variables, which are all measured on scales, the primary instrument is multiple regression. This tool is also used to examine the sensitivity of the material properties and the test system characteristics, on tribological behavior.

The results of the pin-on-plate test system show that PA6G offered the best abrasive resistance while PA66GF30 the worst. The PLA-HF was average among the engineering polymers. Multiple regression models proved that the tribo results showed high sensitivity and relation with  $\sigma_F$ ,  $\sigma_C$ , both alone and in derived dimensionless forms. The change in the surface 3D parameters correlated mainly with  $E$  and  $\sigma_F$ ,  $\sigma_C$ .

For the slurry-pot system, the results show that PLA-HF had the worst abrasive resistance, while the PA6E and PA6G were the best ones. Concerning the wear speed on a daily base, the PLA-HF had a running-in like effect during the first period of testing, caused by the fast wear of the coating layer of the composites. The engineering polymers including the composite PA66GF30 and PA6G ESD showed less fluctuation in daily wear than the PLA-HF.

Based on the coefficients of the regression models, I developed and introduced the "abrasion sensitivity" maps. In the slurry-pot system, the sensitivity analyses enhanced the primary role of tensile features e.g.  $\frac{\sigma_y E}{\sigma_M H}$ ,  $E$  and  $\epsilon_B$ , while the compressive and flexural properties, unlike the pin-on-plate, played a lesser role.

Sensitivity analyses proved that the varying abrasive load conditions bring different material characteristic groups into account. Some of these parameters appeared in both system conditions like  $\frac{\sigma_y}{\sigma_C \epsilon_B}$ . Also  $E$  has been considered as an important factor for the change of the 3D surface parameters.

This reflects on the role of the deformation capability of the surface micro-geometry.

## 7. ÖSSZEFOGLALÁS (SUMMARY IN HUNGARIAN)

Két különböző vizsgálati rendszert terveztem 5 műszaki műanyag (PA6E, PA6G, PA66GF30, PA6G ESD és UHMW-PE HD1000), valamint egy teljesen bio-lebontható kompozit, a kenderrosttal erősített politejsav (PLA-HF) abrúziós kopási tulajdonságainak kutatására és értékelésére. A modell rendszerek a mezőgazdasági gépalkatrészekben jelentkező, különböző abrúziós igénybevételeket szimulálják.

Az első vizsgálati rendszer „polimer tű – abrúziós síkfelület”, azaz pin-on-plate elrendezésű, ahol az álló, 8 mm átmérőjű polimer hengeres próbatesteket három terhelési szinten (9,81-, 29,43-, és 49,05 N), és két eltérő abrúziós csúszási sebességen (0,031 és 0,056 m/s) koptattam, melyhez kétféle szabványos csiszolóvászaron síkfelületet alkalmaztam (P60 és P150). Ez a vizsgálati rendszer a polimer felületek mikro-vágását és deformációját biztosítja. Az abrúziós csúszás során on-line rögzítettem a polimer próbatestek kopását, a súrlódási erőt és a súrlódási hőmérséklet változását. A kiválasztott polimereket abrazív eróziós környezetben is teszteltem, ahol a különböző abrazív koptató közegek (korund, kavicsos öntéstalaj, vályogtalaj és homoktalaj) vizes keveréke örvénylő mozgással ütközik a polimer próbatestek felületének (slurry-pot tribo-system).

Mindkét vizsgálati rendszerben 3D felülettopográfiai mérésekre alapozva összehasonlítottam a kiindulási és a koptatás végi polimer felületek mikrogeometriájának változását. Az összes on-line és 3D mikroszkópiai eredményt statisztikailag is elemeztem az IBM SPSS 25 szoftver segítségével. Többszörös lineáris regressziós modelleket állítottam fel.

A pin-on-plate rendszerben a PA6G nyújtotta a legjobb kopásállóságot a mikro-vágások ellen, míg a PA66GF30, a legkisebb alakváltozási képességgel rendelkező kompozit a leggyengébb. A bio-polimer (PLA-HF) átlagos kopásállósággal rendelkezett, de a súrlódási ellenállása a kenderrostok tépése miatt a többi polimerhez képest a duplája volt. A többváltozós lineáris regressziós modellek a tribo-rendszer eredményei kapcsán magas érzékenységet és kapcsolatot mutattak a  $\sigma_F$ ,  $\sigma_C$ -vel. A felületi 3D paraméterek változása főként  $E$  és  $\sigma_F$ ,  $\sigma_C$  értékekkel korrelált.

A slurry-pot rendszerben (abrazív erózió) a PLA-HF kopásállósága volt a legrosszabb, a szívós és nagy szilárdsággal rendelkező PAE és a PA6G volt a legjobb. A PLA-HF esetén egy „running-in” azaz bekopási szakasz volt elkülöníthető, amelyet a felületi, erősítetlen rétegének a lekopása eredményezett.

A regressziós modellek együtthatói alapján kidolgoztam és bevezettem az egyes vizsgálati rendszereket jellemző „abrúziós érzékenység”-i térképeket. A slurry-pot rendszerek érzékenységi elemzése rámutattak a húzó tulajdonságok elsődleges szerepére, pl.  $\frac{\sigma_y E}{\sigma_{MH}}$ ,  $E$  és  $\epsilon_B$ , míg a nyomó és hajlító tulajdonságok, ellentétben a pin-on-plate rendszerrel, kisebb szerepet játszottak.

Igazoltam, hogy a változó abrúziós hatások különböző anyagjellemző csoportokkal kapcsolatba hozhatók. Ezen paraméterek némelyike, mint pl.  $\frac{\sigma_y}{\sigma_C \epsilon_B}$  a P60, P150 és kavicsos talaj koptató hatásával is korrelált. A rugalmassági modulus ( $E$ ) is fontos tényezőnek tekinthető a 3D-s felületi paraméterek változásában. Ez tükröződik a felületi mikro-geometria deformációs képességének szerepében is.

## 8. APPENDICES

### A1: Bibliography

1. Abhi (2010): *What Is A Polymer- Polymer Engineering Solutions*, Plastic Injection Molding Design Process. Available at: <http://plasticinjectionmouldingdesign.blogspot.com/2010/12/what-is-polymer-polymer-engineering.html#more> (Accessed: 3 August 2017)
2. Accuratus (2013): *Aluminum Oxide, Al<sub>2</sub>O<sub>3</sub> Material Properties*. Available at: <https://accuratus.com/alumox.html> (Accessed: 20 December 2020)
3. Aderikha, V. N., and Krasnov, A. P. (2013): Solid Lubricants, Polymer-Based Self-Lubricating Materials, in *Encyclopedia of Tribology*. Boston, MA: Springer US, 3186–3193. [https://doi.org/10.1007/978-0-387-92897-5\\_1232](https://doi.org/10.1007/978-0-387-92897-5_1232)
4. Alagirusamy, R., Fangueiro, R., Ogale, V., and Padaki, N. (2006): Hybrid Yarns and Textile Preforming for Thermoplastic Composites, *Textile Progress*, 38(4), 1–71. <https://doi.org/10.1533/tepr.2006.0004>
5. Andó, M., Kalácska, G., and Czigány, T. (2008): Cast Polyamide 6 Polymer Composites for Agricultural Machine Applications, *Hungarian Agricultural Engineering, Gödöllő*, 67–69
6. Axén, N., Jacobson, S., and Hogmark, S. (2001): *Friction and wear measurement techniques*. CRC Press
7. Bahadur, S. (2000): The development of transfer layers and their role in polymer tribology, in *Wear*, 92–99. [https://doi.org/10.1016/S0043-1648\(00\)00469-5](https://doi.org/10.1016/S0043-1648(00)00469-5)
8. Bartenev, G. M., and Lavrentev, V. V. (1981): *Friction and wear of polymers*. Elsevier
9. Bates, T. R., Ludema, K. C., and Brainard, W. A. (1974): A rheological mechanism of penetrative wear, *Wear*, 30(3), 365–375. [https://doi.org/10.1016/0043-1648\(74\)90150-1](https://doi.org/10.1016/0043-1648(74)90150-1)
10. Békési, N. (2012): Modelling Friction and Abrasive Wear of Elastomers, in *Advanced Elastomers - Technology, Properties and Applications*. InTech, 341–362. <https://doi.org/10.5772/50498>
11. Bely, V. A., Sviridenok, A. I., Petrokovets, M. I., and Savkin, V. G. (1982): *Friction and Wear in Polymer-Based Materials*. Oxford, UK: Pergamon press. <https://doi.org/10.1016/C2013-0-03331-2>
12. Bhushan, B. (1999): *Principles and applications of tribology*, Wilky-Interscience, Chichester.
13. Bhushan, B. (2000): *Modern tribology handbook, two volume set*. CRC press
14. Biron, M. (2013): Outline of the Actual Situation of Plastics Compared to Conventional Materials, in *Thermoplastics and Thermoplastic Composites*. Second. Oxford, UK: William Andrew Publishing, 1–29
15. Busch, K., Hochmuth, C., Pause, B., Stoll, A., and Wertheim, R. (2016): Investigation of Cooling and Lubrication Strategies for Machining High-temperature Alloys, *Procedia CIRP*, 41, 835–840. <https://doi.org/10.1016/j.procir.2015.10.005>

16. Chanda, M., and Roy, S. K. (2006): *Plastics Technology Handbook*. CRC Press. <https://doi.org/10.1201/9781420006360>
17. Ciraci, S., Yildirim, T., Dag, S., and Gulseren, O. (2007): Ab-initio Atomic Scale Study of Nearly Frictionless Surfaces, in *Superlubricity*. Elsevier, 57–77. <https://doi.org/10.1016/B978-044452772-1/50035-4>
18. Deltombe, R., Kubiak, K. J., and Bigerelle, M. (2014): How to select the most relevant 3D roughness parameters of a surface, *Scanning*, 36(1), 150–160. <https://doi.org/10.1002/sca.21113>
19. Devine, M. J. (1976): *Proceedings of a Workshop on Wear Control to Achieve Product Durability. 23-25 February 1976. Sponsored by the Office of Technology Assessment United States Congress*. NAVAL AIR DEVELOPMENT CENTER WARMINSTER PA. Available at: <https://apps.dtic.mil/sti/citations/ADA055712>
20. Ellis, K. A., Pritzker, M. D., and Fahidy, T. Z. (1995): Modeling the Degradation of Scanning Electrochemical Microscope Images Due to Surface Roughness, *Analytical Chemistry*, 67(24), 4500–4507. <https://doi.org/10.1021/ac00120a012>
21. Encyclios (2020a): *Friction*. Available at: <https://www.encyclios.org/physics/friction/> (Accessed: 12 December 2020)
22. Encyclios (2020b): *Lubricant*. Available at: <https://www.encyclios.org/engineering/lubricant/> (Accessed: 12 December 2020)
23. Gahr, K. H. Z. (1988): Modelling of two-body abrasive wear, *Wear*, 124(1), 87–103. [https://doi.org/10.1016/0043-1648\(88\)90236-0](https://doi.org/10.1016/0043-1648(88)90236-0)
24. Girisha, K. G., Anil, K. C., and Akash, A. (2014): Mechanical properties of jute and hemp reinforced epoxy/polyester hybrid composites, *International Journal of Engineering and Technology*, 2347–4599
25. Gupta, M. K., Srivastava, R. K., and Bisaria, H. (2015): Potential of jute fibre reinforced polymer composites: a review, *International Journal of Fiber and Textile Research*, 5(3), 30–38
26. Harris, T. A., and Kotzalas, M. N. (2006): *Essential concepts of bearing technology*. CRC press
27. Harsha, A. P. (2011): An investigation on low stress abrasive wear characteristics of high performance engineering thermoplastic polymers, *Wear*, 271(5–6), 942–951. <https://doi.org/10.1016/j.wear.2011.03.019>
28. Hokkirigawa, K., and Kato, K. (1988): An experimental and theoretical investigation of ploughing, cutting and wedge formation during abrasive wear, *Tribology International*, 21(1), 51–57. [https://doi.org/10.1016/0301-679X\(88\)90128-4](https://doi.org/10.1016/0301-679X(88)90128-4)
29. Hutchings, I., Gee, M., and Santner, E. (2006): Friction and Wear, in *Springer Handbook of Materials Measurement Methods*. Berlin, Heidelberg: Springer Berlin Heidelberg, 685–710. [https://doi.org/10.1007/978-3-540-30300-8\\_13](https://doi.org/10.1007/978-3-540-30300-8_13)

30. Jeyaprakash, N., and Yang, C.-H. (2021): Friction, Lubrication, and Wear, in Tribology in Materials and Manufacturing - Wear, Friction and Lubrication. IntechOpen. <https://doi.org/10.5772/intechopen.93796>
31. Kalácska, Á., De Baets, P., Fauconnier, D., Schramm, F., Frerichs, L., and Sukumaran, J. (2020): Abrasive wear behaviour of 27MnB5 steel used in agricultural tines, *Wear*, 442–443, 203107. <https://doi.org/10.1016/j.wear.2019.203107>
32. Kalacska, G. (2013): An engineering approach to dry friction behaviour of numerous engineering plastics with respect to the mechanical properties, *Express Polymer Letters*, 7(2), 199–210. <https://doi.org/10.3144/expresspolymlett.2013.18>
33. Kalacska, G. (2017): *Polymers*. Godollo
34. Kalácska, G. (2007): Műszaki polimerek és kompozitok a gépészmérnöki gyakorlatban. 3C-Grafika Kft., Gödöllő
35. Kalácska, G., Zsidai, L., Róbert, K., and Otto, E. (2008): Abrasive wear of polymer/steel gear pairs in different soil types, in The international conference of the Carpathian Euro-region specialists in industrial systems. Citeseer
36. Kaplonek, W., and Lukianowicz, C. (2012): Coherence Correlation Interferometry in Surface Topography Measurements, in Recent Interferometry Applications in Topography and Astronomy. InTech. <https://doi.org/10.5772/35059>
37. Kato, K. (1997): Abrasive wear of metals, *Tribology International*, 30(5), 333–338. [https://doi.org/10.1016/S0301-679X\(96\)00063-1](https://doi.org/10.1016/S0301-679X(96)00063-1)
38. Kato, K. (2000): Wear in relation to friction — a review, *Wear*, 241(2), 151–157. [https://doi.org/10.1016/S0043-1648\(00\)00382-3](https://doi.org/10.1016/S0043-1648(00)00382-3)
39. Keresztes, R., Kalácska, G., Zsidai, L., and Eberst, O. (2008): ABRASIVE WEAR OF POLYMER-BASED AGRICULTURAL MACHINE ELEMENTS IN DIFFERENT SOIL TYPES, *Cereal Research Communications*, 36, 903–906. Available at: <http://www.jstor.org/stable/90002851>
40. Keyence America (2021): *Friction, Wear, and Abrasion Tests and Analysis*, KEYENCE America. Available at: <https://www.keyence.com/ss/products/microscope/vhx-casestudy/chemistry/wear-test.jsp> (Accessed: 20 November 2020)
41. Khondker, O. A., Ishiaku, U. S., Nakai, A., and Hamada, H. (2006): A novel processing technique for thermoplastic manufacturing of unidirectional composites reinforced with jute yarns, *Composites Part A: Applied Science and Manufacturing*, 37(12), 2274–2284. <https://doi.org/10.1016/j.compositesa.2005.12.030>
42. Kim, S. H., and Park, C. H. (2017): Direct impregnation of thermoplastic melt into flax textile reinforcement for semi-structural composite parts, *Industrial Crops and Products*, 95, 651–663. <https://doi.org/10.1016/j.indcrop.2016.11.034>
43. Kitsunai, H., Kato, K., Hokkirigawa, K., and Inoue, H. (1990): The transitions between microscopic wear modes during repeated sliding friction observed by a scanning electron microscope tribosystem, *Wear*, 135(2), 237–249. [https://doi.org/10.1016/0043-1648\(90\)90028-9](https://doi.org/10.1016/0043-1648(90)90028-9)

44. Knight, I. (2016): *Machinery Wear – How to Eliminate It!*, Reliability link. Available at: <http://reliabilitylink.com/machinery-wear-eliminate/> (Accessed: 13 December 2020)
45. Koutsos, V. (2009): Chapter 46: Polymeric materials: an introduction, in ICE manual of Construction Materials, 571–577. <https://doi.org/10.1680/mocm.35973.0571>
46. Kovaříková, I., Szewczykova, B., Blaškoviš, P., Hodúlová, E., and Lechovič, E. (2009): Study and characteristic of abrasive wear mechanisms, *Materials Science and Technology*, 1, 1–8
47. Kumar, R., and Antonov, M. (2020): Self-lubricating materials for extreme temperature tribo-applications, *Materials Today: Proceedings*. <https://doi.org/10.1016/j.matpr.2020.10.824>
48. Kumar, S., and Panneerselvam, K. (2016): Two-body Abrasive Wear Behavior of Nylon 6 and Glass Fiber Reinforced (GFR) Nylon 6 Composite, *Procedia Technology*, 25, 1129–1136. <https://doi.org/10.1016/j.protcy.2016.08.228>
49. Lancaster, J. K. (1969): Abrasive wear of polymers, *Wear*, 14(4), 223–239. [https://doi.org/10.1016/0043-1648\(69\)90047-7](https://doi.org/10.1016/0043-1648(69)90047-7)
50. Larsen-Basse, J., and Sokolowski, S. S. (1975): Influence of atmospheric humidity on abrasive wear — II. 2-body abrasion, *Wear*, 32(1), 9–14. [https://doi.org/10.1016/0043-1648\(75\)90200-8](https://doi.org/10.1016/0043-1648(75)90200-8)
51. Lee, G. Y., Dharan, C. K. ., and Ritchie, R. . (2002): A physically-based abrasive wear model for composite materials, *Wear*, 252(3–4), 322–331. [https://doi.org/10.1016/S0043-1648\(01\)00896-1](https://doi.org/10.1016/S0043-1648(01)00896-1)
52. Li, C. X. (2009a): *Wear and Wear Mechanism*, The University of Birmingham, UK. Available at: [http://emrtk.uni-miskolc.hu/projektek/adveng/home/kurzus/korsz\\_anyagtech/1\\_konzultacio\\_elemei/wear\\_and\\_wear\\_mechanism.htm](http://emrtk.uni-miskolc.hu/projektek/adveng/home/kurzus/korsz_anyagtech/1_konzultacio_elemei/wear_and_wear_mechanism.htm) (Accessed: 24 June 2017)
53. Li, C. X. (2009b): *Wear Testing and Wear Measurement*, The University of Birmingham, UK. Available at: [http://emrtk.uni-miskolc.hu/projektek/adveng/home/kurzus/korsz\\_anyagtech/1\\_konzultacio\\_elemei/wear\\_testing\\_measurement.htm](http://emrtk.uni-miskolc.hu/projektek/adveng/home/kurzus/korsz_anyagtech/1_konzultacio_elemei/wear_testing_measurement.htm) (Accessed: 24 June 2017)
54. Li, X., Zhao, Z., Xiong, J., and Liu, C. (2020): 2D numerical model for studying frictional sliding, *Acta Mechanica Sinica*, 36(3), 742–753. <https://doi.org/10.1007/s10409-020-00955-2>
55. Lim, S. C., and Brunton, J. H. (1985): A dynamic wear rig for the scanning electron microscope, *Wear*, 101(1), 81–91. [https://doi.org/10.1016/0043-1648\(85\)90213-3](https://doi.org/10.1016/0043-1648(85)90213-3)
56. Ludema, K. C. (1996): *Friction, Wear, Lubrication: a textbook in Tribology*, Ann Arbor: CRC Press, Inc, Boca Raton
57. Mahapatra, L., and Mohanty, S. (2007): *The effect of strain rate on jute fiber composites*. National Institute of Technology, Rourkela, India

58. La Mantia, F. P., and Morreale, M. (2011): Green composites: A brief review, *Composites Part A: Applied Science and Manufacturing*, 42(6), 579–588. <https://doi.org/10.1016/j.compositesa.2011.01.017>
59. Maru, M. M., and Tanaka, D. K. (2006): Influence of loading, contamination and additive on the wear of a metallic pair under rotating and reciprocating lubricated sliding, *Journal of the Brazilian Society of Mechanical Sciences and Engineering*, 28(3). <https://doi.org/10.1590/S1678-58782006000300005>
60. Miro, G. (2018): *External Contaminants in Lubricating Oils: A Common but Critical Problem*, ATTEN2, Advanced monitoring technologies. Available at: <https://blog.atten2.com/en/external-contaminants-in-lubricating-oils-a-common-but-critical-problem> (Accessed: 18 January 2021)
61. Mishra, V. (2014): Physical, mechanical and abrasive wear behaviour of jute fiber reinforced polymer composites
62. Moore, M. A. (1974): A review of two-body abrasive wear, *Wear*, 27(1), 1–17. [https://doi.org/10.1016/0043-1648\(74\)90080-5](https://doi.org/10.1016/0043-1648(74)90080-5)
63. Mukherjee, T., and Kao, N. (2011): PLA Based Biopolymer Reinforced with Natural Fibre: A Review, *Journal of Polymers and the Environment*, 19(3), 714–725. <https://doi.org/10.1007/s10924-011-0320-6>
64. Myshkin, N. K., Petrokovets, M. I., and Kovalev, A. V. (2005): Tribology of polymers: Adhesion, friction, wear, and mass-transfer, *Tribology International*, 38(11–12), 910–921. <https://doi.org/10.1016/j.triboint.2005.07.016>
65. Myshkin, N., and Kovalev, A. (2018): Adhesion and surface forces in polymer tribology—A review, *Friction*, 6(2), 143–155. <https://doi.org/10.1007/s40544-018-0203-0>
66. Myshkin, N., and Petrokovets, M. (2004): Mechanical behavior of plastics: surface properties and tribology. *Mechanical tribology, materials, characterization, and applications*. GEL Totten, Hong. New York, Marcel Dekker
67. Nasrullah, J., Tyler, G. L., and Nishi, Y. (2005): An Atomic Force Microscope Study of Surface Roughness of Thin Silicon Films Deposited on SiO<sub>2</sub>, *IEEE Transactions On Nanotechnology*, 4(3), 303–311. <https://doi.org/10.1109/TNANO.2005.847007>
68. Park, C. H., and Lee, W. I. (2012): Compression molding in polymer matrix composites, in *Manufacturing Techniques for Polymer Matrix Composites (PMCs)*. Elsevier, 47–94. <https://doi.org/10.1533/9780857096258.1.47>
69. Pascoe, M. W., and Tabor, D. (1956): The friction and deformation of polymers, *Proceedings of the Royal Society of London. Series A. Mathematical and Physical Sciences*, 235(1201), 210–224
70. Patnaik, A., Satapathy, A., Chand, N., Barkoula, N. M., and Biswas, S. (2010): Solid particle erosion wear characteristics of fiber and particulate filled polymer composites: A review, *Wear*, 268(1–2), 249–263. <https://doi.org/10.1016/j.wear.2009.07.021>
71. Prajapati, A. K., Omrani, E., Menezes, P. L., and Rohatgi, P. K. (2018): RETRACTED CHAPTER: Self-Lubricating Polymer Composites, in *Self-Lubricating Composites*.

- Berlin, Heidelberg: Springer Berlin Heidelberg, 75–103. [https://doi.org/10.1007/978-3-662-56528-5\\_3](https://doi.org/10.1007/978-3-662-56528-5_3)
72. Quagliani, V., and Dubini, P. (2011): Friction of Polymers Sliding on Smooth Surfaces, *Advances in Tribology*, 2011, 1–8. <https://doi.org/10.1155/2011/178943>
73. Quattroplast (2019): *Quattroplast products*. Available at: <https://quattroplast.hu/en/products> (Accessed: 10 February 2019)
74. Quintelier, J. (2007): *Online wear monitoring of polymer matrix composites with advanced measurement techniques*. Ghent University
75. Rabinowicz, E., Dunn, L. A., and Russell, P. G. (1961): A study of abrasive wear under three-body conditions, *Wear*, 4(5), 345–355. [https://doi.org/10.1016/0043-1648\(61\)90002-3](https://doi.org/10.1016/0043-1648(61)90002-3)
76. Rajesh, J. J., Bijwe, J., and Tewari, U. S. (2001): Influence of fillers on abrasive wear of short glass fibre reinforced polyamide composites, *Journal of Materials Science*, 36(2), 351–356. <https://doi.org/10.1023/A:1004812109247>
77. Rajesh, J. J., Bijwe, J., and Tewari, U. S. (2002): Abrasive wear performance of various polyamides, *Wear*, 252(9–10), 769–776. [https://doi.org/10.1016/S0043-1648\(02\)00039-X](https://doi.org/10.1016/S0043-1648(02)00039-X)
78. Rigney, D. A. (1997): Comments on the sliding wear of metals, *Tribology International*, 30(5), 361–367. [https://doi.org/10.1016/S0301-679X\(96\)00065-5](https://doi.org/10.1016/S0301-679X(96)00065-5)
79. Sarankó, Á., Kalácska, G., and Keresztes, R. (2017): Developed polymer pin-on-disc test system for fatigue-sliding models, *Scientific Bulletin Series C: Fascicle Mechanics, Tribology, Machine Manufacturing Technology*, 31, 57–60
80. Sari, M. R., Haiahem, A., and Flamand, L. (2007): Effect of Lubricant Contamination on Gear Wear, *Tribology Letters*, 27(1), 119–126. <https://doi.org/10.1007/s11249-007-9215-z>
81. Sari, M. R., Ville, F., Haiahem, A., and Flamand, L. (2010): Effect of lubricant contamination on friction and wear in an EHL sliding contact, *Mechanics*, 82(2), 43–49
82. Sasada, T., Oike, M., and Emori, N. (1984): The effect of abrasive grain size on the transition between abrasive and adhesive wear, *Wear*, 97(3), 291–302. [https://doi.org/10.1016/0043-1648\(84\)90155-8](https://doi.org/10.1016/0043-1648(84)90155-8)
83. Sawpan, M. A., Pickering, K. L., and Fernyhough, A. (2011): Improvement of mechanical performance of industrial hemp fibre reinforced polylactide biocomposites, *Composites Part A: Applied Science and Manufacturing*, 42(3), 310–319. <https://doi.org/10.1016/j.compositesa.2010.12.004>
84. Sidorov, S. A., Khoroshenkov, V. K., Lobachevskii, Y. P., and Akhmedova, T. S. (2017): Improving Wear Resistance of Agricultural Machine Components by Applying Hard-Alloy Thick-Layer Coatings Using Plasma Surfacing, *Metallurgist*, 60(11–12), 1290–1294. <https://doi.org/10.1007/s11015-017-0443-7>
85. Singh, R., and Bajpai, V. (2014): Coolant and Lubrication in Machining, in *Handbook of Manufacturing Engineering and Technology*. London: Springer London, 1–34. [https://doi.org/10.1007/978-1-4471-4976-7\\_7-1](https://doi.org/10.1007/978-1-4471-4976-7_7-1)



86. Singha, A. S., and Thakur, V. K. (2008): Mechanical properties of natural fibre reinforced polymer composites, *Bulletin of materials Science*, 31(5), 791–799
87. Sinha, S. K., and Briscoe, B. J. (2009): *Polymer tribology*. World Scientific
88. Soemantri, S., McGee, A. C., and Finnie, I. (1985): Some aspects of abrasive wear at elevated temperatures, *Wear*, 104(1), 77–91. [https://doi.org/10.1016/0043-1648\(85\)90247-9](https://doi.org/10.1016/0043-1648(85)90247-9)
89. Stachowiak, G., and Batchelor, A. W. (2013): *Engineering tribology*. Edited by Fourth. Butterworth-Heinemann
90. Stachowiak, G. W., and Batchelor, A. W. (2001): *Engineering tribology*. Second. Butterworth-Heinemann
91. Stachowiak, G. W., and Batchelor, A. W. (2005): *Engineering tribology*. Third, Butterworth-Heinemann. Third
92. Su, Y. (2016): Investigation into the role of cooling/lubrication effect of cryogenic minimum quantity lubrication in machining of AISI H13 steel by three-dimensional finite element method, *Proceedings of the Institution of Mechanical Engineers, Part B: Journal of Engineering Manufacture*, 230(6), 1003–1016. <https://doi.org/10.1177/0954405414564806>
93. Summerscales, J., Dissanayake, N. P. J., Virk, A. S., and Hall, W. (2010): A review of bast fibres and their composites. Part 1 – Fibres as reinforcements, *Composites Part A: Applied Science and Manufacturing*, 41(10), 1329–1335. <https://doi.org/10.1016/j.compositesa.2010.06.001>
94. Svensson, N., Shishoo, R., and Gilchrist, M. (1998): Manufacturing of Thermoplastic Composites from Commingled Yarns-A Review, *Journal of Thermoplastic Composite Materials*, 11(1), 22–56. <https://doi.org/10.1177/089270579801100102>
95. Szabadi, L. (2011): *Többrétegű tűzihorgany bevonatok abrázíós kopása*. Szent Istvan University
96. Tervoort, T. A., Visjager, J., and Smith, P. (2002): On Abrasive Wear of Polyethylene, *Macromolecules*, 35(22), 8467–8471. <https://doi.org/10.1021/ma020579g>
97. Thakur, V. K., Thakur, M. K., and Gupta, R. K. (2014): Review: Raw Natural Fiber–Based Polymer Composites, *International Journal of Polymer Analysis and Characterization*, 19(3), 256–271. <https://doi.org/10.1080/1023666X.2014.880016>
98. Tholt, B., Miranda-Júnior, W. G., Prioli, R., Thompson, J., and Oda, M. (2006): Surface Roughness in Ceramics with Different Finishing Techniques Using Atomic Force Microscope and Profilometer, *Operative Dentistry*, 31(4), 442–449. <https://doi.org/10.2341/05-54>
99. Toplice, D. (2009): *Electro-Corundum (aluminium oxide) for surface treatment*. Available at: [https://ferroecoblast.com/storage/app/media/products/air\\_blasting/abrasives/78-corundum\\_en\\_ti\\_jan2009\\_web\\_en.pdf](https://ferroecoblast.com/storage/app/media/products/air_blasting/abrasives/78-corundum_en_ti_jan2009_web_en.pdf) (Accessed: 12 December 2020)
100. Tribonet (2017): *What Are Lubricants?* Available at: <https://www.tribonet.org/wiki/what-are-lubricants/> (Accessed: 13 December 2020)

101. Varenberg, M. (2013): Towards a unified classification of wear, *Friction*, 1(4), 333–340. <https://doi.org/10.1007/s40544-013-0027-x>
102. Wahit, M. U., Akos, N. I., and Laftah, W. A. (2012): Influence of natural fibers on the mechanical properties and biodegradation of poly(lactic acid) and poly( $\epsilon$ -caprolactone) composites: A review, *Polymer Composites*, 33(7), 1045–1053. <https://doi.org/10.1002/pc.22249>
103. Walczak, M., Caban, J., and Marczuk, A. (2017): Evaluation of Tribological Properties of Polymer Materials Used for Sliding Bearings in Agricultural Machinery, *Agricultural Engineering*, 21(1), 95–103. <https://doi.org/10.1515/agriceng-2017-0010>
104. Wen, S., and Huang, P. (2017): *Principles of Tribology*. Singapore: John Wiley & Sons Singapore Pte. Ltd. <https://doi.org/10.1002/9781119214908>
105. Yan, P., Rong, Y., and Wang, G. (2016): The effect of cutting fluids applied in metal cutting process, *Proceedings of the Institution of Mechanical Engineers, Part B: Journal of Engineering Manufacture*, 230(1), 19–37. <https://doi.org/10.1177/0954405415590993>
106. Yapici, S., Baltaci, Ö. A., Guzel, S., and Mihalic, F. (2014): Application of Polymer Matrix Composite Materials for the Tractor Safety Frames, *Tarım Makinaları Bilimi Dergisi*, 10(4), 317–322
107. Zhu, J., Xie, F., and Dwyer-Joyce, R. S. (2020): PEEK Composites as Self-Lubricating Bush Materials for Articulating Revolute Pin Joints, *Polymers*, 12(3), 665. <https://doi.org/10.3390/polym12030665>

**A2: Publications related to the dissertation***Refereed papers in foreign languages:*

1. **Muhandes, H.**, Kalacska, G., Kadi, N., Skrifvars, M. (2017): Thermoplastic bio-composite based on cellulose fibers, V. Synergy International Conference, Engineering, Agriculture and Green Industry Innovation, Mechanical Engineering Letters, Vol. 15, pp. 7-15.
2. Kalacska, A., **Muhandes, H.**, (2018): 3D topographical analysis of abrasive worn surfaces, Mechanical Engineering Letters, Vol. 17, pp. 47-56.
3. **Muhandes, H.**, Kalacska, G., (2019): A slurry-pot abrasive wear test device for several composite materials, International Journal of Engineering and Management Sciences, Vol. 4, No. 1, pp. 437-444, doi: 10.21791/IJEMS.2019.1.54.
4. **Muhandes, H.**, Kalacska, A., Kalacska, G. (2020): Analyses of abrasive wear behaviour in pin-on-plate tribo-system for several materials, IOP Conf. Series: Materials Science and Engineering 749 (2020) IOP Publishing, doi:10.1088/1757-899X/749/1/012020.
5. **Muhandes, H.**, Kalacska, A., Székely, L., Keresztes, R., Kalacska, G. (2020): Abrasive sensitivity of engineering polymers and a bio-composite under different abrasive conditions. Materials 13(22): 5239. (IF: 3.057)
6. **Muhandes, H.**, Kalacska, G. (2020): Bio-degradable Polymer composites as abrasive wear materials. Polymer Sci Peer Rev J. 1(3). PSPRJ. 000512.

*Refereed papers in Hungarian:*

7. **Muhandes, H.**, Kalacska, G. (2018): Kompozit anyagok abrazív koptató vizsgálata pin-on-plate tribométerrel, Műanyagipari Szemle, 06. sz., 1-10. ISSN 1785-7856.
8. **Muhandes, H.**, Kalacska, G. (2020): Mezőgazdasági gépek polimer alapanyagainak abrziós kopásállósága “slurry-pot” mérések alapján, Műanyagipari Szemle (accepted)

*International conference proceedings:*

9. **Muhandes, H.**, Kalacska, G., Kadi, N., Skrifvars, M. (2018): Pin-on-plate abrasive wear test for several composites and bio-composite materials, ICME, International Conference of Experimental Mechanics, Brussels, Belgium, Proceedings 2018, Vol. 2, No. 469, doi:10.3390/ICEM18-05333.
10. **Muhandes H.**, Kalácska, G. (2019): A study of evolution of friction temperature on several composite materials by a pin-on-plate system, 7th International Scientific Conference on Advances in Mechanical Engineering (ISCAME 2019), Debrecen, Hungary, 7-9 November, 2019, pp. 87-88.
11. Barkó, G., Kalácska, G., **Muhandes, H.** (2018): Sensor systems and data processing, 6th International Scientific Conference on Advances in Mechanical Engineering (ISCAME 2018), Debrecen, Hungary, 11-13 October, 2018, pp. 13-14.
12. **Muhandes H.**, Kalácska, G. (2018): A slurry-pot abrasive wear test device for several composite materials, 6th International Scientific Conference on Advances in Mechanical Engineering (ISCAME 2018), Debrecen, Hungary, 11-13 October, 2018, pp. 113-114.
13. **Muhandes H.**, Salloum, W. (2017): Simulating the bruising damage of olive fruit during drop, 5th International Scientific Conference on Advances in Mechanical Engineering (ISCAME 2017), Debrecen, Hungary, 12-13 October, 2017, pp. 372-379.

## A3: Comparing the materials for wear

The relation between the wear and sliding distance for several polymer types for cases 2, 3, 4, 5, 8, 9, 10 and 11 in the Table 3.4.

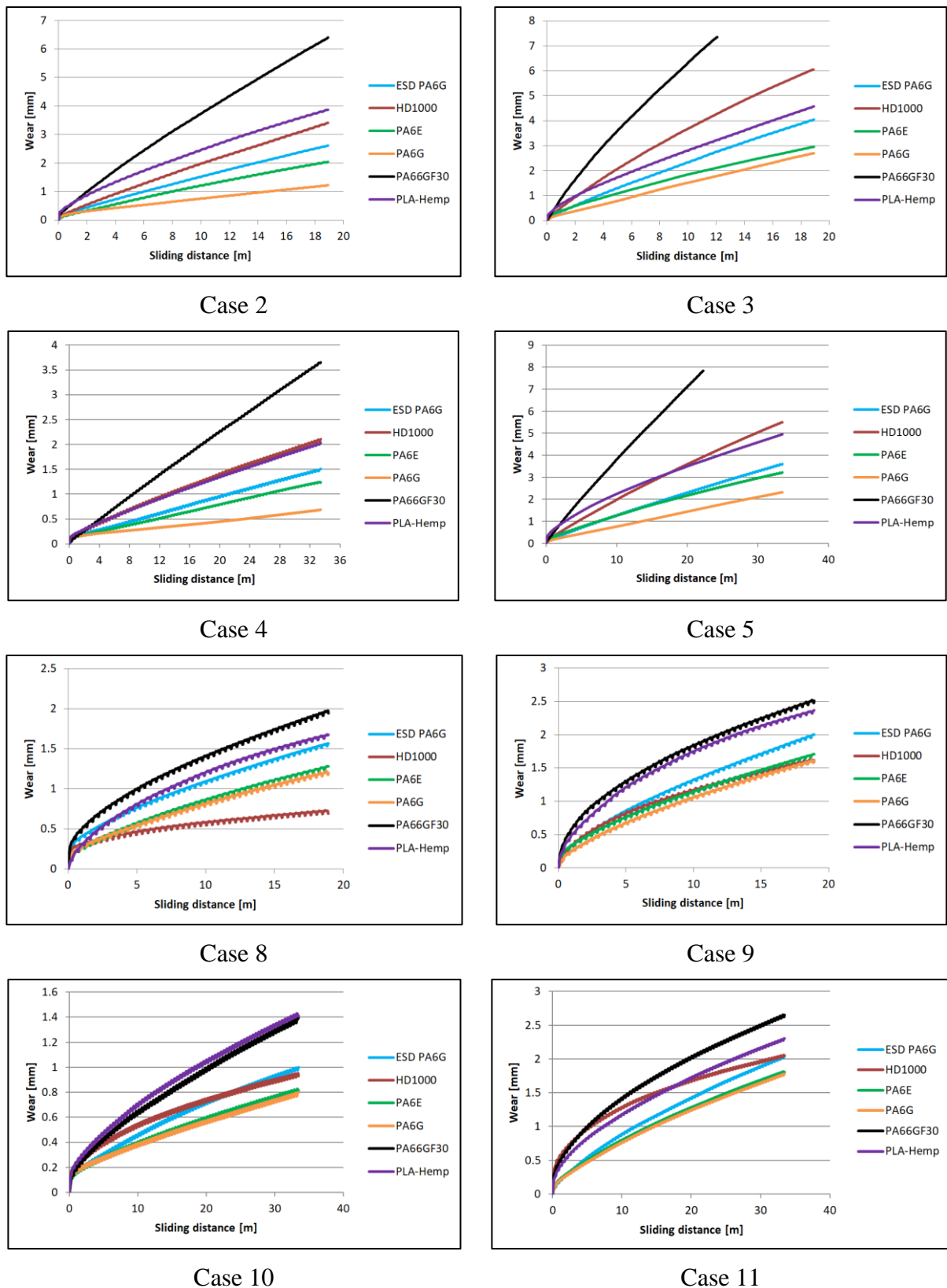


Fig. 8.1. The relation between the wear and sliding distance for several polymer types on P60 and P150 for cases 2, 3, 4, 5, 8, 9, 10 and 11 in Table 3.4

**A4: The wear line equation and the slope value for the 12 test conditions**

For the test number 1:

Type	Wear line equation	Slope value
PA66GF30	$y=0.1198 x+0.2253$	0.1198
PA6E	$y=0.0457 x+0.2175$	0.0457
PA6G	$y=0.0258 x+0.1917$	0.0258
PLA-Hemp	$y=0.0912 x+0.263$	0.0912
HD1000	$y=0.0508 x+0.1724$	0.0508
PA6G ESD	$y=0.0433 x+0.2184$	0.0433

For the test number 2:

Type	Wear line equation	Slope value
PA66GF30	$y=0.323 x+0.4339$	0.323
PA6E	$y=0.1032 x+0.1495$	0.1032
PA6G	$y=0.055 x+0.196$	0.055
PLA-Hemp	$y=0.1822 x+0.5699$	0.1822
HD1000	$y=0.1711 x+0.2288$	0.1711
PA6G ESD	$y=0.1296 x+0.2072$	0.1296

For the test number 3:

Type	Wear line equation	Slope value
PA66GF30	$y=0.5914 x+0.49$	0.5914
PA6E	$y=0.1439 x+0.3436$	0.1439
PA6G	$y=0.1338 x+0.1105$	0.1338
PLA-Hemp	$y=0.2166 x+0.5886$	0.2166
HD1000	$y=0.3115 x+0.4447$	0.3115
PA6G ESD	$y=0.2065 x+0.2386$	0.2065

For the test number 4:

Type	Wear line equation	Slope value
PA66GF30	$y=0.108 x+0.0825$	0.108
PA6E	$y=0.0343 x+0.1087$	0.0343
PA6G	$y=0.016 x+0.1377$	0.016
PLA-Hemp	$y=0.0551 x+0.2238$	0.0551
HD1000	$y=0.0578 x+0.2133$	0.0578
PA6G ESD	$y=0.0415 x+0.1212$	0.0415

For the test number 5:

Type	Wear line equation	Slope value
PA66GF30	$y=0.3457 x+0.2802$	0.3457
PA6E	$y=0.0899 x+0.3262$	0.0899
PA6G	$y=0.0669 x+0.0983$	0.0669
PLA-Hemp	$y=0.1292 x+0.827$	0.1292
HD1000	$y=0.1598 x+0.3285$	0.1598
PA6G ESD	$y=0.1036 x+0.2024$	0.1036

For the test number 6:

Type	Wear line equation	Slope value
PA66GF30	$y=0.5691 x+0.7096$	0.5691
PA6E	$y=0.1185 x+0.3937$	0.1185
PA6G	$y=0.082 x+0.204$	0.082
PLA-Hemp	$y=0.2154 x+0.8066$	0.2154
HD1000	$y=0.2612 x+0.4191$	0.2612
PA6G ESD	$y=0.1586 x+0.3303$	0.1586

For the test number 7:

Type	Wear line equation	Slope value
PA66GF30	$y=0.0422 x+0.3469$	0.0422
PA6E	$y=0.0269 x+0.2223$	0.0269
PA6G	$y=0.0193 x+0.2199$	0.0193
PLA-Hemp	$y=0.0455 x+0.2129$	0.0455
HD1000	$y=0.0229 x+0.3308$	0.0229
PA6G ESD	$y=0.032 x+0.2813$	0.032

For the test number 8:

Type	Wear line equation	Slope value
PA66GF30	$y=0.0808 x+0.5441$	0.0808
PA6E	$y=0.0563 x+0.2716$	0.0563
PA6G	$y=0.0524 x+0.2681$	0.0542
PLA-Hemp	$y=0.0759 x+0.3744$	0.0759
HD1000	$y=0.0229 x+0.3308$	0.0229
PA6G ESD	$y=0.0644 x+0.415$	0.0644

For the test number 9:

Type	Wear line equation	Slope value
PA66GF30	$y=0.1054 x+0.6901$	0.1054
PA6E	$y=0.0757 x+0.3475$	0.0757
PA6G	$y=0.0753 x+0.2641$	0.0753
PLA-Hemp	$y=0.1036 x+0.6015$	0.1036
HD1000	$y=0.0703 x+0.4062$	0.0703
PA6G ESD	$y=0.0919 x+0.3509$	0.0919

For the test number 10:

Type	Wear line equation	Slope value
PA66GF30	$y=0.0355 x+0.2537$	0.0355
PA6E	$y=0.0198 x+0.1848$	0.0198
PA6G	$y=0.0187 x+0.1865$	0.0187
PLA-Hemp	$y=0.0355 x+0.2537$	0.0355
HD1000	$y=0.0211 x+0.2952$	0.0211
PA6G ESD	$y=0.0255 x+0.1891$	0.0255

For the test number 11:

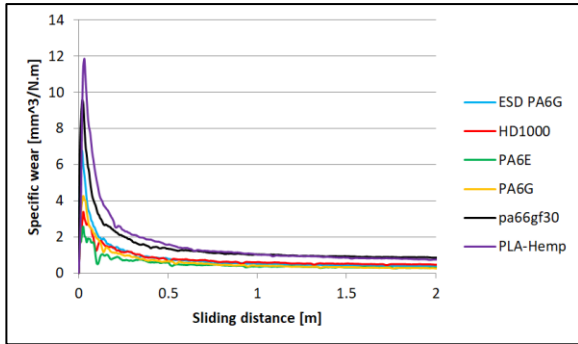
Type	Wear line equation	Slope value
PA66GF30	$y=0.0633 x+0.6897$	0.0633
PA6E	$y=0.0486 x+0.2729$	0.0486
PA6G	$y=0.048 x+0.2494$	0.048
PLA-Hemp	$y=0.0561 x+0.5484$	0.0561
HD1000	$y=0.0428 x+0.7622$	0.0428
PA6G ESD	$y=0.0555 x+0.2753$	0.0555

For the test number 12:

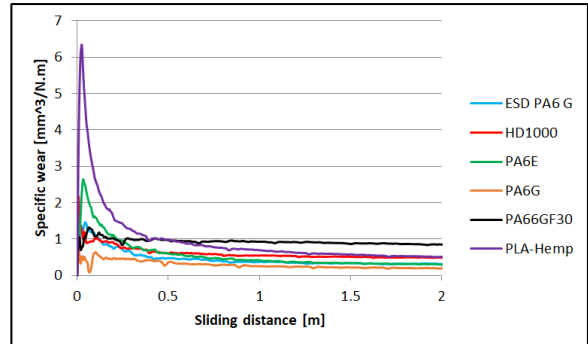
Type	Wear line equation	Slope value
PA66GF30	$y=0.0838 x+0.8158$	0.0838
PA6E	$y=0.0648 x+0.4353$	0.0648
PA6G	$y=0.0641 x+0.5621$	0.0641
PLA-Hemp	$y=0.078 x+0.6076$	0.078
HD1000	$y=0.0552 x+0.6252$	0.0552
PA6G ESD	$y=0.0794 x+0.5831$	0.0794

**A5: Specific wear comparison**

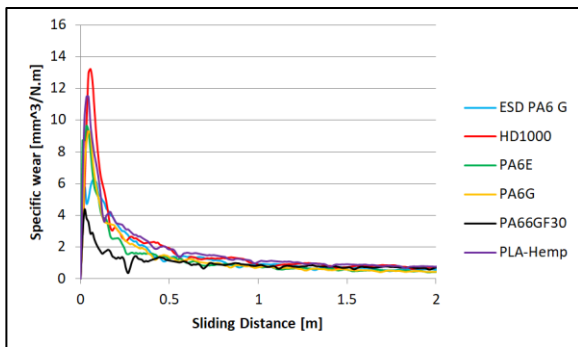
The relation between the specific wear and sliding distance for several polymer types for cases 2, 3, 4, 5, 8, 9, 10 and 11 in the Table 3.4.



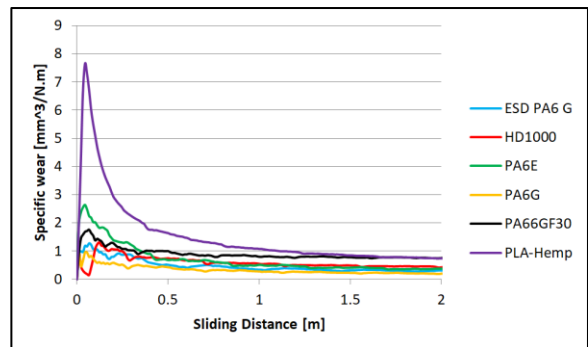
Case 2



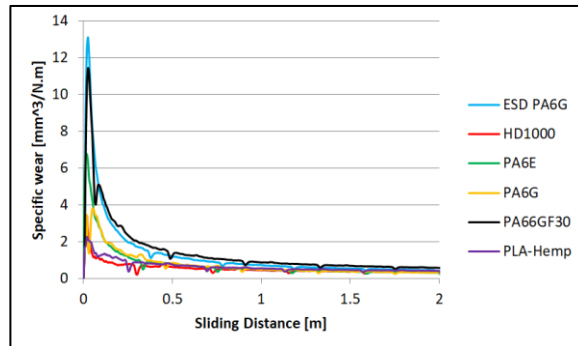
Case 3



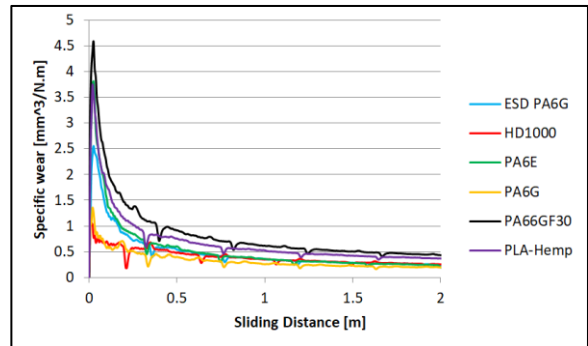
Case 4



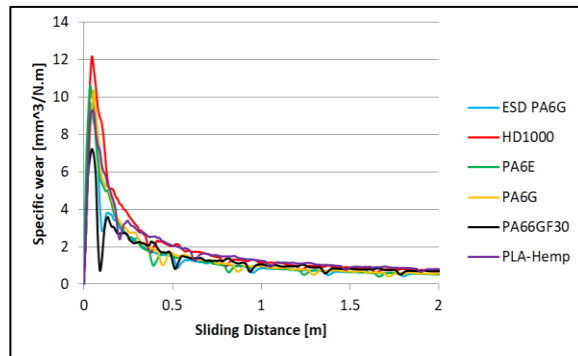
Case 5



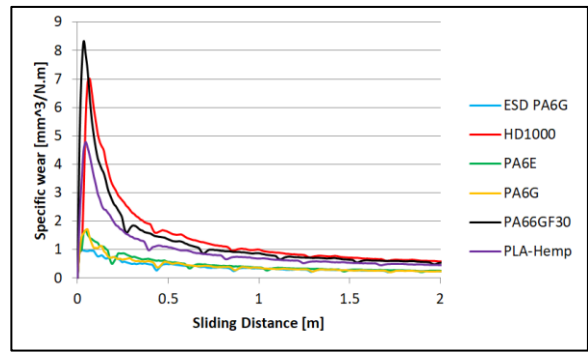
Case 8



Case 9



Case 10



Case 11

Fig. 8.2. The relation between the specific wear and sliding distance for several polymer types on P60 and P150 for cases 2, 3, 4, 5, 8, 9, 10 and 11 (Table 3.4)

**A6: Comparing the materials for friction temperature evolution**

The relation between the temperature and sliding distance for several polymer types for cases 2, 3, 4, 5, 8, 9, 10 and 11 in the table 3.4.

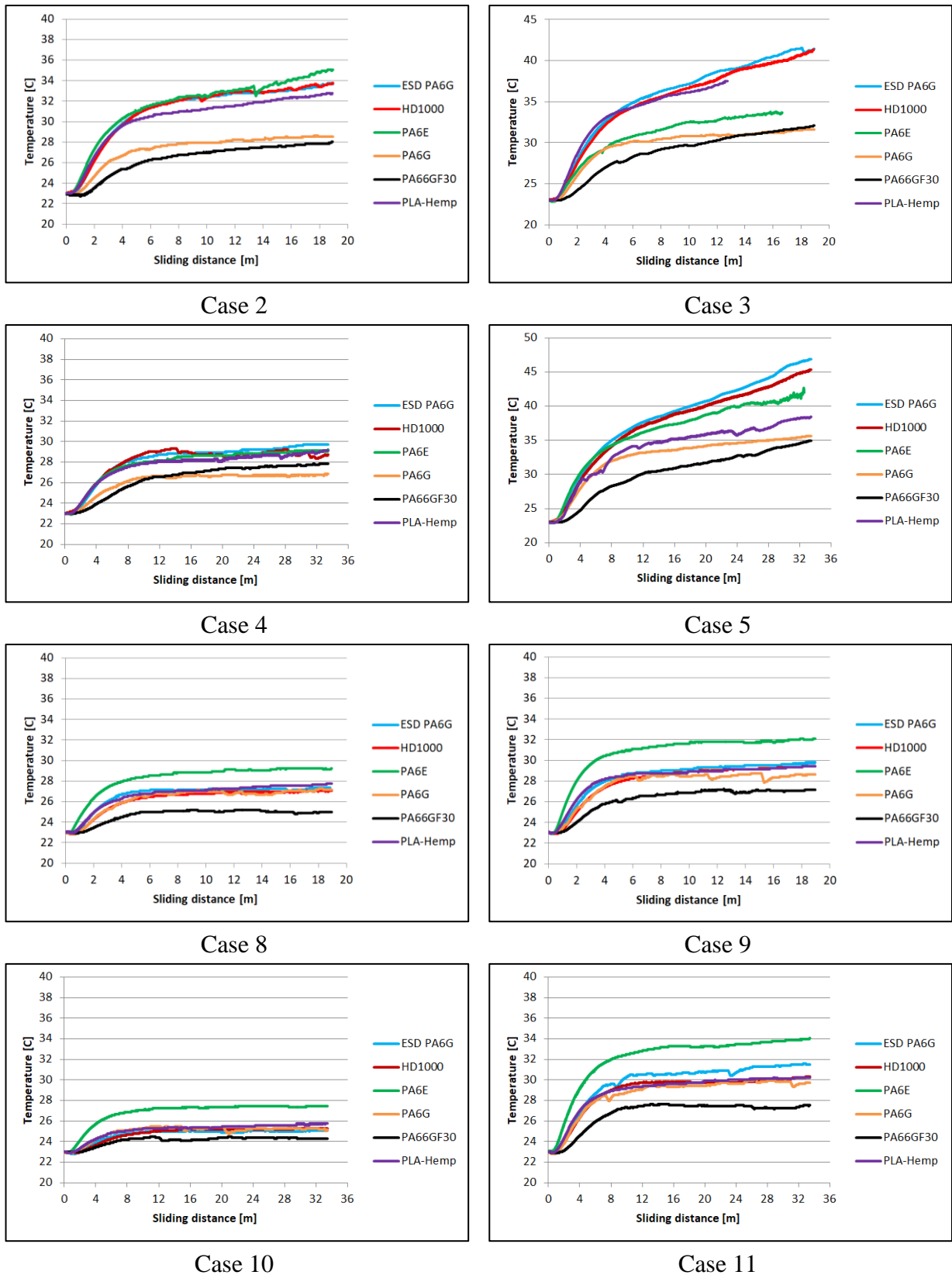


Fig. 8.3. The relation between the temperature and sliding distance for several polymer types on P60 and P150 for cases 2, 3, 4, 5, 8, 9, 10 and 11 (Table 3.4)



**A7: Comparing the materials for friction force**

The relation between the friction force and sliding distance for several polymer types for cases 2, 3, 4, 5, 8, 9, 10 and 11 in the Table 3.4.

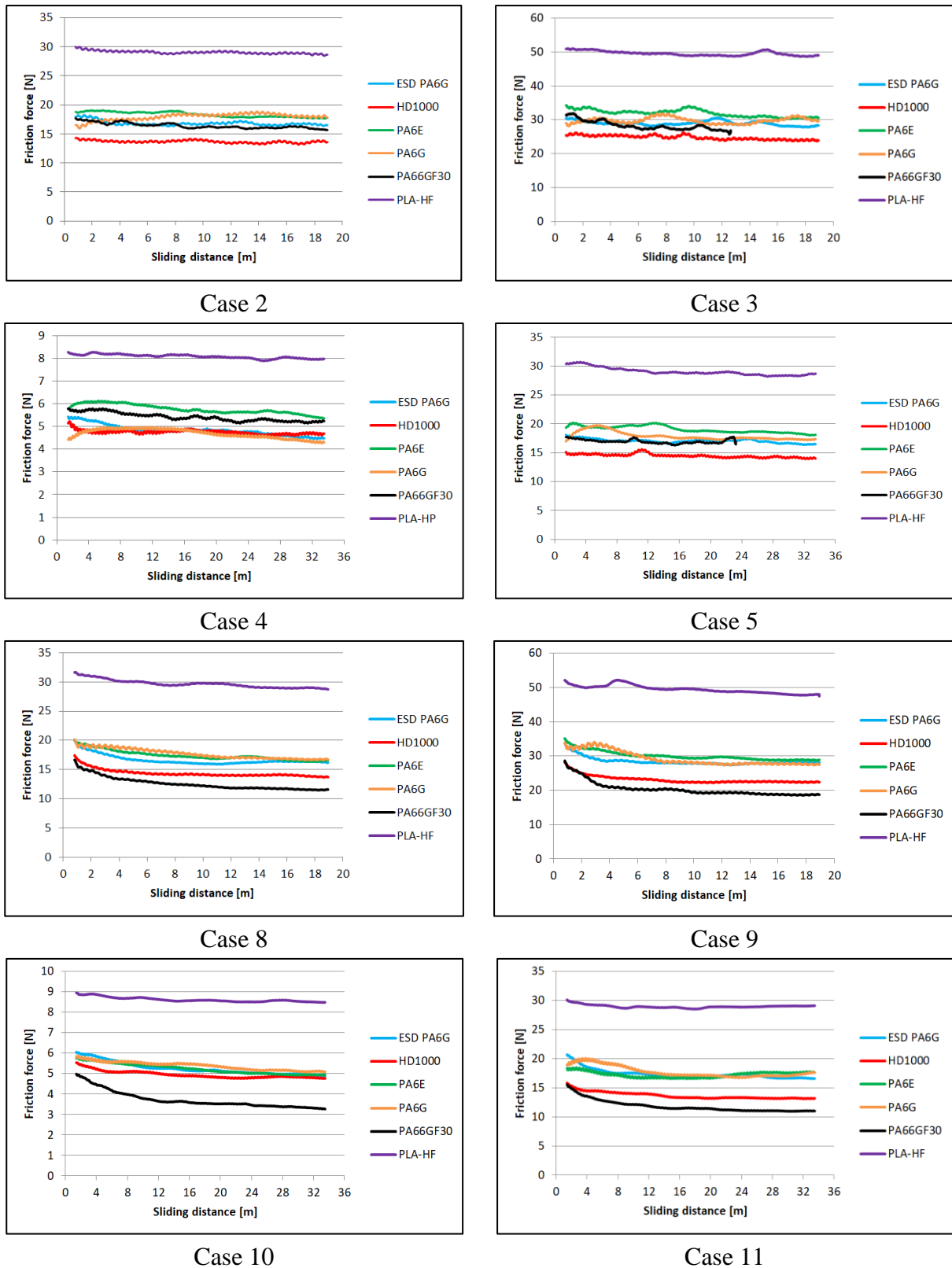


Fig. 8.4. The relation between the friction force and sliding distance for several polymer types on P60 and P150 for cases 2, 3, 4, 5, 8, 9, 10 and 11 (Table 3.4)

**A8: 3D surface microscopy results**

Fig. 8.5 shows Microscopic visualization of the change of surface 3D topography of the tested materials on P60 abrasive, applying the top speed and load (No. 1 condition)

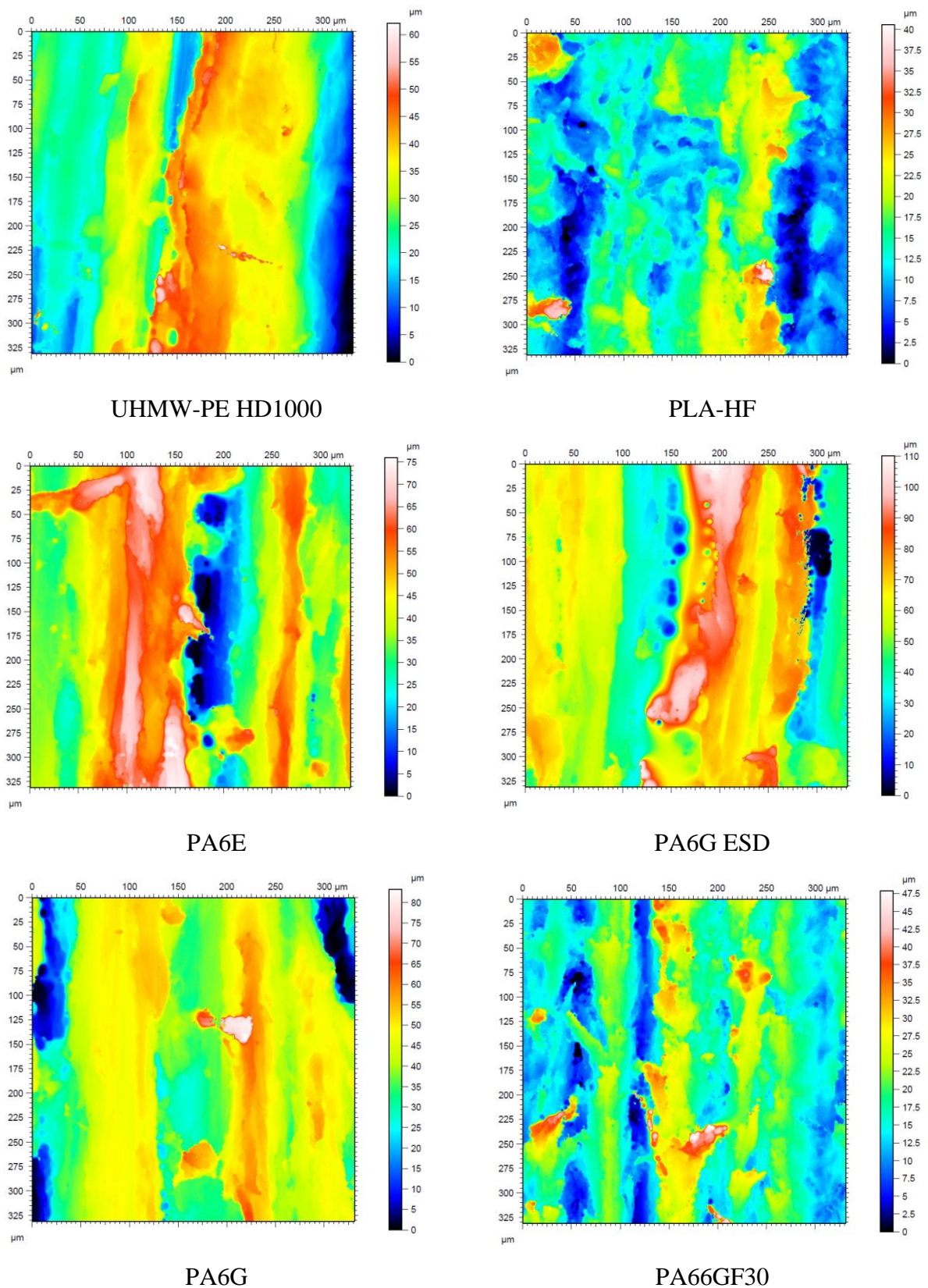


Fig. 8.5. Microscopic visualization of the change of surface 3D topography of the tested materials on P60 abrasive, applying the top speed and load (No. 1 condition)

Fig. 8.6 shows Microscopic visualization of the change of surface 3D topography of the tested materials on P150 abrasive, applying the top speed and load (No. 7 condition)

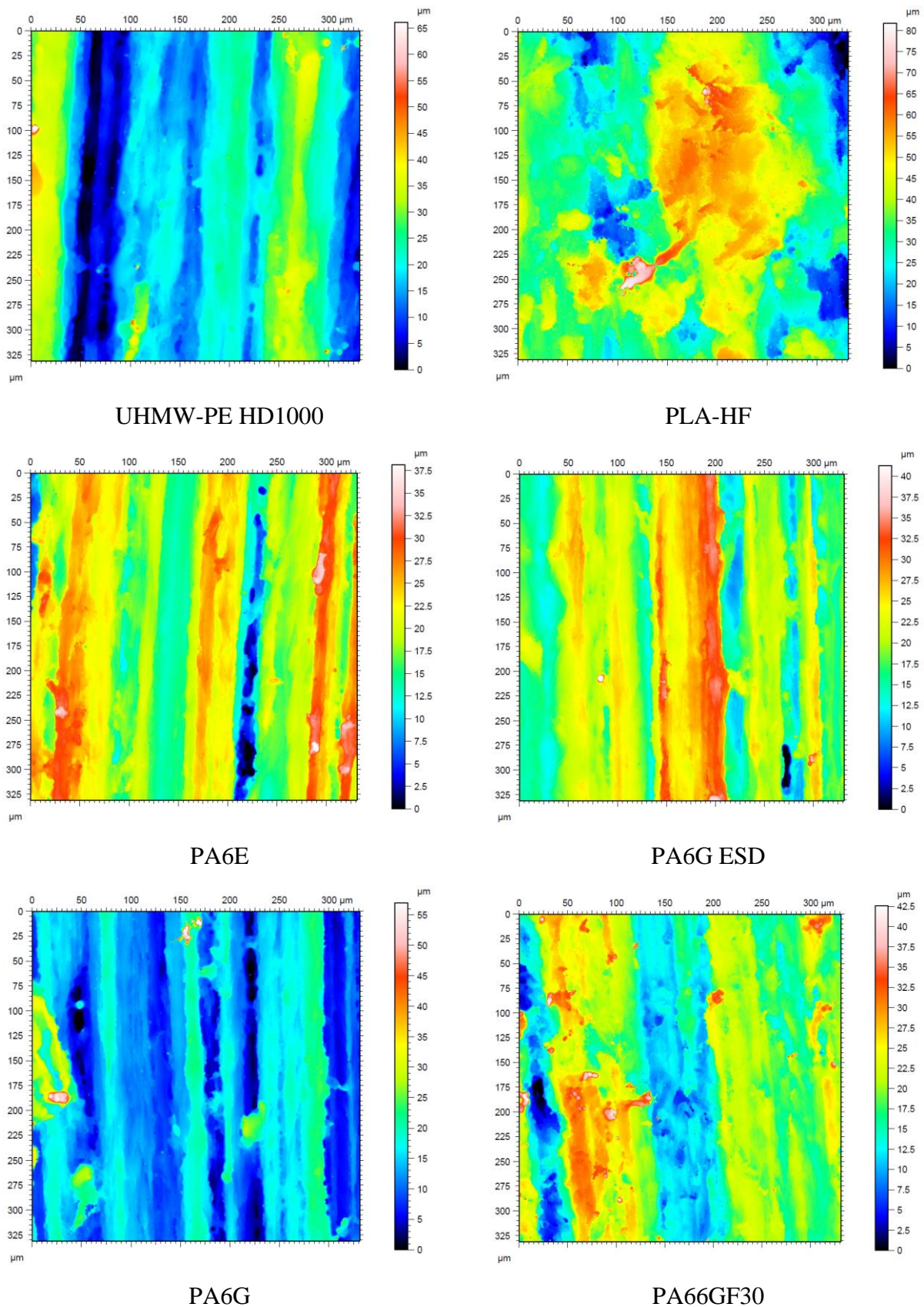


Fig. 8.6. Microscopic visualization of the change of surface 3D topography of the tested materials on P60 abrasive, applying the top speed and load (No. 1 condition)

Table 8.1. Surface characteristics after the tests and the change in % (test condition No. 1)

	<b>HD1000</b>	<b>PLA-HF</b>	<b>PA6E</b>	<b>PA6G ESD</b>	<b>PA6G</b>	<b>PA66GF30</b>
<b>after the test</b>						
Sq ( $\mu\text{m}$ )	10.86	15.04	15.04	19.19	12.46	6.68
Ssk	-0.34	-0.19	-0.34	-0.14	-1.15	0.55
Sku	2.46	3.04	2.92	3.01	5.05	3.77
Sp ( $\mu\text{m}$ )	32.70	38.25	34.31	50.72	41.85	29.89
Sv ( $\mu\text{m}$ )	29.38	40.77	41.67	59.40	41.31	17.96
Sz ( $\mu\text{m}$ )	62.08	79.03	75.98	110.12	83.16	47.85
Sa ( $\mu\text{m}$ )	9.24	11.66	12.18	15.11	9.33	5.22
<b>Change in %</b>						
Sq ( $\mu\text{m}$ )	104%	14%	672%	864%	709%	149%
Ssk	-134%	-214%	-169%	-155%	401%	4%
Sku	-19%	27%	51%	57%	141%	-9%
Sp ( $\mu\text{m}$ )	51%	6%	495%	996%	1131%	57%
Sv ( $\mu\text{m}$ )	285%	49%	1142%	1477%	948%	116%
Sz ( $\mu\text{m}$ )	112%	24%	733%	1212%	1033%	75%
Sa ( $\mu\text{m}$ )	109%	7%	621%	786%	606%	138%

Table 8.2. Surface characteristics after the tests and the change in % (test condition No. 7)

	<b>HD1000</b>	<b>PLA-HF</b>	<b>PA6E</b>	<b>PA6G ESD</b>	<b>PA6G</b>	<b>PA66GF30</b>
<b>after the test</b>						
Sq ( $\mu\text{m}$ )	9.18	3.83	5.52	5.42	6.00	6.00
Ssk	0.16	1.54	-0.39	0.15	1.02	1.02
Sku	2.64	13.50	3.77	3.04	7.39	7.39
Sp ( $\mu\text{m}$ )	46.72	31.31	18.24	20.56	43.24	43.24
Sv ( $\mu\text{m}$ )	19.39	10.40	19.91	20.70	13.71	13.71
Sz ( $\mu\text{m}$ )	66.10	41.71	38.15	41.25	56.96	56.96
Sa ( $\mu\text{m}$ )	7.34	2.76	4.30	4.32	4.60	4.60
<b>Change in %</b>						
Sq ( $\mu\text{m}$ )	73%	-71%	183%	172%	290%	124%
Ssk	-84%	817%	-179%	-42%	-543%	93%
Sku	-13%	463%	95%	58%	253%	79%
Sp ( $\mu\text{m}$ )	115%	-13%	217%	344%	1172%	128%
Sv ( $\mu\text{m}$ )	154%	-62%	493%	449%	248%	65%
Sz ( $\mu\text{m}$ )	125%	-34%	318%	391%	676%	109%
Sa ( $\mu\text{m}$ )	66%	-75%	154%	153%	248%	110%

**A9: The relative wear different polymer samples (daily cumulative) of the weight loss in percentage (%), compared to the zero day weight**

Corundum:

Table 8.3. The relative wear different polymer samples (daily cumulative) of the weight loss in percentage (%), compared to the zero day weight for the corundum medium

	<b>Day 0</b>	<b>Day 1</b>	<b>Day 2</b>	<b>Day 3</b>	<b>Day 4</b>	<b>Day 5</b>
PA66GF30	0%	0.91%	1.83%	3.13%	3.79%	5.62%
	0%	0.82%	1.25%	1.76%	2.51%	3.09%
	0%	0.88%	2.45%	4.49%	5.73%	7.03%
	0%	0.69%	1.16%	1.95%	2.86%	3.73%
PA6E	0%	0.73%	1.06%	1.55%	2.23%	2.96%
	0%	0.40%	0.89%	1.17%	1.48%	1.99%
	0%	1.03%	1.96%	2.36%	3.26%	4.26%
	0%	0.56%	1.08%	1.31%	1.82%	2.35%
PA6G	0%	0.80%	1.52%	1.92%	2.63%	3.53%
	0%	0.36%	0.66%	0.98%	1.33%	1.91%
	0%	0.85%	1.79%	2.46%	3.24%	4.52%
	0%	0.37%	0.90%	1.26%	1.45%	2.05%
PA6GESD	0%	1.39%	2.14%	3.51%	4.25%	5.00%
	0%	0.55%	1.32%	1.92%	2.34%	3.38%
	0%	1.54%	2.39%	3.94%	5.94%	7.50%
	0%	0.40%	1.07%	2.28%	3.31%	4.13%
HD1000	0%	1.17%	1.98%	2.83%	3.37%	4.19%
	0%	0.62%	1.00%	1.41%	1.97%	2.70%
	0%	1.30%	2.39%	3.75%	4.80%	5.95%
	0%	0.72%	1.36%	1.88%	2.34%	3.09%
PLA-HF	0%	7.05%	15.46%	21.33%		
	0%	5.95%	8.78%	10.45%	12.37%	14.64%
	0%	12.40%	16.85%	20.62%	24.63%	29.43%
	0%	5.73%	7.85%	10.80%	13.96%	16.84%

Gravel soil:

Table 8.4. The relative wear different polymer samples (daily cumulative) of the weight loss in percentage (%), compared to the zero day weight for the gravel soil

	<b>Day 0</b>	<b>Day 1</b>	<b>Day 2</b>	<b>Day 3</b>	<b>Day 4</b>	<b>Day 5</b>
PA66GF30	0%	0.44%	0.89%	1.70%	2.25%	2.84%
	0%	0.32%	0.53%	0.78%	0.95%	1.42%
	0%	0.82%	1.63%	2.03%	2.43%	3.28%
	0%	0.51%	0.81%	1.30%	1.39%	1.73%
PA6E	0%	0.37%	0.83%	1.36%	1.72%	2.10%
	0%	0.23%	0.43%	0.75%	1.03%	1.24%
	0%	0.59%	1.24%	1.95%	2.42%	2.86%
	0%	0.34%	0.98%	1.34%	1.63%	1.99%
PA6G	0%	0.38%	0.87%	1.45%	2.02%	2.37%
	0%	0.42%	0.76%	1.07%	1.47%	1.70%
	0%	0.82%	1.58%	2.24%	3.07%	3.76%
	0%	0.33%	0.74%	1.15%	1.54%	1.80%
PA6GESD	0%	0.58%	1.31%	1.74%	2.16%	2.78%
	0%	0.32%	0.73%	1.20%	1.51%	1.90%
	0%	1.54%	2.13%	2.68%	3.39%	3.98%
	0%	0.53%	0.88%	1.46%	1.82%	2.11%
HD1000	0%	0.46%	0.85%	1.44%	2.01%	2.44%
	0%	0.46%	0.66%	0.96%	1.30%	1.55%
	0%	1.09%	1.68%	2.39%	2.93%	3.93%
	0%	0.33%	0.67%	1.06%	1.44%	1.66%
PLA-HF	0%	2.04%	3.96%	5.77%	6.71%	7.72%
	0%	1.56%	2.49%	3.68%	4.88%	5.88%
	0%	3.51%	6.16%	7.72%	9.01%	11.73%
	0%	2.31%	3.80%	4.89%	5.63%	6.71%

Loamy soil:

Table 8.5. The relative wear different polymer samples (daily cumulative) of the weight loss in percentage (%), compared to the zero day weight for the loamy soil

	<b>Day 0</b>	<b>Day 1</b>	<b>Day 2</b>	<b>Day 3</b>	<b>Day 4</b>	<b>Day 5</b>
PA66GF30	0%	0.32%	0.78%	1.11%	1.54%	1.84%
	0%	0.11%	0.40%	0.50%	0.65%	0.84%
	0%	0.75%	0.93%	1.19%	1.59%	2.09%
	0%	0.34%	0.50%	0.69%	1.01%	1.42%
PA6E	0%	0.17%	0.37%	0.63%	0.92%	1.23%
	0%	0.16%	0.29%	0.41%	0.66%	0.83%
	0%	0.37%	0.76%	1.08%	1.41%	1.71%
	0%	0.11%	0.34%	0.59%	0.68%	0.91%
PA6G	0%	0.26%	0.46%	0.71%	1.03%	1.31%
	0%	0.10%	0.26%	0.38%	0.52%	0.72%
	0%	0.32%	0.73%	0.93%	1.12%	1.67%
	0%	0.15%	0.28%	0.46%	0.60%	0.75%
PA6GESD	0%	0.37%	0.70%	0.98%	1.39%	1.71%
	0%	0.43%	0.67%	0.74%	1.08%	1.34%
	0%	0.46%	0.82%	1.65%	2.23%	3.02%
	0%	0.22%	0.59%	0.97%	1.23%	1.50%
HD1000	0%	0.21%	0.52%	0.78%	1.12%	1.46%
	0%	0.13%	0.38%	0.46%	0.79%	0.85%
	0%	0.45%	0.68%	1.22%	1.44%	1.76%
	0%	0.26%	0.43%	0.67%	0.87%	1.09%
PLA-HF	0%	1.02%	1.61%	2.00%	2.64%	3.16%
	0%	0.64%	1.07%	1.26%	1.58%	1.85%
	0%	1.23%	1.88%	2.37%	2.89%	3.45%
	0%	0.90%	1.21%	1.66%	2.05%	2.60%

Sandy soil:

Table 8.6. The relative wear different polymer samples (daily cumulative) of the weight loss in percentage (%), compared to the zero day weight for the Sandy soil

	<b>Day 0</b>	<b>Day 1</b>	<b>Day 2</b>	<b>Day 3</b>	<b>Day 4</b>	<b>Day 5</b>
PA66GF30	0%	0.27%	0.64%	1.08%	1.40%	1.67%
	0%	0.25%	0.44%	0.71%	1.03%	1.23%
	0%	0.33%	0.82%	1.35%	1.92%	2.45%
	0%	0.28%	0.52%	0.86%	1.18%	1.47%
PA6E	0%	0.31%	0.59%	0.74%	0.86%	0.99%
	0%	0.11%	0.27%	0.46%	0.71%	0.78%
	0%	0.27%	0.60%	1.07%	1.64%	1.94%
	0%	0.21%	0.37%	0.55%	0.75%	0.83%
PA6G	0%	0.29%	0.60%	0.74%	0.97%	1.22%
	0%	0.10%	0.27%	0.46%	0.66%	0.89%
	0%	0.23%	0.76%	1.10%	1.61%	2.14%
	0%	0.18%	0.35%	0.55%	0.78%	1.05%
PA6GESD	0%	0.27%	0.58%	0.91%	1.21%	1.52%
	0%	0.30%	0.41%	0.65%	0.94%	1.25%
	0%	0.40%	0.95%	1.57%	2.09%	2.62%
	0%	0.23%	0.61%	0.75%	1.16%	1.32%
HD1000	0%	0.23%	0.52%	0.80%	1.02%	1.35%
	0%	0.11%	0.43%	0.65%	0.80%	1.00%
	0%	0.26%	0.74%	1.29%	1.77%	2.24%
	0%	0.22%	0.49%	0.71%	0.95%	1.10%
PLA-HF	0%	0.87%	1.38%	2.05%	2.54%	2.90%
	0%	0.46%	0.96%	1.53%	1.87%	2.24%
	0%	0.51%	1.49%	2.46%	3.80%	4.85%
	0%	0.70%	1.13%	1.57%	2.36%	2.69%



**A10: The daily relative wear of the weight loss as a percentage (%) compared to the previous day's weight**

Fig. 8.7 shows the daily wear of the weight loss as a percentage for the position 2 results, with four types of slurry

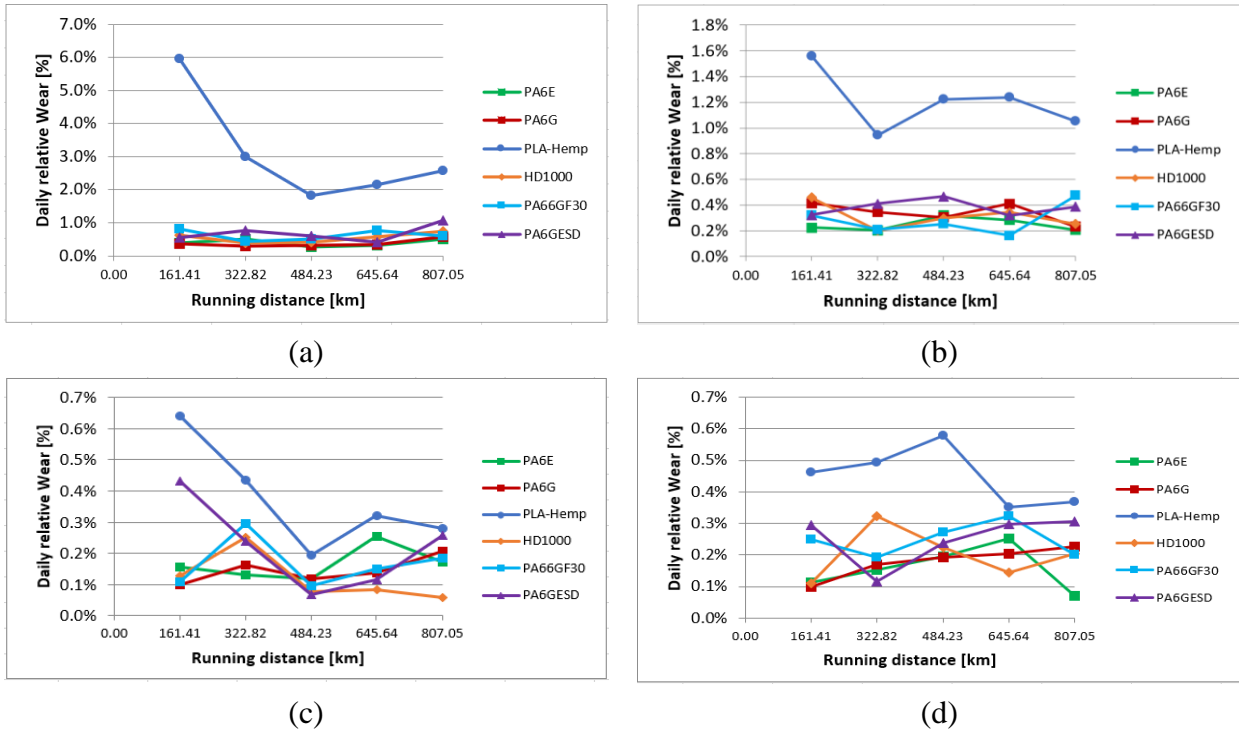


Fig. 8.7. Daily relative wear in position 2 (Fig. 3.13) with (a) corundum medium (b) gravel skeletal soil (c) loamy soil based slurry, and (d) sandy soil

Fig. 8.8 shows the daily wear of the weight loss as a percentage for the position 3 results, with four types of slurry

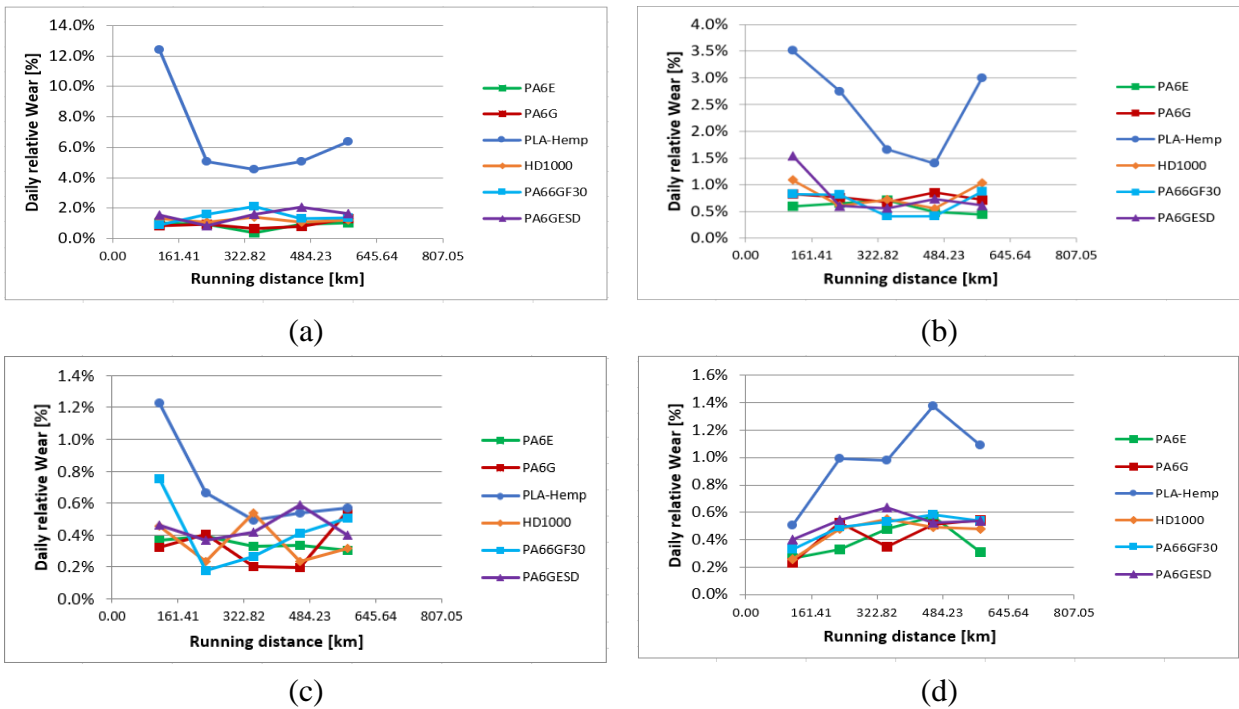
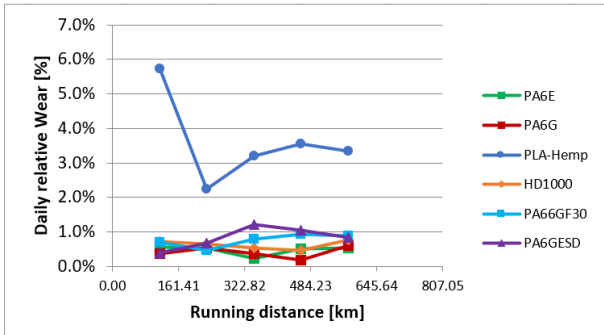


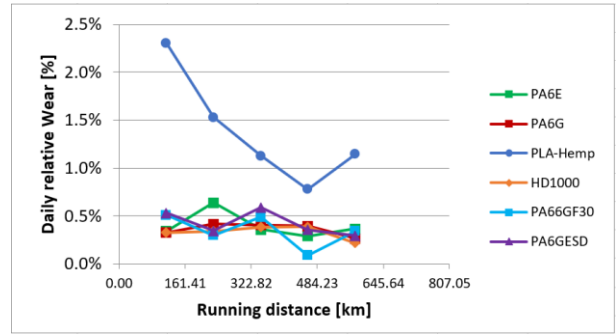
Fig. 8.8. Daily relative wear in position 3 (Fig. 3.13) with (a) corundum medium (b) gravel skeletal soil (c) loamy soil based slurry, and (d) sandy soil

8. Appendices

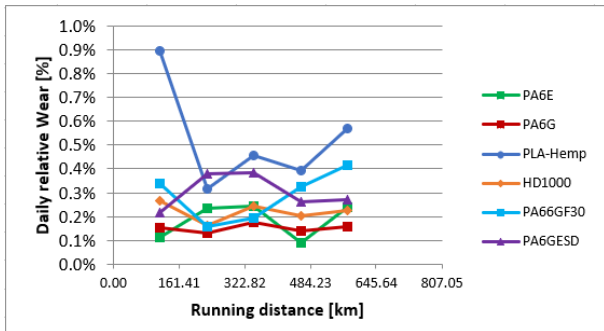
Fig. 8.9 shows the daily wear of the weight loss as a percentage for the position 4 results, with four types of slurry



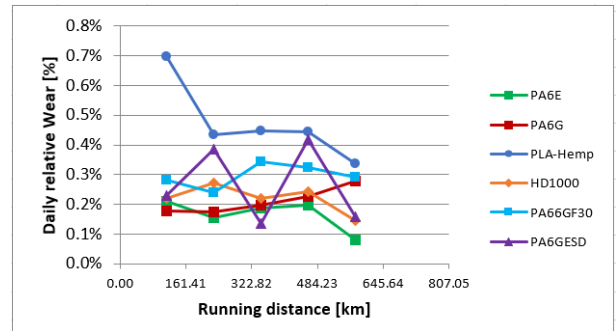
(a)



(b)



(c)



(d)

Fig. 8.9. Daily relative wear in position 4 (Fig. 3.13) with (a) corundum medium (b) gravel skeletal soil (c) loamy soil based slurry, and (d) sandy soil

**A11: The other position results of the 3D surface microscopy results with the corundum medium**

Fig. 8.10 shows the microscopic visualization of the polymer surfaces in the final states with the corundum medium at position 2.

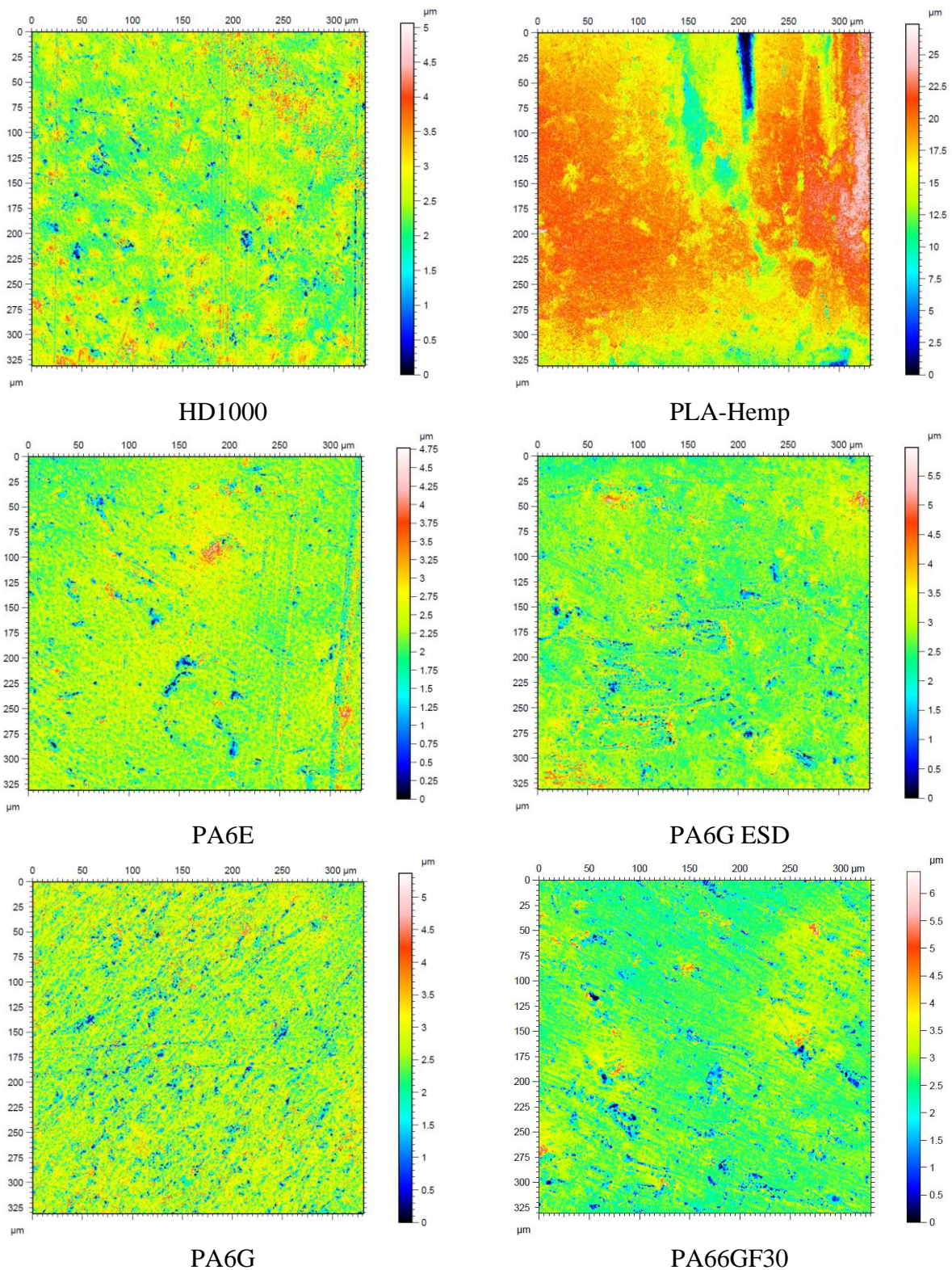


Fig. 8.10. Microscopic visualization of the change of surface 3D topography of the tested materials on corundum slurry at position No.2 (Fig. 3.13)

Fig. 8.11 shows the microscopic visualization of the polymer surfaces in the final states with the corundum medium at position 3.

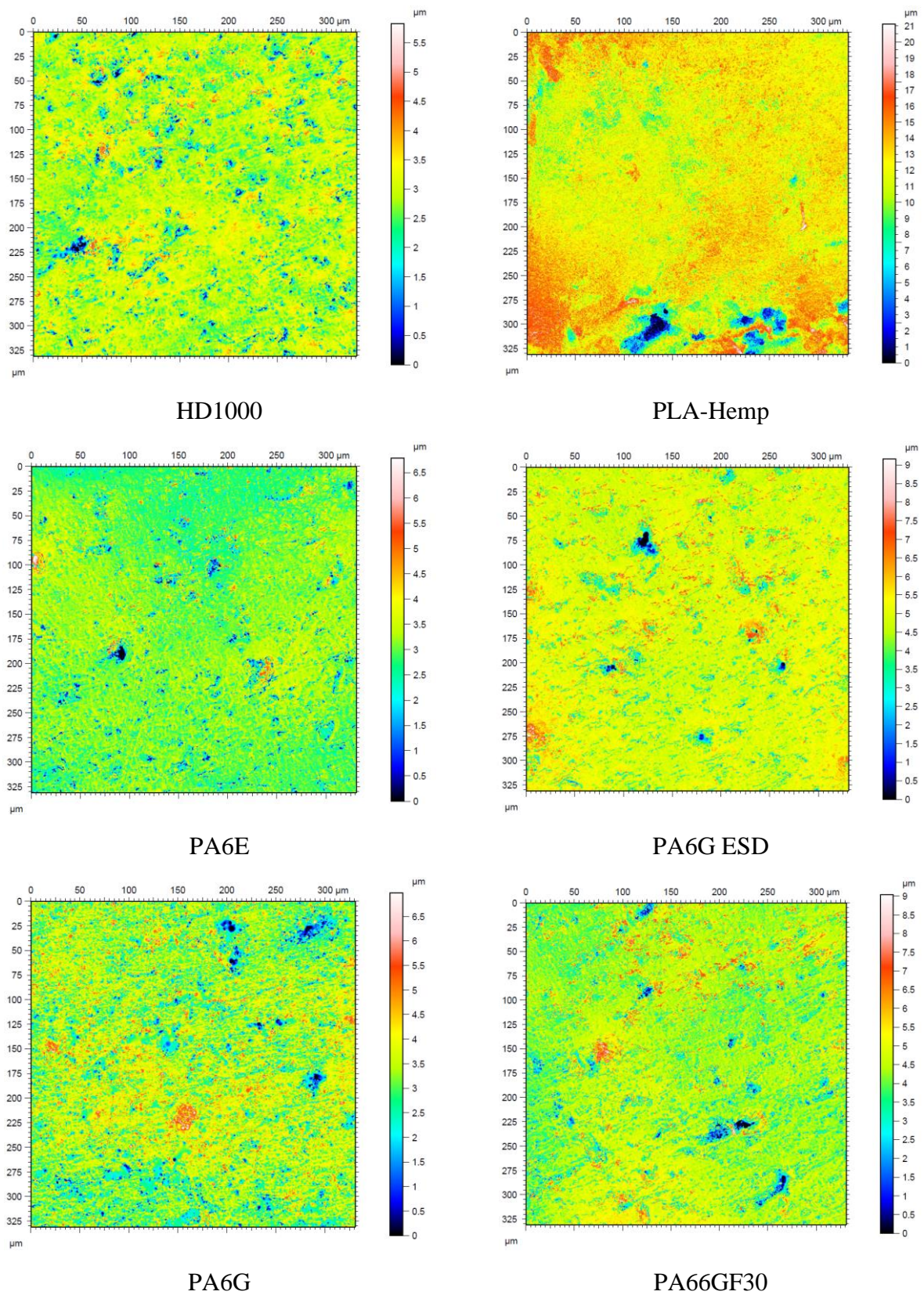


Fig. 8.11. Microscopic visualization of the change of surface 3D topography of the tested materials on corundum slurry at position No.3 (Fig. 3.13)

Table 8.7. Surface characteristics after the tests and the change in % at position No. 2

	<b>HD1000</b>	<b>PLA-HF</b>	<b>PA6E</b>	<b>PA6G ESD</b>	<b>PA6G</b>	<b>PA66GF30</b>
	after the test					
Sq ( $\mu\text{m}$ )	0.49	3.37	0.39	0.48	0.58	0.51
Ssk	-0.44	-0.99	-0.83	-0.67	-0.80	-0.89
Sku	5.94	5.64	8.16	8.26	5.04	8.41
Sp ( $\mu\text{m}$ )	2.61	9.77	2.48	3.27	2.77	3.66
Sv ( $\mu\text{m}$ )	2.45	17.60	2.29	2.71	2.59	2.74
Sz ( $\mu\text{m}$ )	5.06	27.37	4.77	5.98	5.37	6.40
Sa ( $\mu\text{m}$ )	0.35	2.56	0.27	0.33	0.43	0.35
	Change in %					
Sq ( $\mu\text{m}$ )	-91.13%	432.60%	-93.43%	-91.45%	-90.43%	-90.44%
Ssk	-2041.24%	-294.97%	-1870.23%	384.61%	-389.31%	-234.15%
Sku	187.50%	-0.89%	264.21%	321.20%	98.30%	136.00%
Sp ( $\mu\text{m}$ )	-88.95%	137.50%	-91.33%	-77.52%	-85.94%	-90.20%
Sv ( $\mu\text{m}$ )	-78.66%	548.35%	-80.59%	-78.34%	-78.02%	-71.91%
Sz ( $\mu\text{m}$ )	-85.59%	300.86%	-88.19%	-77.90%	-82.97%	-86.42%
Sa ( $\mu\text{m}$ )	-92.45%	456.09%	-94.62%	-93.07%	-91.37%	-91.98%

Table 8.8. Surface characteristics after the tests and the change in % at position No. 3

	<b>HD1000</b>	<b>PLA-HF</b>	<b>PA6E</b>	<b>PA6G ESD</b>	<b>PA6G</b>	<b>PA66GF30</b>
	after the test					
Sq ( $\mu\text{m}$ )	0.52	2.12	0.53	0.69	0.79	0.83
Ssk	-1.39	-1.32	-0.91	-1.11	-0.37	-0.34
Sku	8.59	8.26	9.70	10.80	4.36	6.82
Sp ( $\mu\text{m}$ )	2.97	8.84	3.77	4.25	3.63	4.65
Sv ( $\mu\text{m}$ )	2.85	12.27	3.02	4.91	3.34	4.38
Sz ( $\mu\text{m}$ )	5.82	21.11	6.79	9.16	6.98	9.03
Sa ( $\mu\text{m}$ )	0.35	1.48	0.35	0.44	0.60	0.56
	Change in %					
Sq ( $\mu\text{m}$ )	-90.54%	234.90%	-91.14%	-87.75%	-87.08%	-84.37%
Ssk	-6254.07%	-358.08%	-2053.52%	704.39%	-234.22%	-150.92%
Sku	315.83%	45.03%	333.16%	450.69%	71.48%	91.59%
Sp ( $\mu\text{m}$ )	-87.43%	114.83%	-86.83%	-70.82%	-81.59%	-87.56%
Sv ( $\mu\text{m}$ )	-75.12%	351.94%	-74.35%	-60.78%	-71.63%	-54.98%
Sz ( $\mu\text{m}$ )	-83.41%	209.11%	-83.19%	-66.18%	-77.87%	-80.83%
Sa ( $\mu\text{m}$ )	-92.48%	221.89%	-93.08%	-90.74%	-88.15%	-86.99%

**A12: The other position results of the 3D surface microscopy results with the gravel slurry**

Fig. 8.12 shows the microscopic visualization of the polymer surfaces in the final states with the gravel slurry at position 2.

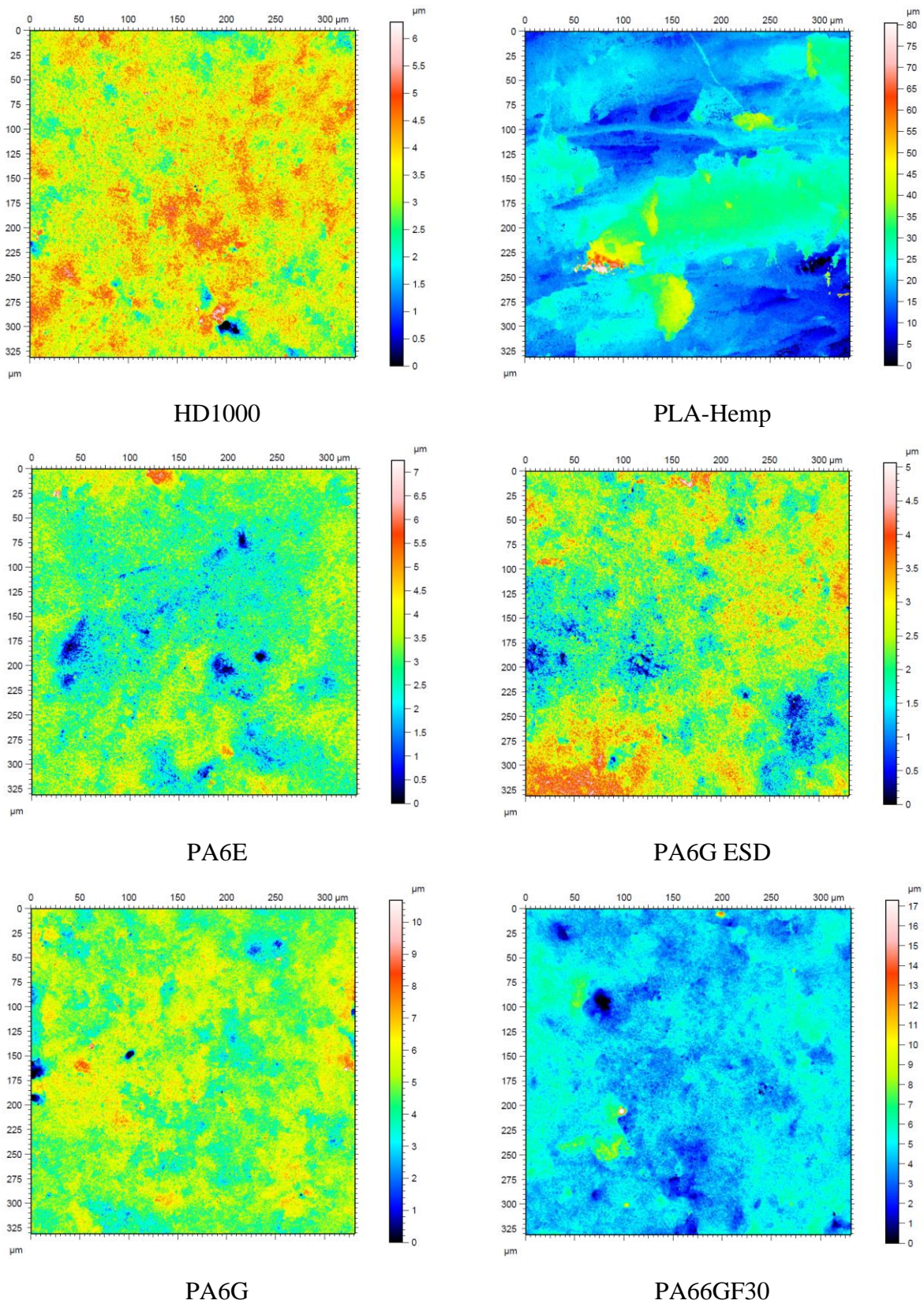


Fig. 8.12. Microscopic visualization of the change of surface 3D topography of the tested materials on gravel slurry at position No.2 (Fig. 3.13)

Fig. 8.13 shows the microscopic visualization of the polymer surfaces in the final states with the gravel slurry at position 3.

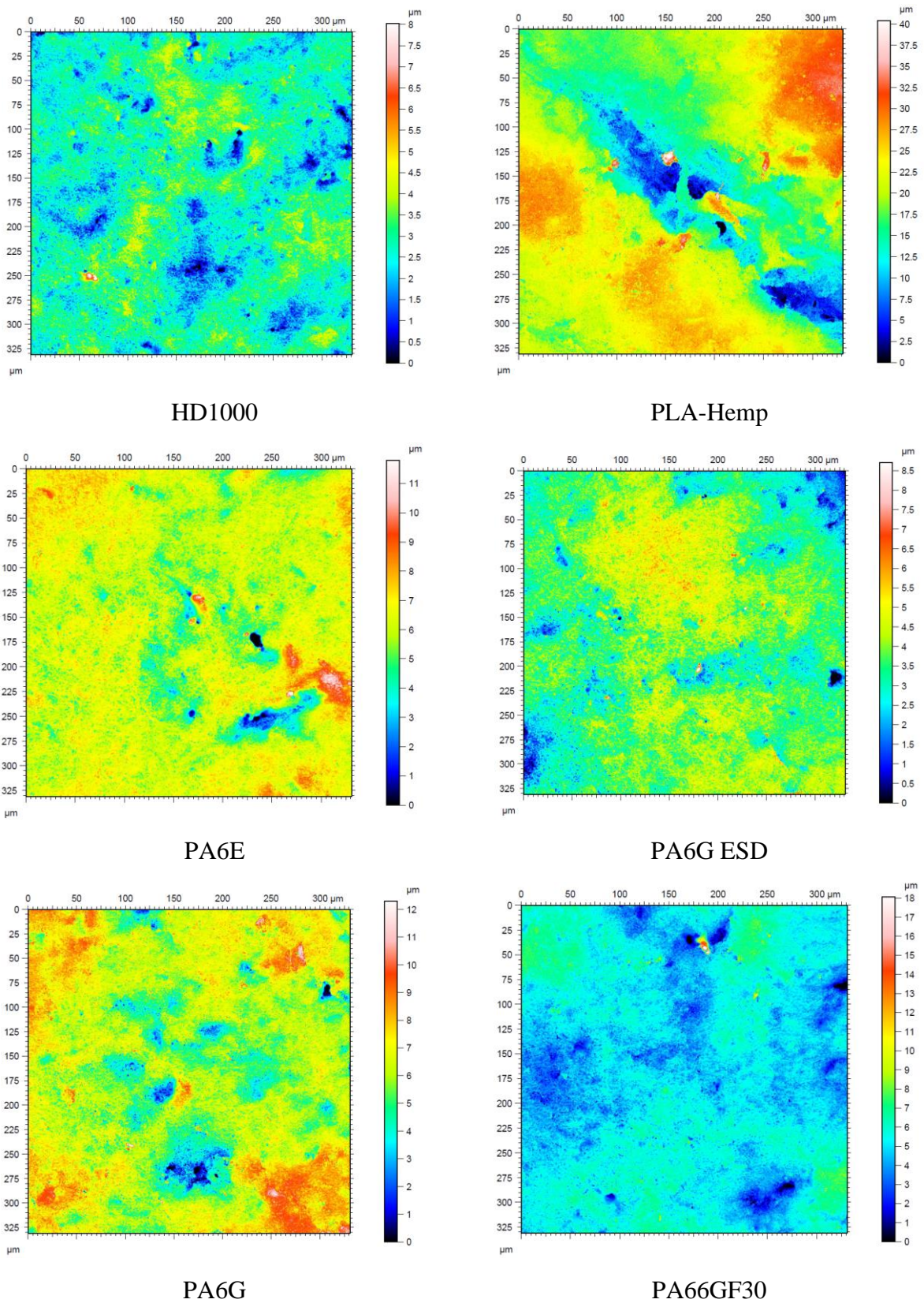


Fig. 8.13. Microscopic visualization of the change of surface 3D topography of the tested materials on gravel slurry at position No.3 (Fig. 3.13)

## 8. Appendices

Table 8.9. Surface characteristics after the tests and the change in % at position No. 2

	<b>HD1000</b>	<b>PLA-HF</b>	<b>PA6E</b>	<b>PA6G ESD</b>	<b>PA6G</b>	<b>PA66GF30</b>
	after the test					
Sq ( $\mu\text{m}$ )	0.64	7.68	0.71	0.69	0.91	0.95
Ssk	-0.33	1.12	-0.28	-0.06	-0.33	0.35
Sku	4.47	7.74	4.34	3.28	5.22	12.02
Sp ( $\mu\text{m}$ )	2.77	58.83	4.29	2.72	5.73	12.67
Sv ( $\mu\text{m}$ )	3.53	21.60	2.96	2.34	4.94	4.62
Sz ( $\mu\text{m}$ )	6.30	80.43	7.25	5.06	10.68	17.29
Sa ( $\mu\text{m}$ )	0.50	5.73	0.55	0.54	0.70	0.71
	Change in %					
Sq ( $\mu\text{m}$ )	-88.37%	1112.40%	-88.11%	-87.74%	-85.01%	-82.06%
Ssk	-1558.23%	119.44%	-690.58%	-53.34%	-219.55%	-47.60%
Sku	116.31%	36.02%	93.60%	67.12%	105.59%	237.40%
Sp ( $\mu\text{m}$ )	-88.27%	1330.05%	-85.00%	-81.33%	-70.94%	-66.12%
Sv ( $\mu\text{m}$ )	-69.25%	695.59%	-74.88%	-81.27%	-58.07%	-52.55%
Sz ( $\mu\text{m}$ )	-82.05%	1077.79%	-82.04%	-81.30%	-66.12%	-63.31%
Sa ( $\mu\text{m}$ )	-89.38%	1146.59%	-89.24%	-88.59%	-86.16%	-83.64%

Table 8.10. Surface characteristics after the tests and the change in % at position No. 3

	<b>HD1000</b>	<b>PLA-HF</b>	<b>PA6E</b>	<b>PA6G ESD</b>	<b>PA6G</b>	<b>PA66GF30</b>
	after the test					
Sq ( $\mu\text{m}$ )	0.71	6.11	1.02	0.86	1.44	1.13
Ssk	-0.18	-0.39	-0.67	-0.40	-0.32	0.02
Sku	4.31	3.13	7.63	3.94	4.23	8.57
Sp ( $\mu\text{m}$ )	5.27	20.47	5.62	5.02	5.98	12.95
Sv ( $\mu\text{m}$ )	2.75	19.91	6.17	3.68	6.31	5.10
Sz ( $\mu\text{m}$ )	8.02	40.38	11.79	8.70	12.29	18.05
Sa ( $\mu\text{m}$ )	0.55	4.84	0.72	0.67	1.08	0.85
	Change in %					
Sq ( $\mu\text{m}$ )	-87.17%	863.72%	-82.97%	-84.80%	-76.36%	-78.85%
Ssk	-899.91%	-177.26%	-1540.67%	188.93%	-214.15%	-97.26%
Sku	108.33%	-45.08%	240.61%	100.93%	66.35%	140.68%
Sp ( $\mu\text{m}$ )	-77.71%	397.55%	-80.35%	-65.51%	-69.69%	-65.35%
Sv ( $\mu\text{m}$ )	-75.99%	633.26%	-47.65%	-70.61%	-46.45%	-47.63%
Sz ( $\mu\text{m}$ )	-77.15%	491.27%	-70.80%	-67.87%	-61.00%	-61.69%
Sa ( $\mu\text{m}$ )	-88.25%	953.60%	-85.83%	-86.00%	-78.45%	-80.35%



**A13: The other position results of the 3D surface microscopy results with the loamy slurry**

Fig. 8.14 shows the microscopic visualization of the polymer surfaces in the final states with the loamy slurry at position 2.

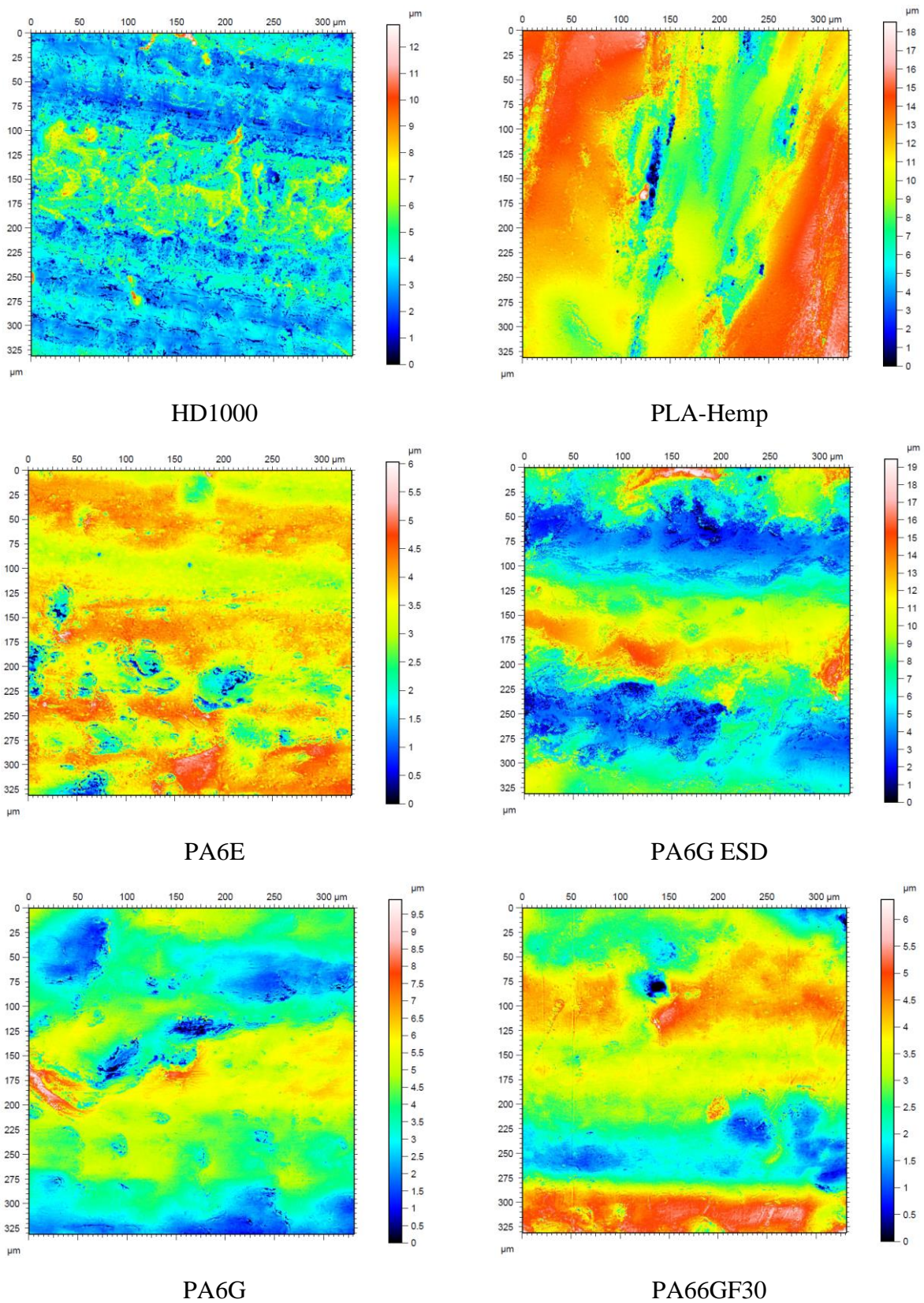


Fig. 8.14. Microscopic visualization of the change of surface 3D topography of the tested materials on loamy slurry at position No.2 (Fig. 3.13)

## 8. Appendices

Fig. 8.15 shows the microscopic visualization of the polymer surfaces in the final states with the loamy slurry at position 3.

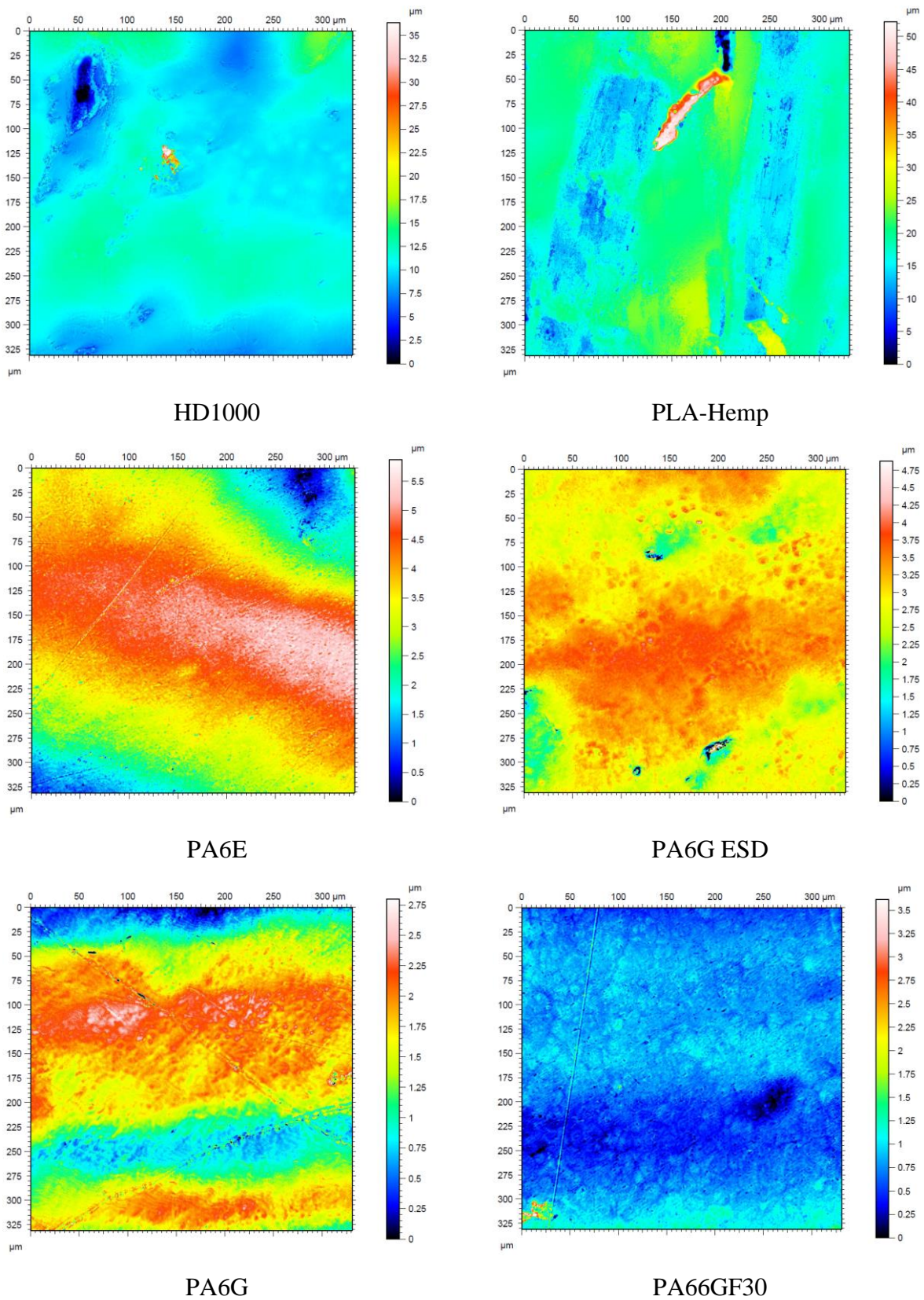


Fig. 8.15. Microscopic visualization of the change of surface 3D topography of the tested materials on loamy slurry at position No.3 (Fig. 3.13)

Table 8.11. Surface characteristics after the tests and the change in % at position No. 2

	<b>HD1000</b>	<b>PLA-HF</b>	<b>PA6E</b>	<b>PA6G ESD</b>	<b>PA6G</b>	<b>PA66GF30</b>
	after the test					
Sq ( $\mu\text{m}$ )	1.32	2.83	0.69	3.22	1.27	1.01
Ssk	0.80	-0.40	-1.18	0.44	0.04	-0.15
Sku	4.97	2.89	6.25	2.61	3.16	2.50
Sp ( $\mu\text{m}$ )	9.10	7.52	2.51	12.29	5.93	3.14
Sv ( $\mu\text{m}$ )	3.73	11.02	3.52	7.15	3.99	3.23
Sz ( $\mu\text{m}$ )	12.83	18.54	6.03	19.44	9.92	6.37
Sa ( $\mu\text{m}$ )	1.00	2.34	0.51	2.67	1.02	0.83
	Change in %					
Sq ( $\mu\text{m}$ )	-76.20%	346.86%	-88.48%	-43.11%	-79.14%	-80.98%
Ssk	3420.40%	-178.15%	-2623.56%	-415.73%	-86.66%	-122.16%
Sku	140.49%	-49.32%	179.09%	33.10%	24.52%	-29.85%
Sp ( $\mu\text{m}$ )	-61.48%	82.73%	-91.23%	-15.62%	-69.93%	-91.60%
Sv ( $\mu\text{m}$ )	-67.48%	305.86%	-70.13%	-42.85%	-66.15%	-66.83%
Sz ( $\mu\text{m}$ )	-63.44%	171.45%	-85.07%	-28.20%	-68.52%	-86.48%
Sa ( $\mu\text{m}$ )	-78.56%	409.15%	-90.02%	-44.03%	-79.71%	-80.82%

Table 8.12. Surface characteristics after the tests and the change in % at position No. 3

	<b>HD1000</b>	<b>PLA-HF</b>	<b>PA6E</b>	<b>PA6G ESD</b>	<b>PA6G</b>	<b>PA66GF30</b>
	after the test					
Sq ( $\mu\text{m}$ )	1.89	4.61	1.11	0.44	0.50	0.22
Ssk	1.11	2.20	-0.61	-0.84	-0.51	1.15
Sku	24.74	16.26	2.80	6.16	2.47	15.76
Sp ( $\mu\text{m}$ )	25.64	33.85	2.26	1.86	1.27	2.87
Sv ( $\mu\text{m}$ )	10.69	18.39	3.61	3.02	1.53	0.74
Sz ( $\mu\text{m}$ )	36.33	52.25	5.87	4.88	2.80	3.61
Sa ( $\mu\text{m}$ )	1.32	3.08	0.90	0.34	0.42	0.17
	Change in %					
Sq ( $\mu\text{m}$ )	-65.86%	627.06%	-81.37%	-92.18%	-91.80%	-95.79%
Ssk	4830.35%	331.04%	-1405.85%	509.64%	-284.83%	73.73%
Sku	1097.15%	185.60%	24.98%	214.06%	-2.69%	342.27%
Sp ( $\mu\text{m}$ )	8.53%	722.99%	-92.09%	-87.21%	-93.58%	-92.33%
Sv ( $\mu\text{m}$ )	-6.79%	577.35%	-69.37%	-75.87%	-87.01%	-92.35%
Sz ( $\mu\text{m}$ )	3.52%	665.08%	-85.46%	-81.97%	-91.12%	-92.33%
Sa ( $\mu\text{m}$ )	-71.75%	569.88%	-82.19%	-92.80%	-91.70%	-96.14%

**A14: The other position results of the 3D surface microscopy results with the sandy slurry**

Fig. 8.16 shows the microscopic visualization of the polymer surfaces in the final states with the sandy slurry at position 2.

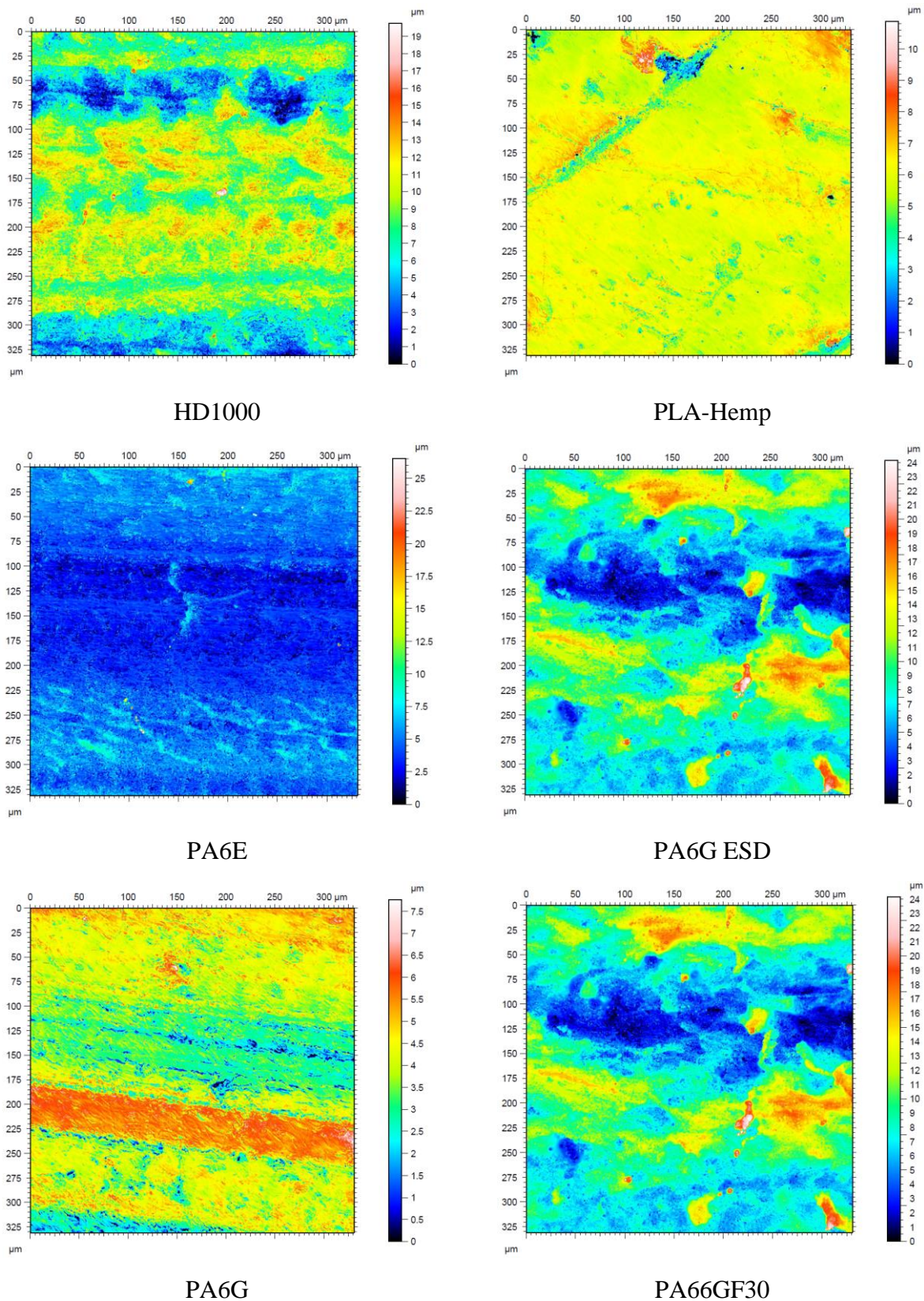


Fig. 8.16. Microscopic visualization of the change of surface 3D topography of the tested materials on sandy slurry at position No.2 (Fig. 3.13)

Fig. 8.17 shows the microscopic visualization of the polymer surfaces in the final states with the sandy slurry at position 3.

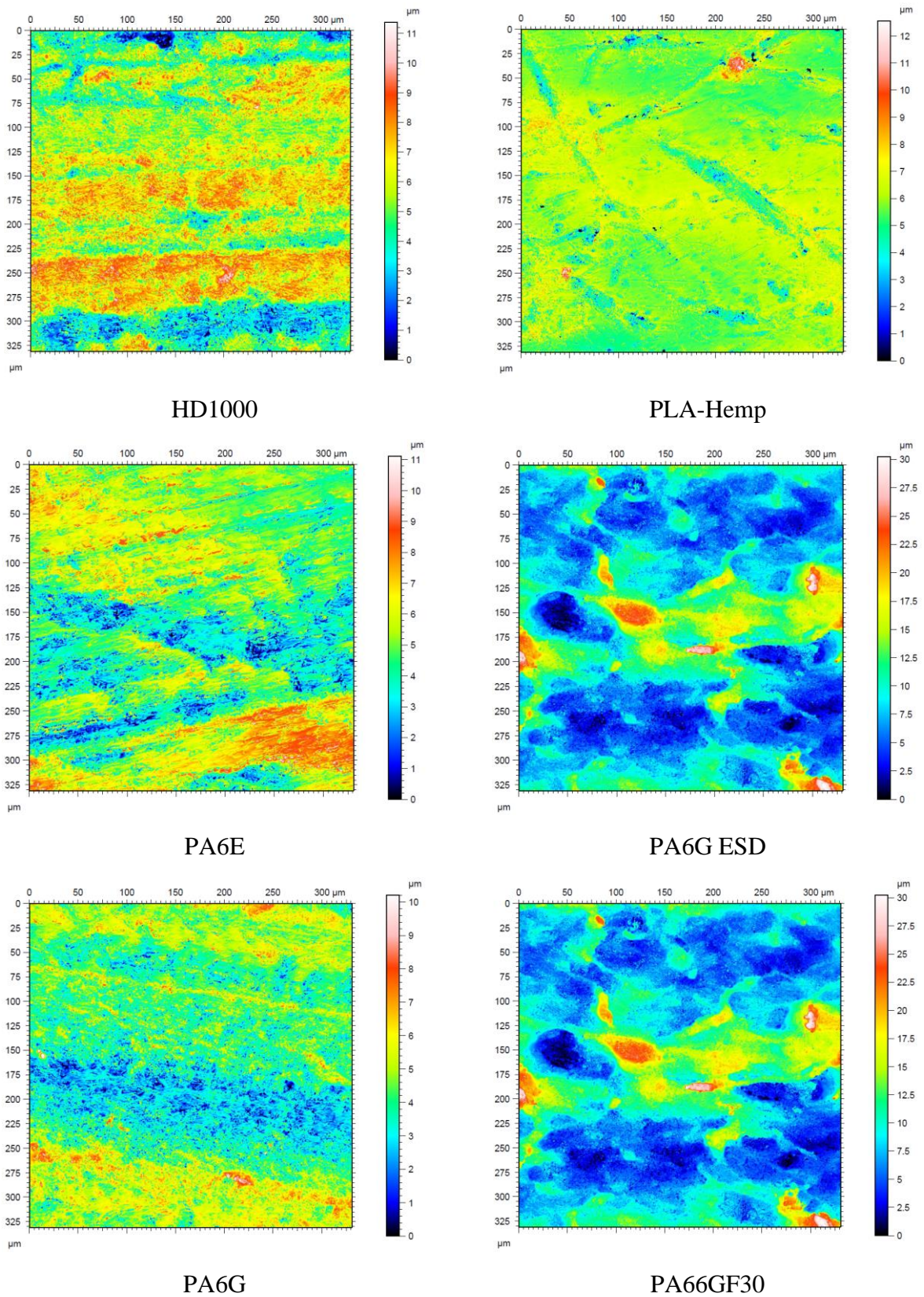


Fig. 8.17. Microscopic visualization of the change of surface 3D topography of the tested materials on sandy slurry at position No.3 (Fig. 3.13)

## 8. Appendices

Table 8.13. Surface characteristics after the tests and the change in % at position No. 2

	<b>HD1000</b>	<b>PLA-HF</b>	<b>PA6E</b>	<b>PA6G ESD</b>	<b>PA6G</b>	<b>PA66GF30</b>
	after the test					
Sq ( $\mu\text{m}$ )	2.71	0.75	1.56	3.57	1.07	1.65
Ssk	-0.31	-1.87	0.80	0.43	-0.34	1.73
Sku	2.84	15.33	10.70	3.24	3.40	10.10
Sp ( $\mu\text{m}$ )	11.43	4.90	22.08	15.84	3.73	13.33
Sv ( $\mu\text{m}$ )	8.33	5.97	4.44	8.30	4.04	4.15
Sz ( $\mu\text{m}$ )	19.76	10.87	26.52	24.14	7.76	17.48
Sa ( $\mu\text{m}$ )	2.18	0.47	1.22	2.82	0.84	1.13
	Change in %					
Sq ( $\mu\text{m}$ )	-51.05%	18.52%	-73.83%	-36.98%	-82.42%	-68.97%
Ssk	-1466.99%	-467.27%	1617.03%	-414.12%	-222.86%	161.69%
Sku	37.61%	169.30%	377.95%	64.94%	33.92%	183.50%
Sp ( $\mu\text{m}$ )	-51.62%	19.14%	-22.76%	8.72%	-81.10%	-64.33%
Sv ( $\mu\text{m}$ )	-27.40%	119.75%	-62.31%	-33.63%	-65.77%	-57.40%
Sz ( $\mu\text{m}$ )	-43.70%	59.14%	-34.30%	-10.84%	-75.37%	-62.90%
Sa ( $\mu\text{m}$ )	-53.48%	2.39%	-75.91%	-40.89%	-83.35%	-73.77%

Table 8.14. Surface characteristics after the tests and the change in % at position No. 3

	<b>HD1000</b>	<b>PLA-HF</b>	<b>PA6E</b>	<b>PA6G ESD</b>	<b>PA6G</b>	<b>PA66GF30</b>
	after the test					
Sq ( $\mu\text{m}$ )	1.71	0.89	1.59	4.43	1.29	0.88
Ssk	-0.29	-0.64	-0.01	1.08	0.00	0.34
Sku	2.98	9.59	3.09	4.64	3.18	3.92
Sp ( $\mu\text{m}$ )	5.67	6.65	6.16	21.38	6.01	4.46
Sv ( $\mu\text{m}$ )	5.70	5.90	4.95	8.85	4.20	2.72
Sz ( $\mu\text{m}$ )	11.37	12.55	11.11	30.23	10.21	7.18
Sa ( $\mu\text{m}$ )	1.37	0.62	1.25	3.43	1.03	0.69
	Change in %					
Sq ( $\mu\text{m}$ )	-69.07%	40.11%	-73.39%	-21.70%	-78.88%	-83.46%
Ssk	-1362.35%	-225.80%	-127.09%	-881.34%	-99.74%	-48.67%
Sku	44.26%	68.47%	37.99%	136.78%	24.99%	9.95%
Sp ( $\mu\text{m}$ )	-76.00%	61.66%	-78.45%	46.74%	-69.52%	-88.08%
Sv ( $\mu\text{m}$ )	-50.32%	117.35%	-58.00%	-29.27%	-64.42%	-72.06%
Sz ( $\mu\text{m}$ )	-67.61%	83.80%	-72.49%	11.62%	-67.61%	-84.77%
Sa ( $\mu\text{m}$ )	-70.78%	35.38%	-75.31%	-28.18%	-79.50%	-83.93%

## 9. ACKNOWLEDGEMENTS

This PhD work has been accomplished at Institute for Mechanical Engineering Technology, Faculty of Mechanical Engineering, Szent István University- Gödöllő, between September 2016 and January 2021.

The PhD program including the present research is supported by Stipendium Hungaricum Scholarship Program. Further, the experimental tests materials were supplied by Quattroplast Ltd. Hungary, And Borås University, Sweden.

I would like to acknowledge my most profound gratitude to my supervisors Prof. Dr. Gábor Kalácska for his valuable recommendations, advice, excellent guidance and continuous encouragement during my PhD research. This dissertation would not have been possible without his considerable academic support and it was my pleasure to work under his supervision and learn the sober scientific research ways. Additionally, I desire to extend my sincere gratitude to all the team of Institute for Mechanical Engineering Technology, especially thanks for prof. Dr. Róbert Keresztes, prof. Dr. Zoltán Szakál, prof. Dr. Székely László, prof. Dr. Nawar Kadi, and Ádám Sarankó for their valuable help, in the laboratory and provide data, throughout my research.

In addition, I would like to express my thanks and gratitude to the head of Doctoral School of Mechanical Engineering prof. Dr. István Farkas for his valuable advice and fatherly dealing throughout my research years which has dramatically contributed to facilitate the completion of the doctoral degree.

The surface 3D topography measurements were carried out in co-operation with University of Ghent, Department of Mechanical Construction and Production, Soete Laboratory with individual help and support from Ádám Kalácska and Dr. Jacob Sukumaran.

This scientific work is dedicated to my family for their support.

Hasan Muhandes

Gödöllő, 2021